Abstracts Booklet

2026

Biomolecular Materials

Principal Investigators' Meeting

Office of Science

Office of Basic Energy Sciences

Materials Sciences and Engineering Division

August 4-6, 2026

Gaithersburg, Maryland

FOREWORD

This volume comprises the scientific content of the presentations made at the 2026 Biomolecular Materials (BMM) Principal Investigators' Meeting, sponsored by the Materials Sciences and Engineering (MSE) division in the Office of Basic Energy Sciences (BES) of the U.S. Department of Energy (DOE). Focusing on the fundamental science supported by the Biomolecular Material Core Research Area (CRA), the in-person meeting took place August 4-6, 2026, in Gaithersburg, MD.

The purpose of the meeting is to bring together all the Principal Investigators with currently active projects in the BMM program for raising awareness among PIs of the overall program content and of each other's research, encouraging exchange of ideas, promoting collaboration, and stimulating innovation. The meeting also allows the Program Manager and BES management to periodically gain a comprehensive overview of the program, helping to identify needs and potential new research directions.

This year's meeting was organized and led by Co-chairs Oleg Gang (Columbia) and Suri Vaikuntanathan (U. Chicago) and included special lunch seminars by National Laboratory scientists Kevin Yager (BNL) and Gary Ren (LBL) on soft matter characterization. Adam Kinney of BES provided updates on Genesis Mission AI activities and Andy Schwartz, Deputy Associate Director for BES provided updates on research funding landscape and activities of newly constituted Office of Science Advisory Committee (SCAC) providing critical advice to all of the Office of Science research programs.

Sincere thanks to Oleg and Suri, all session chairs, guest speakers, Adam, and Andy for dedicating their time and providing a holistic picture of BES's support for science. I would like to thank the meeting attendees for sharing their ideas and new research results, asking insightful questions, and contributing fresh perspectives to the continued development of the field. Sincere thanks also go to Kerry Hochberger of BES and Paul Hudson, April Ward and Kutter Criag at the Oak Ridge Institute of Science and Education (ORISE) for their excellent logistical support for the meeting.

J. Aura Gimm
Program Manager, Biomolecular Materials
Materials Sciences and Engineering Division
Office of Basic Energy Sciences
U.S. Department of Energy

Table of Contents

Agenda ..... **vii**

University Abstracts **14**

Bioinspired Active Transport and Energy Transduction using Liquid Crystals Beyond Equilibrium
*Nicholas L. **Abbott**, and Juan J. de Pablo* *15*

Adaptive Locomotion and Free-Form Maneuverability of Untethered, Single-Material Symmetric Microrobot: Experiment and Modeling
*Joanna **Aizenberg** and Anna C. Balazs* *19*

Conductive Chiroptical Polysaccharides for Dynamic Infrared Electro-Reflectivity
*Cécile **Chazot*** *23*

Design Principles of Biomolecular Metamaterials
*Jong Hyun **Choi*** *27*

Energy-Efficient Self-Organization and Swarm Behavior in Active Matter
*Jerome **Delhommelle** and Stefano Sacanna* *32*

Dynamic materials assembly using stimuli responsive polypeptide coacervates
*Timothy **Deming*** *37*

Nature-Inspired Ionomer Design and Self-Assembly for Robust, Precise Synthetic Ion Channels
*Shudipto Konika **Dishari*** *41*

Active interfaces and membranes
*Zvonimir **Dogic** and Cristina Marchetti* *45*

Hierarchical Assembly in Biomimetic Active Interfaces
*Guillaume **Duclos*** *49*

Bioinspired Morphogenesis of Functional Bicontinuous Materials
*Eric R. **Dufresne** and Brett P. Fors* *51*

Bio-inspired Materials Designs: Reactive, Functional Droplets and Smart Interfaces
*Todd **Emrick*** *54*

Early Formation Stages and Pathway Complexity in Functional Bio-Hybrid Nanomaterials

*Lara A. **Estroff**, Elias Nakouzi and Ulrich Wiesner* *59*

Programmable Dynamic Self-Assembly of DNA Nanostructures
*Elisa **Franco** and Rebecca **Schulman*** *64*

Controlling Lattice Organization, Assembly Pathways and Defects in Self-Assembled DNA-Based Nanomaterials
*Oleg **Gang** and Sanat K Kumar* *70*

Catalytic Enzymes as Active Matter
*Steve **Granick*** *76*

Hybrid Quantum Magnonics for Transduction and Sensing
A framework for exploring and controlling non-equilibrium coherent states in active fluids based on global phase space geometry
*Piyush **Grover**, Jae Sung Park, and Michael M. Norton* *83*

Combining machine learning and feedback control to understand and manipulate active matter
*Michael F. **Hagan**, Seth Fraden, Pengyu Hong, and Zvonimir Dogic* *88*

Chemically fueled dissipative assembly of complex molecular architectures
*C. Scott **Hartley** and Dominik Konkolewicz* *93*

Chaos, Mixing, and Energy Extraction in Active Nematics
*Linda S **Hirst**, Kevin Mitchell, Zvonimir Dogic, and Cristina Marchetti* *98*

Active-Passive Colloidal Experiments and Simulations for Programmable Active Matter
*Daphne **Klotsa**, John F. **Brady**, and David J. **Pine*** *102*

Ion-Ion discrimination in biomimetic ligand appended artificial channels
*Manish **Kumar**, Venkat Ganesan, and Carlos Baiz* *105*

Bio-mimetic material design based on principles of disorder
*Andrea J. **Liu** and Sidney R. **Nagel*** *110*

Understanding and Informed Manipulation of Functional Dynamics on the Nanoscale Through Integrated Experiments and Computation
*Erik **Luijten** and Qian **Chen*** *115*

Multiscale Modeling of Water and Peptide Self-Assembly through Probabilistic Backmappings
*Jacob I. **Monroe** and Ralph E. Martin* *119*

Electrostatic-Driven Self-Assembly Design of Functional Nanostructures

*Monica **Olvera de la Cruz**, Michael J. Bedzyk, and Neha Kamat* *124*

Nonequilibrium Transport: Interfaces, Nucleation, and Bulk Dynamics
*Ahmad K. **Omar*** *129*

Data-Driven Generalized Master Equations for Nonequilibrium Coarse-Grained Dynamics and Response
*Grant M. **Rotskoff*** *133*

Tension and Curvature -Driven Interactions Producing Touch-Sensitive Patterning in Biomolecular Lamellae
*Maria M. **Santore** and Gregory M. Grason* *136*

Emergent functionality generated from excitonic building blocks using DNA origami
*Gabriela S. **Schlau-Cohen**, Mark Bathe and Adam P. Willard* *141*

The Role of Nanoparticle-Based Bonds in Polymer Networks
*S. Eileen **Seo*** *146*

Toward Programmable Self-Navigation of DNA-Based Micrometer-Scale Gliders
*William M. **Shih*** *150*

Transient Microstructures Inspired by Mycorrhizal Fungi Arbuscules
*Meredith **Silberstein*** *154*

Biomimetic Strategies for Field-Driven Defect Annealing in Microparticle Crystals
*Michael J. **Solomon** and Sharon C. Glotzer* *158*

Synthetic Methanotrophs: a methane powered platform for active matter
*Michael S. **Strano*** *163*

Dynamics of Superstructure Formation from Supramolecular Assemblies
*Samuel I. **Stupp*** *168*

Simulation-driven design for experimental realization of 3D complex nanostructures
*Petr **Šulc*** *173*

Hybrid Quantum Magnonics for Transduction and Sensing
*F. Akif **Tezcan*** *175*

Merging non-equilibrium stat mech and AI for the design of intelligent adaptive bio-inspired materials
Polymer Origami – A Blueprint for Hierarchical Folding Multiblock Copolymers
*Thi **Vo*** *183*

Steering the Pathways of Hierarchical Self-assembly at Solid Surfaces

*Tao **Ye**, Yonggang **Ke**, and Gaurav **Arya*** *188*

Laboratory Abstracts 193

Bio-inspired Durable Storage of CO_2
*Chun-Long **Chen**, Jim De Yoreo, Chris Mundy, Kevin Rosso, Wendy Shaw, and Marvin Bayro*..... *194*

Precision synthesis and assembly of ionic and liquid crystalline polymers
*Paul **Nealey**, Matthew Tirrell, Jie Xu, Joan Montes de Oca, Juan J de Pablo, and Wei Chen* *199*

Adaptive Interfacial Assemblies Towards Structuring Liquids
*Thomas P. **Russel**l, Paul D. Ashby, Brett Helms, Ahmad K. Omar, and Peter Ercius*..... *204*

Dynamics of Active Self-Assembled Materials
*Alexey **Snezhko**, Andrey Sokolov, and Andreas Glatz*..... *209*

Agenda

2026 DOE BES Biomolecular Materials Principal Investigators' Meeting

Meeting Co-Chairs: Oleg Gang (Columbia University) and Suri Vaikuntanathan (University of Chicago)

Presentation slides must be submitted via the website no later than **a day prior** to your presentation. Please include the timeslot and your last name in the title of the file (e.g. **Tuesday_0930_Solomon**.ppt).

Tuesday, August 4th 2026:

8:00–8:50 AM	Breakfast and presentation set-up (Put up posters)
8:50–9:00 AM	**Opening Remarks** Aura Gimm, Program Manager, Biomolecular Materials Oleg Gang and Suri Vaikuntanathan, Meeting Co-Chairs
Session 1	**Programmed Self-Assembly and Hierarchical Nanostructures I** Session Chair: Qian Chen
9:00–9:20 AM	Gaurav Arya, Duke University; Yonggang Ke, Emory University; and Tao Ye, UC Merced *Conformationally-Steered Hierarchical Self-Assembly at Solid Surfaces*
9:20–9:30 AM	Discussion
9:30–9:50 AM	Michael Solomon, University of Michigan *Biomimetic Strategies for Defect Annealing in Colloidal Crystallization*
9:50–10:00 AM	Discussion
10:00–10:20 AM	Lara Estroff and Uli Wiesner, Cornell University *Early Formation Stages and Pathway Complexity in Functional Bio-Hybrid Nanomaterials*
10:20–10:30 AM	Discussion
10:30–10:50 AM	**Break**
Session 2	**New Projects – New Directions I** Session Chair: Rebecca Schulman
10:50–11:10 AM	Thi Vo, Johns Hopkins University (Early Career) *Polymer Origami: A Blueprint for Hierarchical Folding of Sequence-Controlled Multiblock Copolymers*
11:10–11:20 AM	Discussion
11:20–11:40 AM	Eileen Seo, Arizona State University (Early Career) *Self-Repairing Polymer Networks Engineered with Nanoparticle-Based Bonds*

11:40–11:50 AM	Discussion
11:50–12:10 PM	Cécile Chazot, Northwestern University (Early Career) *Conductive Chiroptical Polysaccharides for Dynamic Infrared Electro-Reflectivity*
12:10–12:20 PM	Discussion
12:30–2:00 PM	**Working Lunch – Soft matter characterization at National Labs** (MC: Gang) Kevin Yager, Brookhaven National Laboratory *The Present and Future of the Center for Functional Nanomaterials* Gary Ren, Lawrence Berkeley National Laboratory *Advanced Electron Microscopy at the Molecular Foundry: Enabling Studies of Structure, Dynamics, and Spatial Distribution in Soft and Biomaterials*
2:00–3:30 PM	**Poster Session 1 (odd numbers) and Discussion**
Session 3	**Active Matter and Non-equilibrium Dynamics** Session Chair: Zvonimir Dogic
3:30–3:50 PM	Steve Granick, University of Massachusetts Amherst *Catalytic Enzymes as Active Matter*
3:50–4:00 PM	Discussion
4:00–4:20 PM	**Break**
4:20–4:40 PM	Jerome Delhommelle, UMass Lowell, and Stefano Sacanna, New York University *Morphogenic Colloids*
4:40–4:50 PM	Discussion
4:50–5:10 PM	Piyush Grover, University of Nebraska *Dynamics and Control of Active Nematics Using Nonlinear Reduced-Order Models*
5:10–5:20 PM	Discussion
5:20–7:00 PM	**Poster Session 1, continued**
	Dinner on your own

Wednesday, August 5th 2026

8:00–8:55 AM	Breakfast and presentation set-up
9:00–9:30 AM	**SC/BES/MSE Updates** Andy Schwartz, Deputy Associate Director, Office of Basic Energy Sciences (BES)
Session 4	**New Projects – New Directions II** Session Chair: Gabriela Schlau-Cohen
9:30–9:50AM	Meredith Silberstein, Cornell University *Transient Microstructures Inspired by Mycorrhizal Fungi Arbuscules*
9:50–10:00 AM	Discussion
10:00–10:20 AM	Linda Hirst, UC Merced (FAIR) *Chaos, Mixing, and Energy Extraction in Active Nematics*
10:20–10:30 AM	Discussion
10:30–10:50 AM	Eric Dufresne, Cornell University *Bioinspired Morphogenesis of Functional Bicontinuous Materials*
10:50–11:00 AM	Discussion
11:00–11:10 AM	**Break**
Session 5	**AI, Simulation, and Data-Driven Materials Design** Session Chair: Suri Vaikuntanathan
11:10–11:30 AM	Petr Šulc, Arizona State University *Simulation-Driven Design for Experimental Realization of 3D Complex Nanostructures*
11:30–11:40 AM	Discussion
11:40–12:00 PM	Grant Rotskoff, Stanford University (Early Career) *Characterizing the Limits of Nonequilibrium Control for Dissipative Self-Assembly*
12:00–12:10 PM	Discussion
12:10–12:30 PM	Michael Hagan, Brandeis University *Combining machine learning and feedback control to understand and manipulate active matter*
12:30–12:40 PM	Discussion

12:40–2:10 PM	**Working Lunch with BMM updates, Genesis Updates, discussions on potential new programmatic directions** (MC: Gimm) Adam Kinney, Senior Technical Advisor, BES *Genesis Mission Update* Aura Gimm, Program Manager, BES *Biomolecular Materials Program Update*
2:10–3:30 PM	**Poster Session 2 (even numbers) and Discussion**
Session 6	**New Projects – New Directions III** Session Chair: Jason Green
3:30–3:50 PM	Timothy Deming, University of California, Los Angeles *Dynamic Materials Assembly Using Stimuli Responsive Polypeptide Coacervates*
3:50–4:00 PM	Discussion
4:00–4:20 PM	Shudipto Dishari, University of Nebraska–Lincoln *Nature-Inspired Ionomer Design and Self-Assembly for Robust, Precise Synthetic Ion Channels*
4:20–4:30 PM	Discussion
4:30–4:40 PM	**Break**
Session 7	**National Laboratory Programs** Session Chair: Oleg Gang
4:40–5:00 PM	Alexey Snezhko, Argonne National Laboratory *Dynamics of Active Self-Assembled Materials*
5:00–5:10 PM	Discussion
5:10–5:30 PM	Chun-Long Chen, Pacific Northwest National Laboratory *Bio-inspired Durable Storage of CO_2*
5:30–5:40 PM	Discussion
5:40–7:00 PM	**Poster Session 2, continued**
	Dinner on your own

Thursday, August 6th, 2026

8:00–8:55 AM	Breakfast (Take down posters)
Session 8	**Biomimetic Transport and Functional Materials** Session Chair: Jong Hyun Choi
9:00–9:20 AM	Michael Strano, Massachusetts Institute of Technology *Synthetic Methanotrophs: a methane powered platform for active matter*
9:20–9:30 AM	Discussion
9:30–9:50 AM	Manish Kumar, University of Texas at Austin *Transport and Molecular Discrimination in Biomimetic Artificial Water Channels for Lanthanide Separations*
9:50–10:00 AM	Discussion
10:00–10:20 AM	**Break**
Session 9	**Programmed Self-Assembly and Hierarchical Nanostructures II** Session Chair: Elisa Franco
10:20–10:40 AM	Maria Santore, University of Massachusetts Amherst *Tension and Curvature -Driven Interactions Producing Touch-Sensitive Patterning in Biomolecular Lamellae*
10:40–10:50 AM	Discussion
10:50–11:10 AM	C. Scott Hartley, Miami University of OH *Chemically Fueled Dissipative Assembly of Complex Molecular Architectures*
11:10–11:20 AM	Discussion
11:20–11:40 AM	Todd Emrick, University of Massachusetts Amherst *Reactive, Functional Droplets in Bio-inspired Materials and Smart Interfaces*
11:40–11:50 AM	Discussion
11:50–12:10 PM	**Concluding Remarks and Discussion** Oleg Gang and Suri Vaikuntanathan, Meeting Co-Chairs Aura Gimm, Program Manager, Biomolecular Materials
12:10 PM	**Adjourn**

Poster Presentations

(*posters should be up for both days following the numbered assignments. Odd numbers will be manned on Tuesday (8/4), and even ones on Wednesday (8/5))

1. *Electrostatic Driven Self-Assembly Design of Functional Nanostructures*
   Olvera de la Cruz, Northwestern University
2. *Protein Self-Assembly by Rational Chemical Design*
   Tezcan, University of California, San Diego
3. *Adaptive Locomotion and Free-Form Maneuverability of Untethered, Single-Material Symmetric Microrobot: Experiment and Modeling*
   Aizenberg, Harvard University
4. *Controlling Lattice Organization, Assembly Pathways and Defects in Self-Assembled DNA-Based Nanomaterials*
   Gang, Columbia University
5. *Programmable Dynamic Self-Assembly of DNA Nanostructures*
   Schulman, Johns Hopkins University & **Franco**, University of California, Los Angeles
6. *Active Interfaces and Membranes*
   Dogic, University of California, Santa Barbara
7. *Merging non-equilibrium stat mech and AI for the design of intelligent adaptive bio-inspired materials*
   Vaikuntanathan, University of Chicago
8. *Emergent functionality generated from excitonic building blocks using DNA origami*
   Willard (Schlau-Cohen), Massachusetts Institute of Technology
9. *Design Principles of Biomolecular Metamaterials*
   Choi, Purdue University
10. *Understanding and Informed Manipulation of Functional Dynamics on the Nanoscale Through Integrated Experiments and Computation*
    Q Chen, UIUC & **Luijten**, Northwestern University
11. *Dynamics of Superstructure Formation from Supramolecular Assemblies*
    Stupp, Northwestern University
12. *Bio-mimetic material design based on principles of disorder*
    Nagel, University of Chicago
13. *Hierarchical Assembly of Biomimetic Active Matter Driven by Non-Equilibrium Actin Turnover*
    Sessa (**Duclos**), Brandeis University (Early Career)
14. *Principles of Self-Navigation for Cell-Sized Gliders*
    Shih, Dana-Farber Cancer Institute
15. *Data-Driven Learning of Dissipation from Microscopy of Chemically Active Materials*
    Green, University of Massachusetts Boston (FAIR)

16. *Physically motivated linking of resolutions in multiscale models to predict thermal and charge transport in self-assembling soft materials*
    Monroe, University of Arkansas (Early Career)
17. *Transport Mechanisms in Active and Biomolecular Materials*
    Omar, University of California, Berkeley
18. *Evolutionary Structured Liquids from Confined Active Matter*
    Omar (**Russell**), Lawrence Berkeley National Laboratory
19. *Adaptive Interfacial Assemblies Towards Structuring Liquids*
    Russell et al. Lawrence Berkeley National Laboratory
20. *Microscopic Insights into Interfacial Assemblies in Structured Liquids*
    Russell, Lawrence Berkeley National Laboratory
21. *Biomimetic Strategies for Field-Driven Defect Annealing in Microparticle Crystals*
    Solomon, University of Michigan
22. *Precision Synthesis and Assembly of Ionic and Liquid Crystalline Polymers*
    Xu (Nealey), Argonne National Laboratory
23. *Chaos, Mixing, and Energy Extraction in Active Nematics*
    Hirst, University of California, Merced
24. *Dynamics of Active Self-Assembled Materials*
    Snezhko, Argonne National Laboratory
25. *Bio-inspired Durable Storage of CO_2*
    C Chen, Pacific Northwest National Laboratory
26. *Energy-Efficient Self-Organization and Swarm Behavior in Active Matter*
    Delhommelle, UMass-Lowell, & **Sacanna**, NYU
27. *Magic-size clusters and cage topologies as early formation stages in the polycondensation of silica*
    Wiesner (**Estroff**), Cornell University
28. *Predictive Model for Nanoparticle Incorporation into Crystals Reveals Essential Role of Interfacial Solution Structure*
    Wiesner (**Estroff**), Cornell University
29. *Chemical Exchange in Transiently Generated Covalent Polymers*
    Hartley, Miami University of OH
30. *Harnessing Symmetry Breaking and Emergence in Chemically Powered Active Matter*
    Strano, Massachusetts Institute of Technology
31. *Combining machine learning and feedback control to understand and manipulate active matter*
    Hagan, Brandeis University

University Abstracts

Bioinspired Active Transport and Energy Transduction using Liquid Crystals Beyond Equilibrium

Nicholas L. **Abbott** (Cornell University) and Juan J. de Pablo (University of Chicago)

Keywords: Non-equilibrium, bioinspired, hierarchical, liquid crystals, solitons

Research Scope

Biological systems function out of equilibrium, with structure and dynamics that arise from dissipative processes involving the interplay of advective and diffusive transport. The complex dynamic behaviors found in biology often reflect highly non-linear phenomena that lead to surprisingly localized responses to delocalized fields. These principles offer inspiration for new designs of soft materials that harvest and transduce non-localized sources of energy. In this project, we are exploring an emerging class of dynamic, cooperative phenomena that have been observed in liquid crystals (LCs) – solitary waves, or "solitons", as the basis of new designs of active soft matter for achieving rapid and directed transport processes and new modes of energy transduction. These localized responses have analogies to many other physical and biological phenomena, and have only recently been shown to occur in LCs [1]. In LCs, solitons consist of waves of localized orientational perturbations that can travel at high speed and over long distances. Through closely coupled simulations and experiments, this project is addressing open questions regarding the mechanisms by which solitons form in LCs and subsequently interact with fluid interfaces, with the long-term goal of creating fundamentally new ways to transduce soliton energy into new states of matter.

Recent Progress

A particular focus of our recent efforts has revolved around investigations of key factors that are allowing us to gain control over soliton trajectories. The approach involves introduction of elastic distortions in the nematic far-field director by using LC films confined in hybrid cells (i.e. with one surface promoting uniaxial planar anchoring, and a second surface promoting homeotropic/perpendicular anchoring). Using microscopic observations, simulations and high-speed imaging, we have been elucidating the factors that lead to soliton bullets propagating along tunable oblique axes in non-uniform far-field directors (Figure 1). We have discovered that asymmetric flexoelectric torques [2] lead to the frequency dependent oblique trajectories in hybrid anchoring settings and simulations predict asynchronous out-of-plane fluctuations, which are verified in experiments. Overall, our results reveal the interplay between the non-linear action of external fields and the far-field strain on soliton propagation. They also show that confinement can be used to control the direction of propagation of non-linear signals, and demonstrate how LCs

can be used as a model system to test and predict the effects of non-linear excitations on material designs.

This progress was described in PNAS in 2026.

We have also utilized high-speed imaging to study the behavior of solitons at interfaces, in particular fluid interfaces between an LC and an isotropic oil. This work aims to understand the mechanisms leading to the soliton energy being harnessed to trigger emulsification or "budding", in a manner similar to biological processes, or de-emulsification. The need to incorporate a coupling between hydrodynamic effects and structure to describe such interfacial processes has been providing exciting challenges for theoretical and computational efforts in the team. In a second direction of investigation related to interfaces between LCs and isotropic oils, we have investigated the role of AC electric field-induced solitons in the coalescence of isotropic oil emulsion droplets dispersed in LCs. We have discovered that solitons formed near the droplets can bridge two or more droplets, thus pulling the droplets into rapid coalescence (Figure 2). This discovery provides a fundamentally new way to destabilize

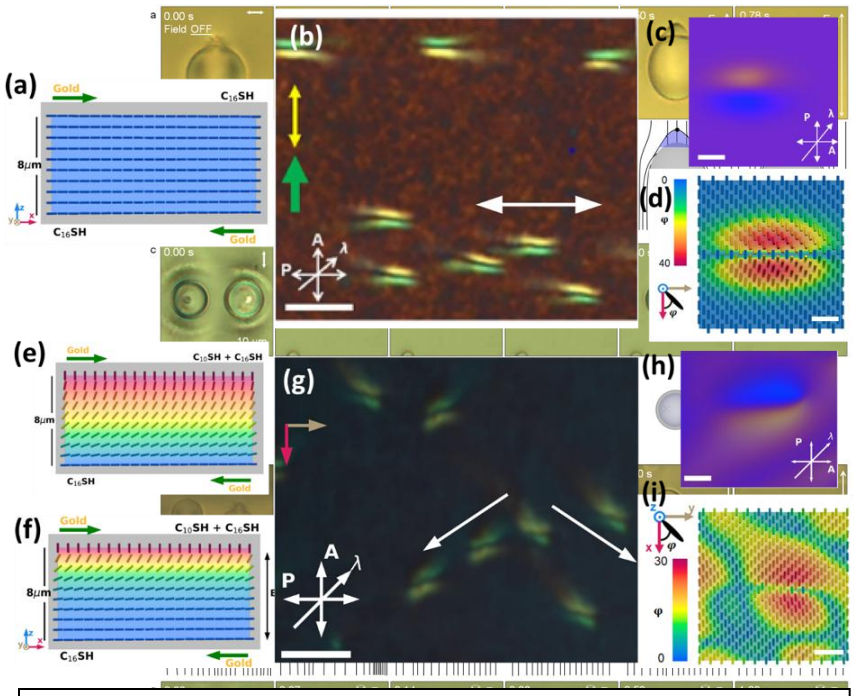


Figure 1. Comparison of solitons formed in LCs with uniform and strained far-field director orientations. (a) Schematic illustration of a planar LC optical cell, assembled using two gold films decorated with a self-assembled monolayer (SAM) of $C_{16}SH$ promoting planar anchoring. Green arrows indicate the direction of gold deposition. (b) Traveling solitons observed in a planar cell. Green arrow indicates the direction of gold deposition on the bottom substrate, the far-field nematic director is indicated by the double-headed yellow arrow, and the propagation axes of solitons is indicated by the white arrow. Scale bar: 50 μm. (c) Optical micrograph and (d) structure of a single soliton traveling in a planar cell, obtained in simulations, showing two symmetric wings. Scale bars: 10 μm. (e) Schematic illustration of a hybrid cell, assembled using one gold film with a C16SH SAM, promoting planar anchoring, and one gold film decorated with a mixed SAM of C_{10}- and $C_{16}SH$, promoting homeotropic anchoring. Green arrows indicate the direction of gold deposition. (f) Schematic illustration of the hybrid cell, with an electric field applied along the z-axis. (g) Propagating solitons in a hybrid cell. The white arrows highlight the two oblique axes of propagation of solitons. Scale bar: 50 μm. (h) Simulated polarized micrograph of simulated soliton at f = 300Hz and (i) simulated director profile of a soliton generated with hybrid anchoring conditions, highlighting the asymmetry of its structure. Scale bars: 10 μm.

emulsions and generalizes our prior reports of soliton-induced emulsification. This progress was described in *Nature* in 2025.

Future Plans

First, we will complete ongoing experiments and simulations that are characterizing the interactions of solitons at boundaries between orientational domains of LCs [4,5]. In experiments to be performed over the coming year, we propose to program complex soliton trajectories by using patterned LC domains. For example, we envisage, a soliton phase selector that filters solitons depending on their phase when they arrive at the boundary – because only solitons of a specific phase will pass across the boundary. This approach has the potential to provide "spatially coherent" fluxes of solitons, in which all solitons, irrespective of their spatial positions, will share the same phase, after crossing the domain boundary. Such coherent fluxes, similar to spatially coherent laser light, will permit predictable manipulation of the solitons in subsequent domains, thus providing an important step toward soliton circuits around which preprogrammed behaviors of solitons can be realized. We will use our high-speed camera to confirm the formation of coherent "beams" of solitons by characterizing the relative phases of the solitons.

Second, whereas our previously reported observations of soliton-

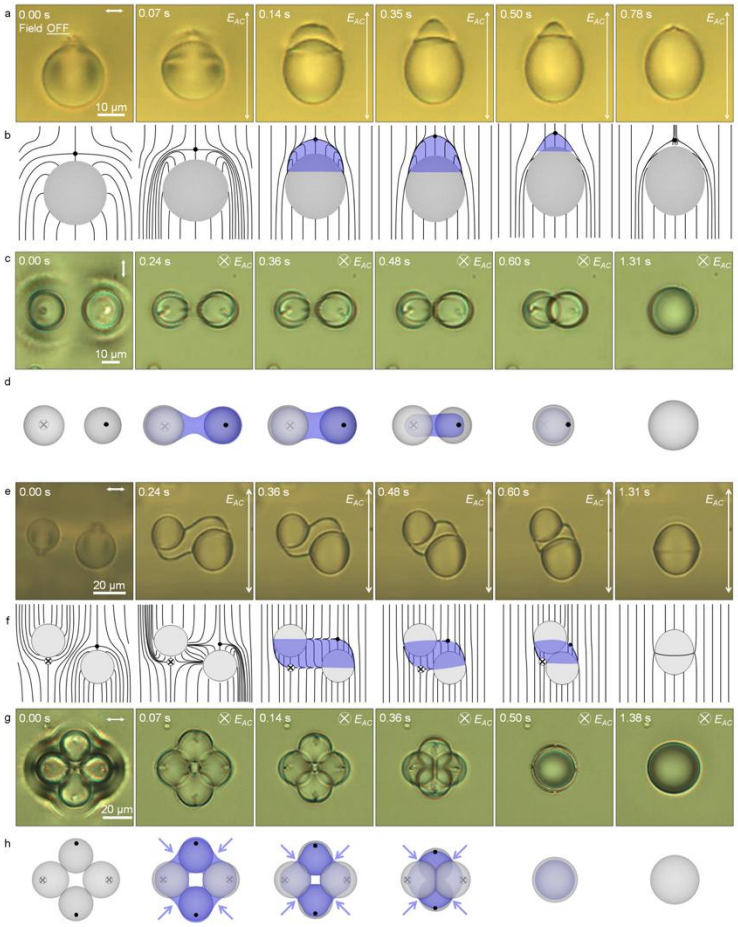


Figure 2. Kinetic pathway mediated by solitons leads to rapid coalescence of isotropic oil microdroplets dispersed in LC. a, Side view of soliton formation and contraction near a single droplet with a LC point defect. The soliton is formed upon application of an electric field (0.6 V/μm, 1 kHz). **b,** Schematic illustration of soliton formation (indicated by purple shading) shown in (**a**). The director profile of the LC is depicted by lines. **c,** Top view of a pair of DS droplets that were accompanied by topological point defects before applying an electric field (0.6 V/μm, 1 kHz). After application of the electric field, a soliton bridges the two droplets, driving their coalescence. The bright and dark points represent defects above and below the droplets, respectively. **d,** Schematic illustrations of the droplets in c. **e**, Side view of a pair of droplets that were accompanied by topological point defects before applying an electric field (0.6 V/μm, 1 kHz). The images show coalescence of two droplets driven by the formation of a bridging soliton. **f,** Schematic illustration of the droplets shown in (**e**). **g,** Top view of a cluster of four droplets before and after the onset of an electric field (0.6 V/μm, 1 kHz) that generated a soliton that bridged the four droplets and caused their coalescence. The droplets were oriented in an antiparallel manner. **h,** Schematic illustration of the droplets in (**g**). All images shown were obtained using a single polarizer. We added 5×10^{-5} w/v % of TBAB to E7 in all experiments shown in this figure.

induced emulsification have focused on planar interfaces (as described above), additional complex behaviors are observed at convex and concave interfaces between the LC and isotropic oil. During the next year, we will explore such behaviors using LC domains dispersed within an isotropic oil continuum. In preliminary observations, we have observed that solitons form within discrete LC domains and can subsequently undergo multiple reflections with the LC-isotropic oil interface (a siloxane oil was used in these experiments). This result hints at ways to concentrate solitons within domains and explore collective phenomena. In work to be conducted during the next year, we plan to understand how the shapes of LC domains impact soliton behaviors. We will control the LC domain shapes by patterning surface chemistry (using microcontact printing of SAMs) that is preferentially wet by the LC over the isotropic oil. Using this method, we will be able to prepare LC domains that are non-spherical in shape, which we predict will allow us to generate net fluxes of solitons. We also hypothesize that regions of the LC-isotropic oil interface that possess high curvature strain will function as local sources of solitons. These predictions will be tested by experiments.

Finally, we plan to continue our studies of soliton-induced coalescence of isotropic oil droplets in LCs. Specifically, we seek to understand the spatial range of the interactions between droplets induced by solitons, and how key properties of the LCs (e.g., dielectric, elastic and flexoelectric) mediate the coalescence process.

References

1. X. Li, R. L. Xiao, S. Paladugu, S. V. Shiyanovskii, and O. D. Lavrentovich, *Three-Dimensional Solitary Waves with Electrically Tunable Direction of Propagation in Nematics*, Nat. Commun. **10,** 1 (2019).
2. A. L. Alexe-Ionescu, *Flexoelectric Polarization and Second Order Elasticity for Nematic Liquid Crystals*, Phys. Lett. A **180**, 456 (1993).
3. S. Das, N. Atzin, X. Tang, A. Mozaffari, J.J. de Pablo, and N.L. Abbott, *Jetting and Droplet Formation Driven by Interfacial Electrohydrodynamic Effects Mediated by Solitons in Liquid Crystals,* Physical Review Letters 131, 098101 (2023).
4. N. Atzin, A. Mozaffari, X. Tang, S. Das, N. L. Abbott, and J. J. de Pablo, *Minimal Model of Solitons in Nematic Liquid Crystals*, Physical Review Letters **131**, 188101 (2023).
5. S. Das, S. Roh, N. Atzin, A. Mozaffari, X. Tang, J. J. De Pablo, and N. L. Abbott, *Programming Solitons in Liquid Crystals Using Surface Chemistry*, Langmuir **38**, 3575 (2022).

Publications

1. X. Tang, N. Atzin, A. Mozaffari, S. Das, N. L. Abbott, and J. J. de Pablo, *Generation and Propagation of Flexoelectricity-Induced Solitons in Nematic Liquid Crystals*, ACS Nano **18**, 10768 (2024).
2. A. de la Cotte, X.Z. Tang, C. Chen, S.J. Kole, N. Atzin, J.J. de Pablo, and N.L. Abbott, *Controlled Propagation of Soliton Bullets in an Engineered Strain Field*, Proceedings of the National Academy of Sciences, **123**(13) e2518064123 (2026).
3. S. Roh, Y. Ha, N.L. Abbott, *Biphasic Liquids with Shape-Shifting and Bistable Microdomains*, Nature, **643** (8074) (2025).
4. C.Y. Li, X.Z. Tang, X. Yu, N. Atzin, Z.P. Song, C.Q. Chen, N.L. Abbott, B.X. Li, J.J. de Pablo, Y.Q. Lu, *Command of Three-dimensional Solitary Waves via Photopatterning*, Proceedings of the National Academy of Sciences, **121**(36) e2405168121, (2024).

Adaptive Locomotion and Free-Form Maneuverability of Untethered, Single-Material Symmetric Microrobot: Experiment and Modeling

Joanna **Aizenberg**[1], Anna C. Balazs[2]

[1]Harvard University, [2]University of Pittsburgh

Keywords: adaptive locomotion, untethered microrobot, liquid crystal elastomer, energy transduction, theoretical modeling

Research Scope

Untethered soft microrobots that move in a chosen direction almost always pay for that capability with added complexity, for instance a built-in shape asymmetry, a hybrid of active and passive materials, or an external stimulus that is scanned across the body. Each of these strategies fixes a preferred gait but leaves little room for the robot to change direction on its own. Thus, autonomous trajectory adaptation remains difficult to achieve. Building directly on our earlier demonstration that magnetically aligned liquid crystalline elastomers (LCEs) can encode multi-step, non-reciprocal deformations within a chemically homogeneous material,[1] we aim to fabricate a symmetric, one-component geometry that can nonetheless walk in a controllable, steerable way.

We address this through combined experiment and theory approaches using an untethered, light-driven LCE microrobot molded as a simple, four-legged quadruped with high (C_{4v}) symmetry. By aligning the nematic director with a magnetic field during polymerization, we encode the anisotropy inside an otherwise unbiased three-dimensional body, effectively decoupling the molecular orientation from the bulk geometry.[2] Under directional illumination, photoisomerization of azobenzene crosslinkers drives a propagating bimorph[1,3] and, together with self-shadowing, produces a temporary imbalance of contact forces between the legs. The robot skids away from the light and then relaxes back to its original symmetric shape once the light is removed, albeit at a new position. This "symmetry-refresh-mediated" mechanism makes each step independent of the previous one, so that the walker can pick a new motile direction upon a simple change in light angle, without reorienting its body, similar to brittle star's motility. Supported by a finite element and a simplified analytical model, we use this mechanism to demonstrate directional locomotion and free-form, holonomic navigation in 2D. We expect that these results can provide a route toward non-traditional, non-electronic soft robots whose maneuverability depends entirely on the material itself and the irradiation conditions.

Recent Progress

To make the photo-responsive walker, we exploited side-on LC monomers crosslinked with azobenzene and used magnetic alignment during molding to set the nematic director **M** (90° - vertical, 45° - tilted, 0° - horizontal) to any chosen angle relative to the structure. Because the modes of light-guided motion depend on this director orientation, the freedom to program **M**

independently of the geometry lets us span the design space and locate the conditions that yield robust, directional gaits. The device itself is a compositionally uniform, mm-scale quadruped cast in a single mold, with four identical pillars connected by a thin dorsal layer (Fig 1). This shape balances biological analogy, mechanical stability, and simplicity for modeling, as well as it can serve as a building block for more elaborate motile geometries.

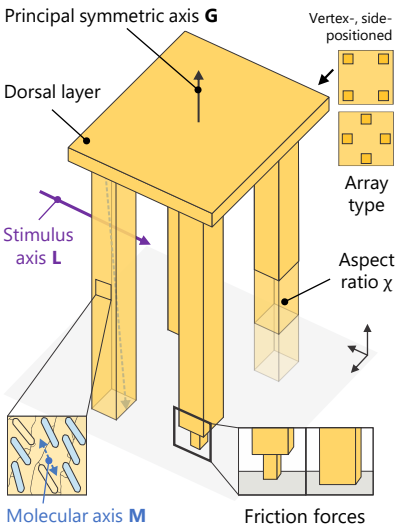


Fig. 1 Schematic representation of the walker, comprising the axis **M**, **G**, and **L** and the geometrical variables (array, aspect ratio, and frictional forces) evaluated both theoretically and experimentally to achieve free-form directional locomotion.

We first tested the material performance on a single, surface-bound pillar to establish how bending responds to temperature and aspect ratio (χ). The bending angle grows with both temperature and χ, and the window above the glass transition (~45 °C) but well below the nematic-to-isotropic transition (T_{NI} ~98 °C) gives the largest amplitudes and the fastest recovery. From this and a systematic screening of pillar dimensions, we fixed an operating temperature of 75 °C and χ = 8 for the microrobot as a compromise between actuation strength, recovery speed, and reliable fabrication. Wide-angle X-ray scattering confirmed that the molecular alignment is highly uniform across the whole mm-size pillar and reproducible between samples, ruling out material inhomogeneity as the origin of the observed deformation.

The directional motion of the four-legged walker in Fig.2 (**M** = 90°, parallel to the **G** axis) arises from a sequence of coupled effects. Diffusive UV light triggers a trans-to-cis photoisomerization that disorders the local nematic phase and creates a transient isotropic/nematic bimorph, bending the illuminated legs toward the source (Fig 2a-b, II). Legs farther from the light (distal) are shadowed by the nearer ones (proximal), so their bending is both smaller and delayed (Fig 2a-b, III). This difference widens the separation between the proximal versus distal feet, shifting the walker weight toward the distal legs, and thus creating a difference in the normal frictional forces at the two leg pairs. Consequently, the proximal feet slide forward while the distal feet stay anchored, producing a net skidding step away from the light (Fig 2a-b, IV). Such displacement is then preserved as the body relaxes

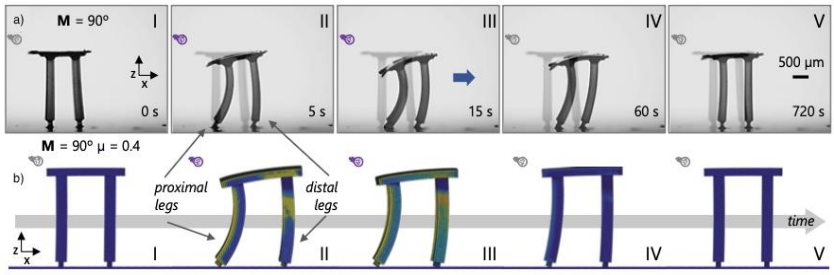


Fig. 2 Side-view, time-series a) micrographs and b) finite elements snapshots (I-V, for 0, 5, 15, 60 and 720 s from turning on the UV light) of a walker undergoing one locomotion cycle. The proximal legs bend phototropically toward the light, while self-shadowing delays and minimizes the bending of distal legs, resulting in a directional skidding motion away from the light.

to its symmetric shape in a new location (Fig 2a-b, V). We captured this behavior with a finite element model, with the light response calibrated from single-post deflection measurement, which reproduces the self-shadowing, the weight redistribution, and the dependence of stride length on the incident angle **Φ** (Fig 3). A simplified analytical model, treating the leg-surface contacts as two 'anchor points', explains how the dorsal layer mechanically couples the leg pairs and why the motion is most effective near **Φ** of about 10°.

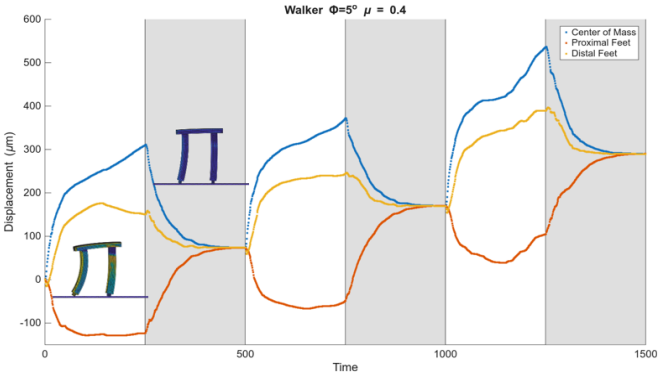


Fig. 3 Simulated walking cycles showing how proximal feet (orange) move toward the light while distal feet (yellow) move away, shifting the center of mass (blue) away from the source. Upon recovery, the feet reconverge to the original shape while retaining a net displacement.

Additionally, the director orientation strongly shapes the outcome. A vertical director (**M** = 90°) gives consistent, unidirectional stepping and cumulative displacement over successive cycles, whereas a tilted director (**M** = 45°) generates internal shear torques that cause the walker to tumble erratically, and a horizontal director (**M** = 0°) produces a splayed deformation that lifts one of the legs into an unhelpful tripod stance and suppresses net motion. The interplay of **M** and the angle **Φ** thus defines a library of situation-specific gaits.

Because the shape resets after every cycle, the walker shows rich in-plane maneuverability with no preferred "front". Upon irradiation, it steps forward and, after a 180° rotation of the light, steps backward with no measurable bias and no body rotation. Introducing a small off-axis offset between the light axis **L** and the symmetry axis **G** causes the walker to reorient progressively, tracking the light through incremental rotations while continuing to move away from it, which we define as a self-correcting mechanism driven by one distal leg acting as a pivot during recovery. Exploiting this reset, we steered the robot along programmed multi-step paths: an "L-shaped" trajectory achieved with a single ~75° rotation of the light source (Fig. 4), and a "zig-zag" path in which alternating ±90° light directions of irradiation sum to a straight net path. Finite element

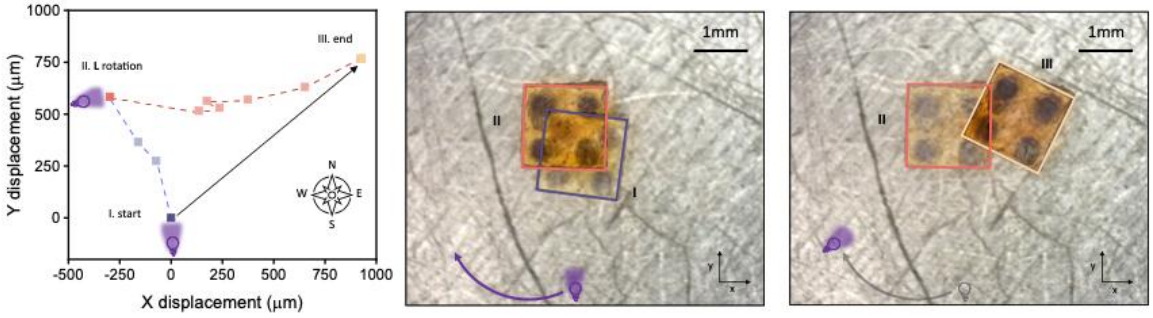


Fig. 4. Free-form 2D navigation of a walker (**Φ** = 10° and **M** = 90°) that follows an L-shaped trajectory: first moving along +y for three cycles, then redirecting toward +x for six cycles after a 75° clockwise light rotation. Micrographs b) before and c) after light rotation showing the initial (blue, I), intermediate (red, II), and final (yellow, III) corresponding walker positions along the trajectory.

simulations reproduced these holonomic trajectories, confirming that free-form 2D locomotion emerges from light control alone, without electronics, external biases, or material asymmetry.

Future Plans

To submit research supported by this grant for publication.

References

1.S. Li, M. M. Lerch, J. T. Waters, B. Deng, R. S. Martens, Y. Yao, D. Y. Kim, K. Bertoldi, A. Grinthal, A. C. Balazs, J. Aizenberg, *Self-regulated non-reciprocal motions in single-material microstructures*, Nature 605, 76–83 (2022).
2. S. Li, M. Aizenberg, M. M. Lerch, J. Aizenberg, *Programming Deformations of 3D Microstructures: Opportunities Enabled by Magnetic Alignment of Liquid Crystalline Elastomers*, Acc. Mater. Res. 4, 1008–1019 (2023).
3. J. T. Waters, S. Li, Y. Yao, M. M. Lerch, M. Aizenberg, J. Aizenberg, A. C. Balazs, Twist again: Dynamically and reversibly controllable chirality in liquid crystalline elastomer microposts, Sci. Adv. 6, eaay5349 (2020).

Publications

1. Y. Yao, A.M. Wilborn, B. Lemaire, F. Trigka, S. Li, F. Stricker, A. Grinthal, M. Zhernenkov, G. Freychet, P. Wasik, R. Bennet, T.C. Cheung, B. Kozinsky, M.M. Lerch, X. Wang, J. Aizenberg, *Rational design of liquid crystalline elastomers with programmable multi-step deformability for ambidirectional actuators*, Science **386**, 1161–1168, (2024).
2. A.B. Tesler, H.A. Nurmi, S. Kolle, L.H. Prado, B. Karunakaran, A. Mazare, I. Erceg, I.B. Soares, G. Sarau, S. Christiansen, S. Stafslien, J. Alvarenga, J. Aizenberg, B. Fabry, R.H.A. Ras, W.H. Goldmann, *Predicting Plastron Thermodynamic Stability for Underwater Superhydrophobicity*, Commun. Mater. **5**, Article number: 112 (2024).
3. S. Wang, S. Li, W. Zhao, Y. Zhou, L. Wang, J. Aizenberg, P. Zhu, *Programming hierarchical anisotropy in microactuators for multimodal actuation,* Lab Chip **24**, 4073-4084 (2024).
4. J.T. Waters, A.C. Balazs, *Achieving controllable and reversible snap-through in pre-strained strips of liquid crystalline elastomers*, Soft. Matter **20**, 15 (2024).
5. X. Xiong, X. Zhou, H. Zhang, M. Aizenberg, Y. Yao, Y. Hu, J. Aizenberg, J. Cui, *Controlled macroscopic shape evolution of self-growing polymeric materials*, Nat. Commun. **16**, 2131 (2025).
6. A.M. Wilborn, H. Almohammadi, P. Qu, Y. Wang, Y. Yang, R. Kay, D.Y. Kim, K. Bertoldi, D. Weitz, J. Aizenberg, *Towards differentiation in untethered microactuators: a soft fabrication strategy*, Adv. Mater. **37**, 51 (2025).
7. M.M. Lerch, A. Shastri, T.B.H. Schroeder, A. Meeks, S. Li, A.V. Shneidman, M. Aizenberg, J. Aizenberg, *Unusual Swelling Behavior of Hydrogels Modified With Spiropyran as Appendage or Crosslinker*, Adv. Funct. Mater. **36**, 27, e18243 (2026).

Conductive Chiroptical Polysaccharides for Dynamic Infrared Electro-Reflectivity

Cécile **Chazot**, Northwestern University

Keywords: Biomolecular Electronics, Chitosan, Conjugated Graft Copolymers, Liquid Crystals, Chiroptical Properties

Research Scope

The long-term goal of this project is to establish new design principles for biomolecular materials that combine hierarchical self-assembly with electronic and optical functionality. Our approach is to unite two sets of properties within a single macromolecular architecture: those of cationic chitosan (CS), the most ionically conducting member of the natural polysaccharide family, which spontaneously forms chiral nematic (N*-LC) mesophases with infrared-selective reflectivity and chiroptical properties that survive solvent drying, and the charge-transport properties of π-conjugated polythiophenes, particularly poly(3,4-ethylenedioxythiophene) (PEDOT). Grafting PEDOT sidechains onto a CS backbone should introduce electronic and mixed ionic-electronic conduction modulated by the long-range helical order of the backbone, yielding materials whose optical response can be dynamically tuned by an electrical stimulus and whose charge transport is tailored by the anisotropy of the self-assembled structure. Because the cholesteric pitch of CS reflects in the infrared, far from the absorption and emission bands of the sidechains, these architectures offer a rare opportunity to decouple and independently control (i) intensive, molecular-level electronic transitions (absorption, emission, and circularly polarized luminescence) and (ii) extensive photonic responses arising from long-range cholesteric order. We pursue this through three core objectives: (1) developing chemical routes to graft PEDOT segments onto CS, (2) understanding how the resulting architectures form and self-assemble from molecular to microscopic length scales, and (3) establishing how this hierarchical structure governs electrical conduction and electro-responsive optical behavior.

During the most recent reporting period, work emphasized laying the chemical and structural foundations required for these later-stage functional studies, particularly the development of CS-g-PEDOT and the study of how the CS backbone self-assembles, and its grafted side chains polymerize.

Recent Progress

In the first year of this award, we functionalized CS with 3,4-ethylenedioxythiophene (EDOT) pendant groups and observed the spontaneous formation of CS-g-PEDOT copolymer architectures in formic acid (FA). FA is a solvent that solubilizes CS and drives its self-assembly into chiral multichain assemblies and compensated (aka mixed left- and right-handed) chiral nematic liquid crystal (N* LC) domains,[1] whose pitch reflects light in the infrared (Fig. 1). Two accomplishments

define this reporting period: the synthesis of a functionalizable EDOT precursor and its controlled attachment to CS, and the discovery that these pendant groups self-polymerize in FA to give a grafted-through copolymer.

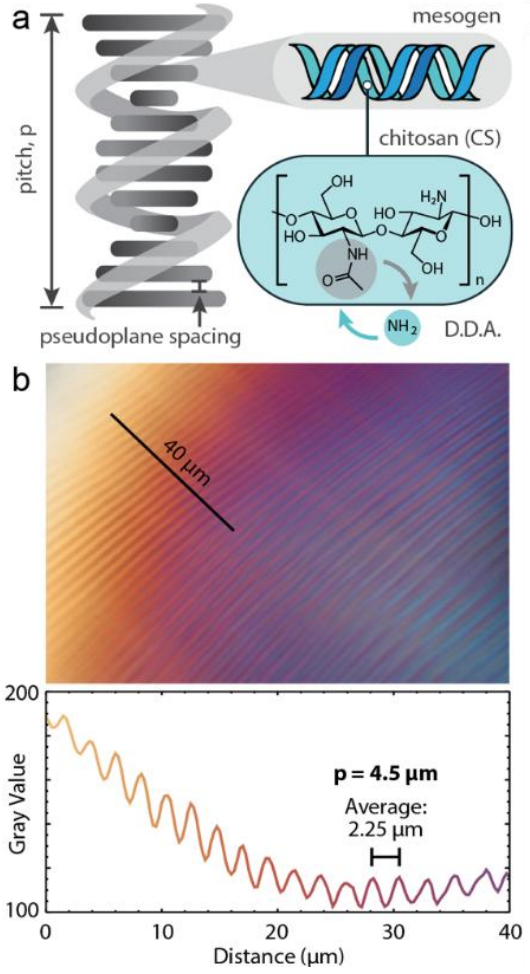


Figure 1: Chiral nematic (N* LC) self-assembly of CS in pure formic acid (FA). (a) Hierarchical chiral ordering of CS chains in FA, from the twisted-fibril mesogen to the cholesteric helix of pitch p. (b) Cross-polarized optical micrograph of a concentrated CS–FA solution, showing the fingerprint texture characteristic of N* LC order. The gray-value trace along the marked line gives a mean half-pitch of 2.25 µm, corresponding to a pitch p = 4.5 µm and therefore to selective reflection in the infrared.

The first accomplishment was the synthesis of the pendant group precursor 3,4-ethylenedioxythiophene bearing a carboxylic acid group (EDOT-COOH), which allows controlled covalent attachment to CS backbones of varying molecular weight and degree of deacetylation (DDA) by amidation (Fig. 2). We prepared it from commercially available hydroxy-EDOT, chosen for its scalability and chemical accessibility: nucleophilic substitution with methyl bromoacetate in an aprotic solvent, followed by saponification and acidification, delivered EDOT-COOH as a light-green solid in 76% isolated yield.[2] Amidation of the CS amine groups with EDOT-COOH then gave our first-generation CS-EDOT precursor, whose structure we confirmed by Fourier-transform infrared spectroscopy (FT-IR) and nuclear magnetic resonance (NMR). At intermediate degrees of substitution (DS), this precursor could be readily solvent-cast into ductile, transparent, free-standing films, whereas neat CS and highly substituted CS-EDOT do not form continuous films and instead crumble under identical casting conditions. These films show no birefringence, indicating a largely amorphous structure and pointing to a plasticizing effect of EDOT functionalization that may partially screen interchain interactions.

Critically, CS-EDOT remains soluble in FA, the solvent that induces chiral multichain self-assembly and N* LC order in pure CS. When we dissolved CS-EDOT at high concentration (~20 wt.%) in FA (with no added EDOT monomer and no oxidant) the solution darkened, indicating spontaneous oxidative polymerization of the EDOT pendant groups into PEDOT (Fig. 2). This mirrors the behavior reported for pure EDOT-FA solutions, in which soluble undoped PEDOT oligomers form without any oxidant at room temperature.[3] After self-polymerization and dilution in excess FA, an insoluble

fraction remained, indicating partial crosslinking of the CS chains. This constitutes the second accomplishment of the funding period: our first CS-g-PEDOT architecture, which appears to be "grafted through": that is, PEDOT chains grow from intrachain and/or interchain EDOT pendant groups. The resulting architecture should therefore be governed by two factors: CS backbone flexibility (set by molecular weight relative to the biopolymer persistence length) and the proximity of reactive EDOT units (set by DS and by the conformation of CS-EDOT chains in FA). We accordingly hypothesize that short CS chains (<100 kDa; here 40 and 60 kDa), which behave as semi-rigid rods in FA, will favor interchain EDOT reactions, whereas a high DS will favor longer PEDOT oligomers that thread through two neighboring CS chains to give the grafted-through architecture (Fig. 2). We expect this effect to be strongest when multichain assemblies such as twisted fibrils are present, assemblies we have observed in both pure and grafted CS in favorable solvents, including pure FA (with no evidence of free protons) and other charged acidic aqueous solutions.

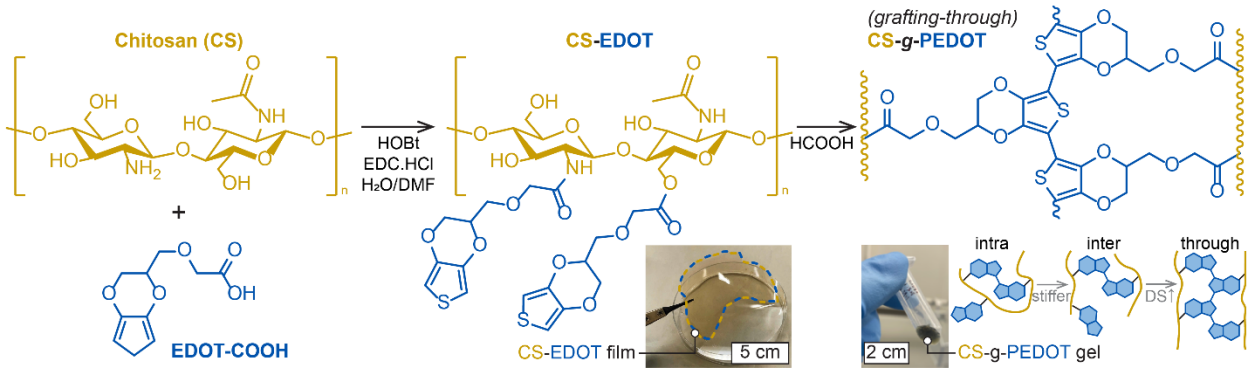


Figure 2: Synthesis of the CS-EDOT precursor and its spontaneous conversion to CS-g-PEDOT. Amidation of the CS amine groups with EDOT-COOH (HOBt, EDC·HCl, H_2O/DMF) yields the CS-EDOT precursor, which self-polymerizes in formic acid (HCOOH) to give the grafted-through CS-g-PEDOT copolymer. Photographs show a free-standing CS-EDOT film and a self-polymerized CS-g-PEDOT gel in FA. The schematic (right) illustrates the hypothesized intrachain, interchain, and grafted-through architectures, set by CS backbone flexibility (molecular weight) and the proximity of reactive EDOT units (DS).

Future Plans

Our next step is to further investigate the hypothesis formulated in this reporting period by varying the molecular weight of the starting CS backbone and its DS with EDOT pendant groups through the starting DDA (75-95%) and the EDOT-COOH concentration in the functionalization step. We will then study the grafting-through reaction of CS-g-PEDOT in FA for these synthesized CS-EDOT precursors and estimate the number of PEDOT repeat units and any short-range order in the film through X-ray diffraction and spectroscopy (Raman, FTIR, photoluminescence) methods. We also plan to conduct cyclic voltammetry and electrochemical impedance spectroscopy (EIS) to assess how doping/dedoping and mixed electronic-ionic conduction proceed in these grafted-through architectures.

References

1. Y. Dong, W. Qiu, Y. Ruan, Y. Wu, M. Wang, and C. Xu, *Influence of Molecular Weight on Critical Concentration of Chitosan/Formic Acid Liquid Crystalline Solution*, Polymer Journal **33**, 387 (2001).
2. C. Beaumont, J. Turgeon, M. Idir, D. Neusser, R. Lapointe, S. Caron, W. Dupont, D. D'Astous, S. Shamsuddin, S. Hamza, É. Landry, S. Ludwigs, and M. Leclerc, *Water-Processable Self-Doped Conducting Polymers via Direct (Hetero)arylation Polymerization*, Macromolecules **54**, 5464 (2021).
3. E. Tomšík, I. Ivanko, J. Svoboda, I. Šeděnková, A. Zhigunov, J. Hromádková, J. Pánek, M. Lukešová, N. Velychkivska, and L. Janisová, *Method of Preparation of Soluble PEDOT: Self-Polymerization of EDOT without Oxidant at Room Temperature*, Macromolecular Chemistry and Physics **221**, 2000219 (2020).

Publications

1. E. C. Grosvenor, K. T. Ghezzi, J. B. Chatterjee, D. S. Silverstein, E. M. Sellin, Z. C. Williams, H. Sai, S. E. Branovsky, Y. Liu, W. Skyrud, S. I. Stupp, J. J. Richards, and C. A. C. Chazot, *Structural Inheritance and Handedness Selection in Biphasic Chitosan Cholesteric Mesophases*, in preparation.
2. J. H. Kim, C. Beaumont, J. Rivnay, C. A. C. Chazot, *Oxidant-Free Grafting-Through Polymerization of EDOT on Chitosan: Architecture Control and Mixed Ionic-Electronic Transport*, in preparation.

Design Principles of Biomolecular Metamaterials

Jong Hyun **Choi**, School of Mechanical Engineering, Purdue University

Keywords: DNA origami, architected metamaterials, auxetic and deployable structures, molecular dynamics, free energy landscape

Research Scope

Architected metamaterials are designed by arranging mechanically coupled building blocks to achieve extraordinary properties and behaviors. There are three classes in such materials: auxetic, topological, and deployable structures. DNA origami is an ideal approach to design and construct nanoscale metamaterials from bottom up. However, there are several challenges, including the lack of design guidelines for DNA metastructures and the insufficient understanding of their mechanics that cannot be fully described by Timoshenko elasticity theory. This research aims to develop design strategies for architected 3D nanostructures based on DNA origami by combining coarse-grained molecular dynamics (MD) and umbrella-sampling free-energy simulations. During this reporting period, we have focused on (1) developing our computational design approach, (2) demonstrating 3D metastructures via DNA self-assembly, and (3) elucidating their structural properties and mechanical behaviors. We showcase all three classes of DNA-based 3D metamaterials with mechanistic insights on design principles. Advances in our understanding of assembly mechanics are also highlighted.

Recent Progress

1. Deployable polyhedral nanostructures

Our computational design approach consists of two steps. Reconfigurable/deformable materials have two or more configurations; for example, open and closed states. A target shape (e.g., open state) is first determined and designed as the most stable state with minimum free energy. The conformation is studied with coarse-grained MD simulations on the oxDNA platform and related free energy profile is calculated with umbrella sampling.[1] Then, the other (closed) configuration after transformation is examined computationally. Since this configuration has a higher free energy, external energy must be provided, e.g., by additional DNA hybridization, to stabilize the state by forming ‘jacks’. This state stores the same amount of elastic energy within its structure. When the jacks are removed, it naturally deploys from the high to low energy states.

This computational design process has been tested and established using a model system called Jitterbug transformer, proposed by R. Buckminster Fuller.[2] This polyhedral structure reconfigures through coordinated rotations of rigid struts connected by flexible joints. The structure expands isotropically from octahedral to cuboctahedral states, and vice versa, during which six square faces

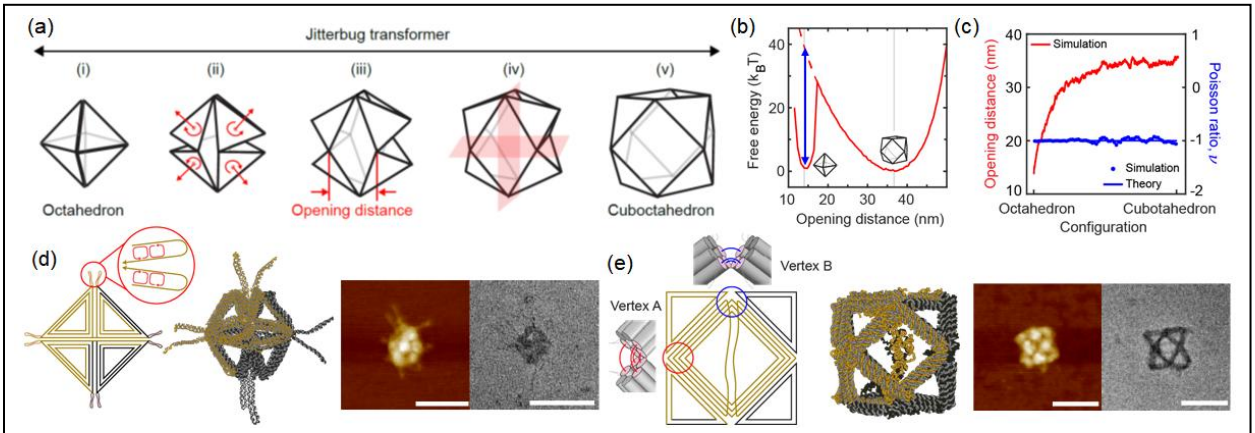


Figure 1. Design of a DNA Jitterbug transformer. (a) Jitterbug transformation between closed octahedral and open cuboctahedral states can be described by a single order parameter, opening distance. (b) Free energy profiles of two topological states are calculated by considering structural and chemical energies. (c) MD simulated structural transition from closed to open states and Poisson's ratio of $\nu = -1$. (d)-(e) DNA designs, MD structures, AFM, and TEM images of (d) octahedral and (e) cuboctahedral configurations. Scale bar: 100 nm.

emerge or disappear (Fig. 1a). The collective motion of its components with kinematic constraints results in a five-fold volume change. To computationally design a nanoscale Jitterbug, we calculated free energy landscape of a DNA wireframe with 28-nm-long edges made of 6 helix bundles (6HB) using opening distance of the squares as the coordinate. The free energy landscape in Fig. 1b shows that the (open) cuboctahedron state has a free energy minimum at ~36 nm. To stabilize the (closed) octahedral state, roughly 40 k_BT energy must be provided by DNA jack staples. We performed Nupack estimation, DNAfold simulation,[3] and virtual-move Monte Carlo calculation in oxDNA to determine the number and length of the jack staples. This free energy profiles indicate that the DNA hybridization energy is required to hold the Jitterbug transitioning from open to closed states, equaling the same amount of elastic energy stored within the structure. Thus, it deploys from the octahedron to the cuboctahedron naturally upon removal of stabilization. Figure 1c shows that the structure releases its stored elastic energy and transitions spontaneously from closed to open states while preserving the Poisson's ratio at $\nu = -1$. We constructed DNA Jitterbug using two scaffolds and observed the transformation between the open and closed states in response to external cues. Figure 1d-e presents AFM and TEM images of the octahedron and the cuboctahedron, consistent with MD structures. We also computed maximum forces and mechanical work associated with reconfiguration, which were approximately 15 pN and 40 k_BT, respectively. Together, these results validate our design approach.

2. 3D auxetic metastructures

We have used computational methods to perform mechanistic studies and generate a set of design rules for DNA metamaterials. We designed a re-entrant triangle using wireframe DNA origami. This triangle is a unit cell from a periodic array and contracts laterally when compressed along the height direction, and vice versa. There are two main components in a DNA wireframe: edges and joints. By varying edge cross-section and joint connection scheme as shown in Fig. 2a-b, we aimed

to understand how each parameter impacts mechanical behavior. We applied compressive loads in oxDNA and evaluated structural response using several metrics.

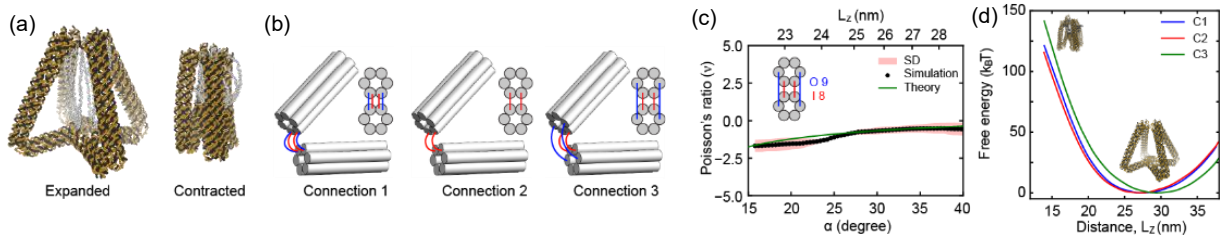


Figure 2. Computational study of a 3D re-entrant triangle unit. (a) Equilibrium MD structures of 3D re-entrant triangle before and after loading in the vertical direction. (b) Three joint-connection types. (c) Poisson's ratio (ν) as functions of re-entrant angle α and internal height L_z. (d) Free energy profiles of different scheme.

We tested 6HB and 2HB edge cross-sections, while three connection types were used for the 6HB design and two types for the 2HB design. For 6HB wireframes, we observed that the edges show little to no deflection and joint-connection type bears the load differently. While they all follow theoretical auxetic motion (Fig. 2c), different ssDNA joint scheme requires distinct joint stretchability (defined as the displacement of ssDNA connection normalized by its contour length). Our computational analyses yielded three design guidelines. First, edge rigidity must be sufficient to concentrate the load at the joints to ensure auxetic response. Second, C1 and C3 joint-connectivities in Fig. 2b should leverage mechanical polarity, with one connector remaining taut while the other provides compliance. This polarity allows the joint to approximate a defined hinge while still accommodating molecular fluctuations. Third, the number of duplexes linked at each joint tunes the transformation energetics. As this connectivity increases, both the energetic cost of contraction and the mechanical work stored during deformation rise.

For 2HB edges, the structure exhibits edge deflection and symmetry breaking. With the thinner beams, deformation is no longer confined to the joints, and the edges absorb a substantial fraction of the load. The choice between the 2HB and 6HB edges thus reflects a trade-off between low-energy actuation and geometric fidelity. The 2HB unit reconfigures with lower energetic input, at the expense of the symmetry and fidelity. The stiffer 6HB framework preserves the intended geometry reliably, albeit at a higher energetic cost (Fig. 2d). When a faithful auxetic response is the priority, the 6HB framework is the more reliable choice. If compactness and low actuation energy are more important, the 2HB unit remains a practical option.

3. Mechanics of DNA assemblies

To perform mechanical studies on DNA constructs, we have assembled large-scale prisms from 7-strand tensegrity triangular motifs via sticky-end association. These crystals are fragile, requiring certain conditions (e.g., high Mg^{2+} concentration $\geq$ 50 mM) for stabilization. One way to strengthen DNA assemblies is enzymatic ligation. By covalently connecting the nicks, they become significantly more stable. To understand the assembly mechanics, we performed MD simulations to investigate the effects of ligation patterns and motif lengths. We applied tensile forces on DNA

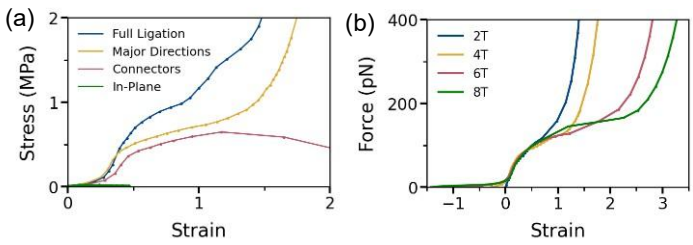


Figure 3. DNA assemblies under tensile loading. (a)-(b) MD simulations show distinct behaviors of DNA assemblies with different ligation patterns and motif lengths, under tension.

prisms made of motifs with a length of 4 helical turns (termed 4T). Various ligation patterns were explored (Fig. 3a): (i) ligations in major directions (along three axes of the triangular motif), (ii) connectors (ligating the strands that hold the oligos along the major directions), and (iii) in-plane (ligating all the strands on a 2D plane) as well as (iv) full ligations. The ligated assemblies show similar trends of entropic elasticity and linear elasticity up to the strain of ~0.5, except for the in-plane ligation which breaks easily due to the lack of resilience against orthogonal tensile loads. Then, there is a transition period between 0.5 and 1.2 of strain before either increasing (full and major-direction ligations) or decreasing (ligated connectors). The transition is attributed to breakage in base-pairs, while single-strand stretch is dominant in the final phase of the extension. Figure 3b presents force-strain plots of fully ligated DNA assemblies as a function of motif length from 2 to 8 helical turns (2T to 8T). Their entropic elasticity points are shifted for clarity. We observed that the longer the motif is, the greater the entropic period is, while linear elasticity is identical for all lengths. The most significant differences are observed with the transition periods due to the lengths as single-strand stretch leads to a drastic increase in all cases. Besides ligation, DNA assemblies can be strengthened by coating inorganic materials. We used CdS and Pd to functionalize DNA crystals. We performed AFM nanoindentation which revealed that the Young's modulus of ligated DNA assemblies is ~1 MPa, in agreement with our simulation data. The DNA crystals functionalized with inorganic materials show three orders of magnitude greater Young's moduli at ~5 GPa.

Future Plans

Reconfigurable DNA structures have been mostly limited to two (open and closed) states. Our future effort will focus on designing metamaterials with multiple topological states. To this end, we plan to explore foldable structures based on Kresling and Yoshimura lattices. The Yoshimura pattern demonstrates linear folding, while the Kresling design leads to chiral folding. Both of these lattices leverage two types of structural components that move outward (mountain fold) or inward (valley fold) during the folding process. We will investigate how edge rigidity and joint stretchability work together to demonstrate mountain and valley folds. We also plan to engineer mechanical frustration in the foldable DNA metastructures which will allow us to demonstrate new topological states.

References

1. A. Sengar, T. E. Ouldrigde, O. Henrich, L. Rovigatti, and P. Šulc, *A Primer on the oxDNA Model of DNA: When to Use It, How to Simulate It and How to Interpret the Results*, Frontiers in Molecular Biosciences, **8**, 693710 (2021).
2. H. F. Verheyen, *The Complete set of Jitterbug Transformers and the Analysis of Their Motion*, Computers Mathematics with Applications, **17**, 203-250 (1989).

3. M. DeLuca, D. Duke, T. Ye, M. Poirier, Y. Ke, C. Castro, and G. Arya, *Mechanism of DNA Origami Folding Elucidated by Mesoscopic Simulations*, Nature Communications, **15**, 3015 (2024).

Publications

1. A. S. Madhvacharyula, R. Li, S. Seo, A. A. Swett, M. R. Kesama, and J. H. Choi, *Predicting Equilibrium DNA Origami Conformations based on Free Energy Profiling and Deep Learning of Structural Images*, (2026). In preparation
2. S. Seo, A. S. Madhvacharyula, A. A. Swett, R. Li, Y. Du, and J. H. Choi, *Computational Design Strategies for Nanoscale 3D Auxetic Metastructures from DNA*, bioRxiv (2026). https://doi.org/10.64898/2026.07.09.737373
3. S. Seo, A. A. Swett, M. R. Kesama, A. S. Madhvacharyula, R. Li, Y. Du, M. Eder, F.C. Simmel, and J. H. Choi, *A Nanoscale Jitterbug Transformer from DNA*, Nature Communications, (2026). https://doi.org/10.1038/s41467-026-74070-4
4. S. Xiao, S. H. Um, M. Xu, D. Dankwa, S. Seo, J.H. Choi, A. Aksimentiev, L. N. Green, and K. Jayant, *Intracellular Neuronal Recordings Across DNA Tiles*, Nature Nanotechnology, 21, 859-868 (2026).
5. M. R. Kesama, J. L. Guo, Anusha, Y. Du, C. Mao, and J. H. Choi, *Programmable Synthesis of DNA Networks in Giant Vesicles via Rolling Circle Amplification*, Nano Letters, **26**, 4866-4873 (2026).
6. A. A. Swett, Y. H. Kim, S. W. Park, M. R. Kesama, N. Siraj, C. Mao, and J. H. Choi, *DNA Crystals as a Template for Patterned Functional Materials*, Small Structures, **7**, e202500693 (2026).
7. Y. H. Kim, A. S. Madhvacharyula, R. Li, A. A. Swett, S. Seo, E. J. Batchelder-Schwab, N. Siraj, C. Mao, and J. H. Choi, *Understanding Structural Mechanics of Ligated DNA Crystals via Molecular Dynamics Simulation*, Nanoscale Horizons, **10**, 3340-3350 (2025).
8. A. S. Madhvacharyula, R. Li, A. A. Swett, Y. Du, S. Seo, F. C. Simmel, and J. H. Choi, *Realizing Mechanical Frustration at the Nanoscale Using DNA Origami*, Nature Communications, **16**, 5164 (2025).
9. Y. Du, R. Li, A. S. Madhvacharyula, A. A. Swett, and J. H. Choi, *DNA Nanostar Structures with Tunable Auxetic Properties*, Molecular Systems Design & Engineering, **9**, 765-774 (2024).

Energy-Efficient Self-Organization and Swarm Behavior in Active Matter

Jerome **Delhommelle** (lead PI), Dept. of Chemistry, University of Massachusetts Lowell

Stefano **Sacanna**, Dept. of Chemistry, New York University
Paul Chaikin, Dept. of Physics, New York University

Keywords: active matter; nonequilibrium assembly; entropy production; colloidal synthesis; nonequilibrium simulations

Research Scope

Living systems achieve remarkable levels of efficiency, adaptability, and coordination. They operate far from equilibrium, where energy consumption, dissipation, and entropy production are tightly coupled to function. Emulating these capabilities in synthetic systems remains a fundamental challenge in materials science and nonequilibrium physics, with direct implications for energy-efficient technologies and emerging functional materials. To address this challenge, we integrate complementary expertise in experimental colloidal systems, particle synthesis, simulations, and nonequilibrium statistical mechanics to probe irreversibility, characterize collective behavior, and uncover design principles for controlling active systems.

Recent Progress

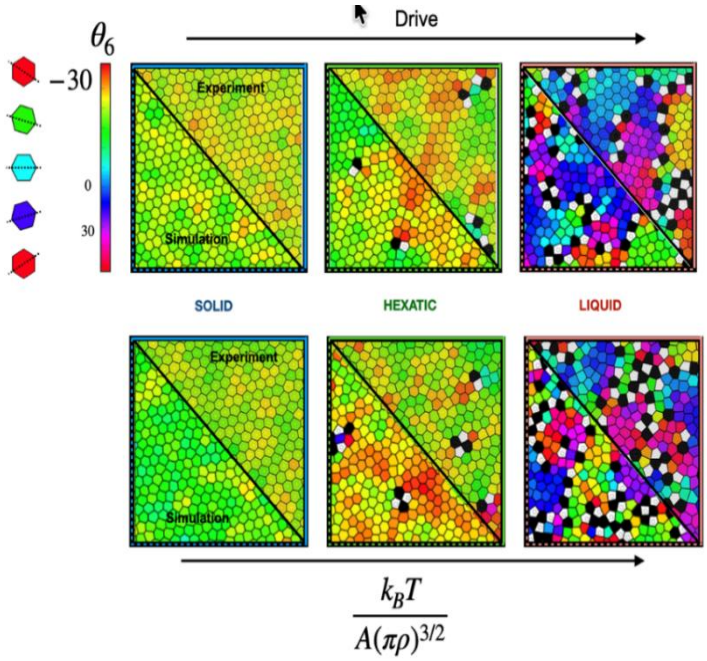


Fig. 1: Top half – melting by stirring. Bottom half – melting by heating. Both melting scenarios were done experimentally and by simulation. White/Black Voronoi cells are five sided and 7-sided disclinations.

Non-Equilibrium Melting in Two Dimensions with Active Matter.

In recently published work, we have investigated probably the best understood melting transition, two-dimensional, defect mediated, Kosterlitz, Thouless, Halperin, Nelson, Young (KTHNY) melting. This occurs naturally by raising the temperature. We wanted to contrast equilibrium from driven non-equilibrium transitions. We introduced dilute concentrations of magnetic colloids to disorder the system by generating random hydrodynamic currents. ***We melted by stirring.*** The surprising result is that the two-stage melting process looks the same (and measurements of correlation functions, critical exponents, and other quantities are the same) if one simply plots the measured properties as a function of the defect densities. For the solid – hexatic transition, the control parameter is the

density of dislocations, for the hexatic – liquid transition the control parameter is the density of disclinations. The system is more a topological transition than a thermal one. The only thing that matters is the density of the defects.

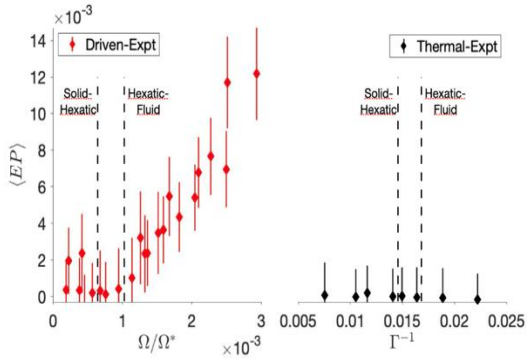


Fig. 2: Entropy production, using an information science-based technique. Note there is no measurable EP for the thermal experiment, but increasing EP upon melting by stirring.

Our technique for measuring the entropy production easily detects equilibrium from non-equilibrium.

$$\dot{S} = \lim_{N\to\infty} \frac{\ln N}{N} \left[\mathcal{C}(\boldsymbol{\chi}_i' || \boldsymbol{\chi}_i{}^{\mathrm{R}}) - \mathcal{C}(\boldsymbol{\chi}_i' || \boldsymbol{\chi}_i)\right]$$

It is simply based on the breaking of detailed balance and hence time reversal symmetry. $\mathcal{C}(\boldsymbol{\chi}_i' || \boldsymbol{\chi}_i)$ is the cross-parsing data compression of the second half of the sequence, $\boldsymbol{\chi}_i$ by the first half $\boldsymbol{\chi}_i'$ and $\boldsymbol{\chi}_i^R$ is the time reversed second half.

Linking local dynamics and entropy production to collective behavior in active matter.

To elucidate how complex environments and interactions give rise to emergent structures and coordinated motion in active matter, we examine the local dynamics of far-from-equilibrium systems, perform a spatial mapping of dissipation and entropy production, and analyze patterns in the map that distinguish active matter from driven passive fluids.

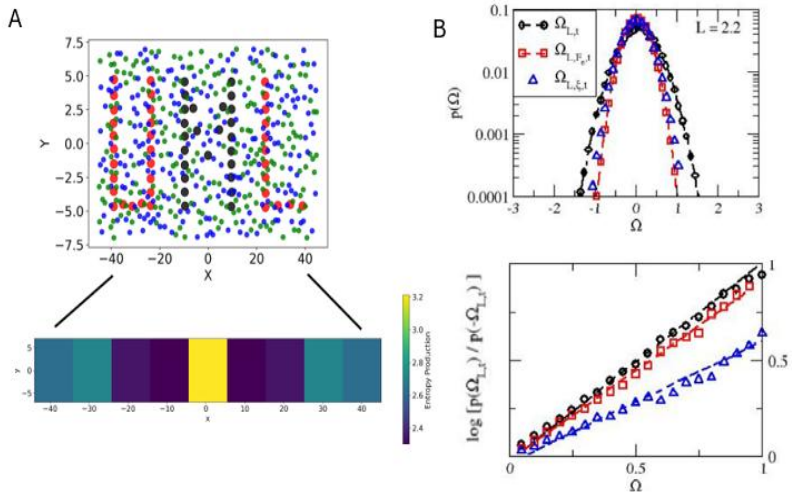


Fig. 3: A) (Top) Passive fluid driven past an obstacle, with an attractive part (red) and a repulsive part (black), resulting in a hotspot (yellow) on the entropy production map. B) (Top) Probability distribution for local dissipation in active matter showing the deterministic (red) and active/stochastic (blue) contributions. While both contributions satisfy a fluctuation theorem (bottom), the active part is associated with an unexpected and markedly reduced slope.

From the system dynamics, we can calculate the dissipation function Ω as

$$\Omega(\Gamma) = \beta \frac{dH}{dt} - \Lambda(\Gamma)$$

in which Γ denotes a phase space point, $\beta = (k_B T)^{-1}$ the inverse temperature, and $\Lambda(\Gamma)$ the phase space compression factor. Calculating the local dissipation $\Omega_{L,t}$ over a region of characteristic length L and a time interval t (or the corresponding entropy production $\Sigma_{L,t}$) allows us to map these quantities over the entire system and identify design principles to control soft matter systems (see Fig. 3.A). We find that, both for driven passive fluids and active matter systems, the local dissipation satisfies a

fluctuation theorem: $ln\left(\Pi_A = \frac{p(\Omega_{L,t}=A)}{p(\Omega_{L,t}=-A)}\right) = \big(1+\kappa(L)\big)A$, where $p\big(\Omega_{L,t}=A\big)$ is the probability that the local dissipation takes the value of A and $\kappa(L)$ a coefficient function of the characteristic length L, that measures the correlation between the local dissipation $\Omega_{L,t}$ and its complementary $\Omega^*_{L,t}$, the latter denoting the dissipation over the rest of the system. Very interestingly, our analysis reveals that these correlations have opposite signs for the active (stochastic) and the passive (deterministic) contributions to local dissipation. This result is yet another evidence of the unique nonequilibrium behavior of active matter (see Fig. 3.B).

Morphogenic Colloids

We moved beyond the initial observation of block-copolymer-driven shape change and established a predictive framework for morphogenesis in synthetic colloidal droplets. We show that controlled remodeling, topology-changing transitions, and spontaneous compartmentalization arise in a compositionally minimal oil-in-water system from the coupling of amphiphile partitioning, osmotic regulation, and interfacial mechanics. We then extended the work from single droplets to collective assemblies, where depletion attractions and external fields turn adaptive shape change into emergent structure.

General framework and design rules. A systematic screen of symmetric PEOx-PPOy-PEOx triblock copolymers, spanning a broad range of PEO/PPO ratios and molecular weights, shows that morphogenesis is governed by general physicochemical principles rather than the chemistry of a particular oil or polymer. Two requirements define the morphogenic regime: sufficient hydrophobic character to drive partitioning and self-assembly within the oil phase, and sufficient hydrophilic content to transport and accumulate water inside the droplet. Excessively hydrophilic copolymers remain in the aqueous phase and stabilize spheres, while strongly hydrophobic copolymers produce isotropic swelling without shape instability. Morphogenesis appears only in the intermediate regime where partitioning, interfacial adsorption, and osmotic swelling coexist. The same pathways recur across chemically distinct oils, including a network-forming silane (TPM), a non-network-forming silane (DMDES), and a fluorinated silane (TMFPS), confirming that the behavior is set by partitioning and interfacial mechanics rather than by molecular detail.

Curvature-elasticity pathways, topology, and compartmentalization. The central advance this period was the identification of topology-changing remodeling pathways governed by curvature elasticity and a reduced-volume constraint. Under hypertonic conditions osmotic swelling is suppressed, and droplets accommodate increasing surface area through large deformations at nearly constant volume, traversing the sequence sphere, prolate, discocyte, and stomatocyte predicted by membrane-elasticity theory for decreasing reduced volume. Using a capillary geometry in which a diffusing P123 front imposes a controlled spatiotemporal concentration profile, we observed both far-from-equilibrium and quasi-equilibrium remodeling; under slowly varying conditions the shape sequence agrees closely with curvature-elasticity theory for fluid membranes. The stomatocyte-to-compartment step is a genuine topological transition rather than a continuous deformation: as the invagination narrows, thermal fluctuations trigger pore closure, sealing the structure and introducing irreversibility into an otherwise reversible landscape. Pore

closure spontaneously internalizes surrounding medium and suspended tracers; fluorescence imaging confirms irreversible uptake, and SEM of polymerized droplets shows closed shells enclosing trapped particles. The process mimics macropinocytosis-like uptake while remaining fully synthetic and requiring no molecular recognition. Fluctuation analysis of dendritic, membrane-like protrusions gives an effective bending modulus of order 10 kBT, and combined holographic and optical measurements show that water and copolymer enter in fixed stoichiometric ratios before any visible shape change, confirming that osmotic swelling and interfacial self-assembly jointly drive remodeling.

Collective behavior: temperature, depletion, and field-driven assembly. Temperature and osmotic pressure act as independent control parameters. Exploiting the LCST of the PPO block, moderate thermal driving produces fully reversible shape oscillations over repeated cycles, while larger deformations trigger the same topology change seen under hypertonic conditions, with irreversible cavity formation. Reversibility is therefore governed by topology rather than morphology: shape changes remain reversible as long as topology is conserved, and pore closure makes them irreversible. Adding high-molecular-weight PEO introduces depletion attractions and converts single-droplet morphodynamics into collective structure. Heating samples containing both PEO and P123 lowers the reduced volume and raises the effective depletion attraction, driving initially gas-like droplet phases into crystalline and, at intermediate aspect ratios, liquid-crystalline order set by excluded-volume packing of deformed droplets. Locally injecting P123 generates a propagating deformation front analogous to a morphogen; Cellpose tracking shows that rising droplet aspect ratio correlates with a transient loss of hexatic order, captured by the global $\psi 6$ parameter, that recovers at long times, linking single-droplet shape change to the order of the assembly. Even without adhesion, worm-like prolate droplets driven by a low-frequency AC field (below 1 Hz, near 5 V cm^{-1}) organize into mesoscale patterns with characteristic length near 100 μm that coarsen over hours; the patterns require droplet anisotropy and vanish for spherical droplets, pointing to shape-mediated interactions now being examined by simulation.

Significance and Outlook. This work turns morphogenic colloids from a phenomenological observation into a predictive, experimentally tractable platform that integrates morphology, topology, and function in a minimal synthetic system. The morphing-induced structural transitions in droplet assemblies show how local shape change regulates large-scale ordering, rigidity, and non-equilibrium organization through the coupling between deformability and inter-particle interactions, directly addressing the broader DOE goal of understanding how collective function emerges from simple interacting building blocks.

Future plans

Future work will couple morphogenic remodeling to chemically active and communicating droplets, joining topology, transport, mechanics, and collective behavior and establishing the system as a model for tissue-like dynamics in adaptive soft matter. We will focus on establishing a comprehensive physical framework for collective morphogenesis in shape-morphing colloidal assemblies through a combination of experiments, image-based analysis, and simulations. Future

work will also leverage both information-theoretical and nonequilibrium dynamics approaches to entropy production to elucidate why and how emergence and coordinated motion arise in active matter.

Publications 2024-2026

1. A. W. Hauser, Q. Zhou, P. M. Chaikin, S. Sacanna, *Light-triggered inflation of microdroplets*. Chem. Mater. 36, 3970 (2024).
2. A. V. Hardikar, A. W. Hauser, T. M. Hopkins, S. Sacanna, P. M. Chaikin, *Osmotic and phoretic competition explain chemotaxic assembly and sorting*. Proc. Natl. Acad. Sci.121, e2410840121 (2024)
3. K. Wang, A. Hardikar, W. Chen, Q. Huang, B. Guo, G. Zhu, H. Ni, R. Sha, N. C. Seeman and P. M. Chaikin *Control and Synchronization of Rapid nanoscale DNA Heat Engine by Local Heating*. Sci. Adv., 11, eadx6316 (2025).
4. C. Desgranges, J. Delhommelle, *Mapping Local Dissipation and Entropy Production in Complex and Active Fluids*. J. Phys. Chem. Lett. 16, 11405 (2025)
5. A. D. Vyas, P. W. A. Schonhofer, T. M. Hopkins, A. D. Hollingsworth, S. Sacanna, S. C. Glotzer, P. M. Chaikin, *Non-Equilibrium Melting in Two Dimensions with Active Matter*. Nat. Phys. 22, 287 (2026).
6. C. Desgranges, J. Delhommelle, *Programming entropy production hotspots via interaction patterning,* Soft Matter 22, 1655 (2026)
7. K. Wang, W. Chen, B. Guo, Q. Huang, G. Zhu, H. Ni, L. Zhang, M. Perez, R. Sha, N. C. Seeman, P. M. Chaikin, *A tunable autonomous RNA-fueled micro-engine.* Nat. Commun. 17, 3164 (2026).
8. C. Desgranges, J. Delhommelle, *Accelerated microswimmer maze solving via spatiotemporally patterned stimuli*. In peer review (2026)
9. F. Fessler, A. W. Hauser, H. Liu, Z. Xu, P. M. Chaikin, S. Sacanna, *Morphogenic Colloids.* Nat. Commun. Accepted for publication (2026)
10. C. Desgranges, J. Delhommelle, P. M. Chaikin, *A comparison of information-theoretic and nonequilibrium dynamics approaches to entropy production,* In preparation.
11. F. Fessler, C. Desgranges, J. Delhommelle, P. M. Chaikin, S. Sacanna. *Electric-field effects on wormlike chains,* In preparation

Dynamic materials assembly using stimuli responsive polypeptide coacervates

Timothy **Deming**, University of California Los Angeles

Keywords: Polypeptides, self-assembly, coacervation, bioinspired, piezoelectric materials

Research Scope

The goal of this research is to test the hypothesis that biomimetic, synthetic polypeptide coacervates can be used to control the assembly and properties of phenylalanine-based dipeptide materials in response to energetic inputs (e.g. heat and/or redox). We plan to accomplish this goal by completion of the following objectives: (I) using molecular tuning of polypeptides and dipeptides in combination with variation of solution pH and counterions to determine how to modulate interactions between coacervate forming polypeptides and nanotube forming dipeptides, (II) applying this knowledge to enable temperature and redox enabled switching of dipeptide-polypeptide materials between nanotubes and coacervates (**Figure 1**), and (III) combining these concepts to guide biomimetic spatial and temporal development of nanotube structure and alignment in peptidic materials using energetic stimuli. Results from these studies are expected to advance understanding and capabilities in the area of external stimuli driven biomimetic materials formation. More specifically, this work aims to introduce new ideas and methods for using stimuli responsive polypeptides to control the dynamics of assemblies, aimed toward the ability to obtain aligned dipeptide nanotube assemblies under mild, biomimetic conditions. These activities are expected to provide new insights for preparation and manipulation of peptide materials with piezoelectric properties that can be controlled by response of chaperone-like polypeptides to external stimuli. Such materials have potential for applications in energy harvesting and sensing.

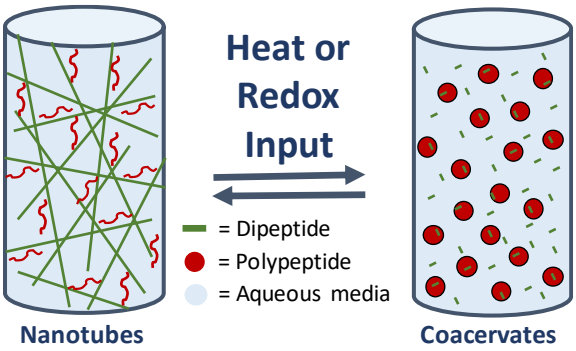


Figure 1 Schematic showing proposed use of heat or redox responsive polypeptides to reversibly switch between different peptide-polypeptide assemblies.

Recent Progress

In the past 7 months, we have achieved many of the goals of our first objective. Specifically, we have prepared the coacervate forming polypeptide **Met-*rac*-C$_{65}$** and have combined it aqueous mixtures with the dipeptide L-phenylalanyl-L-phenylalanine, **FF**. These components were mixed at a variety of concentrations over a range of solution and temperature conditions to determine if **Met-*rac*-C$_{65}$** can be used to inhibit the ability of **FF** to form nanotubes, and if mixtures of **Met-*rac*-C$_{65}$** and **FF** can form disordered liquid coacervates. Finally, we have performed initial studies that demonstrated that FF nanotube formation and dissolution can be externally controlled in

aqueous mixtures with **Met-*rac*-C$_{65}$** by oxidation and subsequent reduction of the polypeptide, respectively (*vide infra*).

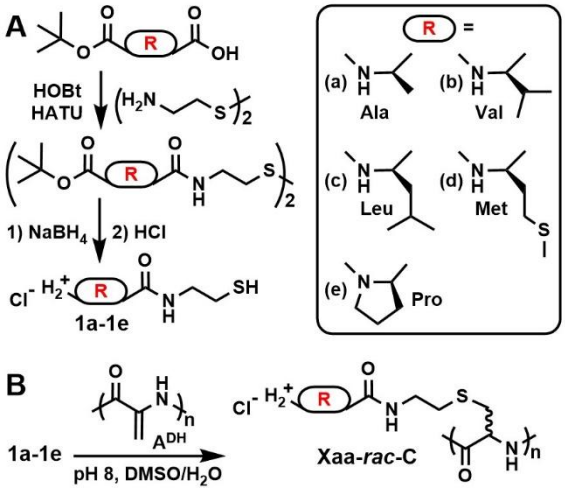


Figure 2 Coacervate forming amino acid functionalized polypeptides **Xaa-*rac*-C** prepared from polydehydroalanine, **A^{DH}**.[2]

Our group has expertise in identifying key molecular features and reactivity found in biomolecules (e.g. proteins) that are utilized in natural energy dissipative processes, and adapting these to synthetic materials and new uses.[1] Our approach focuses on incorporating molecular features of biological processes (i.e. methionine oxidation, protein coacervation) into scalable, synthetic polypeptides so that they can mimic natural properties and functions.[2] Using this strategy in combination with creation of new synthetic methods, we have pioneered development of polypeptides capable of responding in different ways (e.g. water solubilty, chain conformation) to different biomimetic, energetic stimuli.[3] Central to this project, we have pioneered the synthesis and development of well-defined coacervate forming homopolypeptides that mimic many features of natural protein coacervates including coacervation in response to pH, ions, temperature, and redox.[2] The conditions necessary for coacervation can be finely and predictably tuned by molecular adjustment of polypeptide side-chains, as we have shown for the **Xaa-*rac*-C$_{65}$** polypeptides that will be used in these studies (**Figure 2**).[2] We have initially focused on the **Met-*rac*-C$_{65}$** polypeptide, as it forms coacervates with a variety of small counterions. Coacervates of **Met-*rac*-C$_{65}$** can also be dissolved and reformed via reversible redox of the polypeptide side-chain thioether groups (**Figure 3**).[2]

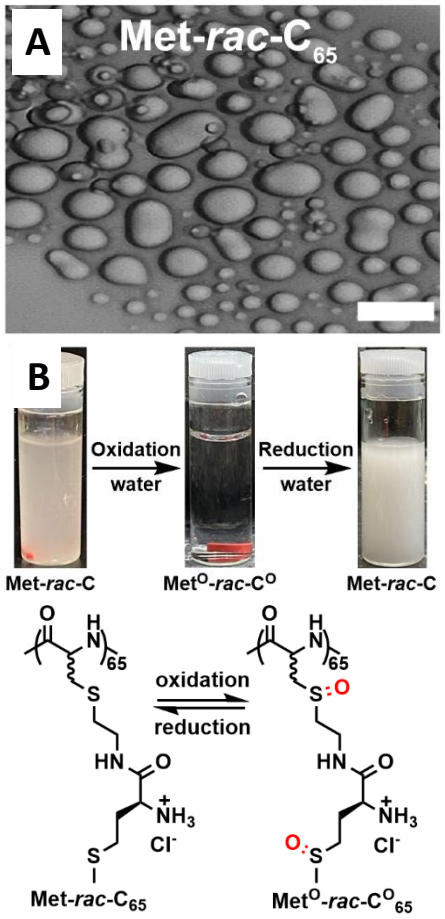


Figure 3 A) Coacervate droplets of **Met-*rac*-C$_{65}$** mixed with tripolyphosphate in water (bar = 20 μm). **B)** Reversible disruption and formation of aqueous coacervate suspensions via oxidation (e.g. peroxide) of **Met-*rac*-C$_{65}$** and reduction (e.g. thiol) of **Met^{O}-*rac*-C$^{O}_{65}$**.[2]

Our group has performed exploratory studies on interactions of polypeptide **Met-*rac*-C$_{65}$** with the dipeptide **FF**. This dipeptide is known to be soluble in water at pH 7 and to assemble into piezoelectric nanotubes when pH is lowered to *ca*. 5.5.[4] We found that mixture of cationic **Met-*rac*-C$_{65}$** with

anionic **FF** in water at pH 6.5 resulted in the formation of phase separated coacervate droplets (**Figure 4**). These droplets could be condensed by centrifugation to obtain a viscous coacervate liquid.

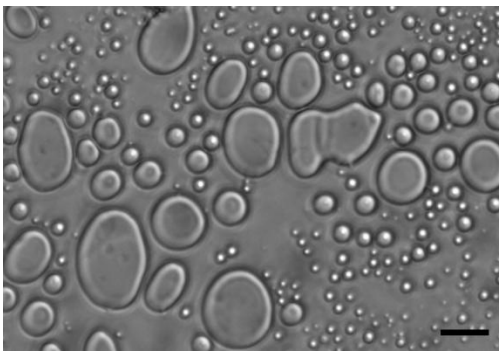


Figure 4 Image of coacervate droplets obtained from mixture of **Met-*rac*-C_{65}** (5.0 mg/mL) and **FF** (2.5 mg/mL) in water at pH 6.5. bar = 10 μm.

We have also initiated studies on the development of stimulus dependent conversion of **Met-*rac*-C_{65}** and **FF** mixtures into **FF** nanotubes. We have varied many conditions: counterions, ionic strength, pH, temperature, concentrations of **Met-*rac*-C_{65}** and **FF**, as well as the addition of different amounts and types of oxidizing agents over different timescales. From these studies, were we able to develop a system capable of converting an otherwise stable **Met-*rac*-C_{65}** and **FF** solution into a suspension of **FF** nanotubes via oxidation (**Figure 5**). To the best of our knowledge, there has been no prior report of **FF** nanotube preparation via oxidation. Subsequent reduction of **Met^{O}-*rac*-C^{O}_{65}** chains present in the aqueous suspension of **FF** nanotubes was able to dissolve the nanotubes and reform the original solution, illustrating reversibility of this process (**Figure 5**).

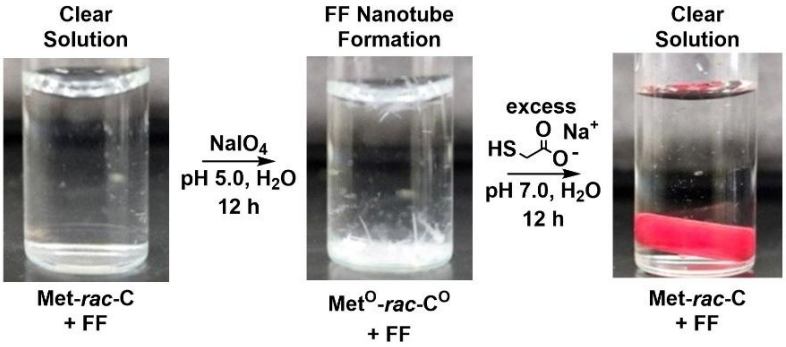


Figure 5 Redox responsive formation and dissolution of **FF** nanotubes using **Met-*rac*-C_{65}**. An aqueous mixture of **Met-*rac*-C_{65}** (3.0 mg/mL) and **FF** (4.0 mg/mL) at pH 5.0 gives a clear solution (left). Oxidation of this mixture with $NaIO_4$ (2 eq/thioether group) converts **Met-*rac*-C_{65}** to **Met^{O}-*rac*-C^{O}_{65}** resulting in spontaneous formation of **FF** nanotubes (middle). Reduction of **Met^{O}-*rac*-C^{O}_{65}** with thioglycolate back to **Met-*rac*-C_{65}** results in **FF** nanotube dissolution (right).

Future Plans

We are now planning to refine our methods to control conversion of **Met-*rac*-C_{65}** and **FF** coacervates into **FF** nanotubes utilizing more controlled oxidation conditions. We will also start studies on oxidation of coacervates in different formats: e.g. droplet, thin film, extruded noodle, in order to control nanotube orientation. We will vary the rate of oxidation with oxidant and oxidant concentration, focused adjustment of pH (5 to 7), and incorporation of different anions in media.

We will also prepare the polypeptide **Val-*rac*-C_{65}** and study its ability to form coacervates with **FF** in response to temperature in order to obtain temperature controlled formation of **FF** nanotubes.

References

1. T. J. Deming, *Sulfur switches for responsive peptide materials*, Acc. Chem. Res. **57**, 661-669 (2024).
2. C. A. Morrison, E. P. Chan, T. Lee, T. J. Deming, *Switchable coacervate formation via amino-acid functionalization of poly(dehydroalanine)*, Biomacromolecules, **25**, 2554-2562 (2024).
3. J. R. Kramer, T. J. Deming, *Multimodal switching of conformation and solubility in homocysteine derived polypeptides*, J. Amer. Chem. Soc., **136**, 5547–5550 (2014).
4. C. H. Görbitz, *Nanotube formation by hydrophobic dipeptides*, Chem. Eur. J., **7**, 5153-5159 (2001).

Publications

None Yet

Nature-Inspired Ionomer Design and Self-Assembly for Robust, Precise Synthetic Ion Channels

Shudipto Konika **Dishari**, University of Nebraska-Lincoln

Keywords: ion-conduction, ionomers, biological ion channel, macrocycles, self-assembly

Research Scope

Biology provides a blueprint for translating nanoscale phenomena into mesoscale materials coordinated behavior. Biological ion channels, despite being exceptionally narrow (< 1 nm in diameter), achieve remarkably efficient and selective transport of water and ions through the precise self-assembly of proteins that are often gated by specific stimuli. Inspired by these natural systems, the PI's earlier work, supported by the DOE Office of Science Early Career Award, demonstrated that incorporating hollow cavity-forming macrocycles, such as calix[4]arene as an ionomer repeat unit, can yield proton conductivities 1-2 orders of magnitude higher than those of state-of-the-art perfluorinated ionomers.[1,2,3,4] These materials also exhibit faster-than-bulk water transport in sub-micron thick films, whereas water and ions in thin films of traditional ionomers experience confinement. This exceptional transport behavior of macrocycle-based ionomers was attributed to the formation of water wires through the sub-nm cavities of calix[n]arenes, analogous to water transport through 4 Å-pores of gramicidin A, a well-known biological ion channel. These findings established calix[n]arenes as a transformative ionomer platform for systems, like electrodes. While these earlier works of ours demonstrated some traces of molecular self-assembly (mostly solvent- and structure-induced) for specific structures of macrocyclic molecules, we did not enforce controlled self-assembly of molecular units. In fact, many traditional ionomers rely primarily on spontaneous phase segregation to create ion transport pathways. If we can gain control over self-assembly of calix-based ionomers via covalent/non-covalent interactions, we would be able to construct more systematic and robust ionic highways, be it in thin films or bulk membranes. This is what the current project is aiming to achieve. By directing the hierarchical self-assembly of functionalized calix[n]arene building blocks, we aim to establish a new design paradigm for high-performance ion-conducting materials.

Recent Progress

Having previously demonstrated the proof-of-concept (Figure 1a), we showed that incorporating macrocyclic calix[4]arenes into ionomers—either as backbone repeat units or as pendant groups—results in significantly higher proton conductivity than Nafion (Figure 1b), the current state-of-the-art proton-conducting ionomers.[1,2] We also demonstrated that non-macrocyclic analogues of these ionomers exhibit proton conductivities several orders of magnitude lower than their macrocyclic counterparts.[2] Building on these findings, we are now pursuing the spatially controlled incorporation of the macrocycles *via* chemistry, like oxirane ring opening.

We have also been able to successfully stack multiple layers of monomeric calix ionomers via a combination of covalent and non-covalent interactions. Most importantly, thin-film systems containing these assembled calix layers exhibited a substantial enhancement in proton conductivity. In one approach, we surface-engineered to design Au electrodes terminated with epoxies that subsequently underwent ring-opening reactions with macrocyclic sulfocalix[4]arene (SC[4], Figure 1c). This ultrathin SC[4] layer exhibited (Figure 1e) exhibited a proton conductivity of 37 mS/cm (Figure 1a, green), representing a remarkable improvement over a ~15 nm thick spin-coated Nafion film, which exhibited a proton conductivity of only 3 mS/cm (Figure 1a, black) under identical conditions. These results confirmed that (i) calix derivatives can indeed be self-assembled into layered architectures, and (ii) even a single self-assembled calix layer achieves an order of magnitude higher proton conductivity than Nafion in thin film form. Together, these findings establish the promise of spatially organized macrocyclic assemblies as a new platform for next-generation ion-conducting materials.

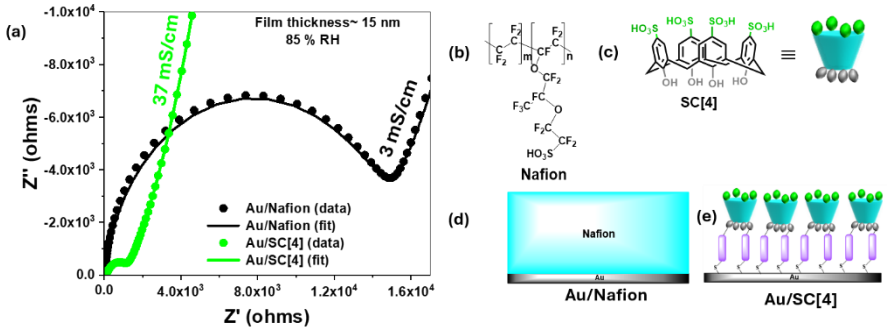


Figure 1. Proof-of-concept demonstration of ultrathin calixarene-based assemblies for enhanced proton conductivity. (a) Nyquist plots comparing proton conductivity of Au/SC[4] assembly (green) vs a Nafion film (black) at 85% RH. The calixarene assembly exhibits markedly higher conductivity despite its reduced thickness. (b-e) Chemical structures and films of Nafion (b,d) and SC[4] (c,e).

Next, building on our success in layering calix molecules, we developed an innovative strategy to spatially localize a calix layer on certain location of Nafion membranes. The resulting membranes again exhibited significant enhancement in proton conductivity (Figure 2a, purple**)** compared with pristine Nafion membrane (Figure 2a, black**)** over the entire temperature range investigated (25-80 ^{0}C). The conductivity advantage increased progressively with temperature, indicating that supramolecular architecture becomes increasingly effective under practical electrochemical operating conditions. At 80 °C, the Nafion-SC[4] (localized) membrane achieved ~50% higher proton conductivity than pristine Nafion membrane, demonstrating that strategic placement of the macrocycles provides a highly efficient pathway for proton transport without altering the bulk chemistry of the ionomer.

To determine whether the improved performance originated from the spatial organization of the macrocycles or simply from their distribution within the matrix, membranes containing a localized SC[4] layer were compared with membranes in which SC[4] was randomly dispersed throughout the Nafion matrix at various loadings (Figure 2a). While increasing the concentration of randomly dispersed SC[4] led to gradual improvements in conductivity (Figure 2a, red, blue, and green**)**,

these gains remained significantly lower than those achieved with the localized self-assembled architecture (Figure 2a, purple**)**. Remarkably, the localized architecture outperforms randomly distributed SC[4] composites, even at high loadings, with the self-assembled membrane reaching conductivities approaching 380 mS/cm at 80 °C. These results clearly demonstrate that the organization and localization of the macrocycles, rather than their distribution alone, can enhance ion transport efficiency.

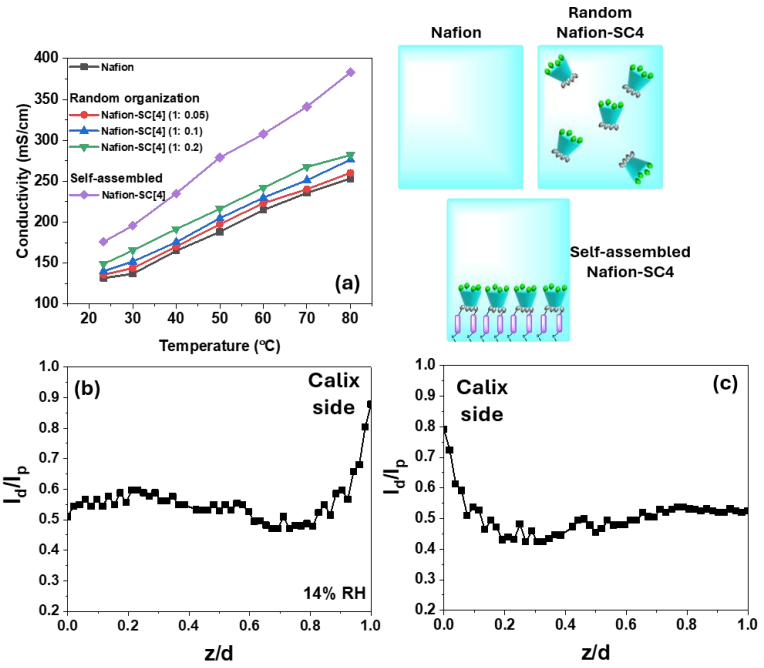


Figure 2. (a) Proton conductivities of self-assembled Nafion and Nafion-SC[4] membranes (both randomly distributed SC[4] with different Nafion-SC[4]ratios and localized SC[4]), highlighting enhanced performance in the self-assembled architecture. Thickness of these membranes were ~ 65 µm. Schematic illustrations of all these membranes are to the right of (a). (b) Proton conduction profile (I_d/I_p) of SC[4]-localized Nafion membrane architecture. (c) Proton conduction profile of same sample upon flipping the membrane. z/d represents thickness (d)-normalized distance (z) from one side of the membrane to the other.

The origin of this enhanced ion transport was further investigated using depth-resolved confocal laser scanning microscopy (CLSM), a technique pioneered by my group.[5] The ion-conduction profile (I_d/I_p) revealed a distinct region of enhanced proton transport that corresponds to the location of the self-assembled SC[4] layer (Figure 2b,c**)**. In the Nafion-SC[4] membrane, the I_d/I_p ratio increased sharply near the SC[4]-functionalized interface (z/d~1), reaching ~0.87, while remaining lower (I_d/I_p ~0.47-0.60) in the bulk and opposite side, having Nafion only. Upon inverting the membrane, the high-conduction region shifted to the opposite interface (Figure 2c). This confirmed that the improvement is localized to the engineered supramolecular interface rather than uniformly distributed throughout the membrane. This provides direct experimental evidence that the self-assembled SC[4] layer offers a superior proton-conduction pathway and demonstrated that ion transport can be spatially engineered within ionomer membranes.

Future Plans

Building upon the demonstrated success in achieving spatially controlled macrocyclic self-assembly and dramatic improvements in interfacial and bulk ion transport, future efforts will systematically optimized macrocycle loading, anchoring chemistry, and processing conditions to

further tailor ionic domain architecture across a range of ionomer platforms. Advanced in-situ and operando characterization will deepen mechanistic understanding of confinement-induced morphology and proton/ion shuttling dynamics.

References

1. S. Chatterjee, E. Zamani, S. Farzin, I. Evazzade, O. A. Obewhere, T. J. Johnson, V. Alexandrov, S. K. Dishari, *Molecular-Level Control over Ionic Conduction and Ionic Current Direction by Designing Macrocycle-Based Ionomers*, JACS Au, **2**, 1144-1159 (2022).
2. S. Chatterjee, O. A. Obewhere, E. Zamani, K. R. Keloth, S. K. Dishari, *Advancing Ionomer Design to Boost Interfacial and Thin-Film Proton Conductivity via a Styrene-Calix [4] Arene-Based Ionomers*, Cell Rep. Phys. Sci., **4**, 1-20 (2023).
3. O. A. Obewhere, K. Acurio-Cerda, S. Sutradhar, M. Dike, R. Keloth, S. K. Dishari, *Unravel-Engineer-Design: A Three-Pronged Approach to Advance Ionomer Performance at Interfaces in Proton Exchange Membrane Fuel Cells*. Chem. Commun., **60**, 13114-13142 (2024).
4. Dishari, S. K. *Ionomers with Macrocyclic Calix[n]arene Moieties for Ion Conductivity and Permselectivity*. 17/996,666, 2021 (patent approved in 2026).
5. S. Farzin, E. Zamani, S. K. Dishari, *Unraveling Depth-Specific Ionic Conduction and Stiffness Behavior across Ionomer Thin Films and Bulk Membranes*, ACS Macro Lett., **10**, 791-798 (2021).

Publications Supported by BES (2022-2026)

1. Dishari, S. K. Ionomers with Macrocyclic Calix[n]arene Moieties for Ion Conductivity and Permselectivity. 17/996,666, 2021 (patent approved in 2026).
2. O. A. Obewhere, K. Acurio-Cerda, S. Sutradhar, M. Dike, R. Keloth, S. K. Dishari, Unravel-Engineer-Design: A Three-Pronged Approach to Advance Ionomer Performance at Interfaces in Proton Exchange Membrane Fuel Cells. Chem. Commun., **60**, 13114-13142 (2024)
3. S. Chatterjee, O. A. Obewhere, E. Zamani, K. R. Keloth, S. K. Dishari, *Advancing Ionomer Design to Boost Interfacial and Thin-Film Proton Conductivity via a Styrene-Calix [4] Arene-Based Ionomers*, Cell Rep. Phys. Sci., **4**, 1-20 (2023).
4. S. Chatterjee, E. Zamani, S. Farzin, I. Evazzade, O. A. Obewhere, T. J. Johnson, V. Alexandrov, S. K. Dishari, Molecular-Level Control over Ionic Conduction and Ionic Current Direction by Designing Macrocycle-Based Ionomers, JACS Au, **2**, 1144-1159 (2022).
5. K. Acurio Cerda, O. A. Obewhere, G. Azom; R. Kumar; S. K. Dishari, *Interface-driven Enhancement of Nafion Thin-Film Conductivity via Controlled Aminothiol Modification.* RSC Applied Polymers. **3**, 1459-1473 (2025)
6. M. Dike, S. K. Dishari, *Linked in with lignin: Ontology*. Nature Chem., **17**, 974, (2025)
7. K. Acurio Cerda, R. Keloth, O. A. Obewhere, S. K. Dishari, *Lignin-based Membranes for Health, Food Safety, Environmental, and Energy Applications: Current Trends and Future Directions.* Curr. Opin. Chem. Eng., **47**, 1-14, (2025)
8. R. Keloth, O. A. Obewhere, K. Acurio Cerda, M. Morton, E. Zamani, S. K. Dishari, *Lignin-Derived Sustainable Cationic Polymers for Efficient High-Temperature Proton Exchange Membrane Fuel Cells.* ACS Sustain. Chem. Eng., **13**, 4132-4147, (2025)
9. O. A. Obewhere, S. K. Dishari, *Engineering Ionomer-Substrate Interface to Improve Thin-Film Proton Conductivity in Proton Exchange Membrane Fuel Cells*, ACS Appl. Polym. Mater. **6**, 4535-4546 (2024).
10. S. Farzin, K. Acurio Cerda, O. A. Obewhere, S. K. Dishari, *Lignin-based Materials for Energy Conversion and Storage Devices* in Sustainability Engineering Challenges, Technologies, and Applications, Editor: Tan, E. C. 1-60 (2023)
11. K. Acurio-Cerda, S. Sutradhar, O. A. Obewhere, R. Keloth, M. Dike, J. Sangster, S. K. Dishari, *Empowering Energy Education: Region-Specific Insights into High School Energy Literacy Infrastructure across Nebraska (fundamental research paper).* ASEE Annual Conference & Exposition (2025).
12. S. Sutradhar, O. A. Obewhere, K. Acurio Cerda, M. Dike, R. Keloth, S. K. Dishari, *Energy Literacy Infrastructure Study across Nebraska and Data-Driven Design of Energy-focused STEM Education and Virtual Outreach Activities for K-12 Students and Teachers. ASEE Midwest Section Conference* (2024)- received ASEE National Best Paper Award, ASEE Zone III Best Paper Award, and ASEE Midwest Section Best Paper Award.

Active interfaces and membranes

Zvonimir **Dogic** and Cristina Marchetti – University of California at Santa Barbara

Keywords: active membranes, active interfaces, wetting, non-equilibrium statistical mechanics.

Research Scope

The research project is organized into two primary aims centered on the study of active matter and its interaction with soft interfaces. The first aim investigates interfacial active matter; specifically, how mechanical forces within bulk active fluids drive deformations of passive interfaces created by conventional phase separation. A key objective is to control wetting transitions in both space and time, which could eventually lead to the development of motile, life-like droplets. The second aim explores a novel category of membrane-based active matter where end-binding molecular motors organize microtubules into dynamic monolayer membranes. Our initial focus is on studying the initial instabilities of this system. In the low activity limit, we observed boundary-induced formation of macroscopic active membranes consisting of one-microtubule-thick monolayer membranes. Such membranes exhibit significant bending deformations powered by the continuous turnover of their microscopic components. In the high activity regime, we study the bulk isotropic instability of the kinesin-4 systems that generates expanding vesicle-like structures. Over long times, active membranes form dynamical bulk materials such as self-healing networks and tissue-like foams that demonstrate steady-state pulsatile contractions.

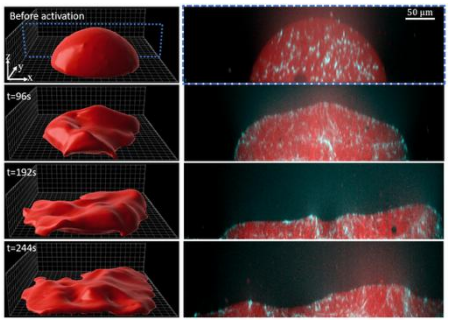


Fig. 1. Release of caged ATP induces changes in the global droplet shape and the local wetting angle.

Recent Progress

Active wetting: We advanced our understanding of how active fluids control the wetting properties of a soft interface in contact with a solid substrate. First, we studied the structure and dynamics of active-dextran-based droplets (Fig. 1). We chemically modified the substrate to control the equilibrium wetting profile from complete wetting to dewetting. Subsequently, we measured the shape of active droplets. We observe that active fluids significantly change the local wetting angle and the global droplet shape. To understand the molecular mechanisms driving such dynamics, we simultaneously image the droplet shape and the microtubule bundles encapsulated within a droplet. For partially wetted droplets, the contact line, where the droplet contacts the substrate, acts as a sink accumulating force-generating microtubule bundles. In turn, these force-generating microtubules exert an additional force on the contact line, modifying the conventional balance of forces and the associated wetting angle (Fig. 2). Inspired by these experimental observations, we developed a theoretical model of the contact point, which relates the local wetting angle to the in-plane curvature of the contact line. Image analysis provides independent measurements of both components, and the linear proportionality constant provides

an estimate of the surface tension of the microtubule bundle (Fig. 3). Thus, active fluids provide a novel mechanical control of the wetting dynamics. In turn, one can use the wetting transition as a novel probe to measure the mechanical properties of extensile microtubule bundles. These are force-generating structural motif that drives microtubule-based active matter out of equilibrium, yet very little is known about their mesoscale mechanics.

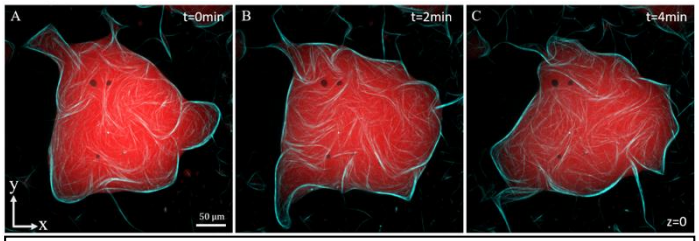


Fig. 2. Active droplet in steady state. Images show the plane where the droplet contacts the solid substrate. Extensile microtubule bundles accumulate along the contact angle.

In addition to isolated droplets on a solid substrate, we also investigated a bulk active-passive interface in contact with the boundaries of the confining sample chamber. We find that above critical activity, the fluid works against gravity and climbs along the walls of the confining tube. In the high activity regime, there is no steady state, but the active interface climbs several millimeters along the confining wall, and once it reaches the top, it spills out of the same. We have characterized the MT-generated autonomous flows within the active wetting layer and correlated that to the dynamics of the upward-growing interface.

Active polar fluids: Properties of active nematic fluids have captured the focus of the wider scientific community and led to extensive experimental and theoretical advances. Over the past two years, we developed an entirely new model system of active fluids, one that has a polar symmetry. In well-studied conventional active nematics, the clusters of conventional kinesin-1 motors push two adjacent microtubules against each other to generate a force-generating unit with nematic (apolar) symmetry. Over the current reporting cycle, we initiated studies of microtubule-based active fluids with kinesin-4 motors. We found a plethora of complex and exceedingly rich dynamical phenomena that largely remain entirely unexplored.

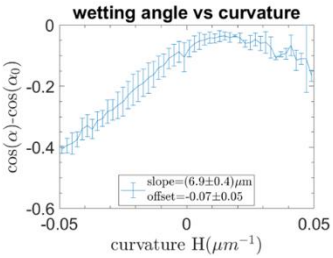


Fig. 3. Local wetting angle is linearly correlated with the in-plane curvature of the contact line for negative protruding curvatures

The kinesin-4 active matter system differs from the conventional microtubule-based active fluids in several ways. First, the system lacks bundling agents. Thus, microtubules form an isotropic semi-dilute suspension with a finite viscoelasticity. Kinesin-4 motors link two filaments and step toward the MT plus end. Such motors endow microtubule filaments with persistent directional motion. Second, the processive kinesin-4 motor accumulates at the microtubule plus end. This generates segmented microtubules whose motor-decorated plus ends have effective attractive interactions. Having mastered the biochemical aspects of the Kinesin-4 system, over the previous period we have completed two major studies which are focused on the initial instabilities of the system.

In the first study, we explored the behavior of the system in the low-activity, low-motor-concentration regime. We developed 3D tracking protocols that allowed us to follow the motion of sparsely labeled microtubules as they undergo driven dynamics. These experiments revealed that the kinesin-4-powered microtubules behave as effective active Brownian rods with polar symmetry. They persistently move in one direction, undergoing active reptation as they move through an entangled suspension. The effective persistence length of such trajectories is hundreds of microns. It is well understood that active Brownian particles accumulate at sample boundaries. Similarly, active Brownian microtubules slowly accumulate at the boundaries. Over time, the wall-induced accumulation of motile filament rods interacts through segmented interactions to generate a macroscopic fluid-like monolayer composed of a one-filament-long monolayer of microtubule filaments (Fig. 4).

At the largest scales, these membranes exhibited continuous height fluctuations that are collectively driven by molecular motors. Surprisingly, the active membrane fluctuations are self-regulating. Once they reach a critical height, they relax back to the minimum-energy flat state. We have characterized the ensuing non-equilibrium dynamics at all relevant length scales (Fig. 5). At the continuum length scales, we measured the coarse-grained height field and the local density as well as the local orientation of microtubules with respect to the membrane normal. We have developed image processing techniques to extract the in-plane and out-of-plane membrane velocities. These measurements reveal a sequence of events that generate self-regulating active height fluctuations. First, the orientation instability generates mesoscale in-plane membrane flows, which increase the local membrane density. Such increased membrane densities lead to out-of-plane buckling and height deformations. Once the membrane reaches the critical height, molecular microtubule interactions relax the deformation, which subsequently leads to the outflow of microtubules. We have completed the experimental characterization of active membranes. Structural characterization revealed that the microtubule-based membrane fluctuations are driven by protrusion modes where the microtubules slide against each other but do not exhibit local splay deformations. This observation suggests that the fluctuation spectrum should exhibit $1/q^2$ scaling, where q is the effective wavelength. Surprisingly, experimental analysis revealed that the active membranes exhibit $1/q^4$ scaling, which is conventionally associated with local splay deformations that are not observed in experiments. To resolve this apparent conflict, we developed a theoretical model of active membranes. Linear stability analysis reveals that activity can drive the effective surface tension to zero or even negative, which can explain the experimental results. These results demonstrate the rich dynamics of active membranes.

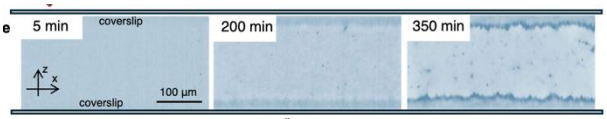


Fig. 4. Assembly of active MT-based membranes driven by kinesin-4.

Low activities of the Kinesin-4 system generated wall-induced membrane formation, while the bulk of the active suspension remained uniform. In the second study, we increased the motor concentration, which increased the effective filament-filament attractions, in turn generating a bulk instability. In this regime, we initially observe the formation of dense globules, dispersed through the bulk suspension. Single filament imaging revealed that such globules have an isotropic structure and the process has intriguing analogies with the conventional spinodal decomposition that is observed in unstable fluid mixtures. After an initial period of globule compactification, we observe a sudden and unexpected transition in the active dynamics. Droplets that initially contract suddenly expand and grow in size. This transition is accompanied by the appearance of local orientation order of microtubules as well as the formation of high-density shell-like structures at the droplet periphery. Eventually, one observes the formation of vesicle-like structures consisting of a one-microtubule-thick monolayer. A theoretical model explains these experimental observations. It demonstrates how the switchable temporal dynamics can be engineered by merging contractile stresses that are generated by the end-binding motors with self-straining stresses generated by effective filament sliding.

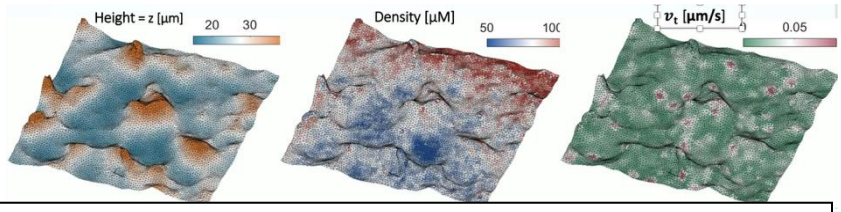


Fig. 5. Quantitative image analysis reveals all continuum fields that describe fluctuations of active membranes, including the height field, the density field, and the in-plane velocity field.

Future Plans.

A series of experimental and theoretical results and associated quantitative analyses highlighted above have been completed. In the short term, these and a few other advances are being prepared for several publications. In the longer term, we aim to extend our studies of active wetting. Current results indicate that the shape of the interfaces and droplets is determined by both local forces generated by the extensile microtubule bundles trapped at the contact line as well as the longer-ranged hydrodynamic flows generated in the interior of the active phases. The proliferating interfaces need further characterization and require theoretical explanation. With the newly developed kinesin-4 systems, we have only characterized the initial bulk instabilities and those induced by the boundaries. Next, we aim to characterize the long-term steady-state dynamics of such systems. Preliminary data demonstrated the existence of a systems-spanning network and foams that are continuously reconfigured by active stresses. We are also planning to study the behavior of the kinesin-4 system in the presence of specific microtubule-based crosslinkers.

Publications:

1. L. Zhao, P. Gulati, F. Caballero, I. Kolvin, R. Adkins, M. C. M. Marchetti and Z. Dogic. “Asymmetric fluctuations and self-folding of active interfaces.” Prof. Nat. Acad. Sci, **51** (2024).
2. P. Gulati, L. Zhao, M. Tateno, O. Saleh, Z. Dogic and M.C. Marchetti, “Bicontinuity in active phase separation,” - https://arxiv.org/abs/2601.03221

Hierarchical Assembly in Biomimetic Active Interfaces

Guillaume **Duclos**

Department of Physics, Brandeis University, Waltham, Massachusetts 02453, USA

Keywords: active matter; active interfaces; active solids; spontaneous symmetry breaking; morphological instabilities

Research Scope

Cells undergo shape change while consuming chemical energy. Their cytoskeletal skeleton bears stress and pushes on the cell wall to drive shape change. We use reconstituted cytoskeletal materials to elucidate how energy-consuming proteins work coherently over multiple length scales to generate complex, yet organized, structures and motion. We are particularly interested in the multiscale impact of active mechanical stresses, which can be produced either by molecular motors or by non-equilibrium turnover of biopolymers. First, we consider liquid interfaces driven by microtubule-kinesin active fluids. At these boundaries, active hydrodynamic flows push and pull on the interface to drive large non-equilibrium deformations. These active flows cause the interface to undergo linear instability, spontaneously break up-down symmetry, and focus the smooth boundary into a sharp cusp. We compare these fluid interfaces with polymerizing actin networks that behave as growing active solids. Continuous assembly loads the network against the surrounding fluid and can trigger fluttering, beating, and chiral motion. Both platforms use hierarchical assembly to turn molecular-scale activity into micron-scale shape change. Studying them together lets us ask how activity, geometry, and material properties control the dynamics of active biomimetic materials.

Recent Progress

At the interface between a passive fluid and a cytoskeletal active fluid, we find that extensile microtubules destabilize an initially flat interface. The first growing mode produces nearly symmetric crests and troughs. As the deformation grows, a second harmonic appears, causing wave crests to broaden and troughs to sharpen. The interface chooses a preferred up-down direction. Flow measurements reveal a layer of counter-rotating vortices near the boundary. This vortex layer rotates the interface and causes the growth of the first two interfacial modes. A hydrodynamic description reduces near the selected wavelength to deterministic KPZ dynamics for the height and Burgers dynamics for the slope. The same transport process continues beyond the first symmetry-breaking event. Higher harmonics onset and form a coherent cascade that sharpens the trough into a logarithmic cusp. Experiments and continuum simulations show the same spectral pathway and the same real-space cusp shape.

Regarding the impact of non-equilibrium turnover, branched actin is nucleated on a colloid and extruded into the surrounding fluid as a cohesive tail. The tail grows straight until viscous drag creates enough compression to overcome bending stiffness. The active solid then enters a growth-driven flutter instability and develops beating, meandering, or spiraling motion. Experiments and simulations show that faster growth lowers the onset length and raises the beating frequency, while a stiffer tail delays the instability and slows the motion. These results show that polymerization

alone can sustain oscillatory and chiral motion in a soft solid. Together, the liquid and solid systems show how unique shape dynamics emerge from active biomaterials far from equilibrium.

Plans

We propose to investigate the impact of non-equilibrium turnover on phase separation. Liquid-liquid phase separation is central to cellular organization because it creates membraneless compartments that concentrate reactions and sort molecules. In cells, these condensates often coexist with cytoskeletal networks that act as active, solid-like mechanical scaffolds. We will couple a programmable DNA nanostar phase-separating system to actin polymerization and turnover. This platform allows us to independently tune activity and mechanical properties of the condensates. We will ask how growth-generated stress, elastic confinement, and network remodeling suppress, modify, or enhance phase separation by changing nucleation, coarsening, and coexistence. We will also test how phase separation changes the onset and shape of the active-solid instability. We will compare experiments and theory. Our goal is to build lifelike materials in which assembly, mechanics, and phase separation regulate one another far from equilibrium.

References

1. T. Sanchez, D. T. N. Chen, S. J. DeCamp, M. Heymann, and Z. Dogic, *Spontaneous motion in hierarchically assembled active matter*, Nature **491**, 431-434 (2012).
2. F. C. Keber, E. Loiseau, T. Sanchez, S. J. DeCamp, L. Giomi, M. J. Bowick, M. C. Marchetti, Z. Dogic, and A. R. Bausch, *Topology and dynamics of active nematic vesicles*, Science **345**, 1135-1139 (2014).
3. M. Kardar, G. Parisi, and Y.-C. Zhang, *Dynamic scaling of growing interfaces*, Physical Review Letters **56**, 889-892 (1986).
4. A. A. Hyman, C. A. Weber, and F. Jülicher, *Liquid-liquid phase separation in biology*, Annual Review of Cell and Developmental Biology **30**, 39-58 (2014).

Publications

No publications supported by this BES award to date.

Bioinspired Morphogenesis of Functional Bicontinuous Materials

Eric R. **Dufresne**[1] and Brett P. Fors[2]

[1]Department of Materials Science and Engineering; Department of Physics, Cornell University
[2]Department of Chemistry, Cornell University

Keywords: phase separation; elasticity; polymer chemistry; polymer networks; bicontinuous structures

Research Scope

Materials with well-defined, bicontinuous nanostructures feature exquisite properties for catalysis, filtration, photonics, and mechanics. Synthetic bicontinuous soft materials are made using two established approaches. Arrested phase separation works with simple molecules and processes and is established at an industrial scale. However, its microstructure is poorly defined, and limited to thin film geometries. Block copolymer self-assembly features precise thermodynamically defined microstructure. However, robust microstructures are limited to spacings on the order of the macromolecular building blocks, typically tens of nanometers.

Alternatively, living systems produce diverse bicontinuous materials with low energy budgets and readily available materials. Astonishingly, the characteristic spacings of these structures are much bigger than the size of their molecular building blocks (Fig. 1a,b). Nevertheless, these nanostructures are made with great precision not only across millions of cells in a single organism but also across all members of a species. Morphological and developmental studies suggest that many of these nanostructures emerge through a form of phase separation.

Inspired by these observations, the Dufresne lab recently developed Elastic MicroPhase Separation (EMPS)[2]. This simple process produces bicontinuous morphologies at the sub-micron scale (Fig. 1c). Like block co-polymer assembly, EMPS produces structures that are defined thermodynamically, *i.e.* independent of quench rate. Like arrested phase separation, it produces structures at scales much bigger than its molecular building blocks and utilizes simple molecules.

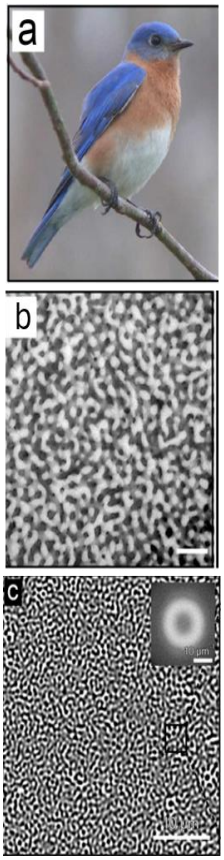


Fig. 1. (a,b) bicontinuous β-keratin nanostructures produce color in bird feathers[1] (c) sub-micron bicontinuous structures by elastic micro-phase separation

The goals of this project are to 1) reveal the mechanisms that underly length-scale selection and stability in Elastic MicroPhase Separation (EMPS) and 2) generalize EMPS, so that it can create bicontinuous monoliths with a wide range of chemistries and functional material properties. This work will articulate simple design rules that enable the large-scale

production of chemically diverse materials with well-defined bicontinuous morphologies for a wide range of applications.

Recent Progress

In the original implementation of EMPS[2], sub-micron bicontinuous morphologies emerge through thermally-drive phase separation of a guest fluid (fluorinated oil) in a host elastomer (silicone). The resulting structures are independent of the quench-rate, appear in a few minutes, and never coarsen. The microstructures fade away slowly (> several hours) from the surface of the elastomer, as the polymer network de-swells. The microstructures are uniform across the sample. Their length scale can be tuned by varying the crosslinking density of the host network. As crosslinking density increases (stiffer networks), the characteristic spacing of the bicontinuous structure shrinks. At low crosslink densities (softer networks), the phase separated guest forms disconnected domains.

While promising, EMPS must overcome multiple limitations before it can be widely implemented to produce functional bicontinuous materials. First, thermal EMPS is very sensitive to the compatibility of the host and guest. It appears to require incubation temperatures near the critical point of mixtures of the guest and uncrosslinked host polymer. This severely limits host-guest combinations. Second, we do not understand the fundamental mechanism of length-scale selection during EMPS, and do not know what range of length scales can be accessed.

We have recently been exploring multiple methods to drive phase separation of guest molecules in host elastomers. We find that polymerization is a robust mechanism to drive phase separation of guest molecules within a host elastomer. While a wide range of guest monomers readily swell a host network, polymerization limits the entropic incentive for mixing and drives them to phase separate. Thus, we expect a much wider range of host-guest combinations to be accessible through polymerization. Further, polymerized structures should be stable against de-swelling of the host network.

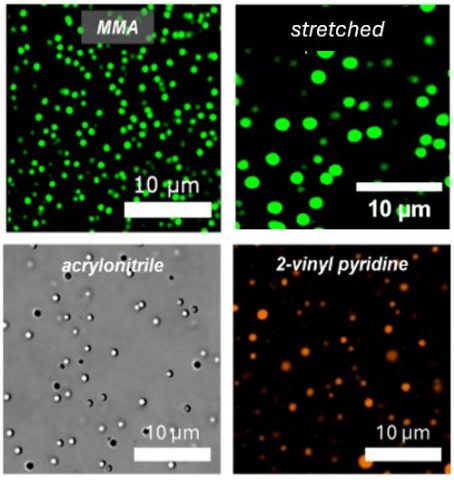


Fig. 2. Polymerization-induced phase separation in elastic matrices[3] (top) poly(methyl-methacrylate) (bottom) poly(acrylonitrile) and poly(2-vinyl pyridine)

Working with silicone elastomers, we have demonstrated polymerization-induced phase separation of methyl methacrylate, styrene, and 2-vinyl pyridine, among others[3], shown in Fig. 2. Polymerization-induced phase separation of these monomers produces monodisperse spherical micron-scale domains for monomer loadings up to about 20%. Domain size varies smoothly with monomer loading. When polymerization of the guest is driven in a uniaxially strained elastomer, the domains are prolate ellipsoids (Fig. 2 top-right). This demonstrates that mechanics of the host couple to the morphology of the domains. At the same time,

however, we do not see a smooth variation of ultimate domain size as we vary the crosslinking density of the network. At high monomer loadings, we observe poorly resolved sub-micron structures, suggestive of bicontinuous structures.

Future Plans

Theory predicts that the ultimate lengthscale in EMPS is determined by a balance of interfacial forces, elasticity, and long-range structural correlations in the host elastomer[4]. We will test this hypothesis through the design, synthesis, and characterization of host elastomers with tunable structural correlations, and explore the impact of these different network architectures on the morphology of phase separated domains.

We will continue to explore the range of chemistries accessible to EMPS. Preliminary experiments suggest that elastic control of domain morphology is limited by a glass transition of the guest polymer. We explore this hypothesis through polymerization-induced phase separation of guests above their glass-transition temperature. Further, we will explore the impact of different polymerization processes (e.g. controlled versus free radical polymerization, chain growth versus step growth) on material structure and properties.

These studies will reveal the practical range of length-scales accessible by EMPS and design rules for functional, bicontinuous structures across a wide range of polymeric materials.

References

1. E.R. Dufresne, H. Noh, V. Saranathan, S.G. Mochrie, H. Cao, and R.O. Prum, *Self-assembly of amorphous biophotonic nanostructures by phase separation*. Soft Matter **5**, 1792 (2009)
2. C. Fernández-Rico, S. Schreiber, H. Oudich, C. Lorenz, A. Sicher, T. Sai, V. Bauernfeind, S. Heyden, P. Carrara, L.D. Lorenzis, R.W. Style, and E.R. Dufresne*, Elastic microphase separation produces robust bicontinuous materials,* Nature Materials **23,** 124 (2024)
3. S. Duraivel, R.J. Dreiling, T.E. Ball, H. Koganti, J. Fu, E.E. O'Banion, B.P. Fors, E.R. Dufresne, *Dispersion Polymerization in an Elastomeric Solvent,* arXiv:2607.09387 (2026)
4. Y. Qiang, C. Luo, D. Zwicker, *Nonlocal elasticity yields equilibrium patterns in phase separating systems*, Physical Review X **14**, 021009 (2024)

Publications

1. S. Duraivel, R.J. Dreiling, T.E. Ball, H. Koganti, J. Fu, E.E. O'Banion, B.P. Fors, E.R. Dufresne, *Dispersion Polymerization in an Elastomeric Solvent,* arXiv:2607.09387 (2026)

Bio-inspired Materials Designs: Reactive, Functional Droplets and Smart Interfaces

Todd **Emrick**, Polymer Science & Engineering Department, University of Massachusetts, Amherst, MA

Keywords: Functional polymers, fluid interfaces, dynamic surfaces, mesoscale materials, polymer zwitterions.

Research Scope

This project focuses on the preparation of novel, bio-inspired materials by translating functional systems in Nature to state-of-the-art synthetic methodology and materials design. With focus on synthetic polymers and fluid interfaces, new macromolecular materials and soft mesoscale structures are emerging from this work and driving advances in materials interfaces, dynamic surfaces, extended filaments, and functional droplets with morphologies and responsiveness reminiscent of biology. In essence, by combining novel organic and polymer synthesis with mesoscale structure fabrication, we access new routes to exploit the combination of interfacial interactions and materials recognition. Specifically, this project targets the cross-section of: **1) designer polymer surfactants that embed functionality directly into zwitterionic sub-units of the polymer structure and 2) soft, polymer-based, mesoscale materials that function as mesoscale surfactants by localizing at fluid-fluid interfaces.** Insights gained from this research advance the fundamental science of materials interface and fluidic droplets and generate novel systems spanning nano-to-mesoscale dimensions. Our work creates novel materials systems that are far simpler than those of biology, thereby advancing the science of energy-efficient materials needed for new discoveries in: *1) materials synthesis spanning multiple length scales and 2) materials design that localizes reactivity at interfaces.*

Bio-inspired materials design. This project is underpinned by ways in which the complexity of biological cells, and their morphologies, instruct the design of dynamic materials. Consider the example of dendritic cells—key connecting components between the adaptive and innate immune systems—that are morphologically unique for their dendrite extensions that participate in signaling mechanisms. Such striking morphologies inspire our discovery of fully synthetic systems with well-coordinated assembly in fluids. The biological structures and processes that inspire this work reinforce our materials design concepts for smart emulsion droplets, with design elements comprising molecular components rooted in biology, such as zwitterions, and synthetic methods that yield novel materials with interfacial impacts. For example, inserting hydrophobic functionality into polar, water-loving polymer zwitterions creates structures with complex solution and interface characteristics, *e.g.,* nanotube formation in liquids or hydrophobic films that are water-adhesive. For mesoscale materials, new insights are derived from fibrillar and sheet-like

structures with surfactant properties extending far beyond those of conventional small molecule or polymer surfactants, and which yield non-equilibrium droplets and inter-connected networks.

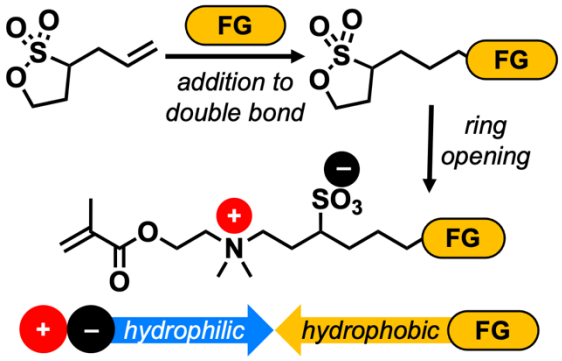


Figure 1. Versatile synthetic route to substituted sulfobetaine methacrylate monomers.

Recent Progress

I. Designer functional zwitterions: synthetic advances and dynamic surfaces. Our strategy to discover routes to novel zwitterionic structures with embeded functionality merges Nature's design principles with efficient coupling chemistry, such as acidity-driven substituion reactions and click chemistry. **Figure 1** illustrates recent progress, where functional group transformations on 1,3-propanesultone ultimately yield substituted sulfobetaine methacrylates. As shown, in one case we utilize fluorocarbon substitution to covalently connect omniphobic fluorocarbon moieties to water-loving zwitterions. In the other case, silylilane units produce related materials that build on efforts to stategically replace PFAS components with fluorocarbon-free alternatives.

Key to these syntheses is the facile preparation of the allyl-substituted propanesultone and subsequent chemical reactions on the double bond, *e.g.,* fluorocarbon groups *via* thiol-ene coupling or silylsilane groups (especially tris(trimethylsilyl silane)) (TTMSS) by free-radical addition. This synthetic methodology produces a library of substituted sultones that, by ring-opening with N,N-dimethylaminoethyl methacrylate (DMAEMA), yield functionalized sulfbetaine zwitterionic methacrylates. These novel monomers were polymerized successfully by controlled free radical techniques, typically by RAFT though also ATRP, to yield polymers of pre-determined molecular weights (typically 8-15 kDa based on monomer:initiator:chain-transfer agent, though higher molecular weights are achievable). A complete set of synthetic details is given in our published manuscripts.[1,2]

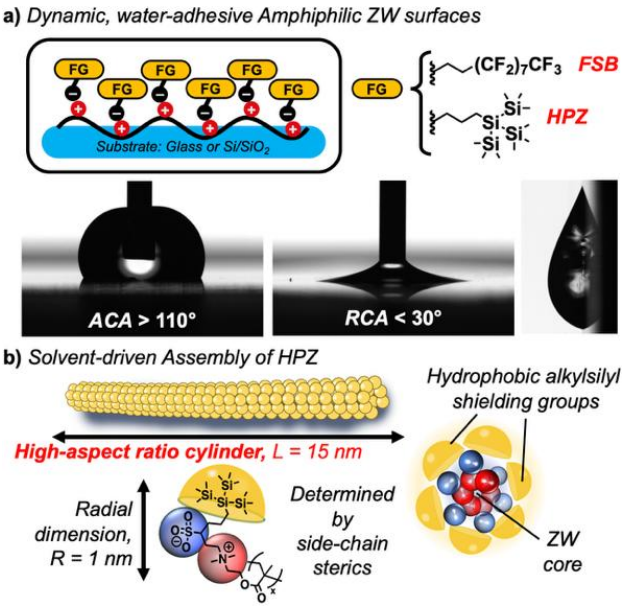


Figure 2. Unique surface (**a**) and solution (**b**) properties of FSB and HPZ polymers.

Figure 2 illustrates new findings from our studies of surface wettability of these unusual polymer zwitterions, performed using contact

angle probe fluids on 50-100 nm thick polymer films. For films of fluorinated polymer zwitterions (FPZs), as might be anticipated, the static water contact angle (WCA) is intermediate between that of Teflon, which repels water, and PSBMA, which is wet by water. *However, for FPZs, dynamnic contact angle measurements revealed water-repelling properties with unexpectedly large WCA hysteresis, on order 100 degrees.* The consequence of this hysteresis is most evident when tilting the substrates on which a water droplet rests: unlike Teflon, with its low hysteresis that causes water to roll off easily upon tilting, on FPZ surfaces water adheres upon titling at a 90-degree angle. As seen, the front edge of the droplet is pinned by a large advancing CA, while the trailing edge of the droplet wets the surface with a low receding CA. Thus, films of FPZs are simultaneously hydrophobic and water-adhering, effectively exhibiting properties similar to those of rose petals (or more generally the petal effect) that retain water owing to Nature's complex topological design, a complexity that is replaced here with simple, smooth films of functional polymers. Moreover, the general solvent resistance of FPZs precludes the need for covalent grafting and thus further simplifies the system relative to surface grafting methodology.

Remarkably, thin films of TTMSS-substituted SBMA polymers perform simililarly, with large (near 100-degree) WCA hysteresis values also leading to retention of water on the otherwise hydrophobic surface. In addition, these silylsilane zwitterions display exceptionally unusual solution properties, much more complex than their fluorocarbon counterparts, a likely consequence of the combined hydrophobicity and steric bulk of the TTMSS pendant groups. The combination of size-exclusion chromatography, NMR spectroscopy (including diffusion measurements), and liquid-phase intermediate angle x-ray scattering (IAXS) provides evidence for the formation of nanoscale cylindrical objects from these silylsilane polymer zwitterions (on order of 15 nm x 1 nm). Microscopic characterization (electron microscopy and stochasitic fluorescence techniques) is underway in attempts to gain direct visual evidence of these objects.

II. Wrapping fluid interfaces with soft objects - mesoscale polymer surfactants. Our approach to designing mesoscale structures exploits photolithographic methodology to pattern polymers into multi-lengthscale objects of well-defined shapes based on the features of the selected mask. While most of our prior work focused on filamentous or ribbon-like objects, **Figure 3** highlights the versatility of this method to obtain sheet-like objects with excellent fidelity, illustrated for ribbons, squares, and triangles. Such mesoscale polymer surfactant (MPS) structures

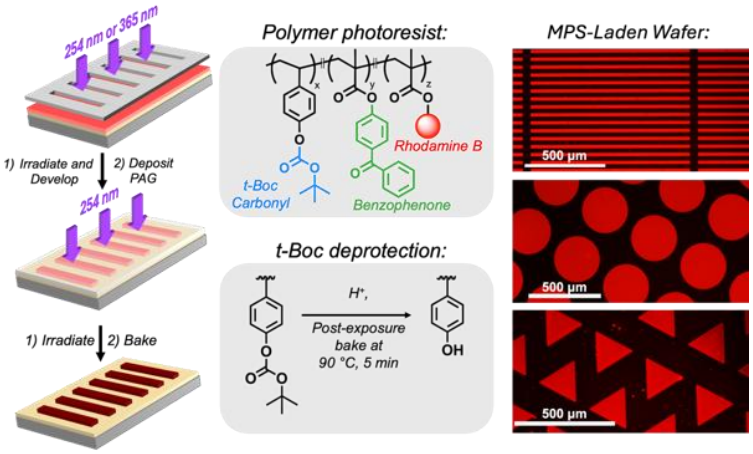


Figure 3. Photolithographic MPS production to yield ultrathin stripes, circles, and triangles.

offer potential insights into the properties of soft, ultrathin objects as they approach, and ultimately wrap, fluid-fluid interfaces, a process enabled by their sub-100 nm thickness.

Key components of our photoresist design include the covalent integration of 1) acid-sensitive t-boc-substituted styrene units; 2) benzophone cross-linkers; and 3) fluorescent tags. Films of these polymer photoresists are well-suited for patterning *via* 254-nm photo-induced crosslinking of the exposed regions, followed by removal of the uncrosslinked regions with a developing solvent. Performing this photoresist patterning atop a release layer (composed of a water soluble polymer) liberates MPS objects into an aqueous fluid where morphological evaluation is performed as a function of the parameters employed, noting that from a single Si substrate on order 1000 MPS objects are produced.

Our recent work on MPS-droplet interfacial contact extends beyond "dendritic droplets" (*i.e.,* droplets with MPS filaments emanating from the fluid interface) to droplet networks and non-equilibrium droplet shapes, as illustrated for different MPS shapes in **Figure 4**.[3] For example, we find MPS filaments bridging emulsion droplets, effectively holding them at some given separation distance based on the length of the filament and extent of wrapping. Building from this concept, we find that bringing an abundance of droplets into contact with the developed photoresist yields droplet-filament networks, where individual filaments wrap around multiple droplets in synthetic networks that resemble the entangled architecture of the rough endoplasmic reticulum and the cellulor resovoirs of vacuoles. In many cases, droplets are trapped in non-equilibrium shapes, especially when MPS filaments are lifted from the release layer as inter-connected structures, which we surmise to wrap multiple droplets, forcing their coalescence into larger droplets, then jamming the oil-water interface into non-equilibrium shapes.

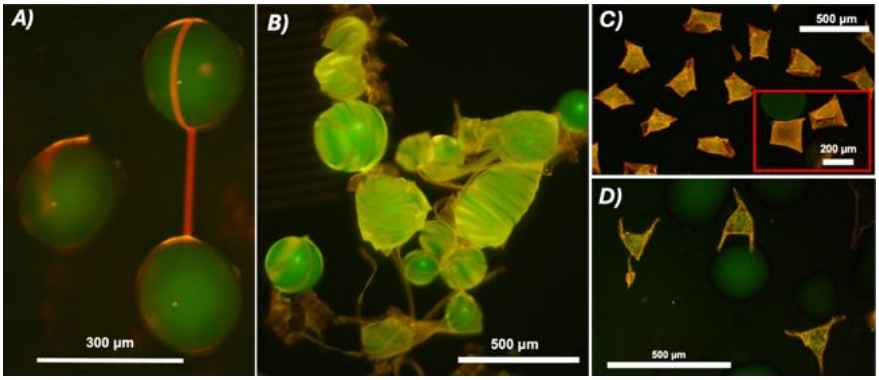


Figure 4. MPS-wrapped oil-in-water droplets showcasing: **a**) bridged droplets, **b**) droplet networks, and **c,d**) droplets packaged into non-equilibrium shapes.

Figure 4 also illustrates the product of MPS sheets (circles and triangles) wrapping the interface of oil-in-water droplets. Here, droplets produced by microcapillary flow focusing were introduced to the releasing MPS-sheets, each wrapped individually as they came into contact with the sheet. As for the MPS filaments, the sub-100 nm thickness enables droplet wrapping in a manner that resembles capillary origami and related processes, but here is performed in a parallel fashion and on a much smaller size scale. Unlike the filamentous objects, this finding offers routes to rapid,

efficient droplet packaging and subsequent triggered release of contents based on the responsive elements of the polymer sheet (*i.e*., bond degradation or on-demand changes to interfacial energy.

Future Plans

Going forward, we seek to capitalize on recent progress with new studies that exploit functionality and reactivity at fluid interfaces through materials advances made *via* biomolecular design. For example, microrheological evaluation of droplet networks holds promise for understanding the adhesive and cohesive impacts of mesoscale surfactants as they wrap and connect droplets, with potential routes to iontronic and/or dropletronic outlets.[4] Concurrently, the ability to individually wrap droplets with mesoscale sheets points to new routes to microencapsulation and in-flow processes that maximize the materials and energy efficiency of encapsulation. Our focus on functional polymers and their interfacial properties will be enabling as these and other studies proceed.

References

1. Steppan, C. G.; Gan, X.; Marquard, H.; White, K.; Mijares, L.; Jeon, D.; Jin, Z.; Morris, S.; Hu, W.; Russell, T. P.; Emrick, T. Hydrophobic Polymer Zwitterions: Impacts of Silylsilane Substitution on Solution and Interfacial Properties. *Angew. Chem. Int. Ed.,* **2025**, e202513143. DOI: 10.1002/anie.202513143
2. Steppan, C. G.; Simon, L.; Blackwood, C.; Emrick, T. Sulfobetaine Zwitterions with Embedded Fluorocarbons: Synthesis and Interfacial Properties. *ACS Macro Letters*, **2024**, 13(6), 761-767. DOI: 10.1021/acsmacrolett.4c00198
3. Steppan, C. G.; Marquard, H.; Kroo, L.; Russell, T. P.; Emrick, T. Wrapping Liquids with Mesoscale Objects: Dendritic Droplets and Packaged Fluids. *Manuscript in Revision for The Journal of the American Chemical Society.*
4. Zhang, Y.; Bayley, H.; Signals through Salt: Building Machines that use the Language of Biology. *Physics Today*, May 7, 2026. DOI: 10.1063/pt.d544a86e8f.

BES-supported publications over the past 2-years

1. Steppan, C. G.; Gan, X.; Marquard, H.; White, K.; Mijares, L.; Jeon, D.; Jin, Z.; Morris, S.; Hu, W.; Russell, T. P.; Emrick, T. Hydrophobic Polymer Zwitterions: Impacts of Silylsilane Substitution on Solution and Interfacial Properties. *Angew. Chem. Int. Ed.,* 2025, e202513143. DOI: 10.1002/anie.202513143
2. Steppan, C. G.; Simon, L.; Blackwood, C.; Emrick, T. Sulfobetaine Zwitterions with Embedded Fluorocarbons: Synthesis and Interfacial Properties. *ACS Macro Letters*, 2024, 13(6), 761-767. DOI: 10.1021/acsmacrolett.4c00198
3. Steppan, C. G.; Marquard, H.; Kroo, L.; Russell, T. P.; Emrick, T. Wrapping Liquids with Mesoscale Objects: Dendritic Droplets and Packaged Fluids. *Manuscript in Revision for The Journal of the American Chemical Society*
4. Yang, Z.; Steppan, C. G.; Pagaduan, J. N.; Emrick, T. Smart Mesoscale Polymer Surfactants on Droplet Surfaces: Biomimicry of Cell Dendrites. *In preparation.*
5. Steppan, C. G.; Mijares, L.; Hu, W.; Emrick, T. NMR Evaluation of PFAS Interactions with Fluorinated Copolymer Zwitterions. *In preparation.*

Early Formation Stages and Pathway Complexity in Functional Bio-Hybrid Nanomaterials

Lara A. **Estroff**[1], Elias Nakouzi[2] and Ulrich Wiesner[1]

[1]Department of Materials Science and Engineering, Cornell University, Ithaca, NY 14853

[2]Pacific Northwest National Laboratory, Richland, WA 99352

Keywords: Organic-inorganic hybrids, self-assembly, nanostructured materials, interfaces, crystallization

Research Scope

The current project is focused on understanding the role of interfaces in guiding the earliest stages of nanostructured organic and inorganic hybrid materials assembly and crystallization pathways, resulting in composites with precisely-controlled structures across length scales, from the near-molecular all the way to the macroscopic scale. *The work has been built around three materials platforms to elucidate solution-based assembly pathways, with an increasing emphasis on the role of the solid-liquid interface composed of solvent molecules, polymer chains, and inorganic materials precursors and clusters.* In the first materials system, we have been probing early assembly stages in the formation of sol-gel derived ultrasmall (<10 nm diameter) fluorescent amorphous silica-core poly(ethylene glycol)-shell (core-shell) nanoparticles (NPs) as well as of surfactant micelle self-assembly directed ultrasmall (~10 nm diameter) amorphous silica cages with different topologies. In both cases structure formation in aqueous solutions occurs via metastable ~2 nm sized primary silica particles. Efforts are geared at understanding how those primary building blocks are assembled into the final structures. In the second system, we have been investigating the role of the solid-liquid interface in directing the incorporation of NPs during crystallization. Using insights from the first materials system, we have been performing studies as a function of ultrasmall fluorescent silica NP (*vide supra*) surface chemistry (e.g., different surface functional groups) and silica cage topology. Finally, in the third system, by inverting the approach taken in the second system, we have been developing methods to elucidate the energy landscape associated with block copolymer self-assembly based nanostructured substrates in controlling nucleation and growth of inorganic materials. Here we are focused on elucidating the role of the solid-liquid interface during such growth phenomena. In all cases, we are interested in revealing the early stages in structure formation. We are striving to understand the "active" role of the solvent in directing hybrid assembly pathways, and importantly in mediating the "cross-talk" (information transfer) between organic templates and growing inorganic materials. To accomplish this goal, we are employing two techniques ideally suited to probing molecular-scale features of surfaces and interfaces important for determining assembly pathways in hybrid materials, but not yet well established in this line of research: High-performance liquid chromatography (HPLC) and three-dimensional atomic force microscopy (3D-AFM).

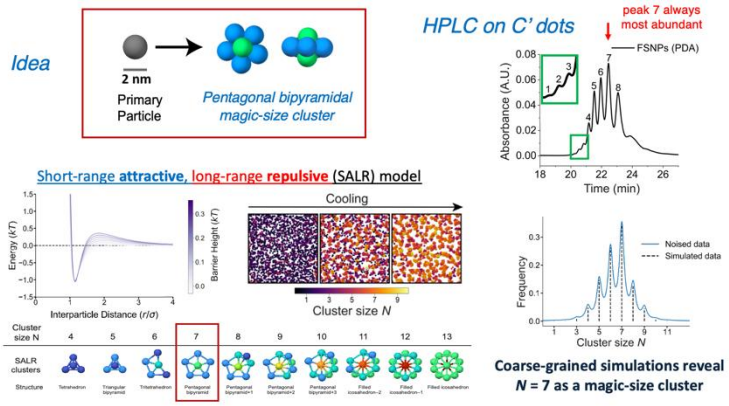


Fig. 1. (Top row), Magic-size cluster (MSC) formation from ~2 nm sized primary silica particles into pentagonal bipyramidal structure (left) and experimental HPLC elugram showing most abundant peak 7 (right). **(Bottom row)**, SALR model-based simulations showing different cluster geometries found (left) and their relative sub-population occurrence, nicely recapitulating HPLC results. (Ref. 3)

Recent Progress

Magic-size cluster (MSC) phenomenon occurring in the aqueous synthesis of ultrasmall fluorescent core-shell silica nanoparticles (NPs). Despite over 20 years of research, little was known about the exact structure of the dye-encapsulating 3–4 nm diameter amorphous silica cores in ultrasmall (diameters <10 nm) fluorescent core-shell NPs with poly(ethylene glycol) (PEG) shells, the first organic-inorganic hybrid nanoparticles that received investigational new drug (IND) FDA approval in the US for human clinical trials. Using a combination of reverse-phase high-performance liquid chromatography (RP-HPLC) and cryogenic transmission electron microscopy (cryo-TEM), we made the surprising discovery of a MSC in the form of a well-defined pentagonal bipyramidal core structure preferentially formed from seven primary silica NPs (Fig. 1) during the synthesis of the core-shell NPs. Such primary silica NPs of around 2 nm diameter are known metastable intermediates in aqueous silica sol-gel synthesis solutions from alkoxysilanes employed as precursors. In the past such magic size cluster (MSC) phenomena had been observed for monodisperse atomic and large (hundreds of nm diameter) colloidal particles. In contrast, we have shown that the primary silica NP building blocks studied here are size dispersed. The use of HPLC enabled the discovery by providing 1 to 10 well-resolved peaks that could be assigned to core-shell silica NP cores build from 1-10 primary particles. Coarse-grained simulations based on short-range attractive and long-range repulsive (SALR) particle interaction potentials provided fundamental insights into the formation mechanism. In particular, they revealed a relatively simple geometrical argument for the unusual stability of the most abundant seven-member MSC (Fig. 1). Results rationalize the successful NP synthesis scale up from 1 mL to 50 L and open a pathway to substantially improved control over ultrasmall particle size distributions, e.g., via chromatographic separations, all critical issues for successful translation of nanoparticles into the clinic.

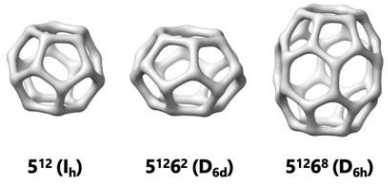


Fig. 2. Amorphous ~10 nm sized silica cages with different topologies and point symmetries. (Ref. 5)

Identification of different ultrasmall amorphous silica cage topologies. Cages are fundamental structural motifs of clathrates and their topological duals, Frank-Kasper phases, are constituents of

mesoporous silica frameworks, and are known from the discovery of carbon-based fullerenes. With one exception, however, they had not been synthesized as discrete particles via surfactant self-assembly directed aqueous sol-gel silica synthesis routes. By varying reactant ratios of surfactant, oil, and silane, we discovered $5^{12}6^{2}$ and $5^{12}6^{8}$ amorphous silica polyhedra (Fig. 2), each coexisting with the previously identified 5^{12} cage, using combined cryo-TEM and single-particle reconstruction. Notably, the $5^{12}6^{8}$ polyhedron represents a topology not previously observed in any mesoporous silica frameworks. In this work, we further demonstrated control over structural features of individual cages (e.g., strut thickness and window size), and we gained first insights into cage formation mechanisms. Structural outcomes were summarized in a ternary morphology diagram alongside prior results, bridging serendipitous discovery and intentional design of silica cages displaying a level of control over silica polymerization rivaling nature. Such cages may provide novel carriers for drug delivery or substrates for catalytic conversions.

Incorporation of secondary phases (nanoparticles) during crystallization. We proposed to and succeeded in advancing well beyond the current literature to achieve a predictive understanding of particle incorporation in crystal growth. The incorporation of nanoscale additives into solution-grown single crystals is an interfacial problem of fundamental relevance to understanding the formation and properties of hierarchical biominerals and bio-inspired hybrid nanocomposites with enhanced mechanical, optical, and electronic properties. To date, almost all work on this topic has focused on empirical observations of particle incorporation and chemical intuition about the role of functional groups. This lack of comprehensive understanding of the underlying mechanisms is largely due to the complexity of the organic-inorganic interactions occurring at the interfaces and limited techniques for probing nanoscale features of this interface under growth conditions. Furthermore, little is known about the role of structured water (hydration layers) at the growth front on controlling nanoparticle incorporation.

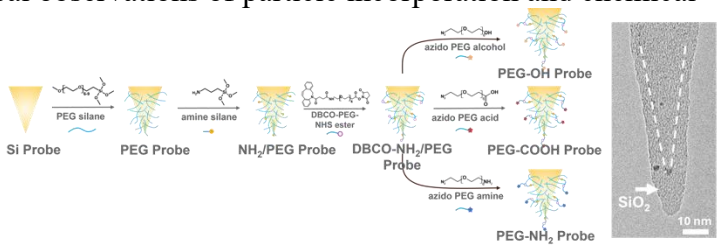


Fig. 3. Technique developed through this project for functionalizing AFM nanoprobes with similar chemistries to silica nanoparticles synthesis. (Ref. 4).

In our approach, we leveraged key capabilities in a way that is only possible in this type of collaborative, multi-PI program: 1) expertise in synthesis of ultrasmall fluorescent silica nanoparticles with well-defined surface chemistries (**Wiesner**), 2) expertise in crystal growth and

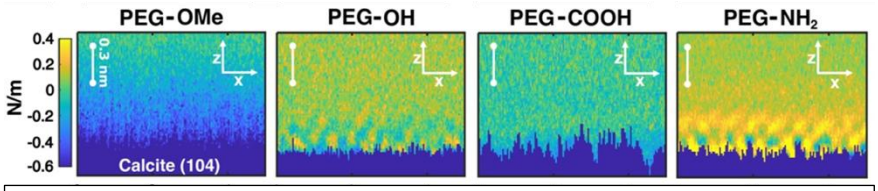


Fig. 4. Interfacial solution structure as measured by 3D AFM and forces encountered by particles of different chemistries as they penetrate hydration layers at the calcite-solution interface (Ref. 4).

biomineralization (**Estroff**), 3) expertise in particle interactions and interfacial solution structure (**Nakouzi**). Each of these capabilities individually is world-leading, and the unique synergy between them has enabled substantial progress during the previous project period on understanding how the organic-inorganic interfacial solution structure drives nanoparticle incorporation into single crystals.

One of the key novelties of our approach is the use of state-of-the-art atomic force microscopy (AFM) tools to directly measure the particle-surface interactions at the relevant solution conditions. We developed a methodology for functionalizing AFM silicon nanoprobes using click chemistry, leveraging our extensive experience with silica surface chemistry (Fig. 3). The functionalized probes were employed in 3D AFM measurements to establish the first reported force mapping datasets using functionalized probes with customized surface chemistries (Fig. 4).

Achieving a predictive understanding of interfacial phenomena requires connecting molecular-scale structure and interactions to emergent interfacial behavior, which remains a major challenge. We solved this problem for the case of fluorescent nanoparticle incorporation in growing crystals. Specifically, using particle fluorescence as a measure to quantify particle incorporation (Fig. 5, left) and 3D AFM to quantify interfacial forces (Fig. 4), we developed and validated the first comprehensive analytical model that successfully predicts nanoparticle incorporation as a function of kinetic *and* thermodynamic parameters, enabling us to quantitatively account for the unique behaviors measured for four different particle surface chemistries (Fig. 5, right). To achieve this success, we used emergent experimental methodology, including best-in-class 3D atomic force microscopy and surface-functionalized nanoprobes to mimic ultrasmall fluorescent nanoparticle surfaces to parameterize and validate our model (Fig. 5). Significantly, we showed for the first time that kinetic barriers originating from interfacial solution structure play a pivotal role in controlling incorporation processes. This recognition of kinetic barriers to surface engagement as a key factor opens an entirely new design space for single crystal composite materials and raises fundamental questions like "*how do we design particle chemistry and topology to minimize/maximize this barrier?*" Our synthesis science framework links interfacial solution structure, particle dynamics, and crystallization kinetics, identifying kinetic barriers as a key design principle for engineering bio-inspired nanocomposites beyond empirical approaches.

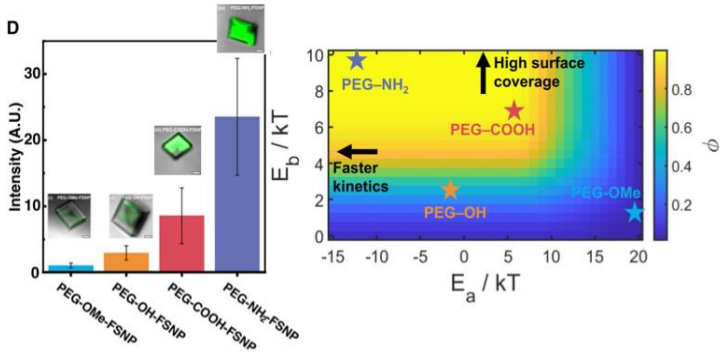


Fig. 5. (Left) We used confocal scanning fluorescence microscopy to measure incorporation efficiencies of surface-functionalized silica nanoparticles in calcite crystals. (Right) We developed a model that successfully predicts the particle incorporation efficiency (φ) using two experimentally measured parameters, namely the kinetic barrier for particle approach to the surface and the particle-surface binding energy. (Ref. 4).

Future Plans. Building on the successes of the last funding period, and inspired by biological systems, we propose a project focused on rationally designing nanostructured materials with precisely controlled structure-property profiles across length scales, from the near-molecular all the way to the macroscopic scale. With our foundational work, we strive to establish a fundamental understanding of how interfacial structures and forces can be harnessed to structure-direct the assembly and growth of amorphous and crystalline inorganic hybrid materials. The proposed work focuses on two materials platforms, one amorphous and one crystalline, to delve into the question of elucidating early formation stages of solution-based hybrid assembly. In the first materials system, we aim to discover new ultrasmall (~10 nm diameter) surfactant self-assembly directed high-symmetry silica cages increasingly using GPC and HPLC to preselect optimal sample compositions. We will also probe the earliest formation stages of these silica cages in water by halting their formation at various early time points. In the second system, we will use our first-of-its-kind comprehensive analytical model for predicting nanoparticle incorporation into single crystals by expanding and diversifying the accessible types of host and guest materials. This will allow us to establish a connection between molecular scale interfacial structure, nanoscale particle incorporation, and mesoscale spatial distribution, ultimately predicting emergent properties at the full material scale. Overall, the objectives of proposed work are: 1) To understand the molecular-scale mechanisms involved in silica nanocage formation; 2) To identify synthetically accessible nanoscale silica cage topologies; 3) To evaluate how solution chemistry (e.g., pH, ionic species) determines the kinetic barrier for surface engagement at mineral-material-fluid interfaces; 4) To demonstrate the generalizability of our newly developed analytical model for predicting particle incorporation into single crystals; 5) To investigate mixed particle surface chemistries and the role of particle topology in particle incorporation; 6) To connect mesoscale particle distributions within single crystals to macroscopic mechanical properties.

Publications Supported by BES 2024-2026

1) Brahana, P.; Zhang, M.; Nakouzi, E.; Bharti, B. Weathering Influences the Ice Nucleation Activity of Microplastics. *Nat. Commun.* **2024**, *15* (1), 9579. https://doi.org/10.1038/s41467-024-53987-8
2) Hedderick, K. R.; Akiki, D. V; Tait, W. R. T.; Oleske, K. W.; Li, Y. M.; Zhang, Q.; Tao, J.; Nakouzi, E.; Wiesner, U. B.; Estroff, L. A. Surface Reconstruction in Hydrated Amphiphilic Block Copolymer Thin Films Probed by Fluid Cell Atomic Force Microscopy. *Macromolecules* **2026**, *59* (8), 4892–4905.
3) Jang, D. J.; Skye, R. S.; Gardinier, T. C.; Lee, R.; Kozbek, A. Y.; Turker, M. Z.; Ma, K.; Tait, W. R. T.; Naguib, N.; Dshemuchadse, J.; Wiesner, U. B. Insights into the Structure of Ultrasmall Fluorescent Core–Shell Silica Nanoparticles. *ACS Nano* **2026**, *20* (15), 12060–12071. https://doi.org/10.1021/acsnano.6c02726
4) Zhang, M.; Liu, K.-T.; Jang, D. J.; Bernat, V. J. B.; Xia, Y.; Li, D.; Kao, H.-M.; Zhu, Z.; Chun, J.; Wiesner, U. B.; Estroff, L. A.; Nakouzi, E. Mapping Interfacial Solution Forces That Drive Fluorescent Nanoparticle Incorporation into Crystals. *ChemRxiv*, January 7, **2026**. https://doi.org/10.26434/chemrxiv-2026-dnj1k
5) Jang, D. J.; Chang, C.-Y.; Lau, C. L.; Ma, K.; Estroff, L. A.; Doerschuk, P. C.; Wiesner, U. B. Towards Libraries of Different Ultrasmall Amorphous Silica Cage Topologies. *ChemRxiv*, June 5, **2026**. https://doi.org/10.26434/chemrxiv.15004374/v1
6) Tait, W. R. T.; Murali, S.; Hsu, C.-H.; Nedsaengtip, J.; Lee, C.; Thedford, R. P.; Kalra, V.; Werner, J. G.; Wiesner, U. B. All-Organic Self-Separating Three-Dimensionally Nanoarchitected Electrochemical Energy Storage Devices. *arXiv*, **2026**. https://doi.org/https://doi.org/10.48550/arXiv.2604.26222

Programmable Dynamic Self-Assembly of DNA Nanostructures

Elisa **Franco** (lead PI), University of California, Los Angeles; Rebecca **Schulman**, Johns Hopkins University

Keywords: biomolecular active matter; DNA nanotechnology; chemomechanical transduction; polymerization ratchets; programmable self-assembly

Research Scope

Biological cells take in energy from the environment and use it to perform a variety of multi-step physical operations in parallel. For example, cell division requires the timed, coordinated assembly of filaments (actin and microtubules) that sort and partition other components, deform and split the cell, and restore cellular organization before the next division. This requires multiple chemical reactions that harness and store energy, and ultimately dissipate it in processes such as polymerization, generating dynamic pulling and pushing forces. This coordinated architecture enables the repeated execution of behaviors, such as microscopic motion, transport, and self-repair, by molecular components that are organized by chemical reactions. Inspired by these architectures, we are using nucleic acid self-assembly to design and build active materials that perform prescribed work, where precise instructions for action can be encoded as molecular sequences. The resulting material systems will produce responsive and programmable materials that can operate under a range of environmental conditions, and help us understand how molecular interactions, mesoscale architecture, and nonequilibrium reaction conditions jointly determine the force, speed, range, and efficiency of prescribed material responses.

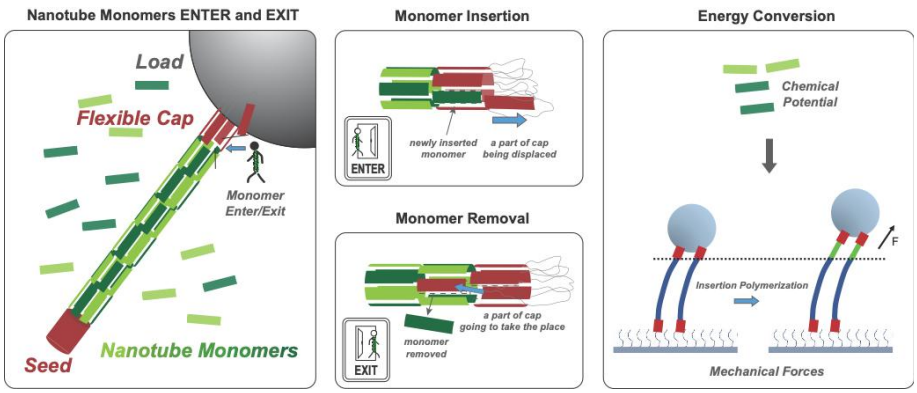


Figure 1. Design of a reversible DNA-based filament motor. The chemical potential from free monomers biases monomer insertion or removal depending on free monomer concentration; monomers attach at sites that are free at a filament-cap junction. The resulting displacement of the cap can be used to perform specific work by, for example, attaching the cap to a specific site. Molecular architecture and endpoint constraints thus determine whether and how filament contour-length change induces motion, elastic stress, or force.

We are designing filament architectures and reaction cycles that leverage polymerization to reliably and efficiently execute specific mechanical tasks, such as positioning components and

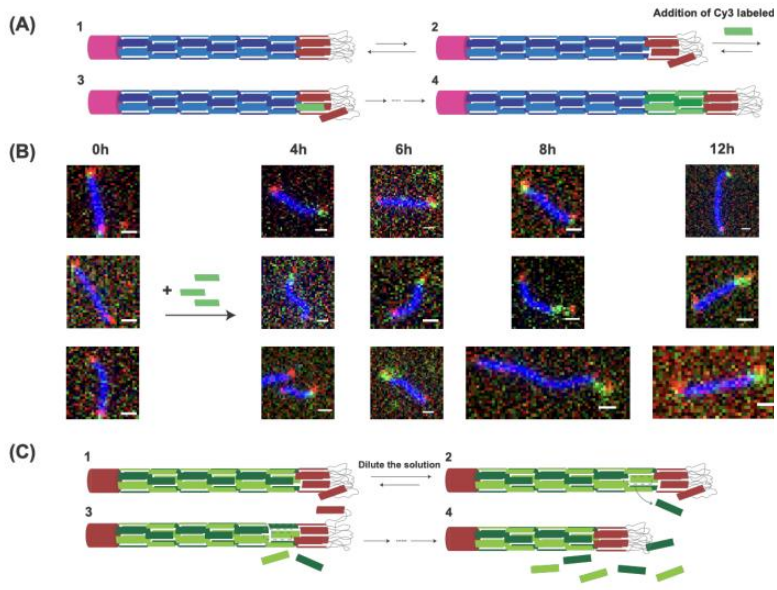


Figure 2. A processive nanotube-cap interface supports reversible filament growth. (A) Local cap-domain detachment from the filament exposes insertion/removal sites. (B) Two-color microscopy localizes newly incorporated monomers next to the cap. Scale bars, 1 µm. (C) Lowering the monomer chemical potential can reverse the flux, shortening the nanotube.

bending materials. We are using computational models and experiments to design, build, and characterize filamentous actuators that 1) apply specific loads to other materials at controlled rates and in specific directions, 2) adjust where and when loads are applied, and 3) respond dynamically to external cues.

Here, we describe the development of a reversible DNA nanotube motor that isolates the elementary operations of a synthetic polymerization ratchet: templated nucleation, processive end tracking, reversible monomer exchange, and load coupling. DNA origami seeds prescribe nucleation and polarity, while a flexible origami cap presents six quasi-independent binding domains at the distal end. Transient release of individual domains exposes sites for tile insertion or removal while the remaining domains retain the cap at the dynamic end. The cap, therefore, acts as a kinetic gate and an addressable mechanical interface.

Raising the monomer chemical potential drives insertion and extension; lowering it below the critical concentration drives removal and retraction. We are using this system to develop a programmable and reversible chemical actuator that can operate under a range of conditions and whose properties could be altered to achieve specific engineering goals. More broadly, this actuator can be used as a primitive in higher-order architectures, such as filament bundles or branched filament networks, to move cargo, reshape soft compartments, and execute staged or cyclic motion.

Recent Progress

A processive interface converts assembly chemistry into directional motion. We engineered seeded and capped nanotubes (SCNTs) in which the origami cap remains coupled to the filament end while individual adapter domains fluctuate between bound and unbound states. Two-color fluorescence experiments were used to visualize how new monomers were incorporated: after preassembling nanotubes from one fluorescent monomer population, a second monomer

population with identical activity but a distinct fluorescent label was introduced. New fluorescence accumulated next to the cap rather than along the nanotube body, demonstrating that elongation occurs through cap-gated insertion at a defined terminal interface. At lower monomer concentrations, we observed monomer removal, while caps remained attached. These results demonstrate how self-assembly can lengthen or shorten a filament and, because the caps remain attached, how these changes might be translated into the directed motion of an addressable endpoint.

Chemical potential sets actuator polarity. We used nanotube growth at different monomer concentrations to measure the critical monomer concentration under defined conditions, which we found to be about 60 nM. We observed that at a monomer concentration of 110 nM, filament dynamics are biased toward insertion and produce an average growth of approximately 1.2 μm over 24 h, roughly 40% of the starting length during a relaxation to the critical concentration. Dilution below the critical concentration reverses the thermodynamic bias and produces approximately 1.0 μm of shortening over 6 h, about 25%. Thus, free monomer concentration and thus chemical potential can control whether filaments extend or retract. Caps remain attached during both growth and shrinkage, suggesting the capacity for bidirectional motion and thus the ability to perform work against a load. We also observed that filaments could grow and then shrink as the monomer concentration was varied, suggesting how a series of actions could be prescribed for a single filament motor.

Filament growth is gated by capping and can store energy in its conformation. We compared three geometries that progressively restrict nanotube motion: seed-tethered uncapped nanotubes (SNT-S), seed-tethered capped nanotubes with a mobile distal end (SCNT-S), and SCNTs tethered through both seed and cap (SCNT-SC). The open geometry elongated fastest. Introducing the cap reduced growth through interfacial gating, as the cap decreased the rates of both monomer attachment and detachment. These experiments suggested a reduction in growth rate upon capping, *i.e.,* a gating factor, of approximately 0.35. We then sought to measure the capacity of filament growth to use the chemical potential in monomer attachment to drive energetically unfavorable conformational changes in filaments; the ability to directly observe these polymer conformations makes it possible to more precisely characterize energy transduction. Two-color imaging confirmed that insertion persisted at the cap under dual anchoring. We also observed that filament growth rates varied with filament conformation. Filaments grew more slowly in conformations for which further growth required energetically unfavorable bending. In some cases, no growth could be observed for long periods. Such reduced growth is a mechanical signature of load-bearing assembly.

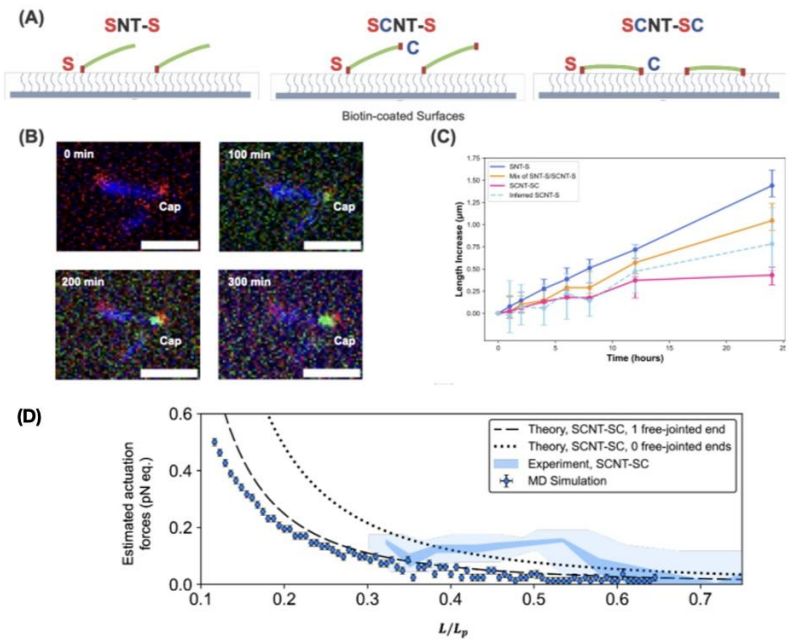


Figure 3. Boundary conditions determine rates of polymerization-driven actuation. (A) Seed-only, cap-gated, and dual-anchor geometries progressively restrict endpoint motion. (B-C) Time-lapse and ensemble measurements show reduced growth as the mechanical constraint increases. (D) Experiment, coarse-grained simulation, and worm-like-chain buckling theory define a length-dependent, sub-piconewton operating regime.

A multiscale mechanical model links molecular design to force. The nanotubes exhibit semiflexible worm-like-chain behavior with a measured persistence length of approximately 8.7 ± 0.5 μm [2]. A classic Brownian-ratchet model for filaments determines an upper limit on the force generated by monomer insertion as a function of chemical potential [1]. We developed a coarse-grained model to predict how filament buckling and confinement affect filament growth rates and the generation and propagation of stresses. The coarse-grained molecular dynamics model reproduces the nanotube persistence length, resolves the onset of buckling under compressive loading, and predicts how force transmission deteriorates as chains become longer and more compliant (Figure 3D). The resulting inverse-square dependence of critical load on filament length is consistent with Euler-type theory and with the sub-piconewton force range inferred from constraint-induced suppression of growth. Together, experiment, simulation, and theory identify the transition from a stiff, productive regime to a compliant, dissipative regime as a function of chemical potential and filament contour length.

Future Plans

Measure the capacity for filament-generated work. We will use the direct displacement of a microsphere load by a single- or multi-filament actuator to measure the capacity of filament growth to perform programmed work. We will tether a bead to a glass surface using a seeded, capped filament. To measure the work performed by filament growth, we will track bead height and trajectory during insertion and removal, together with independent measurements of attachment compliance to produce force-velocity curves. We will use these experiments to better characterize a filament motor's stall force and buckling length and its mechanical efficiency. We will also test whether load-dependent slowing can serve as intrinsic mechanochemical feedback, allowing an actuator to stop at a prescribed mechanical state rather than after a prescribed time.

Maximize actuator performance through design. We will vary contour length, persistence length, cap gating, filament number, crosslink density, and branch geometry, then use experiments and simulations in a prediction-test-refinement loop to understand how these parameters affect actuation speed, range, and stall force [4]. Bundles should increase stiffness and extend the productive force-transmission regime; branched architectures should distribute or redirect loads; dynamic crosslinkers may trade stiffness for reconfigurability.

Control actuation in space and time. RNA activator fields produced by transcriptional hydrogel generators [3] will be coupled to inactive tile monomers, converting a diffusible molecular signal into a spatially patterned chemical potential. We will measure local growth rate, actuator velocity, and stall force across these fields and identify regimes where localized resupply increases performance while suppressing wasteful homogeneous nucleation. Composite caps and strand-displacement controls will independently regulate whether a motor is on, its gating factor, and its polarity. These experiments move the system from externally titrated actuation toward molecularly encoded control over where and when work is performed.

Programming autonomous tasks. Timer and feedback circuits will stage monomer activation, depletion, and cap state to produce cyclic extension-retraction and to coordinate two or more filament types for steering. Initial targets are 1) the upward and downward motions of a bead to achieve a motion cycle and 2) programmable two-dimensional load trajectories. The key scientific question is how temporal programs and mechanical coupling jointly determine task fidelity. We will ask whether a prescribed sequence of molecular signals produces the intended mesoscale trajectory despite load, fluctuations, and component variability. Establishing this link between molecular program and task performance would transform the present filament motor from a biomolecular component into a primitive biomolecular robot.

References

1. C. S. Peskin, G. M. Odell, and G. F. Oster, Cellular motions and thermal fluctuations: the Brownian ratchet, Biophysical Journal 65, 316–324 (1993).
2. A. M. Mohammed and R. Schulman, Directing self-assembly of DNA nanotubes using programmable seeds, Nano Letters 13, 4006–4013 (2013).D. W. Kim, M. Rubanov, A. Grinthal, P. Moerman, and R. Schulman, Building RNA concentration fields, Matter 8, 102208 (2025).
3. D. W. Kim, M. Rubanov, A. Grinthal, P. Moerman, and R. Schulman, Building RNA concentration fields, Matter 8, 102208 (2025).
4. D. Osmanovic and E. Franco, Generating forces in confinement via polymerization, Soft Matter 21, 5312–5322 (2025).

Publications

1. Y. Jiang, K. Akkunuri, E. Shandilya, D. Osmanovic, T. Vo, E. Franco, and R. Schulman, Dynamic and Programmable Self-assembly of DNA Nanostructures as Molecular Motors (manuscript in preparation).
2. G. Moerman, C.-H. Chou, T. E. Videbæk, W. B. Rogers, and R. Schulman, A DNA-encoded recipe to direct multistage colloidal assembly, Proceedings of the National Academy of Sciences 123, e2527410123 (2026).
3. D. W. Kim, A. Grinthal, and R. Schulman, Molecular concentration field design using closed-form steady-state solutions, Soft Matter 22, 1839–1846 (2026).
4. K.-L. Chen, J. Cole, C.-H. Chou, C. W. Lindeman, S. W. Schaffter, P. Moerman, M. Rubanov, K. Sneh, and R. Schulman, Hydrogels with tethered transcription circuit elements for chemical communication and collective computation, ACS Nano 19, 29961–29976 (2025).
5. D. W. Kim, M. Rubanov, A. Grinthal, P. Moerman, and R. Schulman, Building RNA concentration fields, Matter 8, 102208 (2025).
6. E. Kengmana, E. Ornelas-Gatdula, K.-L. Chen, and R. Schulman, Spatial control over reactions via localized transcription within membraneless DNA nanostar droplets, Journal of the American Chemical Society 146, 32942–32952 (2024).

Controlling Lattice Organization, Assembly Pathways and Defects in Self-Assembled DNA-Based Nanomaterials

Oleg **Gang**[1,2,3] and Sanat K Kumar,[1]

[1]Department of Chemical Engineering, [2]Department of Applied Physics and Applied Mathematics, Columbia University, New York, NY.
[3]Center for Functional Nanomaterials, Brookhaven National Laboratory, Upton, NY

Keywords: Self-assembly, DNA nanotechnology, superlattices, nanomaterials, inverse design

Research Scope

This project seeks to establish fundamental principles for programming the assembly of nano-scale objects using sequence-encoded DNA interactions. By integrating experiments, theory, and computation, we aim to identify the key factors that control structural organization, assembly pathways, and defect formation in DNA-guided nanoparticle lattices. We will develop an inverse-design framework that starts from a targeted 3D structure and determines the nanoscale components and interactions required to realize it. This includes accounting for addressable bonds, their energetic landscapes, particle orientations, and the intentional inclusion or removal of nanoscale elements to shape lattice topology. The outcomes of this effort will enable predictive strategies for constructing complex nanomaterials, such as defined lattice geometries and controlled topologies, as well as nanoparticle organizations. The resulting design rules and assembly methods will advance programmable fabrication of 3D nanomaterials and expand the range of functional structures achievable through DNA-directed assembly.

Recent Progress

1. Revealing and Engineering Assembly Pathways of 3D DNA Origami Crystals

Programmable DNA origami enables the construction of highly ordered three-dimensional nanomaterials through precisely engineered interactions between nanoscale building blocks. Although structural design has advanced rapidly, crystal formation has largely relied on empirical slow-cooling protocols lasting several days, limiting both mechanistic understanding and scalable fabrication. We established a quantitative framework for understanding and engineering the thermal assembly pathways of DNA origami superlattices[1]. Using complementary in situ optical microscopy, small-angle X-ray scattering (SAXS), and electron microscopy, we directly monitored crystal nucleation and growth over multiple length scales. These measurements show that DNA origami crystallization follows classical nucleation-and-growth behavior and occurs within a remarkably narrow thermal window (<1°C), with crystals forming within several hours. The assembly represents only a small fraction of conventional multi-day annealing protocols, enabling assembly times to be reduced by nearly two orders of magnitude.

The combined in situ measurements enabled construction of the first time-temperature-transformation diagram for DNA origami crystallization, providing a predictive map linking temperature, nucleation, growth kinetics, and crystal size. The study also identifies the principal

experimental parameters governing reproducible assembly, including DNA sequence, magnesium concentration, and origami concentration, establishing practical design rules for programmable nanomaterial fabrication. Beyond accelerating crystal growth, this mechanistic understanding enables thermal pathway engineering as a new strategy for controlling self-assembly. By exploiting small differences in the melting temperatures of independently encoded DNA-binding motifs, we selectively assembled distinct superlattice architectures from a single mixture solely by modifying the thermal annealing pathway. This approach introduces an additional programmable control without requiring chemical triggers or added molecular components. The resulting kinetic framework substantially reduces fabrication time while enabling precise control over nucleation, growth, morphology, and pathway selection when assembled in bulk and on surfaces[2,3].

1. Programming of Arbitrarily Designed Nanomaterials

The realization of functional 3D nanomaterials requires not only precise placement of nanoscale building blocks but also design strategies capable of encoding increasingly complex architectures. As structural complexity increases, the number of unique building blocks and interactions expands rapidly, limiting fabrication efficiency and assembly fidelity. To address this challenge, we developed a rational inverse-design framework for assembling hierarchically ordered lattices of DNA frames and nanoparticles that dramatically reduces the complexity required to realize prescribed three-dimensional architectures while preserving complete structural programmability[4]. By exploiting the inherent symmetry of a target structure, the framework identifies the minimum set of unique building blocks and bond identities needed to assemble an arbitrarily defined three-dimensional arrangement of nanoscale components.

The fundamental building block is a DNA origami frame, termed a material voxel, which either encapsulates a nanoparticle or remains empty. In our implementation, octahedral DNA frames form directional bonds with six neighbors to assemble into a simple cubic lattice, providing a fully addressable three-dimensional grid for positioning nanoscale objects. Neighboring voxels interact through orthogonal DNA “chromatic” binding sequences. Although assigning a unique sequence to every bond enables complete addressability, this approach becomes impractical for complex structures because it requires an excessive library of orthogonal sequences and introduces kinetic barriers to self-assembly. Instead, our inverse-design framework exploits local symmetry to minimize the number of unique voxels and chromatic interactions, defining a higher-order design motif termed the mesovoxel. A mesovoxel comprises the minimal set of uniquely encoded material voxels whose repetition reconstructs the complete architecture. By encoding structural information into mesovoxels, this strategy substantially reduces design complexity and assembly constraints while enabling programmable fabrication of prescribed nanomaterials. To further streamline the design, we developed the Mapping Of Structurally Encoded Assembly (MOSES) algorithm, which converts an arbitrary 3D material arrangement into an optimized set of DNA voxels by identifying structural symmetries[5]. The algorithm outputs the required voxel identities, stoichiometries, and external-binding and cargo-loading DNA sequences, providing a direct materials assembly recipe.

Future Plans

2. Optically Active Chiral Metamaterials

Chiral nanoscale materials are of great interest due to their ability to manipulate and selectively absorb circularly polarized light based on the chiral handedness of the material. Chiral optical responses result from plasmonic materials without mirror symmetry and features on the order of half a wavelength of light. Due to the difficult nature of fabricating 3D structures with nanoscale precision, many chiroptical metamaterials are limited to longer wavelengths.

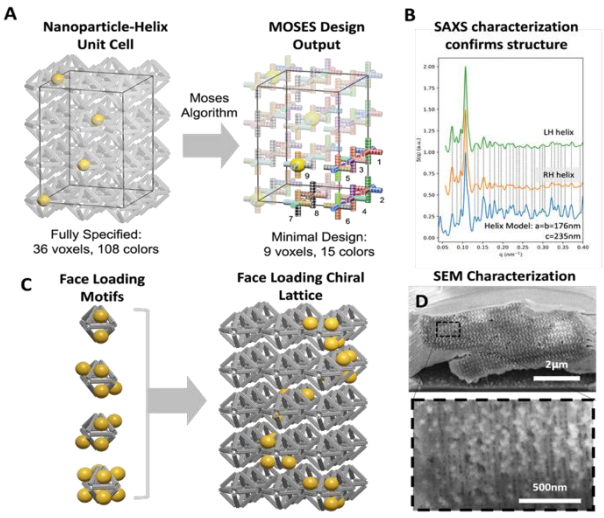


Figure 1. Realizing chiral crystals. A) Chiral nanoparticle helix superlattice design. B) SAXS characterization of assembly. C) External particle binding sites allow for face-loaded particle motifs and enhanced optical properties. D) SEM of face-loaded particle lattices with an inset showing helices.

Using our MOSES algorithm to program a nanoscale lattice, we design a superlattice with repeating helical arrangements of plasmonic nanoparticles, each with a period of ~240 nm (Figure 1A). The mesovoxel output from the MOSES algorithm contains 9 unique voxels with a total of 15 addressable colors. Characterizations based on the SAXS and SEM (Fig. 1B,D) confirm the intended helical nanoparticle structure assembles, and the resulting crystals have micron-scale domains. To enhance the optical properties, we designed several external binding sites to capture nanoparticles on the faces of the frames (Fig. 1C), allowing a 2-fold increase in particle size and decreasing the particle separation from above 70nm to 10-15nm. SEM characterization shows the intended chiral particle superlattices with much smaller inter-particle separation.

3. Assembly pathway control and optimization through tuning interaction strength

Increased design complexity requires more components and a more complex network of interactions, often leading to kinetic limitations. A key goal is to develop methods to control the assembly pathway to avoid kinetic traps. During assembly, however, the system can become trapped in disordered configurations. The defects do not result from individually incorrect bonds, but from collections of valid bonds forming cyclic topologies that are incompatible with the underlying lattice. To identify these kinetic traps, we are developing an algorithm that enumerates local cyclic bonding topologies up to a specified interaction-neighborhood cutoff and classifies them as lattice-compatible or lattice-incompatible (Figure 2). The resulting minimal basis set of crystalline and amorphous motifs is then used to enumerate their possible labeled realizations within a designed established with the MOSES algorithm. This provides a quantitative measure of

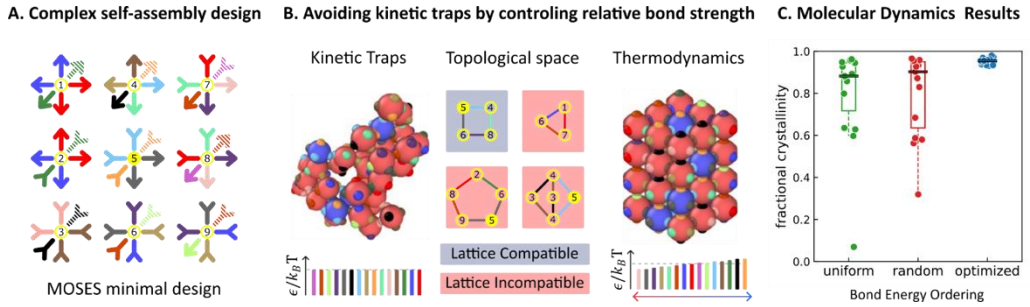


Figure 2. Topology-guided control of assembly kinetics. (A) Minimal MOSES design for the chiral superlattice, consisting of 9 unique material voxels and 15 chromatic bond identities. (B) Minimal basis set of lattice-compatible and lattice-incompatible topological motifs. The labeled realizations of these motifs are used to quantify the participation of chromatic bonds in crystalline and defect-forming structures and to determine the bond interaction strengths. (C) Fractional crystallinity from 15 independent molecular dynamics simulations using uniform bond energies, randomly assigned nonuniform bond energies, and topology-informed bond energies.

how strongly each chromatic bond contributes to desired lattice motifs or to competing defect-forming structures. We use this classification to construct a nonuniform interaction-energy map in which bonds associated primarily with lattice-compatible motifs are strengthened, while bonds that frequently participate in lattice-incompatible motifs are weakened. Fig. 2C compares the final fractional crystallinity from 15 independent molecular dynamics simulations using uniform bond energies, randomly assigned nonuniform energies, and the topology-informed energy mapping. The topology-informed design produces substantially greater crystallinity, demonstrating that motif-based bond-energy programming can suppress kinetic traps and steer assembly toward the intended thermodynamic state.

4. Assembly-by-Elimination of Latices with Interstitials and Interweaves

Creating complex low-density nanoscale architectures remains a major challenge because conventional self-assembly naturally favors densely packed, highly symmetric structures. To address this problem, we are developing the Assembly-by-Elimination (ABEL) strategy (Fig. 3). In this approach, we first assemble a fully connected DNA origami template lattice and then selectively remove prescribed structural elements. The ABEL strategy combines additive and subtractive fabrication within a single self-assembled material. DNA origami cubic frames are first organized into a body-centered cubic template lattice using sequence-programmed interactions. Selected DNA bonds are then cleaved through addressable toehold-mediated

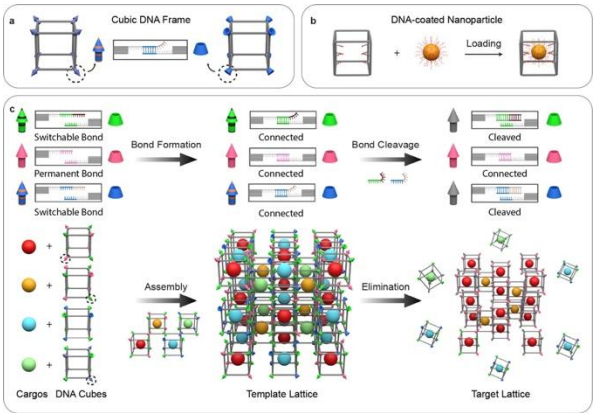


Figure 3. Assembly-by-Elimination (ABEL) strategy. DNA cubic frames with encoded bonds (a) and with or without nanoparticles (b) are self-assembled into a template lattice (c). Selective cleavage of prescribed inter-frame bonds removes targeted elements and transforms the template into low-density architectures with designed topology, including lattices containing engineered interstitials and interpenetrating networks. ABEL strategy allows for creating architectures that are inaccessible or difficult to realize.

strand displacement, disconnecting specific structural elements and allowing them to diffuse from the lattice. This programmable editing transforms a dense parent lattice into targeted low-packing-fraction architectures while preserving long-range crystalline order. The versatility of ABEL was demonstrated by creating multiple architecturally distinct nanostructures that are difficult or impossible to obtain through conventional assembly. For example, a Heusler-type Cu_2MnAl template lattice is selectively transformed into a low-density Cu_2Al framework by removing one sublattice. Compared with direct assembly of the same structure, the ABEL-derived lattice can substantially improve crystallinity, with experiments demonstrating more than a twofold increase in correlation length and significantly sharper SAXS diffraction peaks. These results show that template editing effectively overcomes kinetic and entropic limitations associated with assembling open crystal structures directly.

References

1 Michelson, A. N., Kahn, J. S., McKeen, D., Minevich, B., Redeker, D. C. & Gang, O. Revealing and Engineering Assembly Pathways of 3D DNA Origami Crystals. *ACS Nano* (2025). https://doi.org:10.1021/acsnano.5c09008

2 Teng, F., Zhang, H., Nykypanchuk, D., Li, R., Yang, L., Tiwale, N., Xi, Z., Liu, M., He, M., Zhang, S. & Gang, O. Macroscale-area patterning of three-dimensional DNA-programmable frameworks. *Nature Communications* **16**, 3238 (2025). https://doi.org:10.1038/s41467-025-58422-0

3 Adhikari, S., Minevich, B., Redeker, D., Michelson, A. N., Emamy, H., Shen, E., Gang, O. & Kumar, S. K. Controlling the Self-Assembly of DNA Origami Octahedra via Manipulation of Inter-Vertex Interactions. *Journal of the American Chemical Society* **145**, 19578-19587 (2023). https://doi.org:10.1021/jacs.3c03181

4 Kahn, J. S., Minevich, B., Michelson, A., Emamy, H., Wu, J., Ji, H., Yun, A., Kisslinger, K., Xiang, S., Yu, N., Kumar, S. K. & Gang, O. Encoding hierarchical 3D architecture through inverse design of programmable bonds. *Nature Materials* **24** (2025). https://doi.org:10.1038/s41563-025-02263-1

5 Kahn, J. S., Redeker, D. C., Michelson, A., Tkachenko, A., Hong, S., Minevich, B. & Gang, O. Arbitrary Design of DNA-Programmable 3D Crystals through Symmetry Mapping. *Acs Nano* **19**, 14795-14807 (2025). https://doi.org:10.1021/acsnano.4c17408

Publications

1 Teng, F., Zhang, H., Nykypanchuk, D., Li, R., Yang, L., Tiwale, N., Xi, Z., Liu, M., He, M., Zhang, S. & Gang, O. Macroscale-area patterning of three-dimensional DNA-programmable frameworks. *Nature Communications* **16**, 3238 (2025). https://doi.org:10.1038/s41467-025-58422-0

2 Michelson, A. N., Kahn, J. S., McKeen, D., Minevich, B., Redeker, D. C. & Gang, O. Revealing and Engineering Assembly Pathways of 3D DNA Origami Crystals. *ACS Nano* (2025). https://doi.org:10.1021/acsnano.5c09008

3 Kahn, J. S., Redeker, D. C., Michelson, A., Tkachenko, A., Hong, S., Minevich, B. & Gang, O. Arbitrary Design of DNA-Programmable 3D Crystals through Symmetry Mapping. *Acs Nano* **19**, 14795-14807 (2025). https://doi.org:10.1021/acsnano.4c17408

4 Kahn, J. S., Minevich, B., Michelson, A., Emamy, H., Wu, J., Ji, H., Yun, A., Kisslinger, K., Xiang, S., Yu, N., Kumar, S. K. & Gang, O. Encoding hierarchical 3D architecture through inverse design of programmable bonds. *Nature Materials* **24** (2025). https://doi.org:10.1038/s41563-025-02263-1

5 Chmielewska, J. M., Redeker, D. C., Szustakiewicz, P., Arnon, Z., Powala, F., Paterczyk, B., Michelson, A., Gang, O. & Majewski, P. W. Volumetric Shaping of Nanoparticle-DNA Crystals by Light-Induced Milling. *Nano Letters* **25**, 12884-12891 (2025). https://doi.org:10.1021/acs.nanolett.5c02830

6 Michelson, A., Subramanian, A., Kisslinger, K., Tiwale, N., Xiang, S., Shen, E., Kahn, J. S., Nykypanchuk, D., Yan, H., Nam, C.-Y. & Gang, O. Three-dimensional nanoscale metal, metal oxide, and semiconductor

frameworks through DNA-programmable assembly and templating. *Science Advances* **10**, eadl0604 (2024). https://doi.org:doi:10.1126/sciadv.adl0604

7 Liu, H., Matthies, M., Russo, J., Rovigatti, L., Narayanan, R. P., Diep, T., McKeen, D., Gang, O. L., Stephanopoulos, N., Sciortino, F., Yan, H., Romano, F. & Sulc, P. Inverse design of a pyrochlore lattice of DNA origami through model-driven experiments. *Science* **384**, 776-781 (2024). https://doi.org:10.1126/science.adl5549

8 Arnon, Z. A., Piperno, S., Redeker, D. C., Randall, E., Tkachenko, A. V., Shpaisman, H. & Gang, O. Acoustically shaped DNA-programmable materials. *Nature Communications* **15**, 6875 (2024). https://doi.org:10.1038/s41467-024-51049-7

9 Mao, R., Minevich, B., McKeen, D., Chen, Q., Lu, F., Gang, O. & Mittal, J. Regulating phase behavior of nanoparticle assemblies through engineering of DNA-mediated isotropic interactions. *Proceedings of the National Academy of Sciences* **120**, e2302037120 (2023). https://doi.org:doi:10.1073/pnas.2302037120

10 Chiang, H. T., Kern, N., Wylie, Z. R., Moeez, A., Zhang, H., McKeen, D., Herringer, N. S. M., Gang, O., Ferguson, A. L., Sherman, Z. & Pozzo, L. D. Assembly of small silica nanoparticles using lipid-tethered DNA 'bonds'. *Soft Matter* **21**, 9398-9411 (2025). https://doi.org:10.1039/d5sm00924c

Catalytic Enzymes as Active Matter

Steve **Granick**, University of Massachusetts at Amherst

Keywords: active matter, chemical-to-mechanical, catalyst, energy dynamics

Research Scope

This project establishes fundamental materials science principles for chemically fueled matter, using biological catalysis as a design blueprint for converting chemical free energy into directed, programmable mechanical function. The central problem is how the free energy dissipated by a chemical reaction, together with the noise and entropy production that accompany it, is rectified into coordinated motion and force. We pose this at the scale of individual catalytic molecules and follow the resulting energy transduction upward to mesoscale objects and to assemblies of several catalysts acting together. The long-term aim is programmable design principles for molecule-scale machines.

The work addresses the Basic Energy Sciences transformative opportunity of mastering beyond-equilibrium matter: functional matter organized in time as well as in space, sustained away from equilibrium by continuous chemical input. Its distinctive contribution is to carry active-matter concepts from the colloidal and biofilament scales, where they are established, down to the scale of individual catalytic molecules, and then to reconnect that molecular scale to mesoscale collective behavior. The research is organized around three questions. First, whether a shape-asymmetric mesoscale object placed in a reacting bath rectifies its random rotational diffusion into net directed rotation, and how that directionality is set by shape asymmetry and reaction rate. Second, whether passive molecules and objects are entrained by the hydrodynamic fields that catalytic turnover generates, and how the effect scales with tracer size and catalyst concentration. Third, what collective phenomena emerge when catalytic activity is distributed across several species acting in sequence or on the same molecule, and whether cooperative hydrodynamic coupling scales differently from single-catalyst prediction. A cross-cutting requirement runs beneath all three. Because catalytic chemistry is the energy source that drives every function studied here, the fuel must be reproducible and quantitatively controlled before any driven behavior can be treated as designable. We therefore develop preparation and measurement protocols that render catalytic activity reproducible and controllable by concentration, and we apply them across enzymes of different catalytic mechanism, from highly active oligomers to monomeric enzymes.

Recent Progress

Reproducible and controlled catalytic activity. Using urease, a workhorse enzyme of active-matter studies, we found that the same nominal enzyme yields materially different mobility signatures depending only on preparation: measured by fluorescence correlation spectroscopy, one protocol gave apparent diffusion enhanced above the Brownian level and another gave no measurable

deviation. The determining variables lie in the preparation, and we identified and documented them, covering preprocessing, labeling at a defined functional group, purification of the labeled species, filtration to remove aggregates before measurement, and substrate-induced pH change. A separate quantitative requirement is to hold enzyme and substrate concentrations in the regime where the response is linear in concentration, since outside it the apparent behavior turns nonlinear or erratic and corrupts both the measured value and its interpretation. This control is the precondition for every measurement reported below, and may account for the divergent enhanced-diffusion results reported across laboratories.

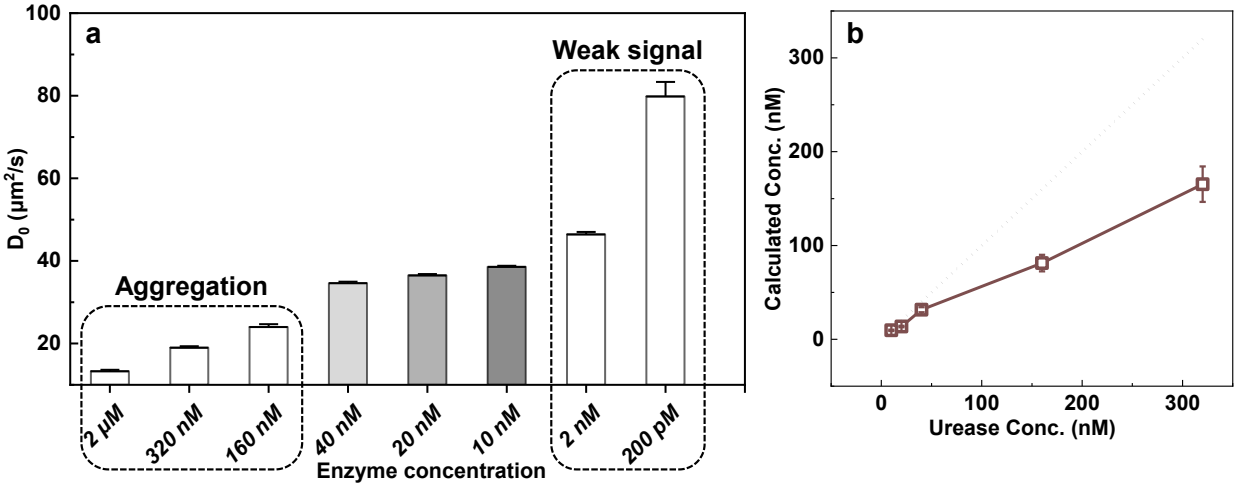


Fig. 1. Urease concentration-dependent diffusion coefficient (D_o) that defines the aggregation threshold, measured using fluorescence correlation spectroscopy (FCS). (a) D_o as a function of urease concentration in PBS buffer. At very low enzyme concentrations, weak fluorescence signals limit accurate measurement, while at very high concentrations enzyme aggregation causes slower D_0. (b) Comparison of nominal enzyme concentration determined gravimetrically and apparent concentration detected by FCS. Deviation from linearity at high concentrations indicates enzyme aggregation, resulting in reduced particle count and underestimation of enzyme concentration by FCS. Error bars represent standard deviation from n = 30 independent measurements.

A single-molecule imaging capability for catalytically driven motion. Molecular-scale transduction has been characterized almost entirely by fluctuation-correlation methods, which average over the ensemble, cannot resolve individual trajectories, and therefore cannot separate a fast or heterogeneous subpopulation from the bulk, nor trace a mesoscale mechanical response to its molecular origin. We built an instrument to remove this limitation. A homebuilt stroboscopic microscope combines highly inclined and laminated optical sheet illumination, a qCMOS detector at 426.9 frames per second, and laser triggering synchronized to millisecond pulses. Together these recover individual trajectories of up to about twenty points and accumulate more than ten thousand single-molecule displacements in two minutes, while suppressing out-of-focus background and

motion blur at the weak labeling densities that activity measurements require.

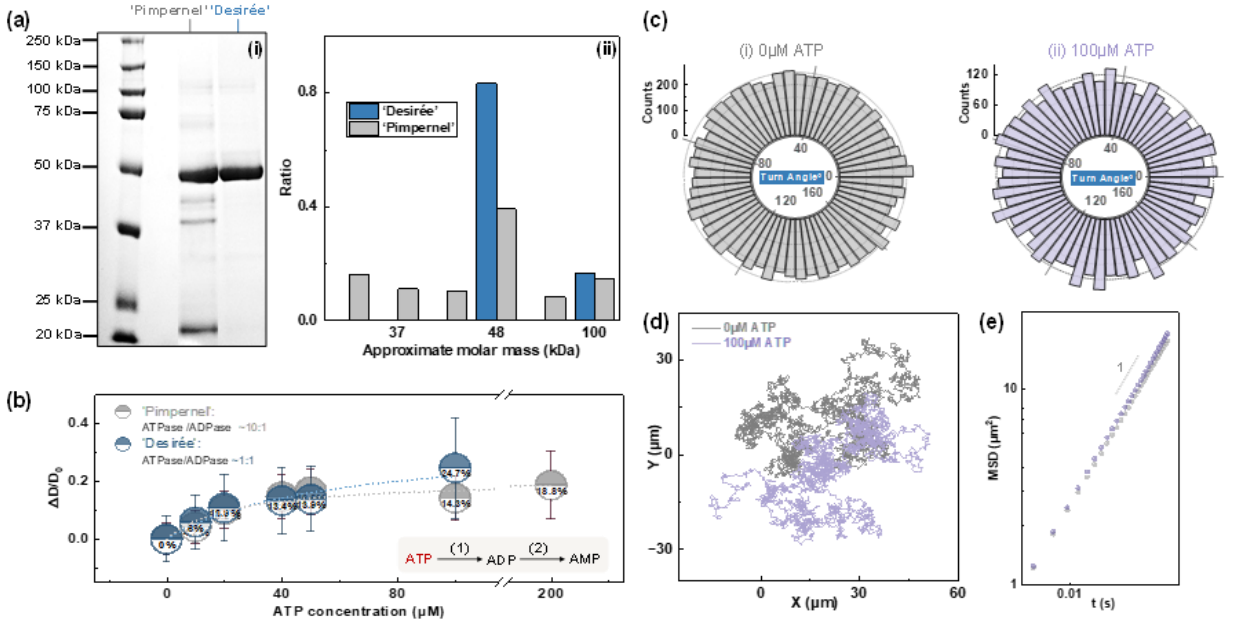


Fig. 2. Apyrase exhibits concentration-dependent enhanced diffusion with normal Brownian statistics. (a) Purity characterization. (i) SDS-PAGE of commercial apyrase isoforms: 'Pimpernel' (Type VI) and 'Desirée' (Type VII). (ii) Component ratios from densitometric analysis. (b) Normalized diffusion enhancement ($\Delta D/D_0$) versus ATP concentration. (c) Turn angle distributions between consecutive displacements. (d) Representative long trajectory reconstructed from pooled short trajectories at 100 μM ATP (scale bar: 2 μm). (e) Ensemble-averaged mean squared displacement (MSD) at 0 and 100 μM ATP. Power-law fits $MSD(t) = 4D't^{\alpha}$ yield $\alpha \approx 1$, confirming normal Brownian diffusion.

Chemical free energy transferred to mechanical work in passive mesoscale objects. The most direct test of chemical-to-mechanical energy transfer is whether a passive object, carrying no catalyst of its own, is mechanically driven by a reaction in the surrounding bath. We performed this test on two objects of contrasting mechanical character. A rigid colloidal bead held in an optical trap showed enhanced position fluctuations during reaction, appearing as white noise across the experimental bandwidth, with the effective diffusion coefficient raised by up to twenty percent in the early stages and decaying continuously to Brownian motion as the reactants were exhausted. The enhancement thus exists only when the system is driven and vanishes when it returns to equilibrium. A soft object reports drive through its shape: using Förster resonance energy transfer to gauge end-to-end distance, we find that a flexible polymer expands in an active urease bath, in proportion to the level of catalytic activity. To our knowledge, this is the first such measurement for a molecular-scale polymer in a chemically active bath.

Directed mechanical work at a shape-asymmetric object. Bacterial baths are known to rotate asymmetric gears in a preferred direction, and the question we posed is whether molecular-scale chemical activity can do the same. We used asymmetrically toothed SU8 microgears as shaped probes, driven by a CuAAC reaction bath. During reaction the gears rotated preferentially along the short edge of the teeth. Tracking the angular trajectories, the distribution of angular step size

at fixed lag time developed a non-zero mean that grew with lag time and returned to zero once the reaction ended. Reducing the catalyst concentration reduced the directional bias. These observations establish that the reaction rectifies the otherwise random rotational diffusion of the gear, and that both reaction rate and concentration set the amplitude of the directionality. At substantially higher reaction concentration the rotation remained persistently unidirectional but in some runs reversed sense, a behavior we tentatively attribute to adsorption and do not yet control.

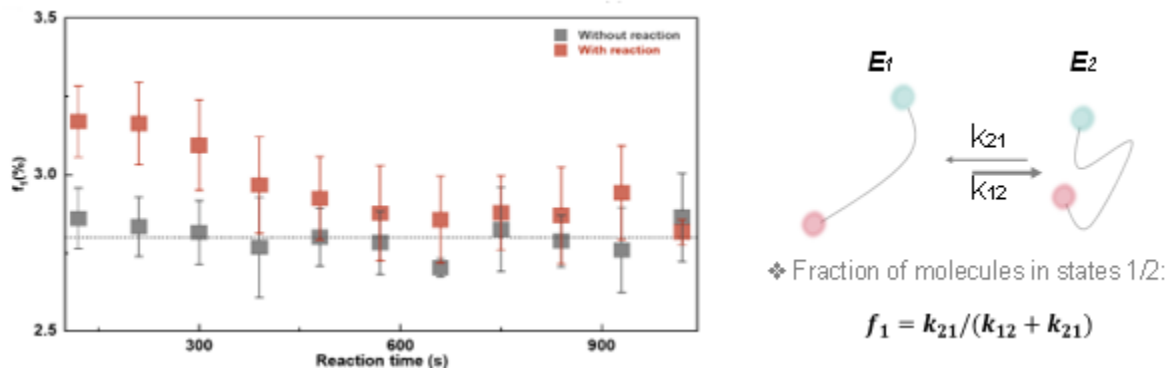


Fig. 3. During hydrolysis of urea by the enzyme urease, FRET measurements show that polyethylene oxide polymer swells. In this example, concentrations are 0. 5 nM urease and 1 mM urea.

Future Plans

Three manuscripts covering the results above are in preparation and moving them to submission is the immediate priority. The next period's science focuses on the shape-asymmetric rectification result, our clearest demonstration of directed work from chemical free energy. We will establish quantitative control over the amplitude and sense of directed rotation as functions of reaction rate and catalyst concentration, resolve the adsorption-linked sense reversal seen at high concentration, and extend the single-catalyst measurements toward multiple catalysts in sequence or on the same molecule, where the open question is whether cooperative hydrodynamic coupling yields collective directional behavior absent at the single-catalyst level. The accumulated single-molecule trajectories may also lend themselves to machine-learning analysis of heterogeneous subpopulations, a direction we expect to explore.

Publications

Q. Pan, S. Granick, Single-Molecule Tracking Confirms Substrate-Dependent Diffusion Enhancement in Monomeric Apyrase, manuscript in preparation.
Q. Pan, S. Granick, Investigating the Impact of Experimental Variables on Catalysis-Enhanced Enzyme Diffusion, manuscript in preparation.
T. Huang, J. Park, H. K. Park, S. Granick, Observation of Chemically-Driven Force Fluctuation in an Optical Trap, manuscript in preparation.

Transient amplification and interfacial instability in chemically active materials

Jason R. **Green**, University of Massachusetts, Boston
Joseph P. Patterson, University of California, Irvine

Keywords: Dissipative self-assembly, transient growth, liquid phase electron microscopy, active condensates

Research Scope

Chemically active materials derive their function from nonequilibrium reaction networks that continuously assemble, remodel, and disassemble structure. Unlike equilibrium materials, these systems can respond strongly to small perturbations, reorganize across multiple length scales, and sustain products that are only transiently stable. Our research program seeks to establish quantitative principles for learning and controlling these dissipative behaviors directly from experiments. To do so, we combine nonequilibrium statistical mechanics, dynamical-systems theory, multiscale modeling, and in situ microscopy of supramolecular materials and peptide condensates.

The long-term goal is to connect microscopic structural dynamics with the thermodynamic costs and control principles of active assembly. In the current project, this means: (i) quantifying structural dynamics from time-resolved microscopy, (ii) building reduced dynamical models that identify amplification, decay, and instability in chemically driven systems, (iii) linking these models to reaction-network and reaction-diffusion descriptions of active matter, and (iv) using the resulting theory to guide experimental design. A central theme emerging from our recent work is that dissipation does more than sustain nonequilibrium steady states: it can also reshape short-time response, interfacial stability, and the dynamic fate of assembled materials.

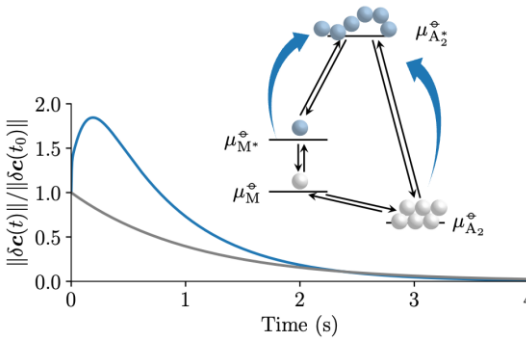


Figure 1. Materials that self-assemble are often designed with the expectation that fluctuations and inhomogeneities will relax toward a steady state. We have shown that the chemical reaction networks can transiently amplify concentration fluctuations to assemble supramolecular materials in thermodynamically unstable states.

Recent Progress

Transient amplification as a design principle for dissipative self-assembly. Our most recent theoretical work [1] shows that chemically driven self-assembly networks can transiently amplify small fluctuations, even when their steady states are asymptotically stable. For a reaction network representative of current dissipative supramolecular materials, we found that perturbations do not necessarily relax monotonically back to steady state. Instead, the linearized dynamics can be nonnormal, allowing small concentration perturbations to grow temporarily and produce a burst of assembled material above the steady-state yield. We derived a precise criterion for this effect from the largest

eigenvalue of the symmetric part of the Jacobian matrix, which identifies when a steady state is reactive and capable of transient growth. Across the parameter space, chemical driving controls the magnitude, timing, and localization of this amplification. Stronger driving generally increases transient growth and can localize it in the target assembled species, providing a quantitative design rule for responsive active materials.

Nanoscale interfacial organization governs whether condensates mature or collapse. In parallel, we used liquid-phase TEM, cryo-TEM, optical microscopy, and modeling to study passive and active FFssFF peptide condensates across nanometer-to-micrometer scales [2]. In passive droplets, we observed metastable multiphase intermediates with membrane-like interfaces, slow maturation, arrested coalescence, and eventual fibril formation. Cryo-TEM resolved interfacial boundaries with thicknesses on the order of a few nanometers, indicating that nanoscale interfacial organization is an intrinsic structural feature of passive FFssFF condensates. Under active chemical or electrochemical driving, these same droplets behaved very differently: multiphase maturation was bypassed, interfaces destabilized, and droplets exhibited rapid shrinkage or spontaneous bursting. Simulations supported a mechanism in which local membrane degradation and faster interior chemical conversion trigger collapse. Taken together with our theory of transient growth, these observations suggest that dissipation governs both the short-time amplification of perturbations and the longer-time structural fate of chemically active materials.

Data-driven analysis of microscopy and nonequilibrium dynamics. These theoretical and experimental advances strengthen the goal of learning dissipative behavior from microscopy. Our earlier work established structural dissimilarity workflows for quantifying structural change in time-resolved imaging, while recent results now provide clearer physical targets for those analyses: transient amplification, interfacial reorganization, delayed relaxation, and collapse. We are using kinetic models, reaction-diffusion simulations, and simulated TEM images to bridge the gap between observables in microscopy videos and latent dynamical quantities such as amplification envelopes, linear stability, and dissipation rates. This joint workflow is creating a practical route from raw movies to predictive models of active materials.

Future Plans

Our next objective is to integrate these directions into a single predictive framework for chemically active materials. First, we will apply data-driven reduced modeling tools to experimental and simulated microscopy videos to infer short-time linear response, identify reactive states, and test whether transient amplification signatures can be recovered directly from image sequences. Second, we will use reaction-network and reaction-diffusion models to map how chemical driving, interfacial stability, and noise determine whether a material exhibits enhanced assembly,

controlled remodeling, or catastrophic collapse. Third, we will compare these predictions against in situ microscopy of electrochemically and chemically driven assemblies, with emphasis on the conditions that favor selective amplification of desirable structures. More broadly, our aim is to move from descriptive imaging of active matter to predictive control of how dissipation shapes structure and function.

References

1. T. H. Ueon, J. P. Patterson, and J. R. Green, *Transiently amplified fluctuations assemble dissipative materials*, Proc. Natl. Acad. Sci. USA **123** e2531136123 (2026)
2. Lilian Zeinalvand, Dipankar Barpuzary, Tae Hyun Ueon, Walter B. Lai, Yuanming Song, Zhaoxu Li, Rakia Dhaoui, Nehal Idris, Karthik Reddy Peddireddy, Rae M. Robertson-Anderson, Douglas J. Tobias, Zhibin Guan, Jason R. Green, Joseph P. Patterson, *Interfacial organization governs maturation and collapse in passive and active condensates*, J. Am. Chem. Soc. **148**, 17967 (2026)
3. W. S. Gibson, J. T. Mulvey, S. Das, S. Selmani, J. G. Merham, A. M. Rakowski, E. Schwartz, A. I. Hochbaum, Z. Guan, J. R. Green, J. P. Patterson, *Observing the dynamics of an electrochemically driven active material with liquid electron microscopy*, ACS Nano **18**, 11898 (2024).
4. P. J. Hurst, J. T. Mulvey, R. A. Bone, S. Selmani, R. F. Hudson, Z. Guan, J. R. Green, J. P. Patterson, *CryoEM reveals the complex self-assembly of a chemically driven disulfide hydrogel*, Chemical Science **15**, 1106 (2024).

A framework for exploring and controlling non-equilibrium coherent states in active fluids based on global phase space geometry

Piyush **Grover** and Jae Sung Park, Mechanical and Materials Engineering, University of Nebraska-Lincoln

Michael M. Norton (former co-PI), Brandeis University

Keywords: Active fluids, active turbulence, nonequilibrium steady states, pattern formation, reaction-diffusion

Research Scope

We are developing theoretical and computational tools using nonlinear dynamics theory to understand the *global phase space* of active fluids. In this project, we have showed that this infinite dimensional phase space in active nematics is populated by *Exact Coherent Structures* (ECS), which are exact solutions of the physical dynamics with distinct and regular spatiotemporal structure; examples include unstable equilibria, periodic orbits, and traveling waves. The ECSs are connected by dynamical pathways called invariant manifolds. Building upon the success of ECS framework in *inertial passive fluids* over the past two decades [1], our main hypothesis is that active/mesoscale turbulence corresponds to a trajectory meandering in this phase space, transitioning between neighborhoods of unstable ECSs by traveling on the invariant manifolds.

The main goals of the project are 1). To develop a framework for predicting and classifying various classes of ECSs, and dynamical connections between them, as well as quantifying their robustness with respect to change in models, parameters and system geometries. The analysis will be based on exploiting various symmetries inherent in the active fluid systems, as well as the interplay between system symmetries and geometric properties of invariant manifolds. This analysis will also illuminate the minimum 'model ingredients' needed to program active nematics into various time-periodic (cyclic) states.

2. To verify the ECS hypothesis in the fully turbulent regime in simulations, as well as using existing data from various active nematic experimental studies. A key aim is to extract a deterministic dynamical skeleton of active turbulence and build reduced order models for prediction and control.

3.The third objective is to develop theoretical and computational machinery for incorporating a controller into the material itself. This type of embedded or 'endogenous' control is the defining feature of biological systems, where chemo-mechanical pathways orchestrate the dynamics of life at all scales. Motivating examples include morphogenesis, whereby feedback between chemical patterns and tissue structure leads to robust structure formation.

Recent Progress: We have partially resolved two major open questions related to the space-time structure of active turbulence in 2D channels [2]. In our prior work, we have computed a large

number of ECSs in the preturbulent regime. The open questions tackled in the current reporting period are:

1). **Can we provide conclusive evidence that the fate of arbitrary trajectories in active turbulence is strongly determined by the scaffolding provided by the ECSs and their connecting orbits**?
Using a combination of analytical arguments and computation, we have established a minimal flow unit (MFU) which is big enough to sustain active turbulence, but small enough so that a collection of about 10 ECSs is enough to qualitatively and quantitatively explain all observed behavior in the system. For this system, we showed that the active turbulent trajectory closely shadows the small set of the ECSs. To establish this shadowing, we showed that the trajectory and ECSs are close according to several metrics that measure trajectory similarity. The measures include computing pointwise distance in the underlying infinite dimensional space, as well as physically meaningful measures of channel-averaged kinetic energy, elastic energy and enstrophy.

A key result is that the ECS structure in the MFU system reveals the origin of **experimentally observed** persistent, but random reversals between the right and left flowing almost uniaxial flow in active nematic channel flows [4]. Our work has uncovered the deterministic skeleton underlying this intriguing behavior. In the MFU, we discovered that the dominating ECSs come in two types: the first type are symmetric copies similar to left and right flowing states, while the

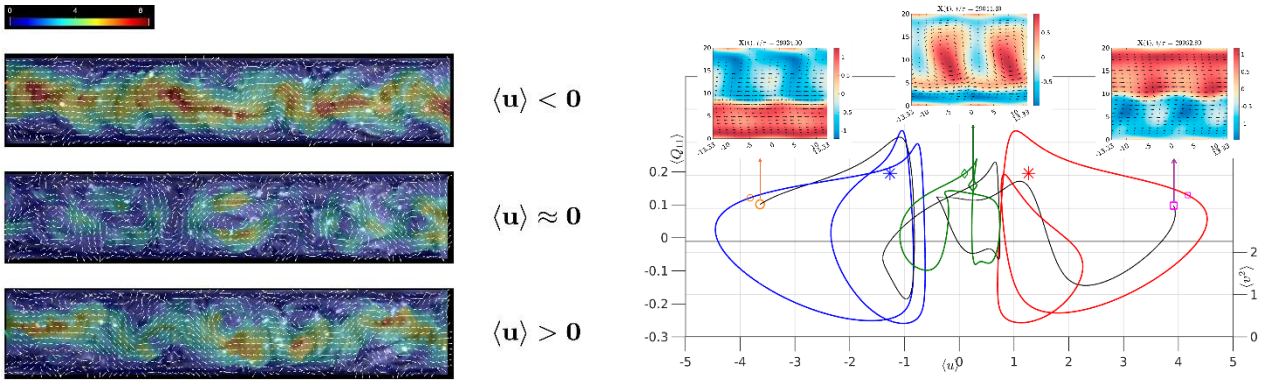


Fig. 1. (a) Velocity field snapshots from active nematic experiments of Doré [4] of a reversal event in a channel. The colormap shows the speed. The flow evolves from a left-flowing almost-uniaxial state (<u> < 0) to a right-flowing almost-uniaxial state (<u> >0) via an intermediate vortex-dominated configuration (<u> ~ 0) (b) Similar reversals in the model shown in reduced phase space in the active turbulent regime, primarily shadowing three ECSs. A segment of the turbulent trajectory is shown in black, while the shadowed left-flowing ECS is in blue, shadowed right-flowing ECS is shown in red, and the two-vortex ECS is shown in green.

second type are those similar to zero net- flow vortex dominated states. Our shadowing analysis conclusively shows that the transitions between the two symmetry related left and right flowing

states often pass close to the vortex dominated state, matching yet another another experimental observation.

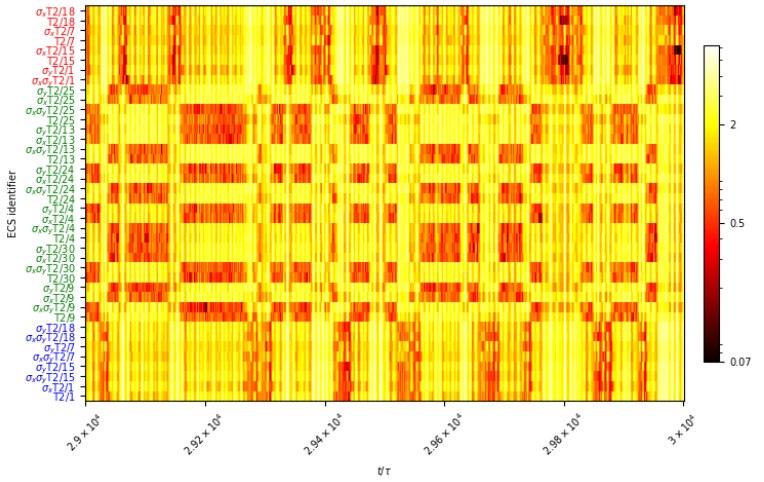


Fig. 2. Distance plot showing the closest encounters between the chaotic trajectory and the ten most relevant ECSs and their symmetry copies. The ECS list on the left follows the same color scheme as in Fig. 1. The plot shows a clear pattern of repeated transitions (i.e., reversals) between `left flowing' (blue) and 'right flowing' (red) ECSs, via the vortex-like (green) ECSs.

How are the ECSs computed in the turbulent regime related to those found in the preturbulent regime?

We use ideas from Equivariant bifurcation and group theory to provide a symmetry-based framework for predicting and organizing the collection of ECS in the preturbulent regime (Fig. 3), and provide strong evidence that the relevant ECSs found in the turbulent regime are slightly symmetry-broken descendants of those in the preturbulent regime. This is established using multiple measures, including a novel remanent symmetry analysis which provides a quantitative measure of the amount of broken symmetry. While it is prohibitive to compute all bifurcation branches from low activity to high activity turbulent regime, this result establishes the utility of cataloguing the preturbulent ECSs using the toolbox of symmetry and group theory. Equivariant bifurcation theory uses the base-state symmetry and its action on the kernel to predict the spatiotemporal symmetry-allowed bifurcating branches.

3). **Progress in control of active fluids**: Co-PI Norton contributed to the Brandeis/UCSB effort on developing a closed-loop control framework and its validation in experimental active nematics [7]. Additionally, the effect of topological defects in calcium signaling waves was investigated theoretically and experimentally in epithelial cells [8]. The main takeaway for control purposes is that nematic cell alignment has a significant impact on signaling waves, and hence, for bio-mimetic devices, optimal design/control of nematic orientation could be used to efficiently direct signals towards or away from targets.

Future work

Our main focus will be on exploiting and characterizing the low-dimensional structure uncovered in the MFU of active nematic channel flow. We will use the autoencoder neural-network architecture, in conjunction with knowledge of the symmetries of the underlying ECS, to learn a

minimal low-dimensional (<10 dimensions) ordinary differential equation (ODE) model for turbulent active nematic channel flow. The model will be capable of reproducing the turbulent statistics seen the full-order continuum/partial differential equation (PDE) model currently used by the community. The value of such models is not just in computational efficiency. Rather, such interpretable models can serve as testing grounds for complicated control strategies currently being designed by the community [5]. Furthermore, such models are amenable to techniques developed over the last five decades in the dynamical systems community and applied to inertial passive turbulent flows with great success [6].

We will design controllers to exploit the structure revealed by the ECSs and their connecting orbits in the MFU. Since we know that highly robust pathways exist between left and right flowing states, we will devise an inverse design methodology to find endogenous control (in form of reaction-diffusion PDEs as envisioned in our previous work [3]) that can couple with the active nematic system, and promote/suppress flow reversals.

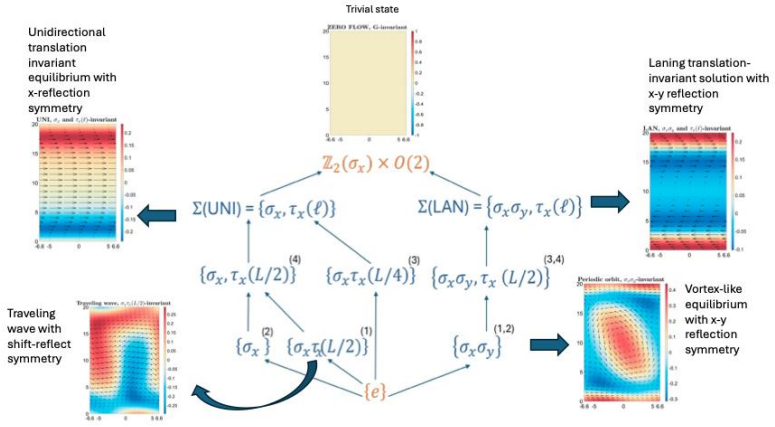


Fig. 3. Primary and secondary bifurcations from the trivial state in 2D active nematic channel flow, arranged using symmetry in a `isotropy lattice'. The primary bifurcations yield uniaxial (UNI) and laning (LAN) solutions. Superscripts indicate the order in which unstable eigenvalues appear for UNI and LAN with increasing activity. Arrows indicate subgroup inclusion. The secondary bifurcations result in a). traveling waves with shift-reflect symmetry and b). vortex-like states with x-y reflection symmetry, both eventually giving rise to defect-laden states. σ_x is x-reflection, σ_y is y-reflection and τ_x is x-translation. The ECS that are shadowed by turbulent trajectories can be traced back to these steady states via remnant symmetry analysis.

References

1. Graham, Michael D., and Daniel Floryan. "Exact coherent states and the nonlinear dynamics of wall-bounded turbulent flows." *Annual Review of Fluid Mechanics* 53.1 (2021): 227-253.
2. A Naranjo, R Pallock, C Wagner, and P Grover, Symmetry, Invariant Manifolds and Flow Reversals in Active Nematic Turbulence, *arXiv:2512.07047*, Dec. 2025 (Under review)
3. M. M. Norton, and P. Grover, Mechanochemical Topological Defects in an Active Nematic, *Phys. Rev. E* **110**, 054605 (2024)
4. Doré, Claire. Active nematic films under confinement: harnessing topological defects, shaping active flows and designing autonomous microfluidic machines. Ph.D. thesis, Université Paris sciences et lettres, 2022.5
5. Alvarado, José, et al. "Optimal control in soft and active matter." *Annual Review of Condensed Matter Physics* 17 (2026).
6. Holmes, Philip. *Turbulence, coherent structures, dynamical systems and symmetry*. Cambridge university press, 2012.
7. Nishiyama, Katsu; Berezney, John; Norton, Michael M.; Aggarwal, Akshit; Ghosh, Saptorshi, et al., "Closed-loop control of active nematic flows", *Physical Review X*, Volume 15, 2025
8. Chardac, Amelie; Norton, Michael M.; Touboul, Jonathan; Duclos, Guillaume, "3D pattern formation of a protein–membrane suspension", *Proceedings of the National Academy of Sciences*, Volume 122, 2025

Publications (last 2 years)

1. A Naranjo, R Pallock, C Wagner, and P Grover, Symmetry, Invariant Manifolds and Flow Reversals in Active Nematic Turbulence, *arXiv:2512.07047*, Dec. 2025 (Under review)
2. M. M. Norton, and P. Grover, Mechanochemical Topological Defects in an Active Nematic, *Phys. Rev. E* **110**, 054605 (2024)
3. Nishiyama, Katsu; Berezney, John; Norton, Michael M.; Aggarwal, Akshit; Ghosh, Saptorshi, et al., "Closed-loop control of active nematic flows", *Physical Review X*, Volume 15, 2025
4. Chardac, Amelie; Norton, Michael M.; Touboul, Jonathan; Duclos, Guillaume, "3D pattern formation of a protein–membrane suspension", *Proceedings of the National Academy of Sciences*, Volume 122, 2025

Combining machine learning and feedback control to understand and manipulate active matter

Michael F. **Hagan**, Brandeis University
Seth Fraden, Brandeis University
Pengyu Hong, Brandeis University
Zvonimir Dogic, University of California Santa Barbara

Keywords: Active matter, machine learning, data-driven methods, optimal control, deep learning

Research Scope: We aim to bridge the gap between active and living matter by implementing external control that stabilizes a target dynamics, through two objectives. In Objective 1, we use optically responsive microtubule-based active fluids and real-time feedback to generate prescribed patterns of active stresses and flows. In Objective 2, we use these active flows to assemble actin filaments into elastic membranes, extending the concept of self-assembly to non-equilibrium active suspensions. Driven by the enveloping active fluids, the membranes exhibit in-plane and out-of-plane driven deformations that lead to system-sized spontaneous oscillations. We then control the active fluid flows to imprint designable strains into a membrane, which in turn drives its folding into prescribed 3D shapes, a key structural motif of biological morphogenesis.

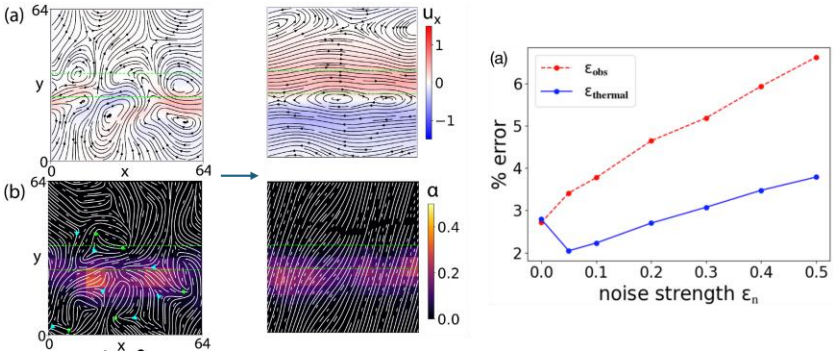


Fig. 1. Model-free reinforcement learning (RL) control of active nematics. Results are shown for a target state that mimics coherent flow of specified magnitude through a channel, without any confining walls. (a,b) The initial and final (a) velocity profiles and (b) director field (lines) and activity profile (color map). (c) The error in the final state as a function of intrinsic ($\epsilon_{\text{thermal}}$) or measurement ($\epsilon_{\text{obs}}$) noise.

Recent Progress: (1) Development of control frameworks for active materials. Hagan performed extensive testing and development on 2D active nematics to establish frameworks for optimal control theory and reinforcement learning (RL) to drive active materials into exhibiting desired behaviors [1]. He showed that optimal control theory can be used to drive active materials into arbitrary states, including those that are not attractors in the absence of control. Hagan and Hong then developed an RL framework that, once trained, can drive the system into target states from arbitrary initial conditions. Notably, the RL framework is exceptionally robust to experimental noise and measurement error (**Fig. 1**). Furthermore, Hagan and Hong identified key limitations in conventional RL approaches that are accentuated by the high dimensionality of our observation space (the director and velocity fields) and action space (the spatiotemporal activity field). With such high-dimensionality, typical RL algorithms are sample-inefficient (and thus require long training times) due to the exploration–exploitation tradeoff: the

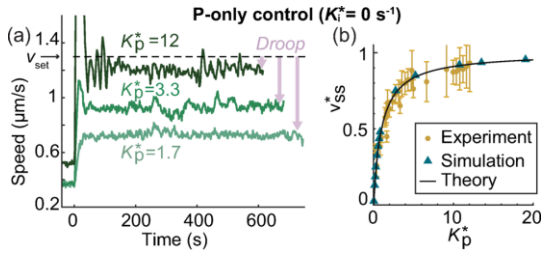


Fig. 2: Proportional-Integral (PI) control of light-activated 2D active nematics in experiments and simulations. The plot shows that P-only control leads to droop, which is captured by simulations and theory.

agent must explore a large action space to discover effective control policies. To overcome this dimensionality bottleneck, we developed β-variational autoencoders (β-VAEs) that compress the inputs into low-dimensional latent representations, and we have initiated model-based RL methods that leverage these latent spaces to achieve more efficient and predictive control. Together, these advances significantly reduce computational cost, enable large-scale RL training, and lay the foundation for data-driven closed-loop control of 3D active materials.

(2) Proportional-Integral (PI) control of 2D active nematics in experiments and theory: as a first step toward implementing control protocols in experiments, **Fraden** and **Dogic** developed an experimental platform that combines optically responsive MT-based nematics with video microscopy and our ML tools to measure spatially averaged speeds in real time and, using PI feedback, adjust the applied light intensity to drive the system toward a target speed. With this approach, **Fraden**, **Dogic,** and **Hagan** demonstrated stabilization of flows in active nematics against external and internal perturbations, including temperature changes, biomolecular degradation, protein aggregation, and sample-to-sample variability. By combining theory and simulation with the experimental observations, we uncovered and understood features such as droop and nontrivial behaviors that arise during control of an active material, such as induced oscillations. (**Fig. 2**) [2].

(3) Control of 3D isotropic fluids in bulk: We extended the suite of theoretical and experimental tools to advance a quantitative model of active isotropic fluids [3]. Experiments showed that optically responsive microtubule-based active fluids develop density contrast when illuminated with a sinusoidally varying activity pattern (**Fig. 3a**). The density contrast depends on the wavelength of spatial modulation. An improvement of a well-established theoretical model of active fluids, which accounts for the isotropic active pressure term, quantitatively explains the experimental data (**Fig. 3b**). Complementary experiments/numerical work and particle-based simulations revealed universal aspects of compressible active isotropic fluids.

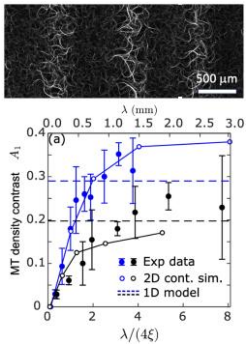


Fig. 3: Controlling the circulation of bulk 3D isotropic active fluids. (top) A sinusoidal activity pattern generates a density contrast of MTs. (bottom) The density contrast depends on the pattern wavelength. A new theoretical model explains the experimental data.

(4) Control of 3D isotropic fluids in circular confinement: Hagan, Dogic, and Fraden are combining experiments, theory, and machine learning to control the active isotropic system in 3D disk and annulus geometries. Previous work showed that this system undergoes spontaneous coherent circulation when the aspect ratio (height/radius) of

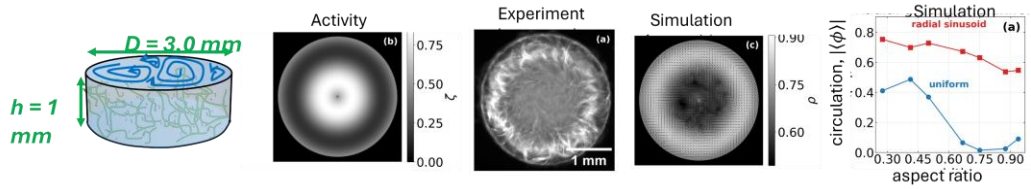


Fig. 4: Controlling circulation of confined 3D isotropic active fluids. (a) Chamber geometry. (b-d) A radially varying activity profile (b) leads changes circulation and density profile in experiments (c) and simulations (d). (e) Simulation results showing that radial profiles lead to higher circulation then uniform activity.

the container is approximately 1, but exhibits incoherent turbulence for asymmetric aspect ratios. We are developing protocols to control the existence and speed of circulation, including achieving circulation in more asymmetric aspect ratios. First, we performed extensive experimental work to identify confinement materials and surface treatments that avoid surface aggregation of the optogenetic motors and microtubules, and robustly achieved circulation under uniform activity for aspect ratios near 1. We then showed that we can change the system density and circulation by imposing nonuniform light profiles (**Fig. 4**). At the same time, we used the new theoretical model (see **Fig. 3b**) with our GPU-enabled in-house solver to simulate the system; the results closely match the experimental observations (**Fig. 4**). Notably, simulations predict that radial variations of activity increase circulation, and allow for circulation over a wider range of aspect ratios compared to uniform activity. The next step is to identify optimal spatiotemporal activity profiles using optimal control and RL.

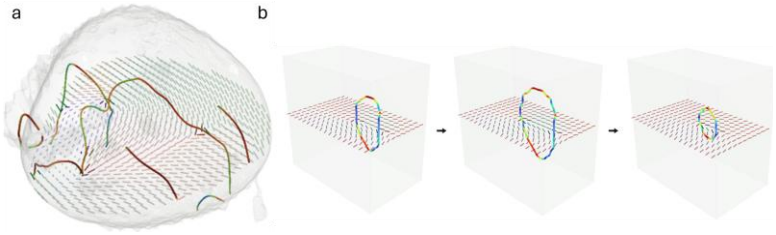


Fig. 5: Controlling disclination loops in 3D active nematics. (a) 3D disclination lines observed in an active droplet extracted from the holographic tomography technique. (b) Simulation of controlling the number (set to 1) and size (varying over time) of disclination loops in a channel. The arrows show the director field near the loop.

(5) Controlling 3D active nematics in experiments and simulations. We significantly advanced our ability to develop and characterize 3D active nematic fluids. We developed a tomographic optical microscopy method that can measure the isotropic dielectric tensor of 3D liquid crystalline samples at about 30 fps, about two orders of magnitude faster than our previous capabilities. This enables studying the dynamics and structure of disclination lines of 3D active nematics, a prerequisite to control them. In particular, we have confined active nematics in deformable droplets and are investigating how active stresses and motile disclination lines couple to the surface deformations (**Fig. 5a**). In parallel, Hagan has

combined control theory, simulation, and his recently developed theoretical analysis of disclination lines or loops in 3D active nematics [4] to control the number and size of disclination lines. In a first step, we simulated a 3D active nematic in a channel using our in-house PDE solver, and implemented feedback control in which the applied activity level is varied based on the number and sizes of disclinations in the simulation (**Fig. 5b**).

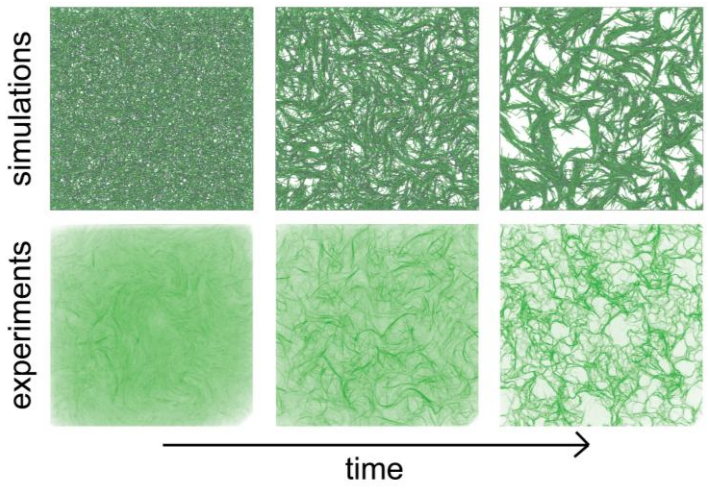


Fig. 6: Active assembly of passive filaments in experiments and simulations. Actin filaments embedded in an MT-based active fluid assemble into a system-spanning network with properties that depend on factors such as cross-linker density.

(6) Controlling the assembly and dynamics of elastic filaments and membranes. We are using the chaotic flows of the active microtubule fluid to assemble fiber-based membranes with tunable architectures that are not realizable using assembly methods that use thermal noise. Once the active flows assemble an active membrane, they continue to actuate non-equilibrium strain fluctuations. For certain molecular parameters, the finite-ranged active drive induces a long-ranged response of the passive elastic network. Over time, such cascading dynamics can generate macroscopic autonomous oscillations [5]. In another regime, the filaments assemble system spanning aggregates that exhibit highly collective motion (**Fig. 6 top**). Inspired by these experiments, Hagan developed a novel method to simulate active fluids via spatiotemporally correlated noise, enabling large-scale simulations of active composite materials [6]. We are applying this method to model the above-described active assembly of actin filaments, to understand the assembly dynamics and the factors that control assembly geometry, velocity, and mechanics (**Fig. 6 bottom**). These observations help explain Dogic's observation of the large-scale collective motion of crosslinked actin filament networks embedded in an active bath, and provide a starting point to developing a theoretical model and training machine learning techniques.

Future Plans: 3D isotropic fluids in bulk: We will better match the theory to experiments by adding nonlinear terms that account for relaxation timescales apparent in the traveling sinewave experiments. We will experimentally implement the first control goal – coherent flow through a "channel" in the center of the chamber – with a protocol computed from optimal control theory. Then we will pursue the same goal using reinforcement learning. 3D isotropic fluids in confinement: We will implement the first control goal – controlling the magnitude and direction of circulation in disks – using optimal control theory and then reinforcement learning. 3D Active nematics: we will experimentally implement control of the number and size of defect loops. Simultaneously, we will extend the theoretical model to account for deformability of the enclosing vesicle. Elastic filaments and membranes: We will complete parameterizing the computational

model to describe the existing experimental data on filament assembly. We will then use a machine learning approach to control the porosity of the assembling filament network, and test this experimentally. In the regime where the system forms membranes, we will compute protocols to control membrane bending fluctuations and oscillations.

References

1. Ghosh, S., A. Aggarwal, P.N. Tran, A. Baskaran, P. Hong, and M.F. Hagan, *Model free control of active nematics using reinforcement learning*. 2026: Manuscript in preparation.
2. Nishiyama, K., J. Berezney, M.M. Norton, A. Aggarwal, S. Ghosh, Z. Zarei, M.F. Hagan, S. Fraden, and Z. Dogic, *Closed-loop control of active nematic flows.* Physical Review X, 2025. **15**(4): p. 041053.
3. Cheng, Y.-C., D. Krommydas, R.L. Rosales-Hasek, S. Shin, P. Gulati, M.F. Hagan, A. Baskaran, C.M. Marchetti, and Z. Dogic, *Spatial Control of Compressible Active Fluids.* 2026.
4. Ma, Y., C. Amey, A. Baskaran, and M.F. Hagan, *Mechanics of disclination emergence in three-dimensional active nematics.* Physical Review Research, 2026. **8**(2).
5. Berezney, J., S. Ray, I. Kolvin, F. Brauns, S. Chen, M. Bowick, S. Fraden, V. Vitelli, and Z. Dogic, *Active assembly and non-reciprocal dynamics of elastic membranes.* Nature Physics, 2026. **22**(4): p. 604-611.
6. Frechette, L.B., A. Baskaran, and M.F. Hagan, *Active-noise-induced dynamic clustering of passive colloidal particles.* Newton, 2025. **1**(7).

Publications

1. Ghosh, S., A. Aggarwal, P.N. Tran, A. Baskaran, P. Hong, and M.F. Hagan, *Model free control of active nematics using reinforcement learning*. 2026: Manuscript in preparation.
2. Ray, S., N. Tavakolian, R. Sweeney, and Z. Dogic, *Controlling fiber network structure and dynamics with active fluid.* 2026.
3. Cheng, Y.-C., D. Krommydas, R.L. Rosales-Hasek, S. Shin, P. Gulati, M.F. Hagan, A. Baskaran, C.M. Marchetti, and Z. Dogic, *Spatial Control of Compressible Active Fluids.* 2026.
4. Nishiyama, K., J. Berezney, M.M. Norton, A. Aggarwal, S. Ghosh, Z. Zarei, M.F. Hagan, S. Fraden, and Z. Dogic, *Closed-loop control of active nematic flows.* Physical Review X, 2025. **15**(4): p. 041053.
5. Choi, K.H., S. Ray, R. Sweeney, Z. Dogic, and S. Takatori, *Mechanics of heterogeneous fiber networks.* arXiv preprint arXiv:2605.11342, 2026.
6. Berezney, J., S. Ray, I. Kolvin, F. Brauns, S. Chen, M. Bowick, S. Fraden, V. Vitelli, and Z. Dogic, *Active assembly and non-reciprocal dynamics of elastic membranes.* Nature Physics, 2026. **22**(4): p. 604-611.
7. Ghosh, S., A. Baskaran, and M.F. Hagan, *Achieving designed texture and flows in bulk active nematics using optimal control theory.* The Journal of chemical physics, 2025. **162**(13).
8. Frechette, L.B., A. Baskaran, and M.F. Hagan, *Active-noise-induced dynamic clustering of passive colloidal particles.* Newton, 2025. **1**(7).
9. Ghosh, S., C. Joshi, A. Baskaran, and M.F. Hagan, *Spatiotemporal control of structure and dynamics in a polar active fluid.* Soft Matter, 2024. **20**(35): p. 7059-7071.
10. Tran, P.N., S. Ray, L. Lemma, Y. Li, R. Sweeney, A. Baskaran, Z. Dogic, P. Hong, and M.F. Hagan, *Deep-learning optical flow for measuring velocity fields from experimental data.* Soft Matter, 2024. **20**: p. 7246–7257.
11. Zarei, Z., J. Berezney, A. Hensley, L. Lemma, N. Senbil, Z. Dogic, and S. Fraden, *Light-activated microtubule-based two-dimensional active nematic.* Soft matter, 2023. **19**(35): p. 6691–6699-6691–6699.
12. Li, Y., Z. Zarei, P.N. Tran, Y. Wang, A. Baskaran, S. Fraden, M.F. Hagan, and P. Hong, *A machine learning approach to robustly determine director fields and analyze defects in active nematics.* Soft Matter, 2024. **20**(8): p. 1869-1883.
13. Lemma, L.M., M. Varghese, T.D. Ross, M. Thomson, A. Baskaran, and Z. Dogic, *Spatio-temporal patterning of extensile active stresses in microtubule-based active fluids.* PNAS Nexus, 2023. **2**(5).

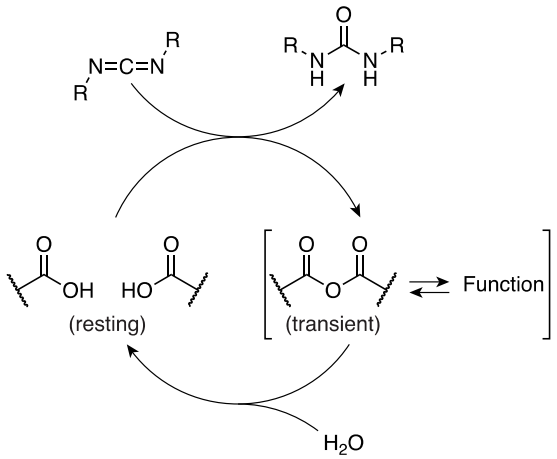
Chemically fueled dissipative assembly of complex molecular architectures

C. Scott **Hartley** and Dominik Konkolewicz, Department of Chemistry and Biochemistry, Miami University

Keywords: Nonequilibrium, carbodiimides, polymer networks, self-assembly, systems chemistry

Research Scope

Many of the remarkable behaviors of biological materials, such as actuation, self-healing, and replication, derive from complex networks of chemical reactions that operate out of equilibrium. In many cases, these systems are driven by the hydrolysis of ATP, which acts as a chemical "fuel". Inspired by nature's example, abiotic reaction networks based on the same principles are currently being developed, yielding materials and molecular machines with time-dependent behavior.[1]



Scheme 1. Treatment of aqueous carboxylic acids with carbodiimides gives transient anhydrides.

Controlling reaction rates within a network is challenging; thus, it is important to develop fuel reactions that can be used broadly. The hydration of carbodiimides is among the most versatile of the abiotic fuel reactions developed so far. In its simplest form, shown in Scheme 1, carbodiimides couple aqueous carboxylic acids to anhydrides, resulting in a transient covalent bond. This simple chemistry has been applied to a wide range of functional systems, from molecular motors to responsive polymer materials.

The goal of this project to control out-of-equilibrium chemical reaction networks and to exploit them in the design of new functional materials. We currently have three Specific Aims: (1) to control the rates of anhydride formation, hydrolysis, and exchange in nonequilibrium systems; (2) to develop polymer network hydrogels with both persistent and transient dynamic bonding; and (3) to couple fuel chemistry to phase transitions in materials for amplified responses.

Recent Progress

Controlling anhydride formation, hydrolysis, and exchange. Controlling the rate of deactivation, or anhydride hydrolysis, in carbodiimide-driven reaction networks is critical for regulating out-of-equilibrium behavior, especially transient property lifetimes in materials. We recently investigated how pyridine derivatives with varying nucleophilicity (pyridine, 4-methylpyridine, 4-methoxypyridine, and DMAP) can be used as catalysts to control this step.[2] Kinetic modeling revealed that while the rate of pyridine attack on the anhydride follows expected nucleophilicity

trends, this effect is offset by the increased protonation of the more nucleophilic pyridines at typical operating pHs. Further, we made the unanticipated discovery that the most commonly used carbodiimide fuel itself, EDC, and its urea byproduct, EDU, are not passive participants; their tertiary ammonium groups catalyze and accelerate anhydride hydrolysis. This work provides a valuable framework for fine-tuning the kinetics of carbodiimide-fueled reaction networks by carefully balancing the nucleophilicity and basicity of the chosen catalyst at a given pH.

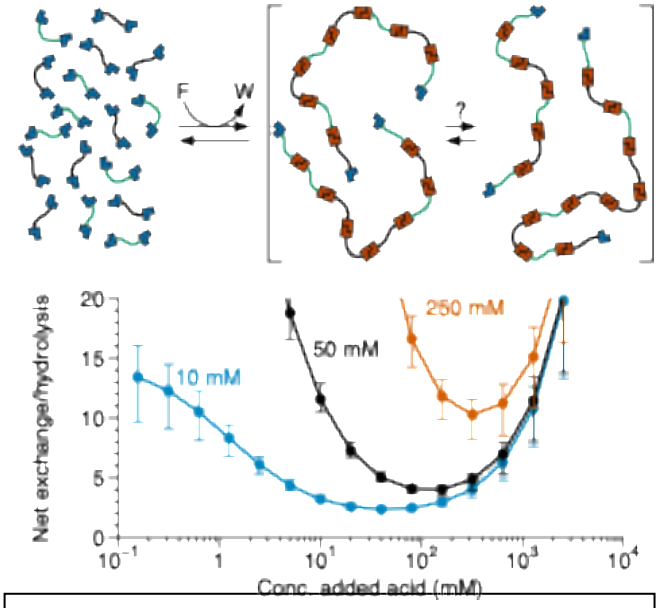


Figure 1. Top: Exchange in a transiently generated polymer. Bottom: Ratios of exchange to hydrolysis for varying concentrations of an anhydride model treated with a rapidly hydrolyzing additive.

We have also built on previous work on chemically driven polymerization to measure the extent to which anhydride bonds dynamically exchange in the transient state, an underappreciated feature of these networks. We used ^{13}C NMR spectroscopy to quantify concentrations in both small molecule and polymer models. We discovered that, under typical conditions, bond exchange is frequent relative to hydrolysis. For instance, introducing a different carboxylic acid to an already-assembled system results in the rapid formation of mixed anhydrides, suggesting that there are multiple exchange events for each hydrolysis, as illustrated in Figure 1. This rapid exchange dictates what can be achieved in out-of-equilibrium design: while it prevents the use of kinetic control to program sequence (because the polymers are scrambled), it can be exploited to generate closed architectures, such as macrocycles, through self-correction mechanisms analogous to those used in thermodynamically controlled self-assembly.

Related to this work, we have completed an additional study on transient covalent polymerization that explores structure–property effects in these systems. These results will provide useful guidelines as we continue to use this system as a general model for nonequilibrium self-assembly.

Materials with transient and persistent dynamic bonding. We recently developed self-healing polymer hydrogels that integrate persistent dynamic metal–ligand coordination with transient, carbodiimide-generated anhydride crosslinks. Initially, we used terpyridine (tPy) ligands coordinated with varying divalent metals (Fe^{2+}, Ni^{2+}, Co^{2+}, Zn^{2+}, Cu^{2+}) to dictate the resting-state stiffness and long-term recovery of the materials.[3] When fueled with EDC, these networks exhibit a temporary, independent boost in mechanical properties as transient anhydrides form.

Building upon this, we have developed a next-generation system using bis(pyridin-2-ylmethyl)amine (DPA) ligands, which allow us to systematically tune coordination strength via

electron-withdrawing (chloro) or electron-donating (methoxy) substituents. Further, replacing aliphatic acrylic acid with aromatic benzoic acid monomers extends the lifetime of the transiently reinforced state by slowing down the rate of anhydride hydrolysis. Unlike the orthogonal behavior observed in the tPy system, the DPA-based networks show synergy between the two dynamic bond types. As shown in Figure 2, the EDC-treated samples exhibit faster healing to the same final end point. Notably, this is not just an effect of reinforcement through additional transient crosslinks. At 15 h, all of the anhydrides have hydrolyzed, and yet the material retains its superior mechanical properties.

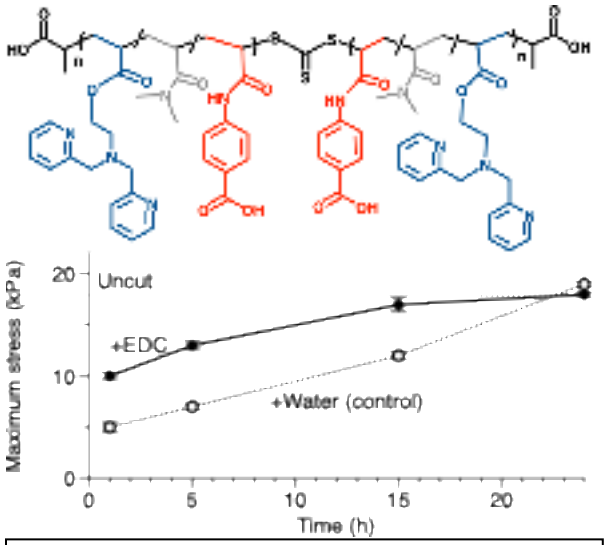


Figure 2. Self-healing of poly(DMAm$_{288}$-BA$_{80}$-DPA$_{32}$) crosslinked with Fe^{2+}.

An advantage of the DPA-based materials is that the monomers are much easier to synthesize, which has allowed us to build a library of materials with varying metal ion, acid structure, chain length, and network architecture. The library can be screened for interesting mechanical properties in the resting and transient states. To take advantage of this efficiency, we have developed a robotic mechanical tester that allows high-throughput screening of materials, with interesting cases then selected for full characterization. We have carried out our preliminary testing of 144 materials and are currently working to fully characterize the materials of interest.

Coupling phase changes to fuel chemistry. A current challenge for the field is translating chemical changes driven by fuel chemistry into large-scale effects on macroscopic properties. We are exploring whether carbodiimide chemistry can be coupled to phase changes, specifically the LCST of poly(NiPAm). Our hypothesis is that treatment of suitable hydrogels with the carbodiimide will trigger the phase transition as hydrophilic carboxylates are converted to hydrophobic anhydrides. This should cause the material to expel water and shrink before returning to its resting state as the anhydrides hydrolyze. We have found that the addition of carbodiimide does decrease the LCST of copolymers of NiPAm and maleic acid. In the example in Figure 3, the LCST of the starting polymer is 27 °C. Treatment with EDC lowers it, causing the polymer to temporarily aggregate so long as the temperature is between the LCSTs

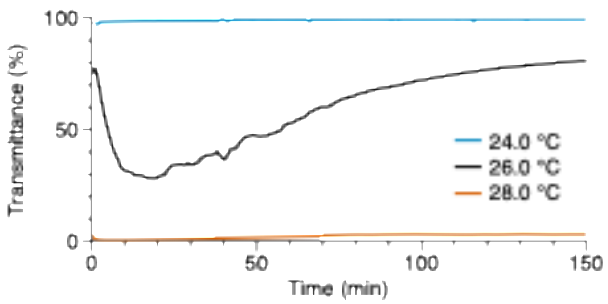


Figure 3. Transmittance vs time for NiPAm and maleic acid copolymers after treatment with carbodiimide, showing that at 26 °C the polymer undergoes transient aggregation.

of the two states. We are currently adapting this chemistry to hydrogel polymer networks that should undergo shape changes through this process.

Other work. In addition to the work described above, we also produced a review on nonequilibrium polymer materials and developed a precursor polymer that only undergoes carbodiimide-driven crosslinking after photochemical activation.

Future Plans

Controlling anhydride formation, hydrolysis, and exchange. We have largely completed the work for this aim, but we have learned a lot about the importance of exchange in nonequilibrium reaction networks. We are currently working to design new systems that would be expected to minimize exchange reactions compared to the polyanhydrides.

Materials with transient and persistent dynamic bonding. There are several directions for these materials that are being pursued. First, the ready availability of the DPA ligands makes it possible to explore a wider variety of network architectures. We are particularly interested in investigating telechelic materials, where the metal–ligand bonding is in the polymer main chain instead of in randomly distributed pendant crosslinks. These materials are expected to exhibit improved mechanical properties through better controlled networks of persistent crosslinks.

We are also investigating the DPA-containing materials as pluripotent materials, that is, materials with multiple distinct functions. The DPA ligands are basic (Figure 2), and thus the metal–ligand exchange chemistry should be pH-sensitive. We are interested in taking advantage of transient acid fuel chemistry[4] to temporarily activate self-healing in these materials, addressing the fundamental tradeoff between healing and creep in dynamic materials. Current results have shown that the gels are is indeed sensitive to pH, and we are optimizing the chemistry to work with transient acids.

A new direction for the project is to create materials with multiple dynamic chemistries that are both controllable through external stimuli. Accordingly, we are combining the fuel-driven transient anhydride chemistry with photochemical dynamic covalent disulfide chemistry.

References

1. L. S. Kariyawasam, M. M. Hossain, and C. S. Hartley, *The transient covalent bond in abiotic nonequilibrium systems*, Angew. Chem., Int. Ed. **60**, 12648–12658 (2021).
2. R. Baral, J. V. Gunn, and C. S. Hartley, *Pyridine catalysis of anhydride hydrolysis within carbodiimide-driven reaction networks*, ChemSystemsChem **8**, e00042 (2025).
3. C. W. H. Rajawasam, N. K. Saha, C. Tran, S. M. Costantino, M. Weeks, K. McCoy, J. L. Sparks, C. S. Hartley, and D. Konkolewicz, *Programmable hydrogels by combining persistent and transient dynamic bonds*, Chem. Eng. J. **534**, 174743 (2026).
4. D. Del Giudice and S. Di Stefano, *Dissipative systems driven by the decarboxylation of activated carboxylic acids*, Acc. Chem. Res. **56**, 889–899 (2023).

Publications

1. W. S. Salvia, G. Mantel, N. K. Saha, C. W. H. Rajawasam, D. Konkolewicz, and C. S. Hartley, *Controlling carbodiimide-driven reaction networks through the reversible formation of pyridine adducts*, Chem. Commun. **60**, 12876–12879 (2024).
2. I. O. Raji, T. C. Wilcox, C. S. Hartley, and D. Konkolewicz, *Photoresponsive polymers for carbodiimide-fueled transient hydrogels*, Polym. Chem. **16**, 947–953 (2025).
3. C. W. H. Rajawasam, D. Konkolewicz, and C. S. Hartley, *Autonomous changes in polymer materials driven by chemical fuels*, ChemSystemsChem **7**, e202400090 (2025).
4. R. Baral, J. V. Gunn, and C. S. Hartley, *Pyridine catalysis of anhydride hydrolysis within carbodiimide-driven reaction networks*, ChemSystemsChem **8**, e00042 (2025).
5. C. W. H. Rajawasam, N. K. Saha, C. Tran, S. M. Costantino, M. Weeks, K. McCoy, J. L. Sparks, C. S. Hartley, and D. Konkolewicz, *Programmable hydrogels by combining persistent and transient dynamic bonds*, Chem. Eng. J. **534**, 174743 (2026).

Chaos, Mixing, and Energy Extraction in Active Nematics

Linda S **Hirst** and Kevin Mitchell, University of California, Merced

Zvonimir Dogic and Cristina Marchetti, University of California, Santa Barbara

Keywords: Active nematic, biomolecular motors, chaotic advection

Research Scope

The objective of this project is to control chaos and mixing in active materials, using a combination of experiment, simulation, and theory. Active materials are a new paradigm in soft condensed matter physics. Nature provides many examples, from flocks of birds to sheets of cells and swarms of bacteria and in the lab, biomimetic active materials include self-propelled colloids and dense phases of biopolymers driven by molecular motors. Although they are non-living, these active materials share the non-equilibrium property of living matter, consuming energy to maintain their complex structures. As such materials do not fit the framework of conventional thermodynamics, their study requires new perspectives and techniques. This project focuses on active nematics, a class of active materials consisting of small rod-like subunits that tend to locally align with one another. We study a prototype biomolecular active nematic composed of kinesin molecular motors and microtubules. The motors consume energy and generate self-sustained flows. These active nematics represent a new class of fluids that exhibit spontaneous, self-driven mixing and in this collaborative project we aim to inject a new perspective into the current understanding of active nematics by uniting concepts from fluid dynamics, chaos theory, and the mathematics of braids.

The two main aims of the project are to

1. Investigate and control the self-mixing dynamics of active nematics by engineering the boundaries of wells and via the insertion of motile microparticles.

2. Connect a form of entropy for the active nematics to the amount of work that can be extracted from the system.

We approach both of these aims in tandem using a synergistic combination of experiment and simulation. We have developed new mathematical models for the experiments, and are testing new simulations based on this new model, designed to guide experimental plans and be used to interpret new experimental results.

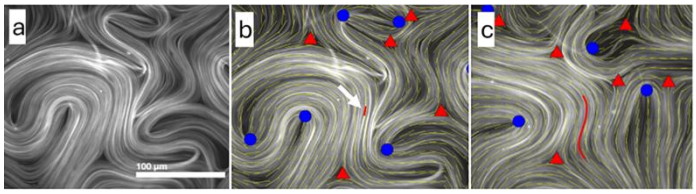
Compared to the long-established field of equilibrium materials, the field of active matter is still rapidly evolving, dominated by just a few materials. With this project we hope to spur interest in new synthetic materials using the principles of active nematics to drive self-mixing flows. Control of these self-mixing flows is the next step to achieve a useful new class of solvents. Such solvents

might revolutionize micro-mixing technologies and produce novel biomimetic mixing environments.

Recent Progress

The experiments in this project use microtubule-based active nematics, that create spontaneous motion via kinesin molecular motors. Using microfluidic techniques to place the material at a 2D oil-water interface, and imaging the resultant nematic order with fluorescence microscopy. The nematic order breaks down at localized points called topological defects. ATP fuel produces extensile motion of the microtubules causing the nematic material to flow chaotically. The topological defects are created and annihilated in pairs, dancing around one another forming a braid in space-time. The material can be confined in wells of various geometries, dramatically influencing defect dynamics. In a recent paper by Hirst and Mitchell [1] we investigated active nematic flows confined to cardioid shaped wells, finding spontaneous mixing in the *golden-braid* – an optimal mixing pattern. Various microprinted particles and shapes can also be inserted, both affecting and responding to the fluid flow. Micro-gears can be placed within the fluid to extract work and potentially perform useful functions and in this project we leverage a platform designed by our collaborators to achieve this set-up [2].

In this project four research groups are working collaboratively. **Hirst**, and experimentalist and **Mitchell** a theorist – both in the UCM Physics Department – are partnered with **Dogic** (experiment) and **Marchetti** (theory) both in the physics Department at UCSB.



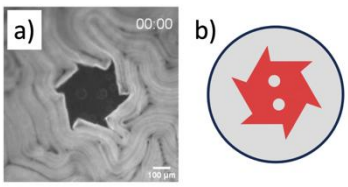
We model microtubule-based active nematics based on the foundational idea that an initial curve following the director field must continue to follow the director field as it evolves. The resulting model shows improved agreement with experiment. a)fluorescence microscope image of active nematic from the Dogic lab, b) The director field is overlayed as yellow segments. Topological defects in the director field are shown as blue circles (+1/2) and red triangles (−1/2). A segment of a bright nematic contour is shown in red and indicated by the white arrow. (c) The active nematic at a later time showing the advected red curve, which clearly remains a nematic contour.

Nematic locking. Although numerous theoretical studies have modeled microtubule-based active nematics, no consensus has emerged on how to fully and quantitatively capture the features of the experimental system. To better understand the theoretical foundations for modeling this system, we have proposed a fundamental principle we call the nematic locking principle—individual microtubules cannot rotate without all neighboring microtubules also rotating. Physically, this is justified by the high density of the microtubules, their elongated nature, and their corresponding steric interactions. We assert that the nematic locking principle holds throughout the majority of the material, but breaks down in the neighborhood of topological defects and other regions of low density. In a new publication lead by Mitchell [3] and UCM grad student Mainul Sabbir and in collaboration with the Dogic lab, a general nematic transport equation, consistent with this principle is derived. We

compare our results with a standard Beris–Edwards approach, commonly used to model this system, to show that it violates the nematic locking principle throughout the majority of the material. Our group proposed a modification to the Beris–Edwards model that enforces nematic locking nearly everywhere. This modification shuts off fracturing except in regions where the order parameter (a proxy for density) is reduced. Simulations show strong nematic locking throughout the bulk of the material, with narrow bands of fracturing, consistent with experimental observation. The new model also eliminates nontrivial stationary state solutions, common in Beris–Edwards simulations but not seen in experiments.

Modeling of inclusions and complex boundaries. An important step has been to successfully modify the theory of active nematics to allow for density variations in the material. This is critical because inclusions create voids in the active material. This new theory of active nematics with density variations is a first principles rethinking of how microtubule-based active nematics should be modified and is an important theoretical advance in its own right. Recently we have successfully implemented walls that bound the active material into, e.g. a disk-shaped region. These walls are soft walls rather than a strict boundary condition. They are achieved by imposing a steep potential energy function on the active material to exclude them from the boundary. We will continue these efforts to design a versatile simulation platform for modeling inclusions in active flows under geometrical confinement.

Training and collaboration wtih UCSB. In addition to the new theory work we have published this year [3,4], an important first phase of the project has been to focus on skill building for two early-stage graduate students at UCM. These students have benefited from working with the Dogic and Marchetti groups at UCSB – our partner in the project. Regular collaborative meetings on Zoom and visits to Santa Barbara by the UCM team have created key skill building opportunities for the UCM students. Sabera Borno Mustary, a second year PhD student in the Hirst lab at UCM spent two weeks at UCSB with the Dogic lab intensively learning methods to prepare active nematics in a configuration suitable for the proposed experiments using inclusions. These methods include formation of 2D and 3D active nematics, two-color sparse labeling (a technique developed in the Dogic lab essential for accurate analysis of the velocity field) and imaging, handling and insertion of gears and small inclusions.



(a) Chiral gear in active nematic from [2], (b) chiral gear confined to a circular well.

Future Plans

A key next step in this project will be for theory student, Sean Ricarte at UCM to develop numerical methods and accompanying Python code to model the motion of inclusions, i.e. small objects, embedded in the active nematic. This will complement the experimental work in the Hirst lab of placing similar inclusions, such as disks or microgears, into the active nematic. This will

create a close synergy between the experimental and theoretical groups' work. To model an inclusion, we will first turn the exterior boundary wall into an internal wall, e.g. bounding an inner solid disk. This step is easy to do. The second step requires allowing the boundary to translate and rotate. To find the force and torque acting on the boundary, we will simply use Newton's third law. Since we already know the force that is active on the active nematic, we can simply use the opposite force acting on the inclusion. Once we can successfully model a single inclusion, we can introduce multiple inclusions (with repulsive potentials to prevent them from overlapping). The dynamics of multiple inclusions embedded in the active material will be an entirely new system to study, as the inclusions themselves will be propelled by the active material. We can also study the impact of the inclusions on the mixing of active nematics, such as the impact on the topological entropy and Lypaunov exponent.

A next step for the experimental side of the project will focus on the work of Sabera Borno Mustary in the Hirst lab at UCM. Borno is collecting data on gear motion in the active nematic using gears fabricated in the Dogic lab at UCSB. A second objective will be to construct a magnetic field apparatus designed to hold the gears under a known force in the active flow, to the rotate and stir the active nematic. These experiments will feed into the theoretical results from the Mitchell lab on work and energy extraction in the active fluid.

References

1. F. L. Memarian, D. Hammar, M. M. H. Sabbir, M. Elias, K. A. Mitchell and L. S. Hirst. *Controlling Chaos: Periodic Defect Braiding in Active Nematics Confined to a Cardioid*, Phys. Rev. Lett. 132, 228301 (2024).
2. S. Ray, J. Zhang and Z. Dogic, *Rectified Rotational Dynamics of Mobile Inclusions in Two-Dimensional Active Nematics* Phys. Rev. Lett. 130 238301 (2023)
3. K. A. Mitchell, M. M. H. Sabbir, S. Ricarte, B. Klein, D. A. Beller; Modeling active nematics via the nematic locking principle. Soft Matter; 21 (47): 9083–9099 (2025).
4. B. Klein, A.J.S. Franco, M.M.H. Sabbir, M.J. Deutsch, R. Kliegman, R.L.B. Selinger, K.A. Mitchell and D.A. Beller, Chaos-generating periodic orbits of topological defects in confined active nematics, *Proc. Natl. Acad. Sci. U.S.A.* 123 (28) (2026).

Publications

1. B. Klein, A.J.S. Franco, **M.M.H. Sabbir**, M.J. Deutsch, R. Kliegman, R.L.B. Selinger, **K.A. Mitchell** and D.A. Beller, Chaos-generating periodic orbits of topological defects in confined active nematics, *Proc. Natl. Acad. Sci. U.S.A.* 123 (28) (2026).
2. **K. A. Mitchell**, **M. M. H. Sabbir**, S. Ricarte, B. Klein, D. A. Beller; Modeling active nematics via the nematic locking principle. Soft Matter; 21 (47): 9083–9099 (2025).

Active-Passive Colloidal Experiments and Simulations for Programmable Active Matter

Daphne **Klotsa** (lead PI) (University of North Carolina at Chapel Hill), John F. **Brady** (California Institute of Technology), David J. **Pine** (New York University)

Keywords: active matter, colloidal self-assembly, hydrodynamic interactions, active doping, Stokesian dynamics

Research Scope

Our combined program investigates how activity, introduced either through synthetic self-propelled colloids or algorithmically in simulation, can be harnessed to control the crystallization, morphology, and reconfigurability of colloidal assemblies. We pursue three complementary strands: (i) synthetic active-colloid experiments using catalytic Janus (hematite/TPM) particles to drive "active annealing" of passive colloidal crystals; (ii) coarse-grained simulations of active-doped colloidal monolayers to establish design rules linking doping fraction, interparticle forces, and packing density to crystallinity and morphology; and (iii) development of a hydrodynamically resolved simulation code, built on our Active Fast Stokesian Dynamics method, that captures full many-body hydrodynamic interactions among active and passive particles near a solid boundary. Together, these efforts aim to establish a predictive framework for designing reconfigurable active-matter assemblies.

Recent Progress

Experimentally, we use catalytic Janus (hematite/TPM) active particles to drive active annealing of passive colloidal crystals. We identified several key mechanisms governing active-passive interactions: propulsion direction reverses depending on electrolyte composition, substrate surface charge, and trace ion leaching from glass and polymer substrates; peroxide-derived radicals degrade steric Pluronic F108 brush layers, weakening depletion-driven crystallization; and commercial silica passive particles suffer dissolution instabilities, which we are now addressing using chemically crosslinked, monodisperse TPM microspheres. We are developing substrate passivation and fuel-purity protocols to achieve stable, reconfigurable assemblies. Computationally, we have shown that doping colloidal monolayers with active particles produces two distinct regimes of crystallization behavior for repulsive versus attractive passive colloids, separated by a critical packing density φc that coincides with the hexatic transition of passive hard disks. Above φc, active doping universally enhances grain-boundary mobility and crystallization; below φc, its effect depends strongly on interparticle forces, promoting annealing for attractive particles but disrupting it for repulsive ones. In both regimes, crystal size varies non-monotonically with active energy, and for attractive particles the crystal morphology tunes continuously from large, porous domains to small, dense crystallites as the doping fraction increases at fixed active energy input. In parallel, we are building an in-house simulation code that resolves full many-body hydrodynamic interactions among active and passive particles near a physical wall, mimicked by a dense stacking of spherical particles, based on our recently developed Active Fast Stokesian

Dynamics method [1]. The code has been validated on single-particle and few-particle test systems.

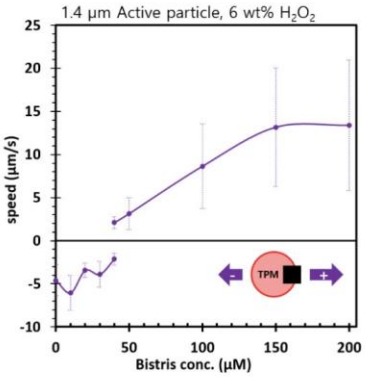


Figure 1. Light-activated particle average velocity across different concentrations of Bis-Tris buffer. Positive indicates the hematite cube facing forward; negative indicates the opposite orientation. Around 40 μM buffer, the active propulsion direction reversed.

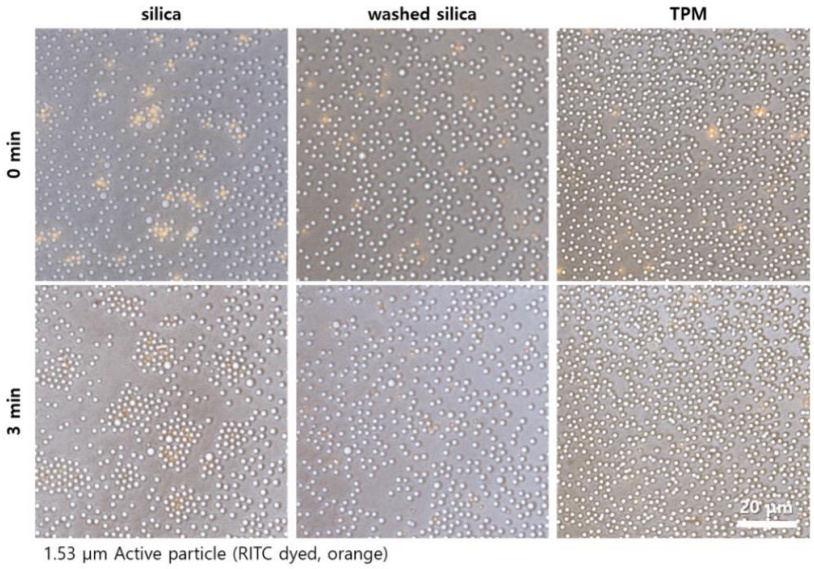


Figure 2. Evidence of dissolution of commercially purchased silica particles compared to non-degrading TPM particles.

Future Plans

We will parameterize the hydrodynamic simulation code to directly match the size, activity, and interaction characteristics of the experimental active and passive particles, enabling quantitative, particle-resolved comparison between simulation and experiment. Experimentally, we will pursue two strategies to prevent degradation-induced melting of depletion-stabilized crystals: using bare TPM particles to bypass polymer-brush degradation, and employing larger macromolecular depletants to stabilize the attractive potential. We will also extend the active-doping simulations to explore activity versus passive-particle packing density and activity versus passive-particle size, further mapping the design space for controlling crystallinity and morphology through active doping.

References

1. T. Zhou and J. F. Brady, *Hydrodynamic interactions destroy motility-induced phase separation in active suspensions*, Phys. Rev. Lett. **136**, 088301 (2026).

Publications

1. T. Zhou and J. F. Brady, *Hydrodynamic interactions destroy motility-induced phase separation in active suspensions*, Phys. Rev. Lett. **136**(8), 088301 (2026).
2. R. Gautam, T. Zhou, J. F. Brady, and D. Klotsa, *Active-doping controls formation and morphology of monolayer colloidal crystals*, to be submitted to Soft Matter.

Ion-Ion discrimination in biomimetic ligand appended artificial channels

Manish **Kumar**, Venkat Ganesan, Carlos Baiz; University of Texas at Austin

Keywords: Biomimetic transport, channels, lanthanides, lithium

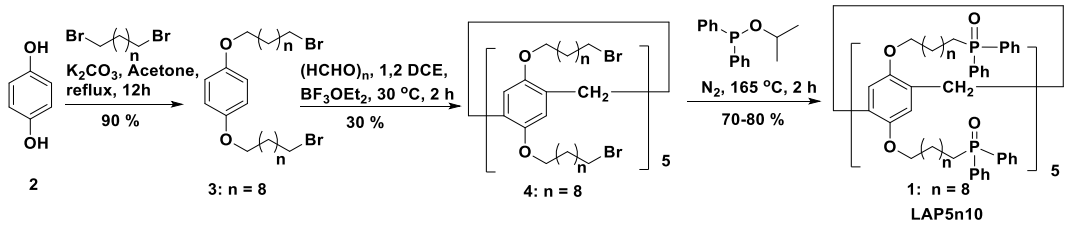
Research Scope

The overall objective of our work in this program is to identify origins of ion selectivity between ions of similar size/valence and hydration states in ligand appended artificial biomimetic channels as a stand in for the wider class of molecularly precise membrane nanochannels (such as membrane proteins). So far, we have developed a class of ligand appended biomimetic channels based on a pillar[5]arene that can discriminate between members of the lanthanide series and between Lithium and its most common co-occurring ions Magnesium and Sodium. Selectivity values include Eu^{3+}/La^{3+} selectivity of >40 and Eu^{3+}/Yb^{3+} selectivity of ~30 for the lanthanide selective channels and ~100 for Li^{+}/ Na^{+}, ~ 500 for Li^{+}/Mg^{2+}, respectively for the lithium selective channels. Molecular dynamics simulations were used to investigate mechanisms of selectivity and indicate water exchange dynamics and confinement as a major factor in lanthanide-lanthanide selectivity in these channels and ligand-ion interaction and size as major factors in Li selectivity over monovalent ions and over divalent ions, respectively. We will continue to investigate mechanism of selectivity using an expanded set of synthetic molecules, simulation techniques and spectroscopic analyses.

Recent Progress

We have created, for the first time, a class of ligand appended pillar[n]arene (LAP) channels that have high lanthanide-lanthanide selectivity and Li^{+} over Na^{+} selectivity. We have synthesized diphenyl phosphine (DPP) appended pillar[5]arene channels (or ligand appended pillar[5]arene, channels represented using the acronym LAP5) with 6 or 10-carbon alkyl chains as spacers represented by the addition of n6 or n10 after the acronym. Thus, these channels are referred to as LAP5n6/ LAP5n10. They are selective for Lithium and Lanthanides over commonly occurring ions. LAP5 channels were synthesized using a three-step process, beginning with the hydroquinone isomer, followed by attachment of alkyl chains, and subsequent Arbuzov reaction involving alkyl chain appended pillar[5]arenes and iso-propoxydiphenylphosphine prepared previously (**Scheme 1**). 1H NMR and ESI-Mass confirmed the formation of LAP5n10 channel.

Scheme 1: *General procedure adopted for synthesis of LAP5n10 channel* ***1.***



LAP5n10 channels show highly selective Li^+ transport. We have incorporated the LAP5n10 channels into lipid membranes, utilizing it as a model system to explore fundamental transport properties and quantify ion selectivity. We demonstrated, using a patch clamp bilayer setup, that the DPP based LAP5n10 channels transport Li^+ ions selectively while excluding other more abundant mono- and divalent metal ions across the lipid membranes (**Figure 1**).

Patch clamp bilayer setups are extensively employed in electrophysiological measurements to quantitively assess the ion transport properties of biological ion channels. Moreover, they have been modified to access the ion transport properties of artificial/engineered channels, enabling reproducible, high-throughput analysis of ion transport rates and ion selectivity. Single channel activity for LAP5n10 with periodic opening and closing events (a characteristic of biological channels) was observed for Li^+ ions and the single channel conductance of this channel for Li^+ was determined to be 13.35 pS, which is equivalent to Li^+-ion transport rates of approximately 1.34×10^7 ions/s per channel under a potential gradient of -160 mV. Notably, minimal activity was seen for other mono- and divalent ions under the same experimental conditions, even at higher LAP5n10 channel concentration (of up to 5 mol%) in the membrane (**Figure 1B).** The current output for each ion at different applied potentials was used to generate an I-V curve **(Figure 1B).** The conductance values obtained from this curve were then applied to calculate selectivities (**Figure 1C**). *In our multichannel patch clamp experiment, the LAP5n10*

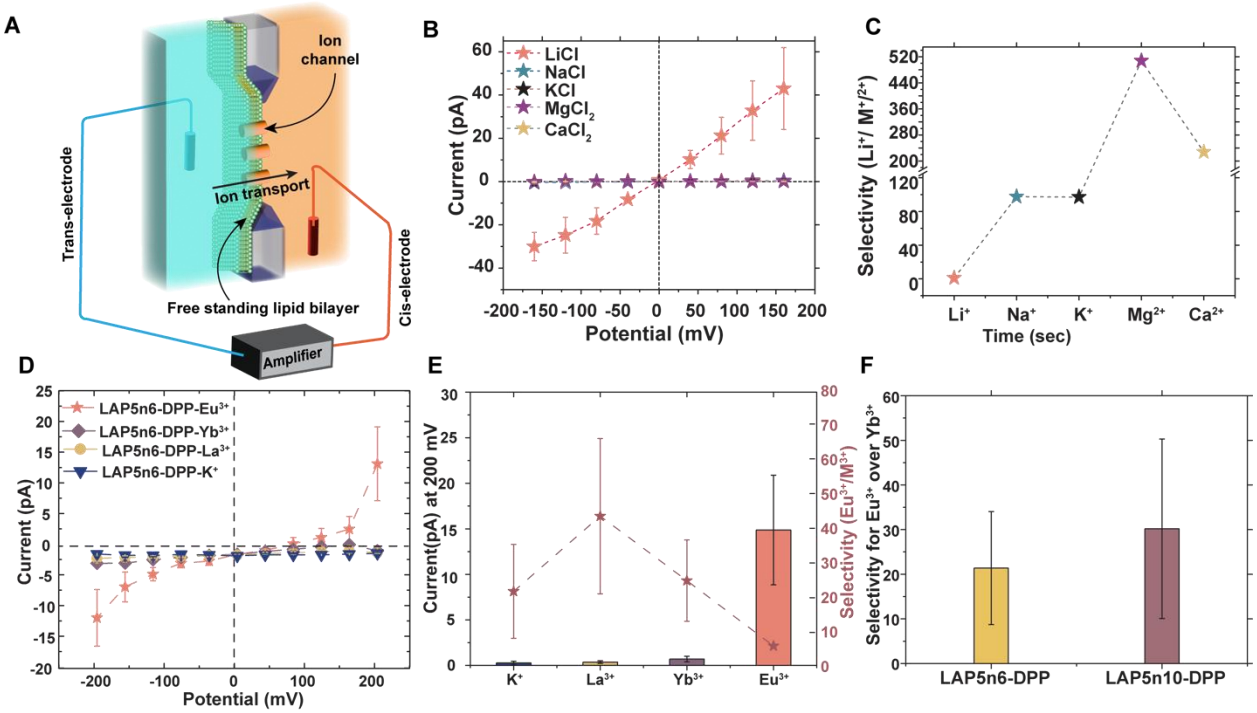


Figure 1. Patch clamp electrophysiological characterization of ion-selective LAP5 channels, when incorporated into painted lipid bilayers reveal high selectivity for Li^+ over other more abundant monovalent ions (Na^+, K^+) and divalent ions (Ca^{2+}, Mg^{2+}); and high Lanthanide-Lanthanide selectivity. **A.** Patch clamp apparatus and a painted lipid bilayer membrane. **B.** LAP5n10 I–V plot for Li^+ and competing ions under symmetrical metal chloride solution conditions, **C.** Li selectivity values over other ions. **D.** LAP5n6 lanthanide transport I–V plot for each ion under symmetrical metal chloride solutions; **E-F.** The conductance calculated from the corresponding I-V plot revealed significant selectivity for Li^+ ions over mono- and divalent ions.

*channel exhibited very high selectivity for Li^+ ions; ~100 times higher than both Na^+, K^+, and between ~ 500 and ~230 times higher than Mg^{2+}, Ca^{2+} ions, respectively (**Figure 1C**).*

LAP5n6 channels show highly selective Lanthanide transport. *When incorporated into lipid membranes.* LAP5n6 channels showed high transport selectivity (~18:1) of the medium lanthanide, Europium (Eu^{3+}), over all measured monovalent and divalent ions, including protons. These membrane channels also have high lanthanide-lanthanide transport selectivity with Eu^{3+}/La^{3+} selectivity of >40 and Eu^{3+}/Yb^{3+} selectivity of ~30 (**Figure 1 D-F**). Additional tests with lanthanides show even higher lanthanide-lanthanide selectivites as discussed in a subsequent section.

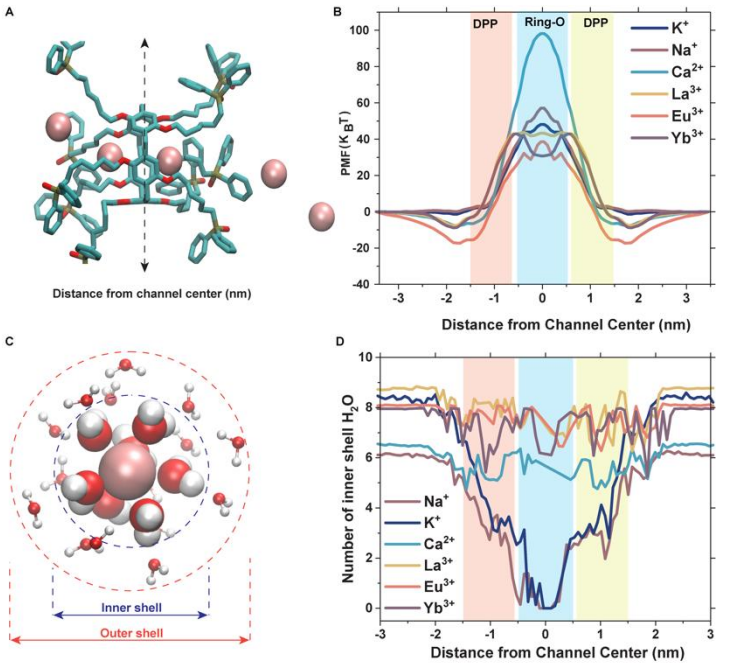


Figure 2: Potential of Mean Force (PMF) calculations based on molecular dynamics simulations provide a mechanistic reason for lanthanide over metal ion selectivity and lanthanide-lanthanide selectivity, based on coordination of ions with channel binding motifs and ion dehydration. A. Illustration of PMF experiment (reaction coordinate) for measurements **B.** PMF traces for all ions tested **C.** Illustration of inner and outer shell complexation for ions. **D.** Number of water molecules coordinated with the ion as it transfers across the reaction coordinate. Error bars represent the standard errors from four independent samples.

We have utilized MD simulations to develop hypotheses regarding selective transport of lanthanides across LAP channels. Our MD simulations have revealed novel coordinated mechanisms governing lanthanide transport selectivity across LAP channels. This selectivity derives from interactions between ion hydration shells and specific channel moieties. Monovalent ions (K^+, Na^+) shed their weakly bound hydration shells at the channel entrance, directly coordinating with terminal-DPP groups via phenyl rings. Their energy profiles show unfavorable minima (1.98-3.53 k_BT), making permeation energetically costly as channel binding sites compete with inner hydration shells (**Figure 2**).

Multivalent ions (Ca^{2+}, La^{3+}, Eu^{3+}, Yb^{3+}) maintain their strongly bound water structures throughout the channel,

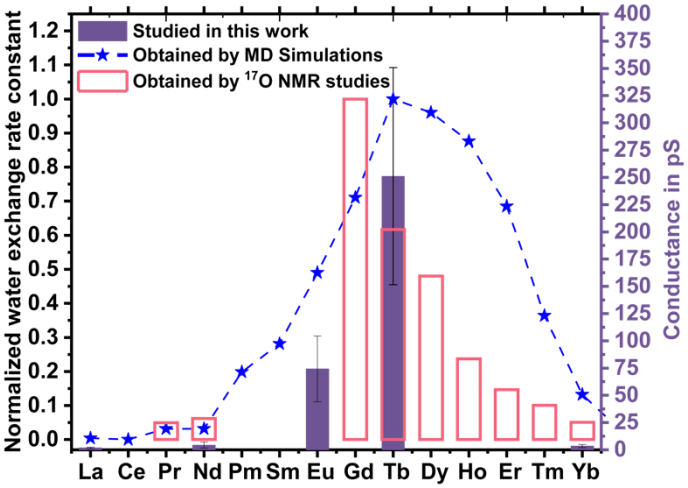


Figure 3: Water exchange dynamics of lanthanide ions plays a crucial role in transport selectivity. Comparison of the water exchange rate constants of lanthanide ions, obtained from ^{17}O NMR experiments and MD simulations, with the LAP5n6-DPP channel's conductance for tested lanthanide ions (La^{3+}, Nd^{3+}, Eu^{3+}, Tb^{3+}, and Yb^{3+}).

coordinating only with phosphine oxide and central ring oxygens. Ca^{2+} and La^{3+} are excluded as their persistent hydration shells exceed the channel's ~ 0.50 nm pore radius.[1]
Despite similar size constraints (Eu^{3+}: 0.364 nm, Yb^{3+}: 0.354 nm), both Eu^{3+} and Yb^{3+} access 8-9 coordinated structures, allowing exchange with channel oxygens. Eu^{3+} demonstrates superior transport efficiency due to its higher water exchange kinetics.

The delicate balance between hydration characteristics and channel dimensions governs selective transport. Ions with rigid, large hydration shells cannot navigate channel constrictions, while those with flexible coordination numbers can adjust their hydration structure to pass through efficiently.This coordination flexibility provides the molecular basis for observed lanthanide transport selectivity across LAP channels.

We have used literature data and experiments to further develop hypotheses connecting ion dehydration and ion transport. As discussed in the previous paragraph, a possible origin for the observed selectivity is the first hydration shell water exchange frequency (**Figure 3**). The water exchange frequency reported for La^{3+}, Eu^{3+}, and Yb^{3+} was $0.095\times10^{9}s^{-1}$, $11.78\times10^{9}s^{-1}$, and $3.17\times10^{9}s^{-1}$ respectively.[2] This trend aligns well with the water exchange rate constants obtained from ^{17}O NMR experiments (**Figure 3**).[3, 4] Further, more broadly the LAP5 channel demonstrated significantly higher selectivity between middle-lanthanides versus both light and heavy lanthanides with the following selectivities Tb^{3+}/La^{3+} (~140), Tb^{3+}/Yb^{3+} (~72), Tb^{3+}/Nd^{3+} (~58), Eu^{3+}/La^{3+} (~41.4), Eu^{3+}/Yb^{3+} (~21.4) and Eu^{3+}/Nd^{3+} (~17), while the selectivity between adjacent middle lanthanide Tb^{3+}/Eu^{3+} was ~3 .We hypothesize from this work that the high selectivity of LAP5-DPP channels for middle lanthanide over light and heavy lanthanides is closely linked to the water exchange dynamics of lanthanide ions that is exploited for separations in the confined central channel of the LAP pore.

Future Plans

We propose that the closeness in size of the hydrated lanthanide ions and the size of the central pore contributes to the sensitivity of selectivity of the LAP channel to the water exchange kinetics of specific lanthanides. In continuing work, we will verify both this proposal on relative size and the overall hypothesis. Additionally, we will use this effort to build on our computational work on channel ring sizes and their impact of water permeability to build out a computational screening framework to evaluate pore size effects on relative ion flux (and thus selectivity), which will be further developed for screening a wide range of ligands. We will then use spectroscopic techniques (17O NMR, 2DIR and Neutron Spin Echo techniques) to evaluate our hypothesis about the local effects of pore size by measuring the effect of specific pore designs on water exchange rates, hydrogen bonding populations, and picosecond level fluctuations of channel structure.

References

(1) Tan, L.-L.; Yang, Y.-W. Molecular recognition and self-assembly of pillarenes. *Journal of Inclusion Phenomena and Macrocyclic Chemistry* **2015**, *81* (1), 13-33.
(2) Duvail, M.; Spezia, R.; Vitorge, P. A dynamic model to explain hydration behaviour along the lanthanide series. *ChemPhysChem* **2008**, *9* (5), 693-696.

(3) Karimi, S.; Helm, L. Water Exchange on [Ln(DO3A)(H2O)2] and [Ln(DTTA–Me)(H2O)2]− Studied by Variable Temperature, Pressure, and Magnetic Field NMR. *Inorganic Chemistry* **2016**, *55* (9), 4555-4563. DOI: 10.1021/acs.inorgchem.6b00363.
(4) Cossy, C.; Helm, L.; Merbach, A. E. Oxygen-17 nuclear magnetic resonance kinetic study of water exchange on the lanthanide (III) aqua ions. *Inorganic Chemistry* **1988**, *27* (11), 1973-1979.

Publications

(1) Behera, H.; Duncan, T.; Samineni, L.; Jogdand, A.; Karnik, A.; Dhiman, R.; Fica, A.; Hsieh, T.-Y.; Ganesan, V.; Kumar, M. Highly Selective Artificial Lithium Channels. JACS (in review) 2026.
(2) Behera, H.; Duncan, T.; Samineni, L.; Oh, H.; Jogdand, A.; Karnik, A.; Dhiman, R.; Fica, A.; Hsieh, T.-Y.; Ganesan, V.; Kumar, M. Lanthanide Selective Artificial Channels . ACS nano. 2025 Apr 4;19(14):13927-40.
(3) Duncan TJ, Behera H, Meng MF, Zhang Z, Marioni N, Tadesse M, Kumar M, Ganesan V. Side-Chain and Ring-Size Effects on Permeability in Artificial Water Channels. The Journal of Physical Chemistry B. 2025 Jan 2;129(2):659-70.
(4) Duncan TJ, Sachar HS, Wang S, Behera H, Kumar M, Ganesan V. Impact of Ligands on the Ion–Ion Selectivity of Ligand-Appended-Pillar [n] arene Channels. The Journal of Physical Chemistry B. 2025 Sep 25;129(40):10311-24.
(5) Oh H, Samineni L, Vogler RJ, Yao C, Behera H, Dhiman R, Horner A, Kumar M. Approaching ideal selectivity with bioinspired and biomimetic membranes. ACS nano. 2024 Dec 24;19(1):31-53.

Bio-mimetic material design based on principles of disorder

Andrea J. **Liu** (lead PI), (University of Pennsylvania) and Sidney R. **Nagel** (University of Chicago)

Keywords: Training; Memory; Landscape; Disorder; Networks; Epistasis

Research Scope

We have pioneered the field of non-biological tunable matter in order to create and control novel material properties. These properties range from tuning moduli and mechanical allosteric interactions to the creation of memories in granular packings, and the training of flow, electrical and mechanical networks to perform desired input-output tasks. We also address fundamental theoretical questions about how microscopic tunability leads to desired collective functionality.

The field of tunable matter, while arising out of purely physical considerations, owes a tremendous debt to biology in that it trains systems to develop function inspired by biomolecular systems such as proteins. Despite their heterogeneity, proteins are not completely disordered; each amino acid can be viewed as having been selected by the evolutionary process so that the folded protein has at least one function that aids survival of the organism. Like their biological inspirations, trained tunable materials are highly heterogeneous but not purely disordered because their functionality arises from correlations.

Our research investigates various new principles to study tunable matter with novel and flexible biologically-inspired functions. We are extending the study of tunable matter in five new directions. (i) Previous work on tunable matter has focused on athermal systems. In the previous funding cycle we have studied the influence of thermal fluctuations on systems tuned at zero temperature. We now propose to tune thermal systems at nonzero prestress, to bring such systems into the framework of tunable matter. (ii) We previously developed a method of shearing systems with periodic boundary conditions in arbitrary directions. We will use this to study how external strain affects buckling and nonlinearities in tuned function. (iii) Previous tuning processes have relied gradient descent, simulated annealing, directed aging and local rules based on contrastive learning. We are investigating a new set of rules based on cooperative learning. (iv) In previous work, we made major advances in characterizing and understanding the topography of the cost landscape locally, in the immediate neighborhood of the tuned minimum. We also developed a global analysis of the landscape for systems with two incompatible tuned functions. We are using these approaches for systems trained for multiple functions to study the extent to which the tuning process affects the topography. (v) In the previous work, we developed local rules for tuning systems with non-reciprocal interactions to develop desired functionalities. We have tuned such systems to desired dynamical fixed points and limit cycles. We now extend our understanding of the link between structure and function provided by our local cost landscape analysis to such systems.

Recent Progress

Effect of temperature on function: Understanding that tuning in function is encoded in the low frequency modes of a network has led us to extend our studies of allostery to *cooperative binding* in networks [1]. Our earlier work, based on mimicking the functional behavior of proteins, trained networks to produce a desired strain at an output location in response to a distant input strain. Now we have tuned for *bidirectional* allostery: a symmetric coupling where the strain propagated between the two sites is independent of which site is perturbed. The effects of temperature can be estimated theoretically using a normal mode analysis. The low eigenmodes of the physical Hessian encoding the learned function are the least robust to temperature. We identified a crossover temperature above which functionality breaks down due to thermal fluctuations. We then introduced a modified tuning process to increase this crossover temperature, showing that function can be robust at biologically relevant temperatures if thermal stability is important (Fig. 1). These protein-function-inspired results have implications for material science at the nanoscale or below [1].

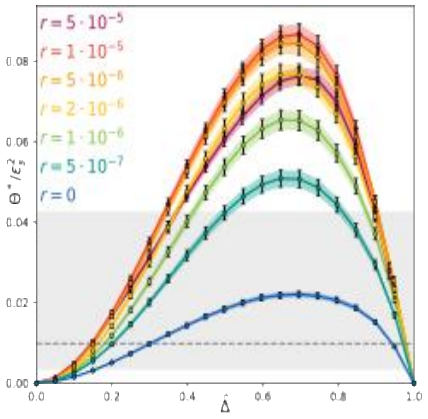


Fig. 1. A dimensionless crossover temperature Θ*, above which function fails, as a function of the ratio of the output response to the input strain Δ at increasing values of the parameter r, which controls the relative importance of thermal stability. Vertical and horizontal bars (too small to see) indicate standard errors. The gray dashed line corresponds to 300 K, obtained by matching our coarse-grained model with typical (median) protein values. The shaded gray region reflects the 25th-75th percentile range across different proteins.

Tensor nature of failure: In order to appreciate how disordered solids fail under sufficiently large perturbations, a material should be regarded as a network of potentially interacting instabilities occurring along different directions of forcing. We developed a tool for simulations with periodic boundary conditions that allows strains to be applied at a continuously variable angle, θ [2]. This reveals an underlying landscape which consists of lines and planes of instabilities. A modified polar plot provides a visualization of this strain landscape while also allowing a graphic measure of an instability's quadrupolar structure. Some lines persist over a broad angular range of applied strain; some pass through one another; others change continuously with angle or end by smoothly decreasing their magnitudes to zero. Appropriate paths through phase space allow instabilities to be circumvented and hence avoided entirely. We show that as the end of an instability line is approached, the separation between the forward and backward instabilities vanishes.

Viable switching of function in tunable networks: An elastic spring network is an example of evolvable matter that can be pruned to couple separated pairs of nodes so that when a strain is applied to one of them the other responds either in-phase or out-of-phase. This produces two pruned networks, with incompatible functions, that are nearly identical but differ from each other by a set of "mutations" each of which removes or adds a single bond in the network. We have generated *ensembles* of network pairs that differ by a fixed number,

M, of discrete mutations and evaluate all mutational paths between the in- and out-of-phase behaviors. With a threshold response for the network to be considered sufficiently fit for either function, so that non-functional networks are disallowed, only some mutational pathways are viable as shown in Fig. 1. We found that there is a surprisingly high critical response threshold above which no evolutionarily viable path exists between the two networks [3]. The few remaining pathways at this critical value dictate much of the behavior along the evolutionary trajectory. The effect of multiple mutations is epistatic, that is, the impact of a mutation is not invariant but depends on what other mutations have already occurred. The analysis clarifies how the number of mutations and the position of a mutation along the pathway affect the evolutionary outcome.

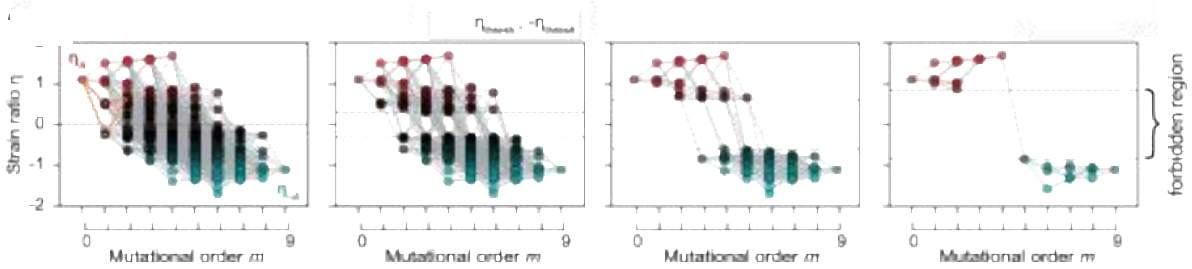


Fig. 2: Viable evolutionary paths with widening forbidden region for M=9. Viable pathways maintain single-step connections between the variants that are sufficiently fit, *i.e.*, that fall outside a forbidden region $[-\eta t_{hresh}, \eta_{thresh}]$ along a trajectory from η_A at m = 0 to η_{-A} at m = M. Plots from Left to Right: η_{thresh} = 0, 0.3, 0.6, and η_c = 0.856, as indicated by the Top arrow. Viable variants with $|\eta| > \eta_{thresh}$ are gradually eliminated as η_{thresh} increases. Above a critical threshold η_c , no viable trajectories between +A and−A exist.

Tuning complex dynamical systems: We have developed local rules for tuning dynamical systems described by coupled ordinary differential equations to have desired behaviors via supervised learning. We showed that for systems that violate time reversal symmetry, local rules with supervision supplied through output nodes cannot reduce to gradient descent on a cost function in any limit. Nevertheless, they typically lead to successful tuning of desired functionality. This opens up a far broader class of systems to scalable tuning than before [4]. As an example, we have tuned a system of Kuramoto oscillators so that an output node (orange in Fig. 3) synchronizes to the same phase as the input node (blue).

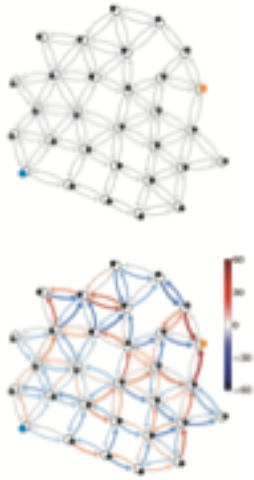


Fig. 3. Training a network of Kuramoto oscillators. (Top) Before training, the network has weak couplings between nearest neighbors. We want to transmit a signal from an input oscillator (blue) to on output oscillator (orange) on the opposite side of the network. (Bottom) After training, some network couplings strengthen or weaken significantly, indicated by edge colors.

Future Plans

Training at T>0: Previous work showed that if we train conformational allostery at *T=0*, we can identify a crossover temperature *T** above which this functionality breaks down due to thermal

fluctuations. We used a variant of the training process for allostery to tune mechanical networks at zero temperature to display cooperative binding functionality. We will now generalize this process to introduce entropic effects into the training itself. We now propose to study the behavior of networks trained for allosteric behavior at a non-zero temperature. This will surely provide microscopically different states than those trained at *T=0*. We are interested in creating these states and investigating how they are similar to or different from those trained at *T=0*. For example, does training at higher *T* make the final solution more robust to being destroyed by temperature? If so, it will convey stability on the function that would not have been attained by training at *T=0*. We will extract lessons from this that will be applicable to other trained functions.

Cooperative learning: Coupled learning provides a well-developed method for a network to be trained to perform a set of pre-determined tasks. Until now, this protocol has required that two copies of a network be created and compared as one of them is strained only at the source and the other is strained at both the source and target. We now introduce a different approach that extends the ideas of contrastive learning. Its main benefits are that (i) it does not require a duplicate network, (ii) it tunes bonds in a more efficient manner so that every move is consequential for the training, (iii) we can tune many tasks simultaneously, and (iv) because of this simultaneity, it can learn in a *cooperative* manner which may lead to faster and better training of more tasks compared to sequential rules.

Encoding with frequencies, simultaneous and cooperative learning: We are now using frequency to extract the signals efficiently. If we oscillate the source and target at different frequencies: $S_j = S_{j0}\cos(\omega_S t)$ and $T_j = T_{j0}\cos(\omega_T t)$, we can extract the signal, without using a second network for contrast, by analyzing the sum and difference frequencies. This presents an enormous advantage when designing analog learning circuits or mechanical networks. One attractive aspect of frequency encoding is that it can train many tasks *simultaneously* by encoding each task at a separate unique frequency. Because it is linear, each learning task is updated separately from all the others; with frequency-encoding, we no longer have to train one task before going on to the next. This has the potential to speed up (by the order of the number of tasks being trained) the total training time. Simultaneous learning has another advantage. The *way* in which the tasks are learned depends on the history of the network. For example, if one task is trained first, then that affects how the next task can be accomplished. That second task has to be performed with fewer degrees of freedom in play because some of those were already set to make the first task work. As one approaches the network's capacity to learn, later tasks are harder and more time-consuming to train. Learning all the tasks *simultaneously* allows optimization of learning as the network settles into the ultimate learned state. We are testing how learning can be enhanced by cooperation.

The work on evolutionary matter detailed above also opens the door to studying the evolution of networks in other physically relevant contexts by including the effects of prestress and nonlinear elastic response. The definition of fitness could also be augmented to include more than one function, which allows us to test our findings against different models of molecular and

macroevolution and susceptibility to an environmental selection pressure. We will probe the cause for the large function switch. Soft modes have been found to accompany training for allosteric function. We are now interested in seeing if the function switch itself is related to a feature in the modes. Finally, while we have concentrated on studying the average values for the entire ensemble, the question remains as to whether all members of the ensemble—for example, systems with large and small critical thresholds—behave similarly.

References

[1] "Cooperative Function with Thermal Fluctuations in Mechanical Networks," B. Pisanty, J. Andrejevic, A.J. Liu, S.R. Nagel, PRX Life (2026, in press). arXiv:2509.20560.

[2] "The landscape of instabilities versus shear angle in simulations," C.W. Lindeman and S.R. Nagel [submitted] (2026). arXiv:2603.12457

[3] "Epistatic pathways in evolvable mechanical networks," S. Alqatari, S.R. Nagel *PNAS* **123**, e2505183123 (2026). https://doi.org/10.1073/pnas.2505183123

[4] M. Stern, A. G. Frim, R. Candas, A. J. Liu, V. Balasubramanian (2026). arxiv: 2603.26969; https://doi.org/10.48550/arXiv.2603.26969

Papers published in past 2 years

[1] L. E. Altman, M. Stern, A. J. Liu, D. J. Durian, PR Applied **22**, 024053 (2024), https://doi.org/10.1103/PhysRevApplied.22.024053
"Experimental demonstration of coupled learning in elastic networks."

[2] Heinrich M. Jaeger, Arvind Murugan, S.R. Nagel *Soft Matter* **20**, 6695–6701 (2024). "Training physical matter to matter."

[3] Savannah D. Gowen, Thomas E. Videbæk, S.R. Nagel *Phys. Rev. Fluids* **9**, 053902 (2024). https://doi.org/10.1063/pt.zork.luqw
"Measurement of Pressure Gradients near the Interface in the Viscous Fingering Instability."

[4] M. Stern, M. Guzman, F. Martins, A. J. Liu, V. Balasubramanian, PRL 134, 147402 (2025), https://doi.org/10.1103/PhysRevLett.134.147402
"Physical networks become what they learn."

[5] Chloe W. Lindeman, S. R. Nagel *New Journal of Physics* **27**, 085001 (2025),
"Minimal cyclic behavior in sheared amorphous solids."

[6] M. Guzman, F. Martins, M. Stern, A. J. Liu, PRX 15, 031056 (2025), https://doi.org/10.1103/f2hb-c9s1
"Microscopic imprints of learned solution in tunable networks."

[7] S. Alqatari, S.R. Nagel, *PNAS* **123**, e2505183123 (2026), https://doi.org/10.1073/pnas.2505183123
"Epistatic pathways in evolvable mechanical networks."

[8] B. Pisanty, J. Andrejevic, A.J. Liu, S.R. Nagel, PRX Life (2026, in press). arXiv:2509.20560."Cooperative Function with Thermal Fluctuations in Mechanical Networks."

Understanding and Informed Manipulation of Functional Dynamics on the Nanoscale Through Integrated Experiments and Computation

Erik **Luijten** (lead PI), Northwestern University; Qian **Chen**, University of Illinois, Urbana Champaign

Keywords: Nanoparticle self-assembly, patchy nanoparticles, electric field effects, liquid-phase transmission electron microscopy

Research Scope

This research project aims to bridge the critical nanoscopic length-scale gap in understanding and emulating the functional dynamics of living systems in synthetic materials and harnessing these materials for macroscopic function. Through an integrated experimental–computational program supported by machine learning (ML) and other data-mining approaches, we will synthesize, image, model, and understand synthetic nanoparticles (NPs, several to 100 nm) that collectively transmit information through force, motility, and energy in a dynamic, self-correcting manner to generate functional structures spanning millimeters to centimeters. Specifically, we seek to uncover the fundamental mechanisms governing NP dynamics and use this knowledge to control their aggregation into materials with tunable, responsive structures and properties. The dynamics we investigate include complex equilibrium behaviors, such as the layered engineering of NP moiré lattices with tunable phononic properties, as well as nonequilibrium dynamics driven by chemical fuels or external fields. Our team has made significant advances in directly imaging large NP assemblies with unprecedented spatial and temporal resolution using liquid-phase transmission electron microscopy (TEM), integrating these observations with advanced computational methods to extract mechanistic insights and extending them to field-driven systems. In parallel, we have established an "atomic stenciling" approach to synthesize patchy NPs with designed surface-charge patterns and steer their dynamics through external energy inputs. We combine the unique real-space observations provided by liquid-phase TEM with predictive modeling of diffusional dynamics, dielectric polarization, charge regulation—the dynamic response of NP surface ionization—and hydrodynamic flow fields. These procedures and insights will enable new pathways toward scaled-up patchy-NP assemblies and establish a real-space understanding of how particle design governs functional dynamics and how this relationship evolves upon assembly under dynamic, non-dilute, and nonequilibrium conditions. The research will advance DOE Biomolecular Materials program priorities in bioinspired materials for harsh and nonbiological environments, predictive modeling through tightly integrated in situ experimental–computational feedback, and scalable manufacturing.

Recent Progress

Atomic stenciling synthesis of patchy NPs. The design paradigm of patchy NPs has sparked a synthesis "arms race" to develop methods that provide precise control over patch number, size, shape, and placement. Existing approaches, including polymer segregation, phase separation of mixed ligands, solvent-induced ligand attraction, dewetting, DNA origami-defined association sites, and curvature-selective ligand attachment, generally remain limited by uniformity and low yields. We have established a new method of atomic stenciling: a bottom-up strategy that uses chemical bonding to mask NP surfaces with nanometer-scale precision. By exploiting the preferential adsorption of iodide on gold {111} facets, we use iodide as a molecular mask and subsequently functionalize the exposed regions with 2-naphthalenethiols. Polystyrene-block-poly(acrylic acid) can then be grafted onto these regions through hydrophobic interactions between the polystyrene block and the 2-naphthalenethiol-functionalized sites, thereby forming well-defined patches. This bottom-up method enables deterministic, high-yield synthesis of patchy gold octahedra, bipyramids, rhombic dodecahedra, cubes, and cuboctahedra (Fig. 1). Polymer scaling theory and molecular dynamics simulations further reveal that the interplay between polymer energetics and entropy during stenciling can generate previously inaccessible patch patterns. Owing to their highly uniform patches, the resulting NPs assemble into extended crystals, including a variety of non-close-packed superlattices that span macroscopic length scales. More broadly, atomic stenciling provides a general route for patterning NPs and substrates with nanometer-scale precision, enabling spatial control

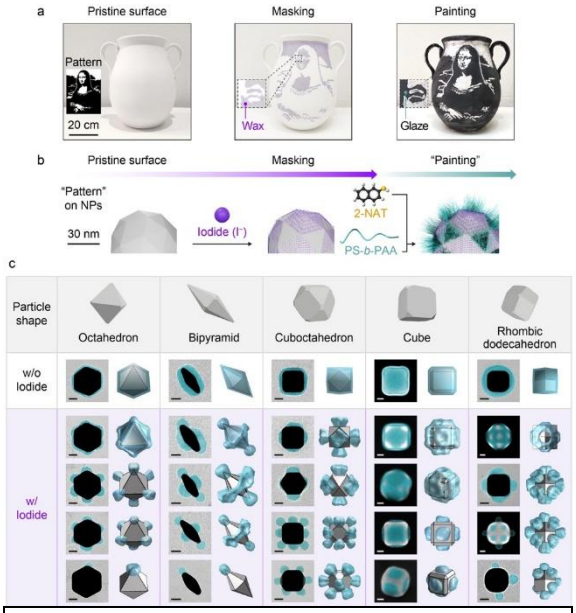


Fig. 1. Patchy NPs via atomic stenciling. (a) Stenciling of pottery. (b) Schematics of stenciling on faceted NP surfaces. (c) Library of patchy NPs: TEM or scanning electron microscopy (SEM) images (left) and scaling theory (right). Scale bars: 20 nm. Chen, *Nature* 646, 592 (2025)

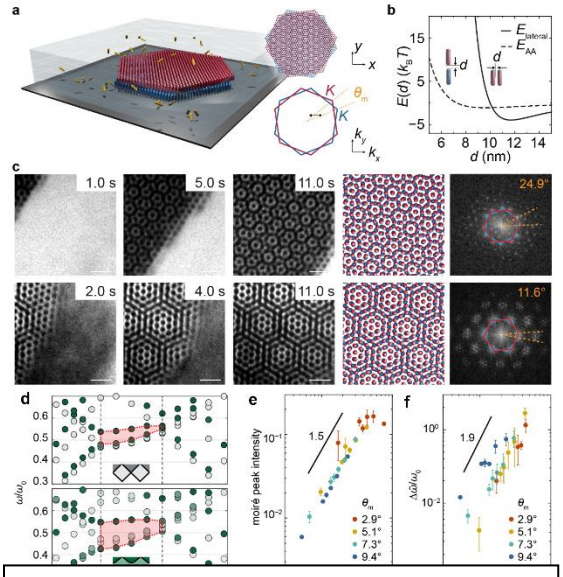


Fig. 2. Moiré of gold nanorods. (a,c) Liquid-phase TEM of moiré. (b) Anisotropic interactions drive moiré growth. (d) Simulated band structures of moiré. (e) Moiré peak height and (f) antisymmetric band splitting at M scales with η. Chen and Luijten, under revision.

over surface chemistry and reactivity for applications in catalysis and integrated metamaterials.

Self-assembled NP moiré lattices and phononic properties. We achieved the first real-time observation of dynamic NP moiré lattice self-assembly using liquid-phase TEM, in which two layers of NP lattices stack with a twist angle. This work establishes a new design principle based on the layered engineering of NP superlattices, inspired by atomic moirés, which are at the forefront of condensed matter physics because they can amplify small geometric variations, such as twist, lattice mismatch, and local registry, into large changes in electronic, optical, and phononic properties. In particular, we showed that gold nanorods can spontaneously assemble into moiré bilayers with a wide range of twist angles, θ_m, governed by inter-NP interactions and nanorod aspect ratio (Fig. 2a–c). Using accurate models, we confirmed that nanorod aspect ratio influences the balance between in-plane and out-of-plane interaction energies (Fig. 2b). By combining analytical theory with molecular dynamics (MD) simulations, we further showed that the resulting strain patterns and modified phononic band structures (Fig. 2d) are governed by a dimensionless interlayer coupling parameter, η. From the MD simulations, we extracted phonon band structures and observed broken degeneracy along the M–K line of the moiré Brillouin zone (Fig. 2d–f). Together, these results demonstrate both the emergence of moiré effects in self-assembled bilayers and the extent to which they can be tuned, highlighting the promise of NP-based moiré structures at the nano- and microscales.

Non-equilibrium dynamics of NPs. We applied the same technique to achieve the first liquid-phase TEM imaging of gold nanosphere self-assembly under an electric field (Fig. 3a,b). Specifically, we applied a coplanar direct-current (DC) electric field that generated an electric-field component perpendicular to the substrate and, consequently, a net attractive electroosmotic flow (Fig. 3b). This flow drove the nanospheres to assemble into hexagonal lattices that were crystalline yet exhibited liquid-like, fluctuating edges (Fig. 3c–e), including transient negative curvature and propagating waves. Single-particle analysis further revealed the nonequilibrium dynamics underlying this behavior. Together, these results demonstrate the direct nanoscale imaging of field-driven, nonequilibrium assembly and suggest new strategies for creating dynamic structures and rapidly deformable systems. In a parallel effort, we investigated self-driven spinners capable of independent three-dimensional reorientation and, consequently, potentially richer collective

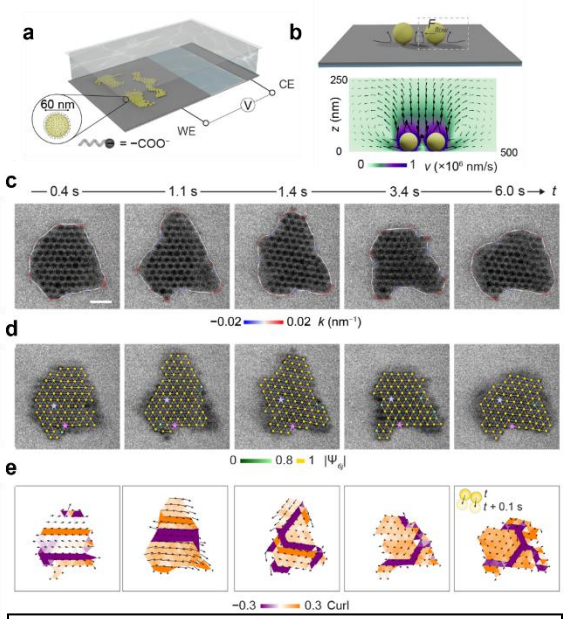


Fig. 3. Electric field driven assembly of gold nanospheres. (a) Schematic of the electric field-based SiN cell. (b) ECEO-induced NP interactions. (c–e) Liquid-phase TEM images (c,d) and displacement analysis of the DC-driven NP assembly. Scale bars: 50 nm.

behavior. Using molecular dynamics simulations coupled with fully resolved three-dimensional direct numerical simulations of hydrodynamics, we examined minimal systems of spheres subjected to intrinsic torque. We showed that rotational motion alone is sufficient to generate translation, collective behavior, and both spatial and orientational order. In addition to the primary rotational flow, each spinner produces a secondary flow directed inward toward its poles and radially outward along its equator. Near a substrate, the axial symmetry is broken, and the resulting flow imbalance generates an attractive motion toward the substrate that increases with Reynolds number. At low concentration, the spinners form a racemic monolayer and predominantly align their rotational axes along the z direction. At substrate packing fractions above approximately 0.7, long-range spatial order emerges, accompanied by geometric frustration in the anti-alignment of neighboring spinners. The system relieves this frustration by reorienting the rotational axes into the x–y plane. The spinners also align pole-to-pole to form antiparallel stripes driven by the secondary flow. We further found that the particle–particle and particle–substrate separation distances govern the emergent order, demonstrating that spinner organization can be tuned through these parameters to design bioinspired materials with controllable properties.

Future Plans

Building on the team's recent advances, including high-yield synthesis of patchy NPs, joint experimental–simulation characterization of NP moiré lattices and their phononic behavior, and liquid-phase TEM coupled to predictive modeling, we will (1) quantify diffusion, energy barriers, and assembly pathways via liquid-phase TEM and large-scale simulation to derive design rules for equilibrium self-assembly tuned to plasmonic and mechanical function; (2) adapt layered moiré engineering to NP assemblies to create new controls over emergent phononic band structures; and (3) elucidate non-equilibrium, field-driven assembly mechanisms by probing electric-field–mediated interactions and comparing nanoscale behavior with micron-scale colloidal counterparts.

Publications

1. A. Kim, C. Kim, T. Waltmann, T. Vo, E. M. Kim, J. Kim, Y.-T. Shao, A. Michelson, J. R. Crockett, F. C. Kalutantirige, E. Yang, L. Yao, C.-Y. Hwang, Y. Zhang, Y.-S. Liu, H. An, Z. Gao, J. Kim, S. Mandal, D. A. Muller, K. A. Fichthorn, S. C. Glotzer, and Q. Chen, *Patchy nanoparticles by atomic stencilling*, Nature **646**, 592 (2025).
2. I. P. Madden and E. Luijten, *Microswimmer separation in complex confining geometries*, Phys. Rev. E **111**, 065403 (2025)
3. Z. Lyu, L. Yao, Z. Wang, C. Qian, Z. Wang, J. Li, C. Liu, Y. Wang, Q. Chen, *Nanoscopic Imaging of Self-Propelled Ultrasmall Catalytic Nanomotors,* ACS Nano **18**, 14231 (2024).

Multiscale Modeling of Water and Peptide Self-Assembly through Probabilistic Backmappings

Jacob I. **Monroe**, Ralph E. Martin Department of Chemical Engineering, University of Arkansas, Fayetteville

Keywords: Coarse-graining, backmapping, molecular simulation, statistical mechanics, normalizing flows

Research Scope

Simulating systems with tight coupling across length scales remains a critical challenge, limiting our understanding of hierarchical molecular assemblies in biological systems, as well as synthetic soft materials with nano- to micro-scale heterogeneities, such as flexible electronics. To address this, we are developing simulation methodologies that benefit from the speed of low-resolution simulations while recovering fine-resolution details. The focus described here is on developing probabilistic backmapping models, which predict ensembles of fine-resolution features given low-resolution information, for water and small self-assembling peptides. These systems are important building blocks on the way to more complex self-assembling soft materials.

Recent Progress

In previous efforts, we developed probabilistic backmapping models of protein sidechains, with all backbone atoms included in the lower-dimensional, coarse-grained (CG) representation. More typically, CG models do not include any original atoms, but only beads representing groups of atoms. As our first effort to backmap entire molecules from only CG beads, we applied our backmapping procedure to phenylalanine dipeptide (FF). Despite consisting of only two residues, FF exhibits a rich set of self-assembled morphologies that are prohibitively expensive to study with all-atom simulations. However, CG simulations must be backmapped in order to understand and estimate properties, in particular the electrical conductivity of FF assemblies. Backmapping multiple FF molecules entails predicting the global translational position and orientation of each molecule as well as atoms in adjacent CG sites. Though global coordinates and CG bead adjacency present significant challenges compared to protein sidechains alone, we have successfully developed models that accurately backmap FF molecules from CG representations, including multiple molecules within a simulation.

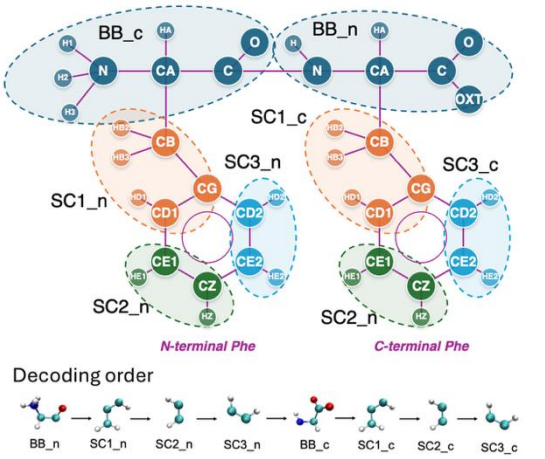


Figure 1: Schematic showing atom assignments to each CG bead (top) and fixed order of backmapping (bottom). Our mapping places CG bead locations at the centers of mass of their constituent atoms.

Our probabilistic backmapping models follow an autoregressive structure, backmapping each CG bead in turn. Each model predicts internal coordinate representations of atoms and is conditioned on CG positions and previously backmapped atoms (Fig. 1). We train a separate model for each CG bead type, with two distinct models required for the first sidechain beads of each residue (SC1_c and SC1_n) due to differences in their molecular connectivity. We train 6 backmaping models in total, each being a rational quadratic spline normalizing flow[1] with masked autoregressive structure.[2] Normalizing flows are conditioned on embeddings that describe the local environment of a CG bead through geometric algebra attention.[3] The structure of our protocol allows its application to any number of molecules and promises extensibility to longer peptides.

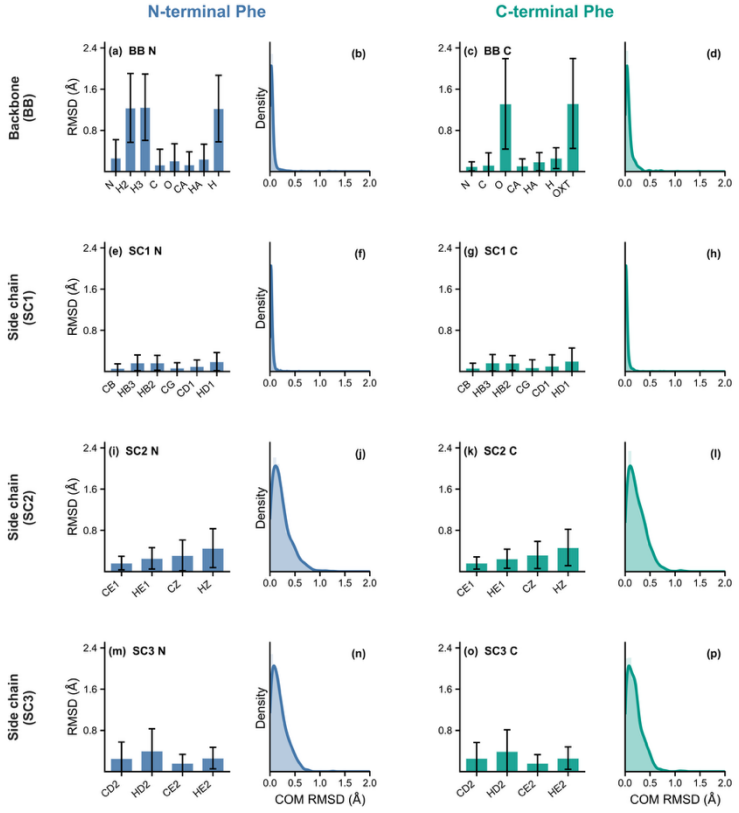


Figure 2: Individual atom RMSD between backmapped and training configurations for each bead (bar plots) and probability densities for the RMSD of the center of mass of backmapped configurations from the center of mass (CG bead location) of training configurations.

We systematically optimized numerous aspects of the models. Including rotational equivariance into the particle embedding allows each model to capture bead orientation in a three-dimensional space without aligning to a fixed reference frame. This substantionally improves performance for all beads, including the N-terminal backbone (BB_n) that predicts the global translation and rotation of the molecule. Selection of the root atom significantly affected the decoding quality – specifically, choosing root atoms in a rigid portion of the molecule is essential. Per-bead decoding quality is reported in Fig. 2 through per-atom and center-of-mass RMSD from training configurations. We also assessed accuracy of reconstructions with Ramachandran free energy surfaces and mutual information analysis. Notably, higher RMSDs and more variability is observed for more flexible species, such as hydrogen atoms.

Distributions of potential energy components for backmapped conformations compare favorably to those of the reference all-atom ensemble. Bonded energy terms (bonds, angles, and dihedrals) are broadened and shifted to higher energies relative to the reference while nonbonded LJ and Generalized Born solvation energy distributions are well-reproduced. Importantly, 84% of generated conformations lead to physically reasonable structures that can be used to initiate simulations at 300 K without energy minimizations. Since configurational log-probabilities are

known, each backmapped conformation can be reweighted to recover the exact total potential energy distribution (or any property of interest) in the all-atom ensemble, representing a crucial advantage of our probabilistic backmapping method. In principle, Boltzmann reweighting using importance weights corrects any mismatch between generated and target distributions. However, the effective sample size (ESS) of the model-generated conformations is small, placing large amounts of statistical weight on only a few samples. Though we see improvement here, low ESS was also identified as a significant challenge in previous work with protein sidechain backmappings. To address this, we recently identified truncated importance sampling[4] through weight clipping as a highly effective strategy to improve ESS, in this case from 0.008% to 0.96%. With truncation, reweighted samples much more closely match the simulated energy distributions.

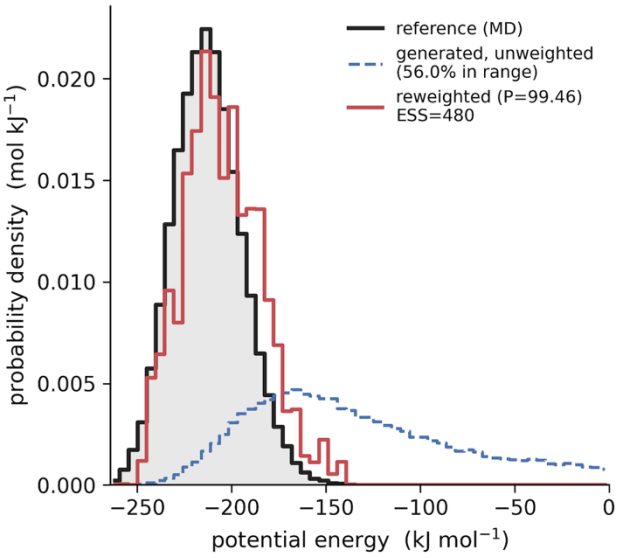


Figure 3: Distributions of potential energies from 50,000 independent configurations generated by models are shifted to higher energies. After truncated importance sampling, ESS increases and the potential energy distribution is reweighted to more closely match the reference.

We applied the same methods as described above to backmap CG representations of liquid water consisting of a single spherical bead at the center of mass of each molecule. We only consider backmapping to rigid all-atom water models (specifically SPC/E) such that only the orientational degrees of freedom of the molecule are predicted. While seemingly simple, large amounts of degeneracy exist in water orientations given fixed CG positions. Further complications arise due to the high level of coorporativity amongst waters in forming extended hydrogen bond networks. Thus, predicting all orientations of waters from CG beads alone requires accurately capturing degeneracy in long-range correlations. For a granular assessment of model performance, we consider backmapping single waters with only CG beads present (scenario 1), and with all atoms present except for the water being backmapped (scenario 2). Encouragingly, inclusion of all-atom information improves radial distribution functions between the molecule of interest and its surrounding waters (Fig. 4a), as well as the distribution of potential energy differences between backmapped and simulated configurations (Fig. 4b). As further evidence of our model's awareness of a water's local environment, Fig. 4c shows scenario 1 and 2 applied to a single water from a simulation with all water CG beads tightly restrained. As such, only reorientations of waters are allowed. Though the model broadens distributions compared to simulation, the preferred water orientation is captured. Tightening of the distribution occurs once information on surrounding atoms is included in scenario 2. Including all-atom information also improves the average number of hydrogen bonds from 2.05 to 2.19. However, comparing to the value of 2.51 from molecular dynamics simulations at 300 K and 1 g/cm^3 shows that hydrogen bonding is underpredicted at even

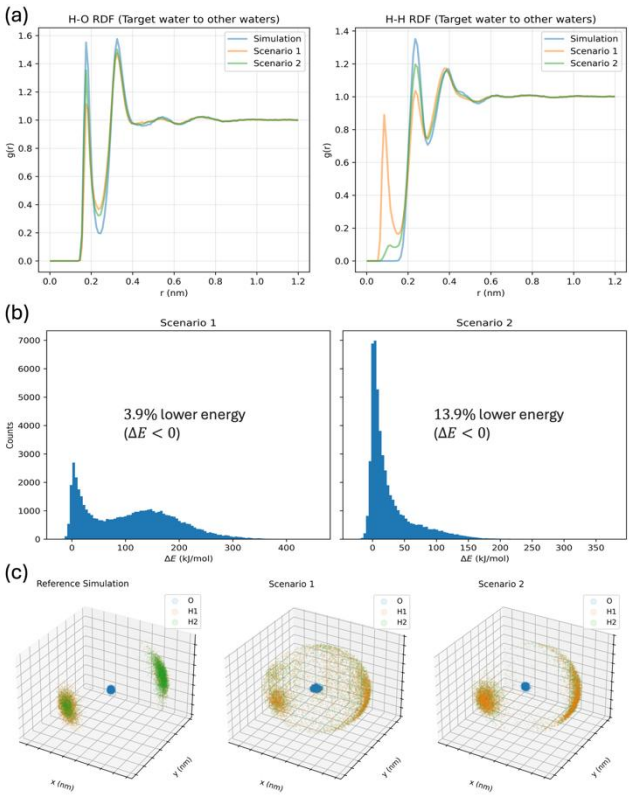


Figure 4: (a) H-O and H-H radial distribution functions of a single target water to other waters from simulation and generated by both backmapping scenarios. (b) Distributions of energy differences between backmapped and simulated configurations. (c) Oxygen (blue) and hydrogen (green or orange) positions for a single water in the restrained simulation and backmapped configurations from both scenarios

a single-water level. This then results in significant reductions in overall system potential energies when backmapping all molecules. To identify key improvements, we are currently correlating local structural order parameters and local orientational entropy with model-predicted likelihoods, hydrogen bonding, and potential energies.

Future Plans

Immediate goals relate to improving the performance of both backmapping models of water and FF peptides. For water, this includes a more detailed analysis of how a water's local environment impacts model performance. Refinement training protocols that penalize high energies during backmappings of entire simulation boxes of water are also underway. While it seems that large improvements may be gained from addressing individual waters' hydrogen bonds, an eventual transition to transformer architectures may be necessary for capturing long-range hydrogen bonding correlations. In the case of FF peptides, more sophisticated importance sampling protocols, such as Rosenbluth-inspired schemes and sequential Monte Carlo, are being tested to further improve ESS. Increasing ESS is essential since it is directly related to computational efficiency and is expected to impact scaling to larger system sizes. Longer term, a key step will be the merging of water backmapping models with those for peptides and other solutes, as well as ions. This will enable large-scale simulations of flexible electronic materials, where CG models are need to reach relevant length and timescales while atomistic resolution is necessary to study conductivity.

References

1. C. Durkan, A. Bekasov, I. Murray, and G. Papamakarios, *Neural Spline Flows*, arXiv:1906.04032 [cs,stat] (2019).
2. G. Papamakarios, T. Pavlakou, and I. Murray, *Masked Autoregressive Flows for Density Estimation*, arXiv:1705.07057 [cs, stat] (2018).
3. M. Spellings, *Geometric Algebra Attention Networks for Small Point Clouds*, arXiv:2110.02393 [cs.LG] (2022).
4. E. L. Ionides, *Truncated Importance Sampling*, Journal of Computational and Graphical Statistics **17**, 295-311 (2008).

Publications

1. J. I. Monroe, *Reweighting Configurations Generated by Transferable, Machine Learned Models for Protein Sidechain Backmapping*, Molecular Systems Design and Engineering **10,** 298–313 (2025).

Electrostatic-Driven Self-Assembly Design of Functional Nanostructures

Monica **Olvera de la Cruz**, Michael J. Bedzyk, and Neha Kamat, Northwestern University

Keywords: chiral molecules, bacterial microcompartments, diffusionphoresis, nanostructures

Research Scope

Biological structures have impressive functionalities that require the organization of heterogeneous molecules into mesoscale structures with precise compositions and architectures. We aim to understand the basic principles that govern such a robust biological assembly and discover ways to actuate these structures to exploit their functions. By assembling heterogeneous molecules, one can mimic the organization and function of specific biomolecular assemblies, such as microtubular structures and bacterial microcompartments. We design and characterize the organization of heterogeneous molecules with polar, non-polar, and charged groups, including proteins and amphiphiles, into specific nanostructures with broken symmetries to explore their functionalities.

The specific aims of this proposal are to: (1) elucidate the influence of heterogeneous chirality and tail length of self-assembling amphiphiles in molecular packing and crystallinity of membrane architectures in different ionic environments; (2) analyze the structural changes of multicomponent membranes with ion pores to generate functional microstructures; (3) investigate how surface structural organization governs the dynamic behavior of synthetic multicomponent membranes functionalized with ion-pores

Recent Progress

One of the important components of the project is to develop control over the assembly of charged molecular/nano-scale components in varied ionic environments.

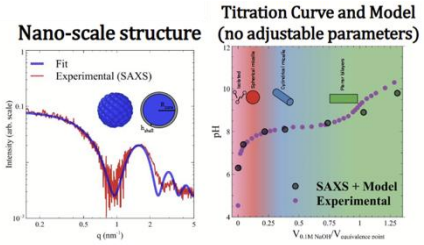


Fig. 1: SAXS intensity profile (red) and the corresponding core-shell form-factor fit (blue) for a $C_{16}K_2$ spherical micelle and pH titration curve of $C_{16}K_2$ in 5 mM NaCl: experimental titration (purple) and back-calculated from SAXS-derived structural parameters combined with the nl-PB model (black). Schematic morphologies at 250 mM NaCl.

Coupling of geometry and charge regulation. Molecular charge determines the assembly morphology, which in turn dictates the molecular ionization as the solution ionic conditions (pH, salt concentration) are varied. By analyzing the assembly of a peptide amphiphile $C_{16}K_2$, with two ionizable lysine headgroups covalently coupled to a 16-carbon tail via small/wide angle X-ray scattering (SAXS/WAXS), nonlinear Poisson-Boltzmann (nl-PB) theory and hybrid Monte Carlo-molecular dynamics (MC-MD) simulations, we showed that the morphology transitions and the underlying degree of ionization are two expressions of the same electrostatic origin [1]. SAXS-derived morphology parameters at low and high ionic strengths when fed into the geometry-

specific nl-PB potentials produced back-calculated titration curves (*Fig. 1*) that matched experiment with no adjustable parameters. This marks considerable progress over the customary charge-regulation that require an empirical effective pK_a with no structural justification. SAXS/WAXS combined with MC-MD simulations produced effective charges of the assemblies that matched those derived from zeta-potential measurements.

Charge regulation modeling. Dissociable functional groups in molecules regulate their hydration, solubility, and molecular interactions, thereby leading to striking properties, such as the assembly geometry changes discussed above. The charge of these dissociable groups is regulated by changes in pH through the association/dissociation of protons and hydroxyl groups. These reactions are crucial in energy processes and for designing the functionalities of novel soft materials. We investigated the pH-dependent phase diagram of co-assembled assemblies by considering an equimolar mixture of acid- and base-functionalized colloidal particles and compared it with a mixture of nanoparticles of fixed positive and negative charges. We found that the system of nanoparticles with fixed charges tends to form a percolated network, whereas in the system containing ionizable groups, denser clusters are favored [2].

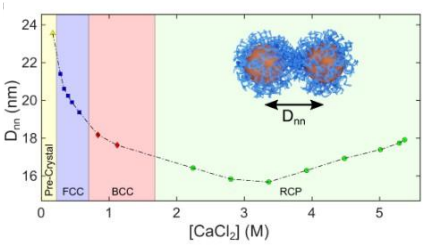


Fig. 2. Nearest-neighbor separation (D_{nn}) versus $CaCl_2$ concentration shows contraction-to-re-expansion.

Charged nanoparticle assemblies in extremely saline solutions: The electrostatic potential of charged objects in aqueous solutions is screened by the surrounding counterions. Classical theories predict that with increasing salt concentration the range of the electrostatic potential decreases monotonically, which should compact arrangements of like-charged objects with increasing salinity. However, we find re-expansion of lattices with increasing salt concentration in assemblies of gold nanoparticles coated with single-stranded DNA (DNA-NP), without the possibility of canonical base-pairing interactions [3]. DNA-NP assembled into FCC lattices contracted with added salt and transitioned to BCC, and to random-closed-packed (RCP) structures when the packing density of the particles starts increasing with increased salinity (*Fig. 2*). MD simulations and WAXS showed that at very high salt concentration, the ionic correlations between the salt ions led to clustering of ions and reduced the concentration of free ions available to screen the electrostatic interactions between neighboring particles resulting in re-expansion of the lattices [3]. Lowering the permittivity strengthened this ion-ion coupling and shifted the re-expansion threshold to lower salt concentration, linking bulk ionic correlations to the assembly response.

Ion fluxes in confinement. Ion fluxes mediated by ion pores are highly interactive processes that give rise to unique functions. We developed a description of self-generated electrolyte flow in capillaries composed of heterogeneous cylindrical micelles or microfluidic devices whose walls feature both nonuniform charge distributions and nonuniform active ionic fluxes [4]. This morphology generates an electrolyte velocity forbidden in the absence of charge and fluxes. We demonstrated that these flow states emerge when modulated boundary patterns of charge and flux are offset by a flux-charge phase difference, corresponding to the separation between the sites of their peak densities on the wall (*Fig. 3*). Our numerical work demonstrated that this mechanism can be realized with a microfluidic generator powered by enzyme-coated patches that catalyze reactants in solution to produce ion fluxes, or by ion fluxes generated through ion pores. Local ionic elevation or depletion, which disrupts a nonuniform double layer, promotes self-induced gradients that yield persistent body forces to generate bulk fluid motion. Our work provided a theoretical framework for understanding the combined effects of active and charged boundaries in biological and soft-matter systems, with applicability to electrofluidic and iontronic applications.

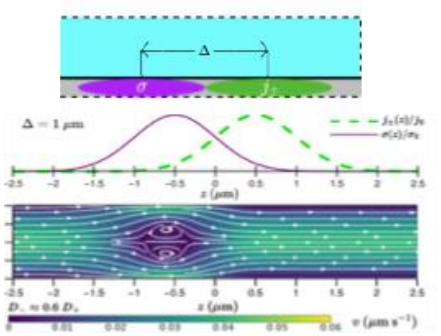


Fig 3. Flows generated by ion fluxes and charge patches are enhanced from diffusivity mismatch in microfluidic chamber as a function of the separation

Quincke colloids. We examined populations of self-oscillating Quincke colloids [5]. Depending on the initial distribution, these active oscillators spontaneously organize into distinct collective states characterized by temporal synchronization and directional alignment, termed synchronematic order. In fluid-like clusters, this order is short-ranged and decays over a length scale set by the competition between hydrodynamic interactions and athermal noise. In crystalline clusters, these interactions drive global synchronization and circular alignment-synchronematic crystals-whose collective frequency increases with cluster size due to non-reciprocal interactions

Future Plans

Coupling of geometry and charge regulation in chiral amphiphiles. We aim to complete the phase diagram of commonly observed chiral shapes by identifying the conditions under which the helical assemblies transform to twisted ribbon structures and extend the chiral assembly studies to the case of enantiomeric mixtures to determine under which conditions left- and right-handed amphiphiles mix homogeneously, segregate into domains, or generate new packing motifs, and how the local molecular arrangements propagate into membrane-scale chiral morphology. Since bending rigidity strongly shapes soft membranes, we will vary amphiphile tail length and enantiomeric ratio to test whether rigidity mismatches favor segregation, or uniform mixing. SAXS/WAXS, circular dichroism, cryo-EM, and polarized microscopy will map the lipid tail and

headgroup organization and defects across enantiomeric ratios, with molecular dynamics and Monte Carlo simulations providing a mechanistic framework for the observed motifs.

Charged nanoparticle assemblies' response to temperature. We hypothesize that dehydration of the nanoparticles and the enhanced ionic correlations at high salinities will produce assemblies with negative thermal expansion (NTE) coefficients. Based on our previous results discussed above, dehydration leads to more compact assemblies. The dehydration is entropically favored with increasing temperature. At molar salt solutions, the bulk solution consists of ionic clusters, which could be broken down at elevated temperatures. This could increase the concentration of free ions to screen interparticle interactions. Both these effects should lead to NTE assemblies.

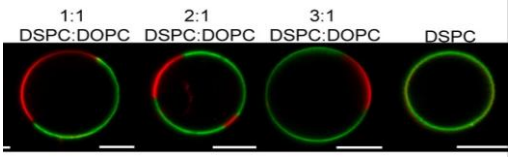


Fig. 4. Microscopy images of phase separation of saturated lipids and unsaturated lipids (red). Scale bars are 10 μ. Image from [7].

Charge regulation in all-atom MD simulations: To advance understanding of ionizable soft materials, we will develop a method to account for acid-base association-dissociation reactions in atomistic, explicit-solvent force-field models. We propose performing charge exchange between the ionizable groups and water molecules by creating/eliminating H_3O^+ (or OH^-) ions by switching water molecules between the neutral and protonated/deprotonated states. Local pH and interfacial electric fields play critical roles in interfacial redox processes, electrocatalysis, and energy processes. Our method and simulations will determine the local pH of water at interfaces.

Ion fluxes in confinement. Ion pores will be incorporated into vesicle membranes using peptides that self-assemble into pores upon interaction with membranes or through cell-free protein expression. We will leverage our finding that phase-separating membranes and hydrophobic mismatch between membrane peptides/transporters and membranes can be used to vary the spatial organization of proteins within synthetic membranes [6]. Self-directed motion can be achieved via nonuniform pore placement on the phase-separated vesicles (*Fig. 4*) [7]. Our work will provide a platform to insert enzymes or ion pores into specific vesicle positions, empowering them with self-diffusiophoresis.

Chiral Quincke Colloids. In collaboration with Alexey Snezhko's at Argonne National Laboratory, we are extending our study of self-oscillating Quincke rollers to a regime in which the particles perform circular chiral trajectories. These chiral oscillators are realized using pear-shaped Quincke rollers, whose shape anisotropy produces differential friction and, consequently, a persistent torque that continuously bends their trajectories into circular motion. Depending on initial conditions, individual rollers spontaneously select either clockwise or counterclockwise motion with equal probability, giving rise to two clearly distinguishable chiral states. We will incorporate hydrodynamic and electrostatic interactions to describe the motion of Quincke rollers to reproduce

the spontaneous selection of chiral trajectories. The broader goal is to establish a predictive model for the nonequilibrium states of matter observed experimentally in chiral active suspensions.

References

1. J. M. McCourt, L. Lopez-Flores, S. Kewalramani, N. B. Welke, M. Olvera de la Cruz, M. J. Bedzyk, *Coupling of Charge Regulation and Geometry in Soft Ionizable Molecular Assemblies*, J. Phys. Chem. B 129, 3814 (2025).
2. L. Lopez-Flores and M. Olvera de la Cruz, *Charge regulation effects on colloidal mixture nanoparticles,* J. Chem. Phys. **163**, 034303 (2025)
3. R.J.E. Reinertsen, S. Kewalramani, F. Jimenez-Angeles, S.J. Weigand, M.J. Bedzyk, M. Olvera de la Cruz, *Reexpansion of Charged Nanoparticle Assemblies in Concentrated Electrolytes*, PNAS **121**, e2316537121 (2024).
4. A. Shrestha, E. Kirkinis, M. Olvera de la Cruz, *Self-generated electrokinetic flows from active-charged boundary patterns*. Physical Review Research **7**, 023223 (2025).
5. S. Leyva, Z. Zhang, M. Olvera de la Cruz, K. Bishop, *Self-oscillating synchronematic colloids,* Nature Communications **17**, 1841 (2026)
6. J.A. Peruzzi, J. Steinkuhler, T.Q. Vu, T.F. Gunnels, V.T. Hu, P. Lu, D. Baker, N. P. Kamat, *Hydrophobic mismatch drives self-organization of designer proteins into synthetic membranes*, Nat Commun. **15**, 3162 (2024).
7. *T.Q.* Vu, J.A. Peruzzi, L.E. Sant'Anna, E.W. Roth, N.P. Kamat, *Lipid Phase Separation in Vesicles Enhances TRAIL-Mediated Cytotoxicity*, Nano Letters. **22**, 2627 (2022))

Publications

1. J. M. McCourt, L. Lopez-Flores, S. Kewalramani, N. B. Welke, M. Olvera de la Cruz, M. J. Bedzyk, *Coupling of Charge Regulation and Geometry in Soft Ionizable Molecular Assemblies*, J. Phys. Chem. B 129, 3814 (2025).
2. L. Lopez-Flores and M. Olvera de la Cruz, *Charge regulation effects on colloidal mixture nanoparticles,* J. Chem. Phys. **163**, 034303 (2025).
3. R.J.E. Reinertsen, S. Kewalramani, F. Jimenez-Angeles, S.J. Weigand, M.J. Bedzyk, M. Olvera de la Cruz, *Reexpansion of Charged Nanoparticle Assemblies in Concentrated Electrolytes*, PNAS **121**, e2316537121 (2024).
4. Y. Xiong, A. Aggarwal, M. Olvera de la Cruz, *Chemo-Mechanical Coupling in Hydrogels: Dynamics in the Diffusion-Limited Regime*, Advanced Functional Materials **35** 2507078 (2025).
5. Shrestha, M. Olvera de la Cruz, Shrestha, *Enhanced phoretic self-propulsion of active colloids through surface charge asymmetry* Physical Review E **109**, 014613 (2024).
6. C. Waltmann, A. Shrestha, M. Olvera de la Cruz, *Patterning of multicomponent elastic shells by Gaussian curvature Phys. Rev. E* **109**, 054409 (2024).
7. N. Pogharian, P. M. Vlahovska, M. Olvera de la Cruz, *Effects of Normal and Lateral Electric Fields on Membrane Mechanical Properties*, J. of Physical Chemistry B **128**, 9172 (2024).
8. A. Shrestha, E. Kirkinis, M. Olvera de la Cruz, *Self-generated electrokinetic flows from active-charged boundary patterns*. Physical Review Research **7**, 023223 (2025).
9. S. Leyva, Z. Zhang, M. Olvera de la Cruz, K. Bishop, *Self-oscillating synchronematic colloids,* Nature Communications **17**, 1841 (2026).
10. V. Agrawal, M. Olvera de la Cruz, *Electrostatically driven pattern formation in mixed charged–neutral multicomponent elastic membranes* PNAS **123**, e2536038123 (2026).

Nonequilibrium Transport: Interfaces, Nucleation, and Bulk Dynamics

Ahmad K. **Omar**, Department of Materials Science and Engineering, University of California, Berkeley

Keywords: transport phenomena, active interfaces, chiral dynamics, nonequilibrium

Research Scope

Living and biological systems across an outstanding range of length scales can display dynamical properties that appear fundamentally different from those of conventional synthetic materials. The breaking of parity and time-reversal symmetry at the microscale frees biomolecular materials from the constraints these symmetries impose on the transport coefficients of traditional "passive" systems. Indeed, from the chiral motion of starfish embryos that generate "odd" transport coefficients to the predator-prey interactions among microorganisms resulting in traveling states, the living world motivates the need to advance our fundamental understanding of active transport mechanisms. Such an understanding could pave the way towards the design of next-generation materials with novel dynamical properties that could improve performance and potentially unlock new applications. Taking inspiration from a variety of recent experiments characterizing biomolecular material transport, this research leverages theory and computation to develop a microscopic understanding of some of the exotic dynamical properties exhibited by these materials. We address theoretical questions surrounding the origins of odd diffusion, explore the implications of violating Newton's third law on multicomponent diffusion, and develop a theory for the dynamics of active interfaces and nucleation. Alongside these theoretical advancements, we build and develop tools for the characterization of these transport coefficients that can be used in both computational and experimental settings. Moreover, as the line between structure and dynamics is blurred for these out-of-equilibrium systems, we will explore the implications of these transport mechanisms on material structure and stability.

Recent Progress

The statistical mechanics of equilibrium interfaces has been well-established for over a half century. In the last decade, a wealth of observations have made increasingly clear that a new perspective is required to describe interfaces arbitrarily far from equilibrium. These include the reports of a *negative surface tension* of active liquid interfaces despite the interface appearing stable. Beginning from microscopic particle dynamics that break time-reversal symmetry, we have systematically derived the interfacial dynamics of coexisting motility-induced phases. Doing so allows us to identify the athermal energy scale that excites interfacial fluctuations and the nonequilibrium surface tension that resists these excitations. Our theory identifies that, in contrast to equilibrium fluids, this active surface tension contains contributions arising from nonconservative forces which act to suppress interfacial fluctuations and, crucially, is distinct from the mechanical surface tension of Kirkwood and Buff (see Fig. 1). We find that the interfacial stiffness scales linearly with the intrinsic activity of the constituent active particle trajectories, in

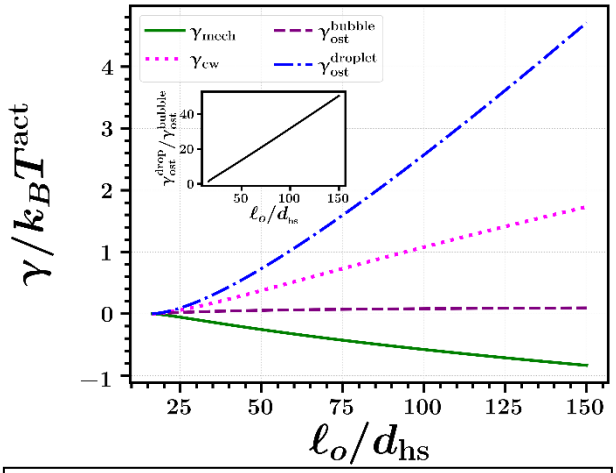


Figure 1: The *three* surface tensions of out-of-equilibrium fluids as a function of activity with an additional distinction between the Ostwald tensions of bubbles and droplets. *At equilibrium, all these tensions are identical.*

agreement with simulation data. We demonstrate that at wavelengths much larger than the persistence length, the interface obeys surface area minimizing Boltzmann statistics with our derived nonequilibrium interfacial stiffness playing an identical role to that of equilibrium systems.

We were able to build on our interfacial fluctuation perspective to develop a theory for nucleation and growth of nonequilibrium fluids. Homogeneous nucleation, a textbook transition path for phase transitions, is typically understood on thermodynamic grounds through the prism of classical nucleation theory. However, recent studies have suggested the applicability of classical nucleation theory to systems far from equilibrium. We have formulated a purely mechanical perspective of homogeneous nucleation and growth, elucidating the criteria for the properties of a critical nucleus without appealing to equilibrium notions. Applying this theory to active fluids undergoing motility-induced phase separation, we identify *three distinct surface tensions* (see Fig. 1) -- the mechanical, capillary, and Ostwald tensions – that play a central role in our theory. While these three surface tensions are identical in equilibrium, our work highlights the distinctive role of each tension in the stability of active interfaces and the nucleation and growth of motility-induced phases.

Importantly, we have extended our theory to apply to systems with *chiral* dynamics in two dimensions. Spatial parity symmetry is routinely broken in experimentally realized active matter systems. We have recently derived a theory for the phase coexistence and interfacial fluctuations for a system that microscopically violates spatial parity. We find suppression of the phase separation as chirality is increased as well as the development of steady-state currents tangential to the interface dividing the phases. These odd flows are irrelevant to stationary interfacial properties, with stability, capillary fluctuations, and surface area minimization determined entirely by the capillary surface tension. Using large-scale Brownian dynamics simulations, we found excellent agreement with our theoretical scaling predictions.

Future Plans

Our work on active interfacial theories suggests that interfacial phenomena in achiral active Brownian particles should be remarkably similar to that of equilibrium fluids. Yet, some phase-separated active systems display *a large population of bubbles* distributed in the dense phase that is at odds with equilibrium liquids where appreciable bubble formation is energetically prohibitive. We thus conducted large-scale simulations to understand the origin of bubble formation by probing

its dependencies. In the athermal system, in which there is no translational Brownian noise, bubbles are entirely absent, consistent with our theoretical expectations. Shockingly, a small amount of translational noise (as measured through the dimensionless noise strength, $\mathcal{T}$) results in *marked bubble proliferation* (see Fig. 2)*!* Whether this transition is truly discontinuous or simply incredibly sharp remains an outstanding question, but the difference in bubble populations coincides with a sharp distinction in dense-phase dynamics. Dynamics in the athermal dense phase are sluggish, reflected in a subdiffusive mean-square displacement while those for the thermal system are fast and diffusive at all times. We are currently working to make this dynamical and structural link more explicit with a theoretical perspective linking bubble formation and bulk transport. An additional fascinating dependence is revealed when comparing monodisperse and polydisperse systems. The hexagonal order present in the dense monodisperse liquid appears to be a crucial ingredient for bubble proliferation, in addition to thermal noise.

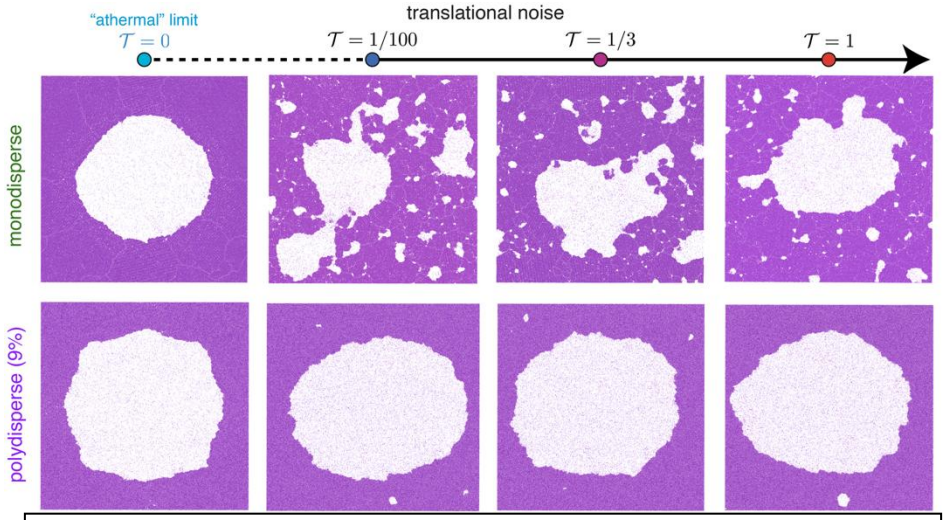


Figure 2: Representative snapshots of simulations at various values of thermalization for both monodisperse and polydisperse cases. Bubbles within the liquid phase were uncommon in all polydisperse and all athermal simulations.

This program has long sought to understand bulk linear transport phenomena in systems arbitrarily far from equilibrium. Linear constitutive laws describe transport across a remarkable range of systems, including many in which the local-equilibrium hypothesis underlying linear irreversible thermodynamics cannot hold. It is well established that driving a system out of equilibrium can lead to new classes of macroscopic transport phenomena that are forbidden near equilibrium. We are currently examining two representative nonequilibrium systems through simulations and a mechanical perspective: a system with pairwise nonreciprocal interactions between distinct species and a system with applied one-body parity-breaking nonreciprocal torque. For the pairwise interacting system, nonreciprocity is found to gives rise to characteristic oscillatory relaxation in the dynamic structure factor, even in a homogeneous state. In the chiral system, an applied torque breaks parity symmetry and leads to diffusion perpendicular ("odd") to density gradients. We can extract the diffusion tensors from simulations using several approaches and find good agreement between our numerical results and mechanical theory. For both model systems, our mechanical

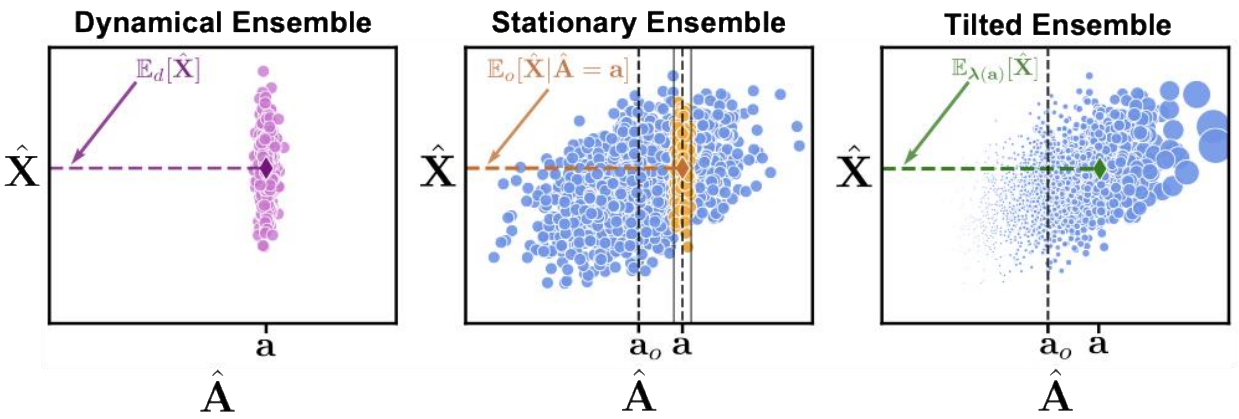


Figure 3: Schematic illustrating the regression-hypothesis and tilting construction used in the main text. (a) A dynamical ensemble produces a mean response for a given realization of the slow variable. (b) From the conditional-regression viewpoint, this mean response is expressed as a stationary conditional expectation at the specified value of the slow variable. (c) When the slow variable is sufficiently concentrated, the conditional stationary ensemble can be approximated by an exponentially tilted ensemble with the same mean. Dot size indicates statistical weight.

perspective connects microscopic features of the dynamics to macroscopic nonreciprocity and provides a practical mechanical route for probing unusual transport phenomena directly from the microscopic equations of motion.

Finally, we are working to show that the transport coefficients governing linear constitutive laws can be expressed as a linear regression coefficient in a reference ensemble. This identification follows from a time-dependent projection operator whose action can be well approximated by cumulants in a reference state. Importantly, this construction yields a route to go beyond linear transport, facilitating the calculation of transport coefficients of arbitrary order expressed as steady-state cumulants of observables. This procedure will further provide explicit bounds on two key approximations, and a unified perspective which recovers linear irreversible thermodynamics and Green-Kubo relations for odd transport as special cases. Because we can apply this procedure to any intensive variable, this approach is not limited to transport and can be used to systematically relate different intensive variables in and out of equilibrium.

Publications

1. L. Langford and A. K. Omar, *Theory of Capillary Tension and Interfacial Dynamics of Motility-Induced Phases*, Physical Review E **110**, 054604 (2024)
2. L. Langford and A. K. Omar, *Phase Separation, Capillarity, and Odd-Surface Flows in Chiral Active Matter*, Physical Review Letters **134**, 068301 (2025)
3. C. Hargus, A. Deshpande, A. K. Omar, and K. K. Mandadapu, *The Flux Hypothesis for Odd Transport Phenomena*, Physical Review Letters **134**, 097105 (2025)
4. L. Langford and A. K. Omar, *The Mechanics of Nucleation and Growth and the Surface Tensions of Active Matter*, Journal of Chemical Physics **163**, 064901 (2025)
5. L. Langford and A. K. Omar, *Hexatic Order Coupled with Thermal Noise Produces Bubbles in Two-Dimensional Active Matter*, arXiv:2603.17320 (2026)
6. Y.J. Chiu*, E. M. Weiner*, and A. K. Omar, *Multicomponent Linear Transport in the Absence of Local Equilibrium*, arXiv:2505.23906 (2025)

Data-Driven Generalized Master Equations for Nonequilibrium Coarse-Grained Dynamics and Response

Grant M. **Rotskoff** — Department of Chemistry, Stanford University

Keywords: coarse-graining; generalized master equations; non-Markovian (memory) dynamics; nonequilibrium response; score-based diffusion methods; machine learning

Research Scope

Predictive kinetic models of complex molecular system, in many cases, rely on a coarse-grained description that emphasizes a few stable states. Two assumptions pervade standard approaches to coarse-graining: 1) that the reduced dynamics are Markovian, and 2) that the system is in thermodynamic equilibrium. Memory is an unavoidable consequence of projecting high-dimensional dynamics onto a handful of observables, and many systems of interest are actively driven and settle into nonequilibrium steady states. The aim of this work is to build reduced dynamical models directly from data that capture memory exactly, remain thermodynamically consistent and physically valid, and remain accurate and out of equilibrium. Ensuring these properties allows us to move towards predictive models of how coarse-grained kinetics respond to perturbations. The approach is grounded in nonequilibrium statistical mechanics and connects to recent machine-learning advances in score-based (diffusion) modeling.

Recent Progress

Kinetic analyses of single-molecule and simulation data are typically built on Markov state models (MSMs), which discretize configuration space and assume memoryless transitions between states. Because memory is generically introduced by coarse-graining, MSMs can misrepresent the true dynamics. Generalized master equations (GMEs) address this by explicitly encoding memory through a kernel, but they are notoriously difficult to parameterize and, in the discrete-time setting native to experiments, are usually only formally approximate.

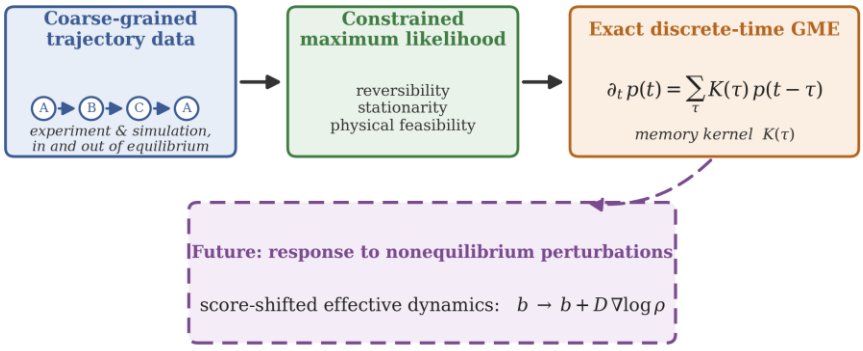


Figure 1. Data-driven workflow. From discrete-time trajectories (experiment or simulation, in or out of equilibrium), a constrained maximum-likelihood procedure parameterizes a formally exact generalized master equation with memory kernel K(τ), enforcing reversibility, stationarity, and physical feasibility [1]. Planned work (dashed) extends this to nonequilibrium response via score-shifted effective dynamics [2].

We recently introduced a maximum-likelihood framework that parameterizes formally exact, physically feasible, discrete-time GMEs directly from experimental and simulation data, in and out of equilibrium [1]. The central object is a discrete-time memory kernel inferred from observed transition counts. The algorithms impose reversibility and stationarity as explicit constraints, are guaranteed to return valid evolution equations (stable, probability-preserving propagators), and conditionally maximize the likelihood of the observed data. Crucially, the method operates on the discrete-time data experiments actually produce and applies to nonequilibrium steady states, while many methods rely on assumptions of thermodynamic equilibrium. Our approach provides a principled, statistically optimal route from raw trajectories to kinetic models that are simultaneously accurate and physically well posed (Fig. 1).

Future Plans

The GME framework describes nonequilibrium dynamics; we next plan to understand how to deduce the response to perturbations from the coarse-grained dynamics of these systems. Classical linear response interprets a perturbation through equilibrium fluctuations in a conjugate observable, but this reasoning breaks down out of equilibrium. Response around a nonequilibrium steady state requires additional dynamical information, and perturbations that change the diffusion constant or temperature cannot be captured by conventional path-ensemble averaging. In recent work we showed that such responses can nevertheless be computed by constructing an effective physical process whose dynamics acquire an extra drift proportional to the score, $\nabla \log \rho$, of the instantaneous density—the same object at the heart of modern diffusion models—so responses follow even when the score is only learned [2].

We plan to unify these two lines of work. Specifically, we will 1) generalize the score-shifted, effective-dynamics response formalism from continuous stochastic differential equations to the discrete-time, non-Markovian GME setting; 2) derive memory-aware response functions and learn the requisite score (or response kernel) from the same trajectory data used to parameterize the GME; 3) carry the reversibility, stationarity, and feasibility constraints through to the response, so that predictions remain thermodynamically valid. The resulting pipeline both learns exact nonequilibrium coarse-grained dynamics and predicts their response, bridging generalized master equations and score-based methods.

References

1. C.-W. J. Liu, J. Klinger, and G. M. Rotskoff, Optimal parameterization of nonequilibrium generalized master equations from discrete-time experimental data, arXiv:2606.28289 (2026).
2. Klinger, J.; Rotskoff, G. M. Computing Nonequilibrium Responses with Score-Shifted Stochastic Differential Equations. *Phys. Rev. Lett.* **2025**, *134* (9), 097101. https://doi.org/10.1103/PhysRevLett.134.097101.

Publications

1. Ye, M.; Pert, E. K.; Lee, M. S.; Li, Y.; Nishimura, A.; Li, R. L.; Ngo, S. H.; Huang, W. Y.; Rotskoff, G. M.; Macfarlane, R. J. Nanoparticle Superlattices Assembled via Rapid Solvent Destabilization of Macromolecular Ligands. *ACS Nano* **2025**. https://doi.org/10.1021/acsnano.5c10677.
2. Klinger, J.; Rotskoff, G. M. Computing Nonequilibrium Responses with Score-Shifted Stochastic Differential Equations. *Phys. Rev. Lett.* **2025**, *134* (9), 097101. https://doi.org/10.1103/PhysRevLett.134.097101.
3. Pert, E. K.; Hurst, P. J.; Waymouth, R. M.; Rotskoff, G. M. Coacervation Drives Morphological Diversity of mRNA Encapsulating Nanoparticles. *The Journal of Chemical Physics* **2025**, *162* (7), 074902. https://doi.org/10.1063/5.0235799.
4. Causer, L.; Rotskoff, G. M.; Garrahan, J. P. Discrete Generative Diffusion Models without Stochastic Differential Equations: A Tensor Network Approach. *Phys. Rev. E* **2025**, *111* (2), 025302. https://doi.org/10.1103/PhysRevE.111.025302.
5. C.-W. J. Liu, J. Klinger, and G. M. Rotskoff, Optimal parameterization of nonequilibrium generalized master equations from discrete-time experimental data, arXiv:2606.28289 (2026).

Tension and Curvature -Driven Interactions Producing Touch-Sensitive Patterning in Biomolecular Lamellae

Maria M. **Santore** and Gregory M. Grason; Department of Polymer Science and Engineering

University of Massachusetts, Amherst

Keywords: elasticity, assembly, lattice, transition, crystallization

Research Scope

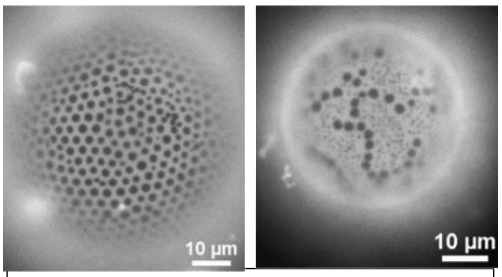


Figure 1. Assembled configurations of monomodal and bimodal domains

The discovery and understanding of touch-sensitive elasticity-driven patterning mechanisms in flexible ultrathin composite sheets is advanced in this program through the integration of theory and experiment focused on biomolecular lamellae containing coexisting fluid and solid (crystalline) phases. Sought after properties not achieved with classical ultra-thin solid sheets such as graphene, nor in canonical fluid membranes and lamellae include the ability to reversibly shift between complex contours having different non-zero Gaussian curvatures, to reversibly assemble solid constituents into arrays and networks in response to mechanical stimuli, and to switch pattern spacing and topology using mechanical triggers with response times as short as a second. Examples of patterns include soccer ball-like pseudo-hexagonal lattices with varied spacings, parallel stripes, and interconnected chains, some with selectivity in the arrangements of different sized constituents in bimodal systems. These sheets also undergo sharp transitions between different patterns and complex global shapes.

This program exploits the 4 nm thick lamella of giant unilamellar phospholipid vesicles containing fluid and crystalline membrane domains to establish mechanisms of pattern formation. These two phase biomolecular membranes comprise 2D fluid regions with integrated 2D solids, both having bending and stretching elasticity. The fluid membrane flows while large solid in-plane moduli effectively eliminate shear deformation. Thus the solid shear elasticity underlies the geometrically non-linear coupling between Gaussian curvature and in-plane strain of 2D sheets. Combined analytical and finite element modeling along with experiments leads to a predictive framework that guides understanding of complex function and establishes generality.

Recent Progress

Membrane-Templated Morphologies of Ultra-thin Crystals We demonstrated how the combined bending and line energies in composite membranes select for the morphologies of growing crystals, for the case of vesicles having 30% DPPC and 70% DOPC, producing crystals that make up 13% of membrane area independent of vesicle size.[1] We further determined how the competition between bending and line energy is shifted by the membrane tension, such that experimental tension is predictive of crystal morphology. This understanding established that complex flower-shaped crystals grew on larger higher-tensioned vesicles compared with the more compact crystals on small vesicles, a dependence on vesicle size opposing established arguments for the assembly of colloidal crystals on spheres.[2] Most recently, detailed analytical modeling of evolving membrane tension, taking into account separately measured membrane properties from the literature and including no adjustable parameters, predicts evolution of membrane tension for a broad composition of vesicle membranes and predicts a greater array of behaviors for morphology development in membranes of different compositions. For instance, we can now explain and predict morphological transitions from compact to flower shapes that occur at elevated concentrations of the crystallizing species, and we can extend the treatment developed for phospholipids to morphology in other membrane-templated 2D crystals, or employ synthetic polymer-surfactant membranes, establishing the generality of our discoveries.

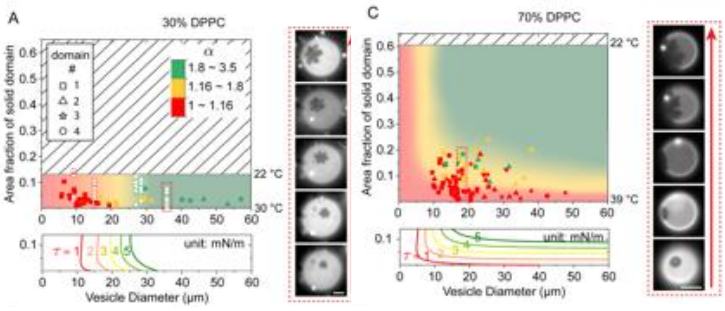


Figure 2. Different tension evolutions and corresponding state spaces for fixed and evolving crystal morphology.

Robust Single 2D Crystal Mechanics and Extreme Elastic Deformation. Solid deformation is expected to profoundly influence assembly. We explore the mechanics of solid domains (single crystals) and highlight their distinctions from single lipid multi-crystalline vesicles. In the latter, the inability of the solid to assume the Gaussian curvature of a closed vesicle forces the solid membrane to form multiple crystallites separated by disordered regions.

We study vesicles containing one or two large single crystals grown upon progressive cooling from individual nuclei. Applying suction to the face of single crystal revealed just how robust these 4 nm crystals are: No yielding into the micropipette was seen as suction was increased, placing a lower bound on its modulus. Further, suction applied to a crystal face was not transmitted to the surrounding low tension or flaccid membrane. These vesicles remained flaccid with the fluid membrane phase unstretched. As suction on the crystal was increased, ultimately at a pressure exceeding 4 kPa, the crystal failed and was lost into the pipette, demonstrating a large stress to failure for these 2D biomolecular crystals.

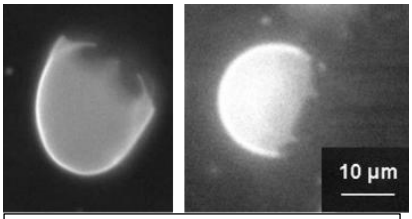


Figure 3. Floppy crystal, suctioned against pipette

Separately, application of micropipette suction to the edge of a large slightly hexagonal crystal triggered it to collapse in order to fully enter a micropipette (Figure 4) one fourth its diameter. The interior aqueous vesicle liquid and the in-tact fluid membrane prevented the crystal from being lost down the pipette. It is not clear if the crystal scrolled cylindrically to enter the pipette or if it folded, umbrella-like. The crystal remained integrated with the fluid membrane; however, a subsequent reduction of suction enabled the crystal to eject from the pipette, whereby it invaginated into the vesicle and was only partially visible. Increasing suction of the fluid membrane caused the crystal to resurface and revealed that its shape was minimally affected by the mechanical abuse. Some alteration of the crystal shape and loss of interior liquid suggests membrane rupture and resealing. While the elastic character of such single crystals is clear, it is not obvious if the crystal broke and then healed.

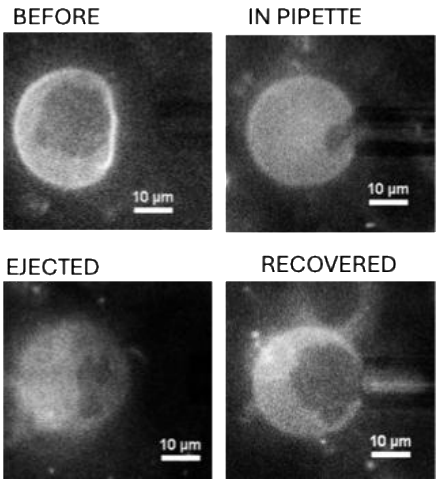


Figure 4. Compact domain initially, aspirated, ejected (partially invaginated domain), reappearance of domain after suction of membrane fluid

These behaviors of single elastic 2D crystals contrast those of multi-crystalline vesicles of a single lipid, where vesicles can be aspirated at modest suctions into a pipette. Release reveals yielding and that the membrane has been molded into the shape of its projection.

Elastic pattern selection in single solid domains on inflated vesicles We considered the elementary case of a single, circular solid domain and using a combination of finite-element simulations of composite vesicle elasticity and Foppl-van Karman theory for the elementary case of a single, circular solid domain on a vesicle, we showed vesicle shapes exhibit a generic pattern of shapes with increasing inflation. This sequence, in Figure 5 top proceeds from smoothly rolled shapes at zero tension to isometrically folded shapes above a threshold tension. Raising tension (inflation) further we find a transition to increasingly non-isometric solid domain configurations adopting first a pattern of crumples then fine, radial wrinkles, before exhibiting smoothly stretched spherical cap shapes. Notably, this latter elastic pattern sequence has been previously shown from microscopic elastic sheets at fluid (e.g. air/water) interfaces,[3-5] but our study is the first to determine the regime of crumple to wrinkle transitions in the context of bilayer vesicle

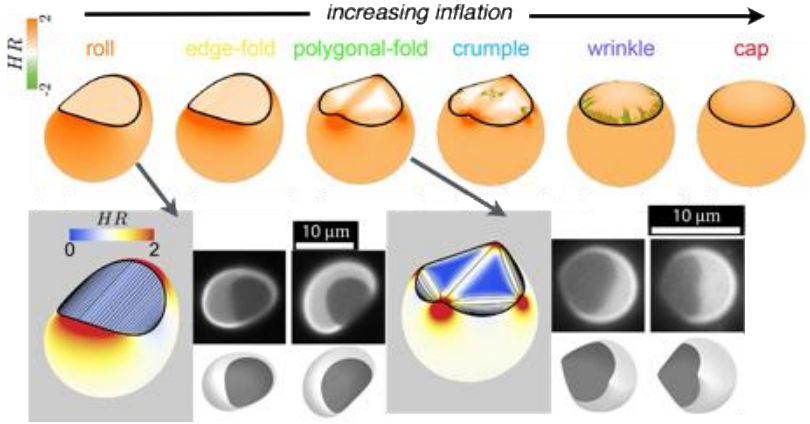


Figure 5. Calculated and observed elastic patterns on a solid domain.

systems. We show that these complex patterns are determined by the ratio of membrane tension relative to two mechanical scales, one controlled by isometric bending and the other non-isometric spherical distortion of the solid domains. We further predict that isometrically folded solid shapes are especially likely for even only slight inflation of GUVs. Consistent with this prediction, fluorescence microscopy of DPPC-DOPC composites with single, large solid domains (Figure 5 bottom) shows striking evidence of both smoothly rolled and polygonally-folded solid domain patterns.

A State Space for Solid Domain Assembly. A state space summarizes the impact of key variables on the structure and properties of dynamic crystal assemblies, providing insights into the interactions, the stability of assemblies, and a working map for creating functional materials. Key variables include the vesicle inflation or excess area, and domain number or size, and overall solid area. For vesicles of a broad size range containing about 18% solid area fraction (Figure 6A), we mapped the state space to identify variable ranges producing patterns that were pseudohexagonal arrays or chains. This revealed an extremely sharp boundary or first order transition between the two pattern types: In the limit of low excess area, a small change (1%) in excess area produces a dramatic reconfiguration of patterning. In the distant part of the state space at high excess area, pseudohexagonal lattice patterns persist over a broad range of crystal sizes, numbers, and excess area. Here the pattern can adjust to perturbations and retain order. Ongoing studies of the impact of solid area suggest a similar first order phase transition in the limit of low excess area, with the exact excess area corresponding to the transition being determined. Newly discovered in the limit of high excess area are shape transitions corresponding to reconfigurations of pseudohexagonal patterns. In Figure 6C a vesicle contains two flat-ish islands of relatively closely-spaced hexagonal assemblies separated by a domain-free border. This object spontaneously reconfigures to a sphere covered uniformly by a pseudo-hexagonal lattice of greater spacing.

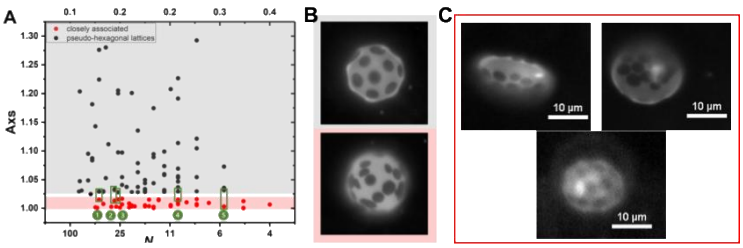


Figure 6. A. state space of assemblies for 18% solids. B. transition at low excess area. C. transition at high excess area

Future Plans

Next steps will continue to address the ranges of assemblies that can be achieved in elastic ultrathin composite sheets, focusing on the role of elasticity and curvature on their phase and shape transitions to develop a predictive mechanistic understanding.

References

1. H. Wan, W. Xin, G. Jeon, G. Grason, and M. M. Santore* *Flower-Shaped 2D Crystals Grown in Curved Fluid Vesicle Membranes*, Nature Communications **15**, Article number: 3442 (2024)
2. G. N. Meng, J. Paulose, D. R. Nelson, and V. N. Manoharan, *Elastic Instability of a Crystal Growing on a Curved Surface*. Science **343**, 634-637 (2014).
3. H. King, R. D. Schroll, B. Davidovitch, N. Menon, Elastic sheet on a liquid drop reveals wrinkling and crumpling as distinct symmetry-breaking instabilities. *Proceedings of the National Academy of Sciences of the United States of America* **109**, 9716–20 (2012).
4. J. D. Paulsen, *et al.*, Optimal wrapping of liquid droplets with ultrathin sheets. *Nature Mater* **14**, 1206–1209 (2015).
5. Y. Timounay, *et al.*, Crumples as a Generic Stress-Focusing Instability in Confined Sheets. *Phys. Rev. X* **10**, 021008 (2020).

Publications

G. Jeon, A. N. A. Prempeh, M.M. Santore, G. M. Grason *Frustrated Shapes of Solid Domains in Fluid Membrane Vesicles: From Rolls and Folds to Crumples and Wrinkles*", under review for New Journal of Physics (2026), preprint DOI: 10.48550/arXiv.2606.26433

H. Wan, G. Jeon, G. Grason, and M.M. Santore,* *Sculpting 2D Crystals via Membrane Contractions before and during Solidification*, Langmuir **42**, 6887-6902 (2026). doi.org/10.1021/acs.langmuir.5c06439

H. Wan, G. Jeon, G.M. Grason, and M.M. Santore,* *Thermal Preconditioning of Membrane Stress to Control the Shapes of Ultrathtin Crystals*, Soft Matter **20**, 6984-6994 (2024). doi.org/10.1039/D4SM00739E

G. Jeon, G., Fagnoni, J. H. Wan, M.M. Santore, and G.M. Grason,* *Shape Equilibria of Vesicles with Rigid Planar Inclusions*, Soft Matter **20**, 5754-5769 (2024). doi.org/10.1039/D4SM00439F

W. Xin, and M. M. Santore* *Bending-Driven Patterning of Solid Inclusions in Lipid Membranes: Colloidal Assembly and Transitions in Elastic 2D Fluids*, Proceedings of the National Academy of Science Nexus, **3** (8) pgae331 (2024). doi.org/10.1093/pnasnexus/pgae331

Emergent functionality generated from excitonic building blocks using DNA origami

Gabriela S. **Schlau-Cohen**, Department of Chemistry

Mark Bathe, Department of Biological Engineering
Adam P. Willard, Department of Chemistry
Massachusetts Institute of Technology

Keywords: DNA nanotechnology, excitonic materials, light harvesting, solar energy conversion

Research Scope

Our research program establishes a class of materials that support emergent functionality of electronic excited states, *i.e.*, excitons. In Nature, essential biological functions emerge from the precise geometric arrangement of protein networks. In particular, the molecular machinery responsible for photosynthetic solar energy conversion is exquisitely sensitive to structural organization, owing to the need to manage high energy electronic excitations. While replicating this spatial precision in artificial light-harvesting systems has remained long-standing challenge, DNA-based excitonic architectures offer a synthetic route to achieve programmable photophysical functionality. The structural variety and geometric precision afforded by higher-order DNA origami architectures enable the development of bioinspired excitonic systems with broad and tunable functionalities that mimic or potentially exceed those found in Nature. Previously, we demonstrated that DNA can position embedded chromophores to control the intermolecular interactions that dictate excitonic properties. Using this control, we developed DNA-based excitonic building blocks selective for the foundational properties of energy transfer, charge transfer, and excimer formation. We are advancing in the complexity and precision of these structures to explore how excitonic processes, such as energy transport, charge separation, and singlet fission, emerge from the number, scale, and combination of distinct building blocks.

Recent Progress

A major focus of this work has been the modular design of excitonic circuitry with programmable emergent electronic properties. In these systems, collective functionality arises from the coaction of interfaced DNA-based excitonic building blocks, each engineered for specific and selective functions such as energy capture or charge conversion. In recent work, we have introduced a toolkit of such excitonic building blocks to manage the flow of energy, electrons, and photons.

Transport of delocalized excitons through DNA-based molecular photonic wires. Natural photosynthetic systems leverage the strong excitonic coupling between scaffolded chromophores to transport captured light energy as delocalized excitons. Inspired by this natural design, we used DNA nanotechnology to engineer molecular photonic wires (MPWs) with weak, intermediate, and strong interchromophore coupling to achieve transport across long-range distances (Figure 1A).[1]

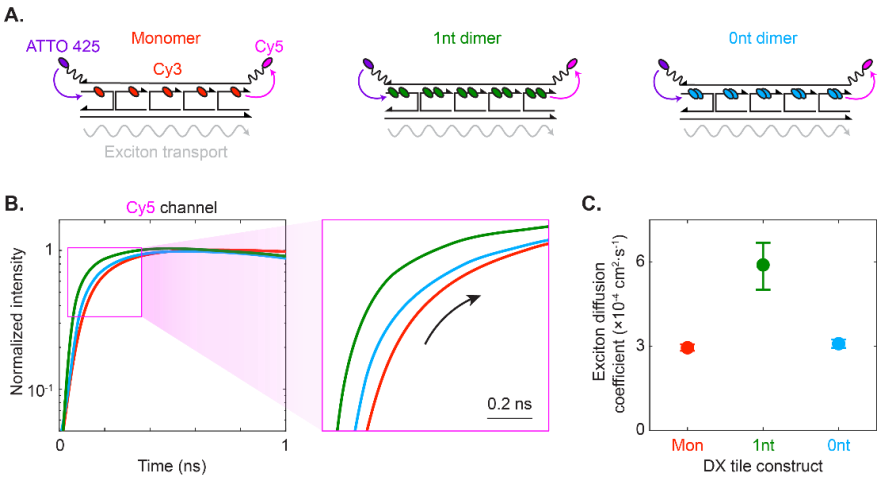


Figure 1: Engineering delocalization for energy transport. (A) DNA DX tile MPWs. Subunits of Cy3 monomers and coupled dimers separated by one or zero nucleotides (nt) are scaffolded onto a DX tile with a donor (Atto 425, purple) and an acceptor (Cy5, pink) at opposing ends. (B) Left: Experimental time-resolved fluorescence traces showing the rise of the Cy5 acceptor of each MPW in A. Right: Zoom-in of acceptor rise. (C) Exciton diffusion coefficients extracted from numerical modeling.

Combining time-resolved fluorescence spectroscopy with microkinetic modeling demonstrated that intermediate coupling (~k_BT) yielded the fastest rates of exciton transport by balancing two competing parameters: chromophore density and the nature of the excitonic coupling (Figure 1B). The optimum identified matches the coupling strengths found in photosynthetic systems, suggesting a universal principle for rapid diffusion of excitons (Figure 1C). Overall, this work provides a blueprint to guide the design of nanoscale machinery best suited for dynamical processing applications, where rapid exciton transport is required.

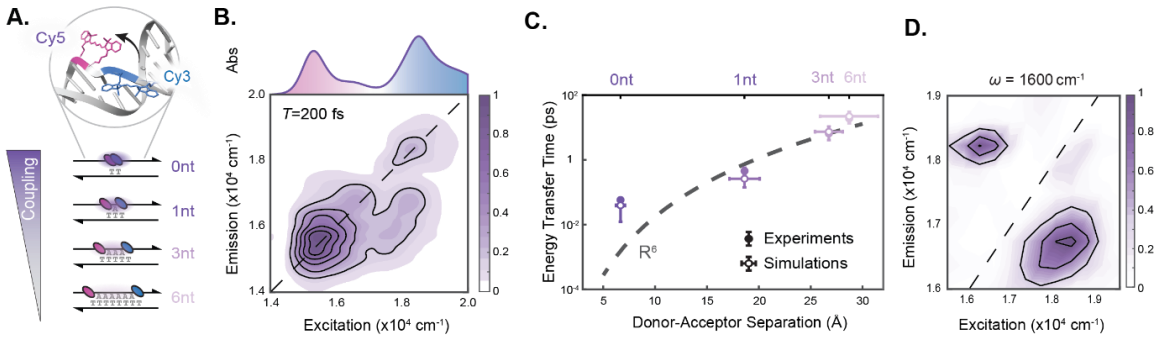


Figure 2: **Transitioning from incoherent to coherent energy transfer.** (A) Schematics of Cy3-Cy5 dimers templated on DNA duplexes, with donor-acceptor separations varying from 0nt to 6nt. (B) Absolute 2D spectrum of the 0nt dimer at T = 200 fs, with the corresponding linear absorption spectrum shown above. (C) Experimental and theoretical energy transfer times across donor-acceptor separations. (D) Beating frequency map at 1600 cm-1 from the real rephasing signal of the Cy3Cy5 0nt dimer.

Controlling the electronic coupling in chromophore heterodimers. Efficient energy capture and transport rely on densely packed networks of chromophores, where close proximity gives rise to interchromophore couplings. To isolate the contributions of these couplings, we engineered DNA–

Cy3–Cy5 heterodimers with precisely tuned coupling strengths by varying the inter-chromophore separation from 0 to 6 nucleotides (nt) and resolved their ultrafast dynamics using two-dimensional electronic spectroscopy (2DES) (Figure 2A-C).[2] Molecular dynamics (MD) and quantum-mechanical simulations identified a transition from classical incoherent transfer in weakly-coupled dimers to exciton delocalization in the strongly-coupled dimers. The 2DES spectra revealed vibronic mixing between the donor and acceptor chromophores (Figure 2D). These findings provide mechanistic insights into how strong coupling drives dynamics in molecular systems and establish design guidelines for next-generation excitonic platforms.

Programming the dynamics of excimer-like photoproducts via geometric confinement in DNA origami. We used DNA six-helix bundles (6HBs) templated with perylene diimide (PDI) aggregates to dictate the dynamics of exciton trapping and relaxation by leveraging the geometric constraints of the scaffold (Figure 3A).[3] Steady-state spectroscopy and MD simulations showed that the 6HB motif confines chromophores to dimer-like interfaces, with distinct aggregate organizations depending on the sequence positioning and chromophore density. Transient absorption spectroscopy revealed the rapid generation of exciton traps known as excimer-like photoproducts (Figures 3B-C), with their formation and structural relaxation timescales directly prescribed by the local pairwise interactions enforced by the scaffold and thereby programmable through the DNA structure.

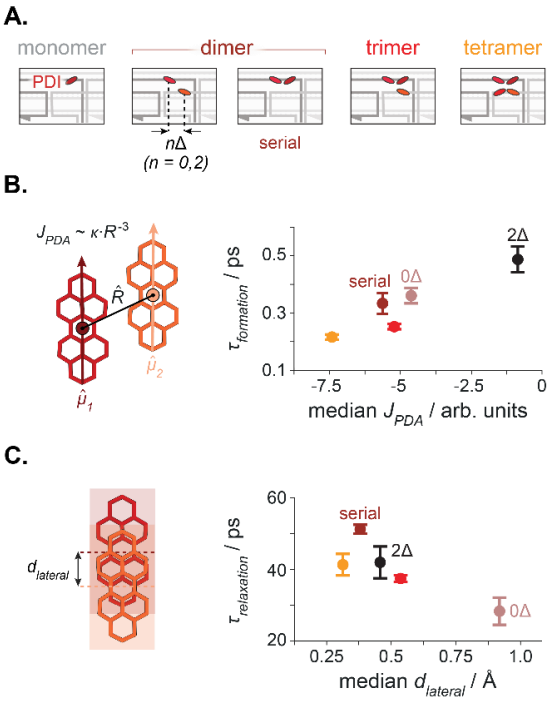


Figure 3. Photoproduct dynamics programmed by geometric confinement. (A) DNA 6HB PDI aggregate series. (B) Timescales of excimer-like photoproduct formation as a function of the median geometric coupling obtained from molecular dynamics (MD) simulations. (C) Structural relaxation timescales of the excimer-like state as a function of median lateral slip obtained from MD.

Deriving the Landauer principle from the quantum Shannon entropy. The Landauer principle establishes a fundamental connection between information and thermodynamics, stating that erasing a single bit of information in a classical system requires a minimum energy proportional to the entropy change. We established a quantum Landauer principle that quantifies the free energy required for quantum state changes, such as qubit erasure, to guide the design of quantum technologies.[4]

Complex-valued intermolecular coupling enables directional exciton transport. Complex-valued intermolecular coupling regulates coherent exciton transfer by incorporating the phase of

electronic interactions. In highly symmetric molecules like porphyrins, circularly polarized light generates a current within the macrocycle that can couple with a low-symmetry linear chromophore with an imaginary coupling component, forming the basis of complex coupling. We successfully demonstrated that the directionality of exciton flux can be dynamically modulated by tuning the complex coupling. This work highlights the potential of leveraging complex coupling as a design principle to drive the flux of excitons in optoelectronic devices.[5]

Future plans

Our ongoing and planned work focuses on broadening the toolkit of DNA-based excitonic building blocks and their integration in several areas, particularly the following two major directions:

Many-body coupling asymmetrically tune energy transfer. Delocalization is a key mechanism for exciton dynamics within strongly coupled chromophore domains, but has only been examined systematically in dimers. We are establishing a DNA-templated chromophore trimer platform that selectively places excitonic delocalization on either the donor or acceptor side. We are employing 2DES and multiscale modeling to resolve the underlying dynamics. Our results are revealing that delocalization within the donor domain suppresses energy transfer, whereas delocalization within the acceptor domain enhances it. This work establishes an asymmetric design rule, with delocalization placed at the energy accepting side, and offers quantitative guidance for engineering energy flow in synthetic excitonic systems.

Advent of singlet fission in DNA-acene materials. Singlet fission (SF) presents a pathway to generate an entangled triplet pair, but its efficiency is strictly governed by near-field intermolecular geometry. To address these constraints, we are utilizing DNA duplexes to systematically organize tetracene aggregates with sub-nanometer precision. By varying dimer separations from 0-5nt, we achieved tunable excitonic coupling, confirmed by a progressive blue-shift in linear absorption spectra. Preliminary ultrafast measurements indicated rapid population growth where the triplet excited-state absorption (ESA) is expected. Next steps will focus on verifying triplet yields and resolving the formation mechanism through replicate measurements, ultimately establishing a proof-of-principle for our DNA-templated acene architectures.

References

1. M. N. Scott, J. L. Banal, W. Jia Chen, C. Brooks, X. Wang, S. M. Hart, A. Dodin, M. Bathe, A. P. Willard, G. S. Schlau-Cohen, *Transport of Delocalized Excitons through DNA-Based Molecular Photonic Wires,* ACS Nano, **19**, 38509-38520 (2025)
2. Y. Ji, H. J. Heelweg, J. Gorman, S. M. Hart, A. Kundu, M. Bathe, A. P. Willard, G. S. Schlau-Cohen, *Delocalization Enables Robust Vibronic Coherence in DNA-Chromophore Heterodimers*, submitted.
3. M. N. Scott, J. Gorman, H. J. Heelweg, Y. Ji, A. P. Willard, M. Bathe, G. S. Schlau-Cohen, *Programming the Dynamics of Excimer-Like Photoproducts via Geometric Confinement in DNA Origami*, in preparation.
4. H. J. Heelweg, A. Dodin, A.P. Willard, *Deriving the Landauer Principle from the Quantum Shannon Entropy.* J. Phys. Chem. Lett., **16,** 1397-1402 (2025)
5. M. A. Castellanos, A. P. Willard, *Complex-Valued Intermolecular Coupling Enables Directional Exciton Transport in Excitonic Circuits*, J. Phys. Chem. C*,* **129**, 5493-5501 (2025)

Publications

1. Y. Ji, H. J. Heelweg, J. Gorman, S. M. Hart, A. Kundu, M. Bathe, A. P. Willard, G. S. Schlau-Cohen, *Delocalization Enables Robust Vibronic Coherence in DNA-Chromophore Heterodimers*, submitted.
2. Y. Park, A.P. Willard, *Modeling Interfacial Electron Transfer Using Path Integral Molecular Dynamics,* J. Chem. Phys, **164** 064119 (2026)
3. M. N. Scott, J. L. Banal, W. Jia Chen, C. Brooks, X. Wang, S. M. Hart, A. Dodin, M. Bathe, A. P. Willard, G. S. Schlau-Cohen, *Transport of Delocalized Excitons through DNA-Based Molecular Photonic Wires,* ACS Nano, **19**, 38509-38520 (2025)
4. M. A. Castellanos, A. P. Willard, *Complex-Valued Intermolecular Coupling Enables Directional Exciton Transport in Excitonic Circuits*, J. Phys. Chem. C*,* **129**, 5493-5501 (2025)
5. H. J. Heelweg, A. Dodin, A.P. Willard, *Deriving the Landauer Principle from the Quantum Shannon Entropy.* J. Phys. Chem. Lett., **16,** 1397-1402 (2025)

The Role of Nanoparticle-Based Bonds in Polymer Networks

S. Eileen **Seo**, School of Engineering of Matter, Transport and Energy, Arizona State University

Keywords: nanotechnology, polymer, self-repairing, nanoparticle, self-assembly

Research Scope

Bio-inspired, self-repairing materials prolong their lifespans against physical damage, providing a more sustainable path to lower carbon and life-cycle costs. Most self-repairing polymers require reversible noncovalent bonds and high segmental mobility to facilitate self-repair in polymer networks. Due to limitations on crosslinking chemistries that can impart self-repairing, these systems have mostly been demonstrated in gels and elastomers, which are relatively soft with Young's moduli of ~10^3–10^4 Pa and low glass transition temperatures (T_g). These materials are prone to creep and undergo significant deformation under load, making them unsuitable for high-performance applications. A long-standing trade-off between self-repairing kinetics and mechanical robustness has been the major limitation in expanding the scope of these materials. The core of this research program leverages nanoparticle-enabled control over polymer structure and function (**Fig. 1**). Guided by molecular and nanoscale design principles, my group pioneered dynamic nanoparticle–based strategies for mechanically robust, self-repairing materials and enabled low-energy, near-IR–activated photothermal assembly into a solid object. The objective is to synthesize nanoparticles bearing tailored ligands that can form multiple noncovalent interactions with the polymer matrix, thereby creating multifunctional nanoparticle-based crosslinks. The fundamental research focus lies on resilient, multiscale materials that demonstrate coordinated functionality akin to biological materials and withstand harsher environments, aligning with the mission of Biomolecular Materials in the DOE's Basic Energy Sciences program. Our group will explore bio-inspired designs for adaptive, multi-responsive materials whose interfacial behavior and morphology are regulated at the nanoscale through external stimuli and translated into macroscopic material performance.

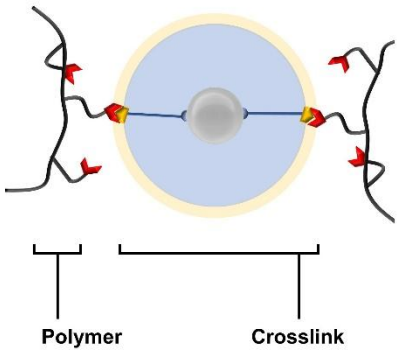


Figure 1. The concept of surface-tailored nanoparticle-based crosslinks to engineer polymer networks.

Recent Progress

Mechanically Robust, Self-Repairing Polymer Nanocomposites with Tailorable Nanoparticle-Based Bonds. A trade-off between mechanical strength and self-repairing kinetics can be overcome through judiciously designed nanoparticle-based bonds. We hypothesized that dynamically tuning the number of interfacial hydrogen bonds and ligand flexibility shifts the nanoscale bond exchange rate (i.e., the overall rate of binding and unbinding) and bulk mechanical properties (e.g., slow versus fast self-repairing ≈ stiff versus soft). In this study, we investigate how the number of

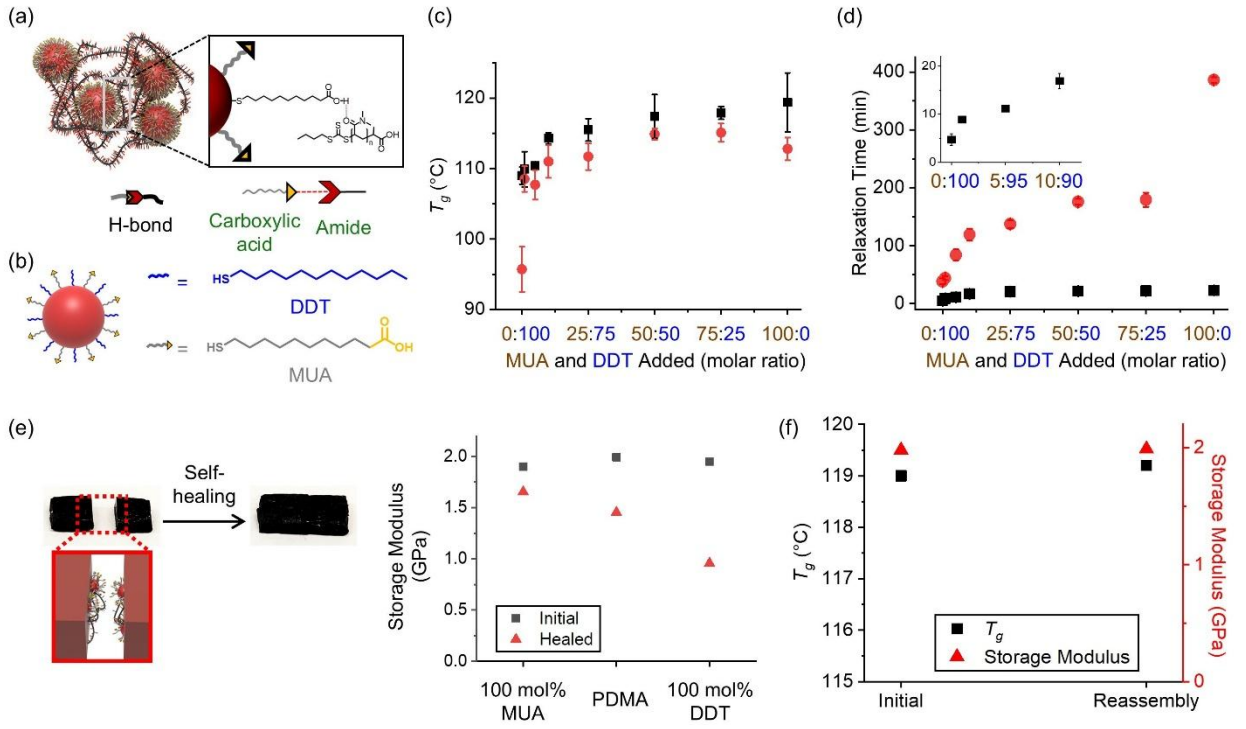


Figure 2. (a) Schematic of the polymer nanocomposite with complementary interfacial hydrogen bonding interactions between polymers and surface-functionalized nanoparticles. **(b)** Varying stoichiometric ratios of 11-mercaptoundecanoic acid (MUA) and 1-dodecanethiol (DDT) on nanoparticle surfaces. **(c)** T_g and **(d)** characteristic relaxation time of polymer nanocomposites with two different nanoparticle sizes and a range of ligand densities. **(e)** Optical images of a polymer nanocomposite before and after self-repairing, and the recovery of storage moduli before and after self-repair. **(f)** T_g and storage moduli of the initial and reassembled nanocomposites.

interfacial hydrogen-bonding interactions between polymers and surface-functionalized nanospheres alters bulk mechanical properties at extremely low nanoparticle concentrations (the volume fractions of 5 and 18 nm diameter nanoparticles are 1.1×10^{-5} and 5.3×10^{-4} v%).[1] Assembly of poly(*N, N*-dimethyl acrylamide) and carboxylic acid-functionalized gold nanoparticles was performed to synthesize a stand-alone polymer network (**Fig. 2a**). UV–Vis spectroscopy was used to track the localized surface plasmon resonance peak of dispersed nanoparticles and confirm that no nanoparticle aggregation occurred during the assembly process. We observed that weakly interacting polymers effectively stabilize nanoparticles in a solvent in which nanoparticles are typically not stable during processing and functionalization. Key variables, including nanoparticle concentration, size (5 and 18 nm), and ligand density (11-mercaptoundecanoic acid and 1-dodecanethiol via co-functionalization), were systematically varied and characterized for T_g, stress relaxation, modulus (via dynamic mechanical analysis), and self-repairing kinetics and recovery. The ligand density was varied by co-functionalizing nanoparticle surfaces with different ratios of 11-mercaptoundecanoic acid and 1-dodecanethiol to control the number of potential hydrogen-bonding interactions at the interface between nanoparticles and polymers (**Fig. 2b**). Self-repairing efficiency was quantified by comparing the storage modulus before and after fracture using tensile testing.

Ligand density on the nanoparticles plays a critical role in precisely tuning the thermomechanical properties, as evidenced by systematic changes in the bulk material's T_g corresponding to variations in surface ligand density (**Fig. 2c**). Notably, nanocomposites containing carboxylic acid-functionalized nanoparticles with poly(*N, N*-dimethyl acrylamide) exhibited the fastest self-repair kinetics (compared to controls: neat polymer without nanoparticles and polymer nanocomposite with dodecanethiol-functionalized nanoparticles), a significant T_g increase (120 °C; > Δ30 °C), slower stress relaxation rate, and storage moduli in the GPa range, demonstrating exceptional mechanical performance for a self-repairing polymer (**Fig. 2c, d, e**). Lastly, reversible disassembly and reassembly offer a promising route to recyclability, addressing a longstanding challenge in composite materials arising from their heterogeneous composition and strong interfacial adhesion. We demonstrate reversible assembly behavior, with full recovery of mechanical properties (storage modulus and T_g), using an energy-efficient density-separation method, highlighting opportunities for material repurposing and enhanced sustainability (**Fig. 2f**).

Rapid Light-Driven Self-Assembly of Polymer Nanocomposites. This project has been extended to expedite assembly by combining the thermoresponsive polymer poly(*N*-isopropylacrylamide) with surface-functionalized thermoplasmonic nanorods that form hydrogen bonds with the polymer matrix (i.e., assembly occurring in less than 5 s upon irradiation).[2] Initial work requires the removal of solvents to obtain a solid nanocomposite, which is a rate-limiting step. Poly(*N*-isopropylacrylamide) exhibits a lower critical solution temperature (LCST) of ~35 °C, leading to phase separation above this temperature. To use light to induce rapid self-assembly, we combined poly(*N*-isopropylacrylamide) with amine and carboxylic acid-functionalized gold nanorods. Near-infrared light can be converted to heat via optical heating of plasmonic nanorods, where incident light induces collective oscillations of conduction electrons, and their nonradiative damping results in sharp temperature rises around nanoparticles. Because heating is induced by light, the photothermal effect is highly localized. Using this platform, we demonstrate that low-energy near-infrared light can generate heat and induce phase separation of polymer

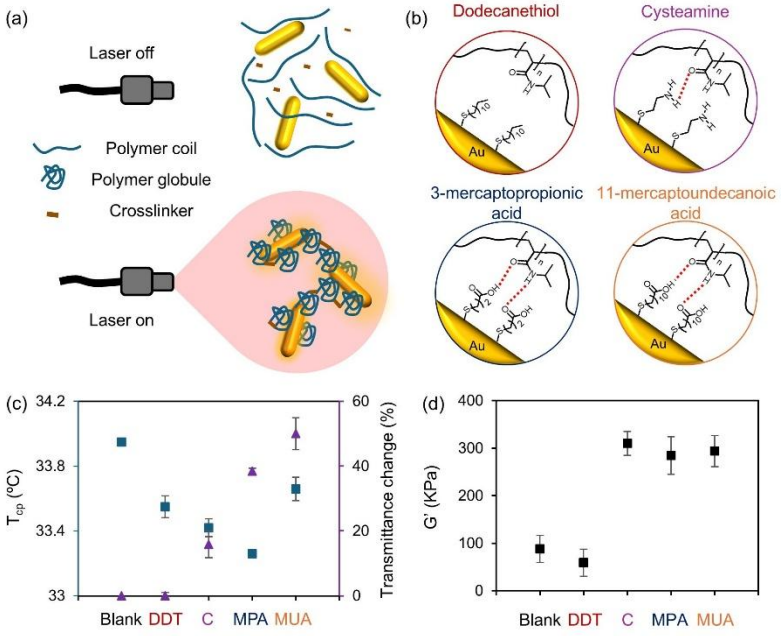


Figure 3. (a) Schematic of light-driven self-assembly of polymer nanocomposites. **(b)** Interfacial interactions between poly(*N*-isopropylacrylamide) and surface-functionalized gold nanorods with different ligands. **(c)** Cloud point and flocculation behavior at 70 °C with a heating rate of 1 °C/min. **(d)** Shear storage moduli of nanocomposites. The formulation consisted of 10 wt/v% poly(*N*-isopropylacrylamide) (126 kg/mol) and 0.002 wt/v% gold nanorods.

nanocomposites from the solution phase (**Fig. 3a**). This "phase separation" or self-assembly behavior, as well as the final mechanical properties, can be altered by tuning interfacial interactions (**Fig. 3b**). With favorable hydrogen bonding interactions at the interface, the cloud point (the coil-to-globule transition of polymers closely related to the LCST behavior) decreases (i.e., favorable interfacial interactions drive the assembly to occur at a lower temperature) and the flocculation behavior is enhanced due to increased interaction between phase-separated microspheres, leading to an extended polymer network (**Fig. 3c**). More importantly, additional hydrogen bonding interactions at the interface improves the stiffness of the dynamic polymer nanocomposite material after assembly (**Fig. 3d**). A central advantage of the method is that it couples near-infrared light penetration with self-assembly dynamics, which is useful for patterning materials that benefit from mild, localized activation rather than high-energy irradiation. This strategy expands microlithography beyond conventional photochemistry by using photothermal control to organize material structure during processing. The broader impact is a fabrication platform for polymer nanocomposites that can be patterned by controlling when and where assembly is triggered.

Future Plans

We will expand the library of nanoparticle-based crosslinks by incorporating additional interfacial interactions, including ionic bonds and synergistic combinations of hydrogen and ionic bonding, alongside polymer matrices tailored to complement these interactions. Homopolymers, random copolymers, and block copolymers will be synthesized to access a broader spectrum of mechanical, self-repairing, and stimuli-responsive behaviors. In block copolymer systems, morphology is expected to play a pivotal role by directing nanoparticle-based crosslinks to specific domains, providing an additional level of structural and functional control. In collaboration with an expert in advanced solid-state NMR spectroscopy, we will elucidate interfacial bonding interactions in polymer nanocomposites under varying thermal and humidity conditions and develop a quantitative framework that links nanoscale interfacial interactions to macroscopic nanocomposite properties.

References

1. J. -C. Yu, R. A. Browne, S. E. Seo,* *Mechanically Robust, Self-Healing Polymer Nanocomposites with Tailorable Nanoparticle-Based Bonds,* Macromolecules **57,** 9059-9066 (2024).
2. J. Sarmas-Farfán, J. -C. Yu, T. Gonzalez Calvo, J. L. Self, S. E. Seo,* *Self-Assembly Driven Microlithography via Near-Infrared Light Activation*, ACS Appl. Polym. Mater. **8,** 4822-4832 (2026).

Publications

1. J. -C. Yu, R. A. Browne, S. E. Seo,* *Mechanically Robust, Self-Healing Polymer Nanocomposites with Tailorable Nanoparticle-Based Bonds,* Macromolecules **57,** 9059-9066 (2024).
2. C. A. Mirkin, S. E. Seo et al., *33 Unresolved Questions in Nanoscience and Nanotechnology*, ACS Nano **19,** 31922-31968 (2025).
3. J. Sarmas-Farfán, J. -C. Yu, T. Gonzalez Calvo, J. L. Self, S. E. Seo,* *Self-Assembly Driven Microlithography via Near-Infrared Light Activation*, ACS Appl. Polym. Mater. **8,** 4822-4832 (2026).

Toward Programmable Self-Navigation of DNA-Based Micrometer-Scale Gliders

William M. **Shih**
Dept. Cancer Biology, Dana-Farber Cancer Institute; Wyss Institute for Biologically Inspired Engineering, Harvard University; Dept. Biol. Chem. and Mol. Pharm., Harvard Medical School

Keywords: DNA origami, active matter, molecular motors, crisscross assembly

Research Scope: Biological active matter systems show how molecular-scale interactions can generate organized motion, transport, and mechanical work at the scale of cells. We aim to establish a synthetic model system in which the geometry and nanoscale patterning of micrometer-scale objects determine their motion across a surface. Using our recently developed crisscross DNA origami technology [1], we seek to build DNA gliders whose shape and interaction sites are specified by design, allowing structure-level design parameters to be connected to experimentally observable trajectories.

We aim to study programmable DNA origami gliders using two complementary surface-based propulsion assays [2]. In the molecular-motor assay, glass surfaces are coated with chimeric dynein motor proteins engineered to walk on DNA instead of microtubules [3]. These motors interact with motor-binding motifs placed on the DNA origami gliders by design, providing a direct route for coupling nanoscale sequence patterning to surface-based glider motion. In the electrokinetic assay, DNA gliders are driven on illuminated ITO electrodes, where local electric fields and electrokinetic flows couple to the shape and orientation of the structures [4]. Together, these assays test how programmable molecular structure can be used to control motion across larger length scales.

Recent Progress: A major emphasis of the current work has been the development of a design and manufacturing platform for fluorescent crisscross DNA origami gliders. We established a design and manufacturing pipeline for crisscross DNA origami gliders (Figure 1a). Crisscross structures are challenging to produce because each design contains many distinct DNA origami slats, and each slat contains hundreds of individual DNA strands. To make this process experimentally tractable, we developed a workflow that connects CAD-based structure design, DNA sequence assignment, liquid-handler instruction generation, robotic handling of thousands of DNA strands, folding and purification of individual DNA origami slats, assembly of the final crisscross structure, and imaging-based validation. This pipeline enables iterative design and testing of micrometer-scale DNA structures and provides the fabrication basis for programmable glider experiments. The associated computational framework for designing micron-scale crisscross DNA megastructures was recently accepted for publication in Nature Communications [5]. Using this platform, we experimentally realized a range of crisscross DNA origami structures, including multilayer geometries that provide greater design freedom than planar structures (Figure 1b). We used this platform to develop fluorescence-labeling strategies compatible with crisscross assembly, which enabled real-time fluorescence imaging of the structures (Figure 2a and 2b).

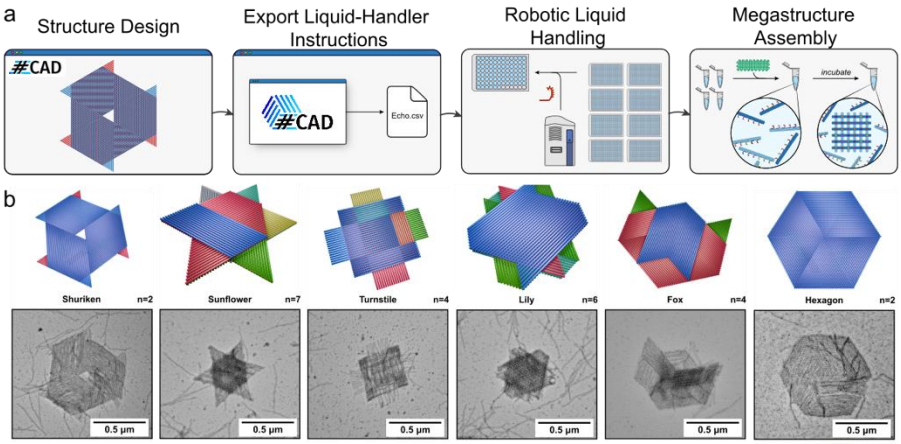


Figure 1. Crisscross DNA origami manufacturing pipeline and example realized structures. **a)** Manufacturing pipeline from left to right. Structure design using in-house software, encoding of the design into DNA sequences, export to liquid-handler instructions, automated robotic handling of thousands of DNA strands, laboratory processing of DNA origami slats, and final megastructure assembly. **b)** Example structures realized with the manufacturing pipeline. The gallery shows renderings from our software and transmission electron microscopy images.

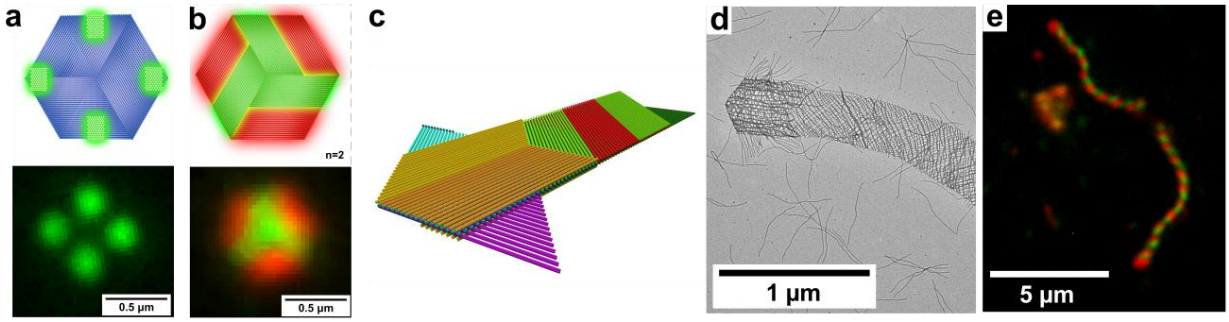


Figure 2. Fluorescently labeled crisscross structures and snake-like glider design. **a)** Rendering and fluorescence image of a hexagon decorated with fluorescent patches attached through binding handles. **b)** Rendering and fluorescence image of a hexagon composed of red- and green-labeled slat types. **c)** 3D rendering of the snake-like crisscross design, with fluorescent red and green tail slats that polymerize indefinitely. **d)** TEM image of the snake-like structure. **e)** Red-green fluorescence overlay showing the red-only head and repeating red-green tail pattern.

Using these fluorescence-labeling strategies, we designed and experimentally realized an elongated snake-like crisscross glider (Figure 2c-e). The structure consists of a finite head region and a polymerizing tail composed of alternating fluorescent slats. The snake-like architecture was chosen as a common test geometry for both propulsion strategies. For dynein-based assays, the extended body can accommodate motor-binding motifs along a defined structural axis. For electrokinetic assays, the elongated geometry provides an anisotropic object whose orientation can be coupled to field-induced forces, flows, and rotational alignment.

We assessed dynein-mediated propulsion using DNA nanotubes as a control system, following the published gliding assay by Ibusuki et al. [3] (Figure 3). Consistent with the published assay, DNA nanotubes associated with dynein-coated surfaces at 200 mM KCl but not at 400 mM KCl. However, the bound nanotubes remained immobile, and no measurable gliding was observed. ATP-consumption assays confirmed motor activity (Figure 3b), suggesting that processive dynein-driven motion, rather than motor inactivity, is the unresolved bottleneck.

To study glider motility under externally driven conditions, we developed an electrokinetic assay based on illuminated ITO electrodes (Figure 4). DNA structures are negatively charged and can therefore be localized near an electrode by an applied electric field. Unexpectedly, compact crisscross structures accumulated specifically in the illuminated region of the ITO surface, suggesting that illumination locally increases the electric field at the electrode and attracts negatively charged DNA structures (Figure 4a,b). Elongated DNA nanotubes behaved differently.

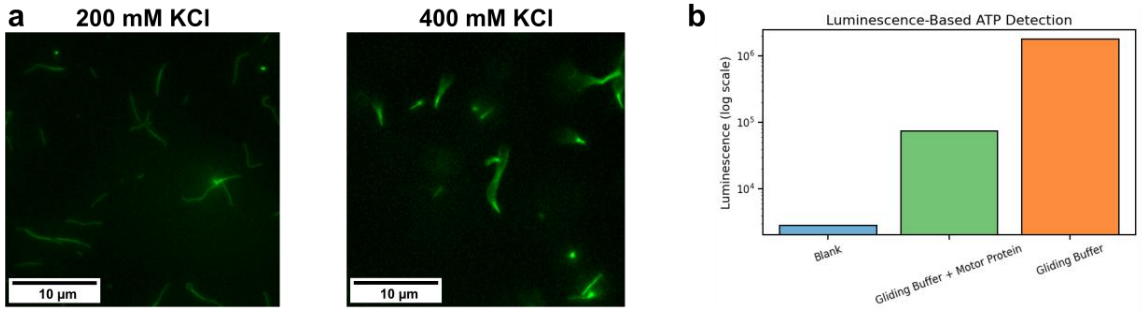


Figure 3. Assessment of dynein-mediated DNA glider motility. **a)** Fluorescence images of DNA nanotubes on dynein-coated surfaces under two KCl concentrations. DNA nanotubes associated with the surface at 200mM KCl but not at 400 mM condition. No measurable gliding was observed. **b)** Luciferase-based ATP-consumption assay. Reduced luminescence in the motor-containing sample compared with the ATP-containing buffer control indicates ATP consumption by the dynein motors.

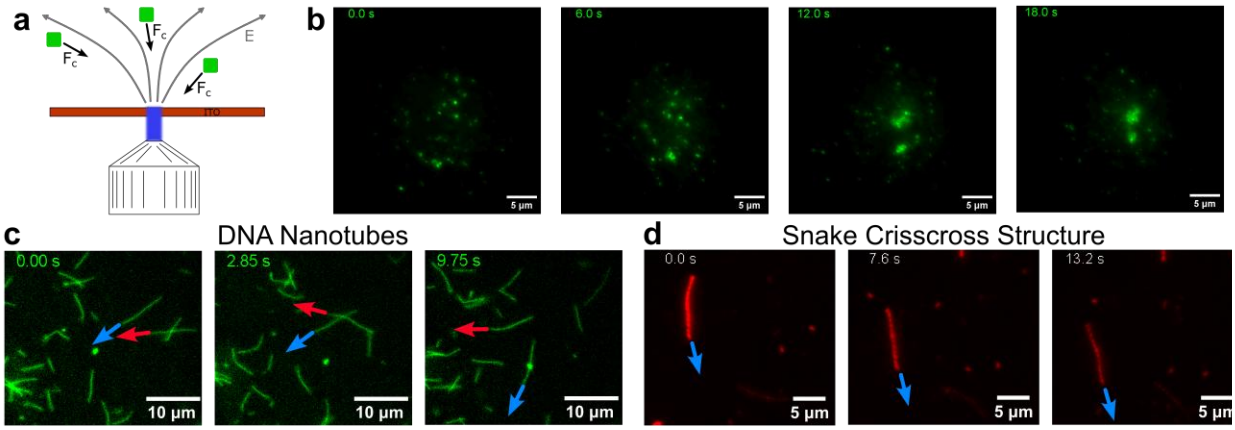


Figure 4. Electrokinetic motion of DNA structures on illuminated ITO electrodes. **a)** Schematic of the electrokinetic assay, in which DNA structures are attracted toward the illuminated region of an ITO electrode. **b)** Time series showing accumulation of compact crisscross structures in the illuminated region. **c)** Time series showing directed motion of DNA nanotubes along their long axis and toward higher illumination intensity. **d)** Time series showing directed motion of a snake-like crisscross structure within the illuminated field region.

Instead of only accumulating, they showed directed motion that combined migration up the light gradient with motion along their long axis (Figure 4c). A similar orientation-dependent motion was observed for the snake-like crisscross structure (Figure 4d). These observations provide initial evidence that elongated DNA glider geometry can couple to electrokinetic flows, linking the structural axis of the object to the direction of motion.

Future Plans: We will next determine the mechanism underlying the illuminated-ITO glider assay and identify how the observed motion depends on applied voltage, illumination intensity, electrode geometry, buffer composition, and glider shape. In particular, we will test how local field gradients, surface electrochemistry, electroosmotic flows, and structure orientation contribute to the combined gradient-directed and orientation-dependent motion of elongated DNA structures.

Once the mechanism is understood, we will use this coupling to design gliders with controlled trajectories. In this system, voltage and illumination define where motion is activated, while the programmed glider geometry determines how the structure moves within the activated region. This separation between external control and local geometry-dependent response could enable DNA-based active materials for programmable motion, sorting, localization, and transport. Dynein-mediated propulsion will remain a complementary molecular-motor route, but the near-term focus will be on establishing quantitative design rules for the illuminated-ITO assay.

References

1. C. M. Wintersinger, D. Minev, A. Ershova, H. M. Sasaki, G. Gowri, J. F. Berengut, F. E. Corea-Dilbert, P. Yin, and W. M. Shih, Multi-micron crisscross structures grown from DNA-origami slats. *Nature Nanotechnology* 18, 281–289, 2023.
2. T. D. Ross, D. Osmanović, J. F. Brady, and P. W. K. Rothemund, Ray Optics for Gliders, *ACS Nano* 16, 16191–16200, 2022.
3. R. Ibusuki, T. Morishita, A. Furuta, S. Nakayama, M. Yoshio, H. Kojima, K. Oiwa, and K. Furuta, Programmable molecular transport achieved by engineering protein motors to move on DNA nanotubes, *Science* 375, 1159–1164, 2022.
4. F. Ma, X. Yang, H. Zhao, and N. Wu, Inducing Propulsion of Colloidal Dimers by Breaking the Symmetry in Electrohydrodynamic Flow, *Physical Review Letters* 115, 208302, 2015.
5. M. Aquilina, F. Katzmeier, M. A. D. Nijenhuis, S. S. Wang, C. Becker, Y. Zhao, S. H. Seok, J. Finkel, H. Cui, J. Lee, S. Lee, and W. M. Shih, A computational framework for designing micron-scale crisscross DNA megastructures. *Nature Communications*. accepted (2026). Preprint available at bioRxiv, https://doi.org/10.64898/2026.01.23.701435.

Publications

M. Aquilina, F. Katzmeier, M. A. D. Nijenhuis, S. S. Wang, C. Becker, Y. Zhao, S. H. Seok, J. Finkel, H. Cui, J. Lee, S. Lee, and W. M. Shih, A computational framework for designing micron-scale crisscross DNA megastructures. *Nature Communications*, accepted (2026). Preprint available at bioRxiv, https://doi.org/10.64898/2026.01.23.701435.

Transient Microstructures Inspired by Mycorrhizal Fungi Arbuscules

Meredith **Silberstein**, Cornell University

Keywords: phase transition, manufacturing, tip growth, metal-coordination bond

Research Scope

Polymer nano, micro, and meso-structure are critical for functionality in many applications. For example, many electrochemical energy related technologies require large surface areas as catalyst support in conjunction with channels to enable fluid access to make these sites active. Polymers with multiscale structures also enable membrane separation processes (*e.g.* water, air, chemicals). These hierarchical structures are most often created through subtractive manufacturing, additive manufacturing, and/or phase separation, however, each of these approaches has critical deficiencies in terms of accessible geometries. Further, they are typically static, maintaining their form and function once established, limiting our ability to realize functionality on demand in the most efficient use of resources.

Biology suggests an alternative route to creating hierarchical structures. Approximately 80% of land plants have a symbiotic relationship with arbuscular mycorrhizal fungi, by which fungi penetrate the plant root cell wall and grow arbuscules (compact, branched, hollow, structures) within plant cells only when the plants need access to additional nutrients. Interestingly, the arbuscular structure is transient, and after 1-3 days, the components are recycled. We are mimicking the essential components of this system to establish a new manufacturing method for hierarchical transient transport microstructures. Our materials rely on polymers whose transition from liquid to solid is controlled by salt content – a fully reversible mechanism. Our research approach combines experimental and computational work, using and advancing state-of-the-art modeling approaches for materials that with both solid-like and liquid-like natures.

Specifically, the research plan focuses on deposition and transience within a single cellular unit. Metal-ligand coordination bonds will be employed as the non-covalent interaction crosslinking the otherwise linear polymers. The research approach is organized into three aims. Aim 1: Hollow microstructure formation by salt inducible second order phase transition. Aim 2: Lateral branch formation via bulging instabilities. Aim 3: Complete dissolution of the microstructure via swelling of the microstructure followed by competitive chelation of the salt.

Recent Progress

Over the past year, we made substantial progress in establishing both the theoretical and experimental foundations needed to realize controllable hollow microstructure formation (Aim 1). A major accomplishment was completion of a constitutive material model describing polymer solidification driven by salt diffusion, including specific implementation and parameterization for alginate–Cu and alginate–Ca systems. This model captures the coupled transport and solidification

processes central to the proposed manufacturing concept and provides a predictive basis for design. We have applied this material model in a custom finite element implementation to simulate tip growth deposition.

We identified several important physical conditions governing hollow structure growth. First, the simulations indicate that adhesion of the polymer to the growing tip is a key requirement for sustained tip growth rather than simple extrusion. Second, while dual-nozzle architectures in which polymer is fed within the salt solution can give a balloon like tip growth, those in which salt is fed internally, and polymer externally appear significantly more favorable for tip growth. These results provide the first mechanistic guidance for design of transient transport microstructures in this platform. In addition, we initiated parameter sweeps to determine how process variables influence wall thickness and cylinder diameter, beginning to establish quantitative structure–processing relationships.

Informed by these simulations, we implemented a physical manufacturing system for dual-nozzle tip growth deposition of polymers based on salt-driven solidification. The system employs a coaxial nozzle architecture with independently controlled polymer and salt flows to localize crosslinking at the fluid interface and enable hollow cylinder formation. Using this platform, we demonstrated formation of cylindrical structures across a range of flow conditions (Figure 1). Validation is underway to determine tip growth versus extrusion.



Figure 1. Two example depositions of hollow cylinder composed of polymers solidified by salt.

The dissolution of the structure and recovery of the material components is essential for realizing the transient concept (Aim 3). We developed an experimental protocol for systematically quantifying the dissolution of different candidate materials in matched solutions – a procedure we term decantation as the salt is progressively removed resulting in liquid polymer floating up from the solid, salt coordinated polymer. We have conducted dissolution experiments on metal coordinated PDMS with different types of salt, using an aqueous-EDTA solution. In parallel, we have adapted the simulation framework from the deposition process to study this dissolution

process. Sample results showing both simulations and experiments are shown in Figure 2. The EDTA solution chelates cations at the polymer interface, enabling them to diffuse away rapidly into the bulk solution. This concentration gradient then drives a slower diffusion of salt ions from the bulk solid polymer to the interface. The removal of salt decreases the density of the polymer below that of the solution, which drives polymer to the surface. Surface tension is a critical component of the phenomenology, setting the condition for when part of the polymer breaks away from the bulk.

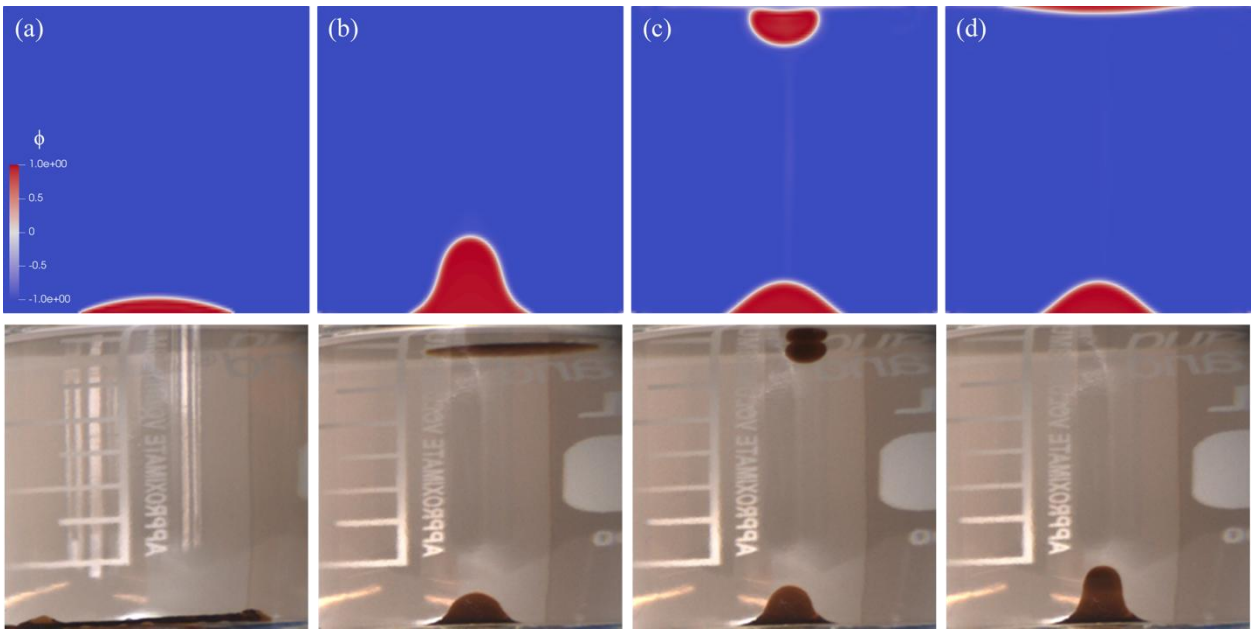


Figure 2. Metal-coordinated PDMS dissolution by aqueous EDTA solution. Top: Snapshots of finite element simulations of the dissolution process showing volume fraction of polymer. Bottom: Snapshots of experimental result.

Future Plans

To broaden our study of tip growth deposition, we will use the implemented material model and simulation framework, finish a broad parameter sweep of the manufacturing conditions, and study their influence on the resulting cylindrical structure. We will then interpret these results through a set of critical non-dimensional parameters. In parallel, and using the simulation results, we will work on our experimental implementation to get clear evidence of tip growth. We will develop methods to image, flow test, and mechanically test the manufactured channel. We will also probe the extrusion (rather than tip growth) regime to verify those results as well. We are aiming for a unified picture of concentric nozzle, second order phase transition driven, hollow tube manufacturing that can be extended to different polymers, salts, and dimensions.

Then we will move onto the next phase of this deposition process, which is realizing branching within the hollow cylindrical structures. As with earlier stages of this project, we will take a

combined computational and experimental approach. We will experimentally characterize rate dependent fracture under bulging conditions, utilize this information to update our material models, determine required deposition conditions via simulation, and then impose these conditions experimentally.

Publications

1. E. W. van Wijngaarden, M. P. Brunette, A.G . Goetsch, I. L. Brito, D. M. Hershey, and M. N. Silberstein. *Rheinheimera sp. T2C2 Bacterial Biofilm for Bioremediation of Cobalt(II)*. ACS Applied Polymer Materials. **8**, 7168-7180, (2026).
2. T. Hana, S. Aiden S, K. Orme, T. Kolozsvary, Z. Bernheimer, H. Cai, M. T. Lam, S. Chen, R. Tobias, M. K. Tragn, R. Doherty R, M. N. Silberstein, and B. R. McDonald. *Tailoring Crosslinks Through Time – A Paradigm for Tough Hydrogels*. Chemical Reviews. **126**, 2006–2082, (2026).
3. L. He, H. Cai, R. S. Gona, T. C. Rohe, M. S. Gangan, T. Lai, D. R. Sullivan, M. N. Silberstein, and A. S. Meyer. *3D-Bioprinted Marine Bacteria for the Degradation of Polyhydroxybutyrate Bioplastics.* ACS Applied Polymer Materials. **8**, 6086-6100 (2026).
4. M. Tepermeister M, M. N. Silberstein. *Conceptualization and Implementation of a Faster Than Real Time Simulation Tool for Ionic Material and System Modeling*. Physical Review Applied. **23**, 054047, (2025).
5. H. Cai, M. Tepermeister, C. Yuan, M. N. Silberstein. *Regulating Hydrogel Mechanical Properties With an Electric Field.* Materials Horizons. **12**, 5388-5399, (2025).

Biomimetic Strategies for Field-Driven Defect Annealing in Microparticle Crystals

Michael J. **Solomon** and Sharon C. Glotzer, University of Michigan Ann Arbor

Keywords: crystallization, annealing, confocal microscopy, Brownian dynamics simulation, colloids

Research Scope

The purpose of this project is to seek scientific principles that expand our understanding of defect annealing to produce high-quality crystals in materials self-assembled from microscale building blocks. Our guiding inspiration is life's capacity to create high-quality crystal structures from microscopic building blocks, yielding materials that produce important functional properties like structural color. To discover such principles, we have developed techniques based on electric field assisted self-assembly to anneal defect structures in colloidal crystal monolayers of microparticle spheres, discs, and ellipsoids. We resolve the spatiotemporal evolution of these structures at the single-particle level by confocal microscopy and use computational simulation to yield mechanistic understanding of the annealing pathways. The fundamental questions this project addresses are: (1) How does the orientation-dependence of an applied electric field couple to the fundamental lattice symmetry of colloidal crystals? (2) How may such electric fields be configured to generate rapid transitions between different, high quality crystal phases of anisotropic colloids? (3) How does the shape of an active particle affect its dynamics and defects in a crystal lattice comprised of passive colloids? These scientific questions motivate our work plan. The scientific outcome of this work are new principles that enable the coupling of fields sculpted in space and time to specific features of colloidal crystals—including their symmetry and the anisotropic particle shape of their building blocks—to control the quality of their order both locally and globally. The impact on basic energy sciences are governing principles that translate into new strategies for spatiotemporal control of annealing in self-assembled materials comprised of microscale building blocks like colloids, polymers, and proteins, with implications for structural color and thermal management materials.

Recent Progress

We report recent progress toward: (1) annealing of colloidal crystals by rotating electric fields; (2) reconfiguration of liquid crystal structure by rotating electric fields; (3) active ellipsoids with variable trajectories as dopants for colloidal crystal annealing.

Annealing of colloidal crystals by rotating electric fields. Defects such as grain boundaries significantly limit the structural quality and functional performance of colloidal crystals formed through directed self-assembly. Periodic external stimuli can anneal defective colloidal crystals by driving particles in the crystal to collectively reorganize, traverse free energy barriers, and adopt lower free energy states with reduced defect levels [1]. In this study, we present a strategy for defect annealing using rotating alternating current (AC) electric fields [2] with six-fold symmetry

to progressively convert polycrystals into a single colloidal crystal by removal of grain boundaries. The applied field cyclically rotates among electrode pairs, generating dielectrophoretic (DEP) forces that drive particles along closed, triangular trajectories. These field-induced cyclic movements cause local particle rearrangements that promote grain boundary defects to migrate to the edge of the crystal and eventually be expelled. Using confocal microscopy, we tracked particle-level dynamics and quantify structural evolution through the hexatic order parameter, crystal phase angle, and Voronoi analysis. We identified optimal operating conditions for annealing, with complete defect removal achieved for certain field amplitudes, frequencies and cycle periods. We developed a molecular dynamics simulation model of the system that captures the interplay between DEP forces, dipolar interactions, and cycle time, reproducing experimental trends and extending the accessible parameter space beyond that of the experiments. The simulations demonstrate that annealing behavior is governed primarily by the magnitude of the applied field rather than the relative strength of dipolar interactions, suggesting generalizability across various materials (c.f. Figure 1). We also explore through simulation and experiment the hypothesis that the annealing performance is governed by the amount of active energy that is injected into the system due to the applied electric field, less the dissipation generated by drag.

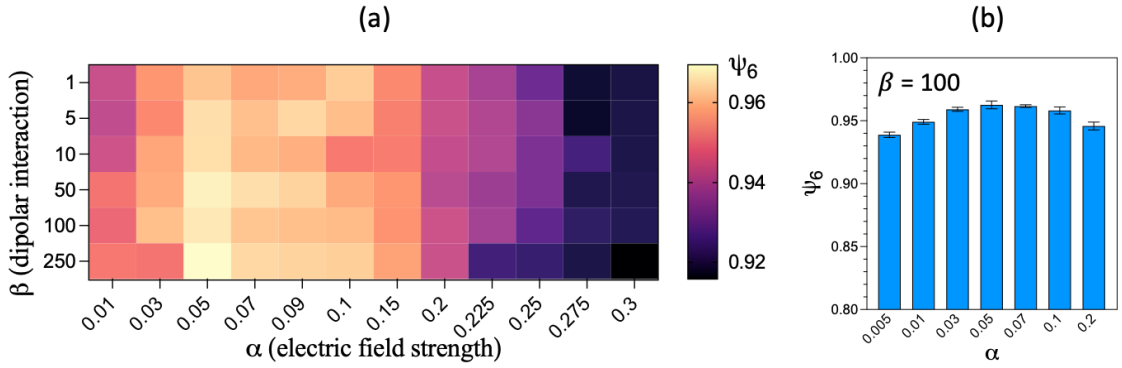


Figure 1. (a) Heatmap showing that the annealing behavior is governed primarily by the magnitude of the electric field strength (through α) rather than the relative strength of dipolar interactions (through β). ψ_6 is an order parameter that characterizes crystal quality. The parameter α controls the magnitude of the electric field strength and β controls the dipole interaction between particles. (b) At constant dipolar interactions (β = 100), we find an optimal electric field strength that achieves the best observable crystal quality.

Reconfiguration of liquid crystal structure by rotating electric fields. Anisotropic colloids align with the field direction under electric field applications in addition to dielectrophoretic translation. Here, we study the dynamics and structures of self-assembled ellipsoids in a six-fold rotating electric field. First, we investigated the dynamics by varying rotating frequency and cluster size. After sedimentation of polystyrene ellipsoids (Figure 2a) in 0.05 mM NaCl in water, we applied the rotating electric fields by connecting a pair of electrodes to the AC electric field one pair at a time; one is connected to the waveform source ("+") of 1 MHz and 20 V_{pp}, and another is to ground ("0"). Others were disconnected ("-"). In this case, the connection is "+--0--" for electrodes 1 to 6 (Figure 2b). The connection was switched to "--+--0" and then "-0--+-" with an interval switching

time τ_s; the rotation cycle was completed after $3\tau_s$ through the 3 distinguishable rotation states. Upon field applications, particles assembled at the center of the device due to dielectrophoresis. After 900 seconds, smaller clusters with longer τ_s were more loosely packed and the particles rotated freely. For larger clusters and at smaller τ_s, the clusters were more compact with less rotational motion, varying from static to edge-rotating (Figure 2 c,d). We then tuned the cluster shape and orientational order (Figures 2 e,f) by varying the connectivity patterns and the rotating sequence. By changing the rotating sequence of "+--0--" pattern from cycling through 6 states (C6 sequence) to 3 states (C3 sequence), the cluster shape changed from hexagon-like to triangle-like with higher orientational order.

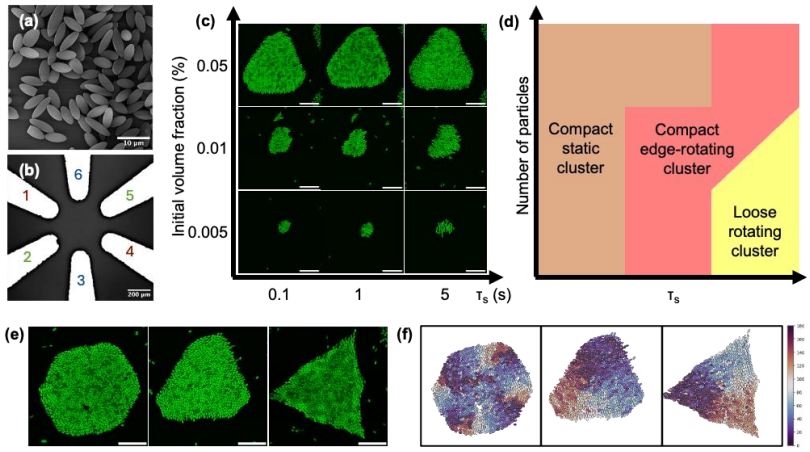


Figure 2. (a) Ellipsoids of aspect ratio 2.6 ± 0.25 were synthesized by thermo-mechanical stretching of spheres of diameter 3.9 ± 0.045 µm. (b) Image of the six-fold electrodes labelled from 1 to 6 in a counterclockwise direction. (c) Images of the self-assembled ellipsoids at the center of the device after 900 seconds of rotating electric field application at different initial volume fraction and switching times (scale bars: 50 µm), and (d) the respective phase diagram based on the dynamics. The self-assembled ellipsoid clusters (initial volume fraction 0.05%, τ_s = 1 s) are shown by their (e) confocal images (scale bars: 50 µm) and (f) detected ellipses with the colorbar as their orientation in degrees. The images in (e) and (f) from left to right represents "+--0---" with C6 sequence, "+--0---" with C3 sequence, and "++00--" with C3 sequence.

Active ellipsoids with variable trajectories as dopants for colloidal crystal annealing. Active colloidal particles differ from Brownian particles because they convert external energy, such as light, electric fields, magnetic fields, or chemical reactions, into directed motion. Here we characterize how the Janus balance and aspect ratio of active colloidal particles affect their propulsion dynamics, with the intention of using these particles as dopants affecting crystal quality. In this study, we synthesized 4µm spherical polystyrene (PS) active particles with varying platinum (Pt) coatings by embedding them in polyvinyl alcohol (PVA) films of different thicknesses. This method was applied to spheres and two types of anisotropic active particles: end-coated ellipsoids and side-coated ellipsoids. Image sequences taken by confocal laser scanning microscopy (CLSM) revealed that end-coated ellipsoid particles tended to exhibit ballistic trajectories, whereas side-coated ellipsoids preferentially followed helical paths, suggesting that variations in Pt-coated regions significantly impact propulsion behavior. These trajectories were identified in the two-

dimensional propulsion profiles by distinguishing between the linear profile of the ballistic trajectory and the sinusoidal profile of the helical trajectory. To further investigate the effect of Janus balance and aspect ratio on active particle motion, we designed a molecular dynamics (MD) simulation framework and constructed coarse-grained ellipsoidal particles with surfaces divided into 32 sub-regions. By selectively activating 2 to 5 adjacent sub-surfaces, we generated 28 distinct active configurations, examples of which are shown in Figure 3a. The resulting simulation library established a quantitative relationship between the ratio of end-to-side active forces and trajectory curvature, revealing three propulsion regimes: ballistic straight-line motion, low-curvature circular motion, and high-curvature circular motion, as plotted in Figure 3b. This simulation-based approach can serve as a valuable tool for guiding experimental studies.

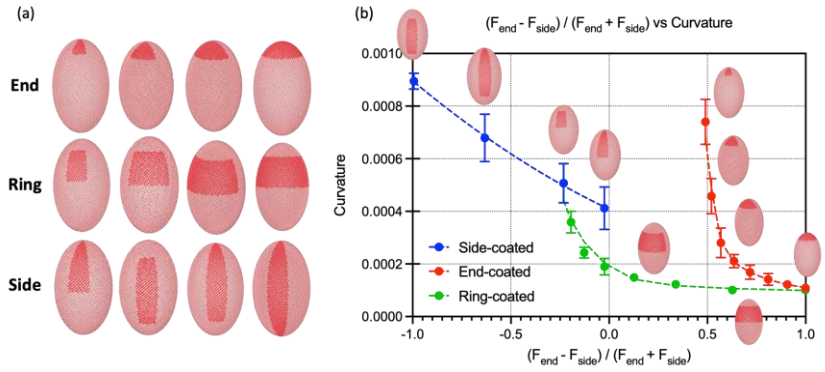


Figure 3. (a) Examples of distinct active ellipsoid configurations studied by simulation. (b) The simulation library of trajectory curvature as a function of the end-to-side force ratio shows three propulsion types: ballistic straight-line motion (blue curve, for side-coated particles), circular motion with high curvature (red curve, for end coated particles), and circular motion with low curvature (green curve, for ring-coated particles).

Future Plans

In the next phase of the project, we will: (1) Change the symmetry of the applied field in the computational model of rotating electric field device to explore the role of this variable on annealing; (2) Control the tilt angle of liquid crystals produced from colloidal ellipsoids by spatial control of electric fields according to the programmable method explored in this abstract; (3) Mechanistically understand how the active patch geometries of anisotropic particles determine the nature of their active trajectory.

References

1. P.-K. Kao, B. J. VanSaders, S. C. Glotzer, M. J. Solomon, *Accelerated annealing of colloidal crystal monolayers by means of cyclically applied electric fields.* Scientific Reports **2021**, *11*, 11042.
2. J. Zhang, J. Yang, Y. Zhang, M. A. Bevan, *Controlling colloidal crystals via morphing energy landscapes and reinforcement learning*. Scientific Advances. 2020, *6*, eabd6716.

Publications

1. S. Mohd Khairi and M.J. Solomon, *Reconfigurable optical response of colloidal discoid liquid crystals by reversible switching between planar and homeotropic alignment*, Cell Reports Physical Science **6(11)** 102926 (2025).
2. T. Liu, C-M Young, T.C. Moore, S.C. Glotzer and M.J. Solomon, *Defect structures in colloidal crystals and their effect on grating diffraction structural color*, ACS Applied Materials and Interfaces **17** 8171-8182 (2025).

Synthetic Methanotrophs: a methane powered platform for active matter

Michael S. **Strano**, Department of Chemical Engineering, MIT

Keywords: chemically powered active matter; synthetic methanotroph; urea-formaldehyde polymerization; synthetic organism

Research Scope

Living organisms that utilize methane as their sole carbon energy source, known as methanotrophs, represent a remarkable class of chemically powered systems. These bacteria oxidize methane at ambient temperature and pressure using membrane-bound enzymes, channeling the resulting chemical energy and carbon intermediates to synthesize new biomass, self-repair damaged cellular components, and move through their environment. This leads us to ask whether this biological design principle can be extracted and realized in synthetic materials: can we build systems in which this type of active chemistry drives matter assembly, repair, and locomotion, independently of living cells? This version of *chemically powered active matter* expands the foundations of the former using biomimetic methanotrophy. The chemistry pioneered in this work offers active matter systems the prospect of not just energy and power for functions, but the ability to *grow* in the context of carbon fixation. This extends active matter concepts to the most powerful versions found in nature: living plant extension and growth, biofilm formation, and tissue repair. The benefits to fundamental materials science are manifold.

Our past work created gel materials capable of active and continuous CO_2 fixation utilizing photosynthetic proteins producing materials that strengthened and repaired over time in the presence of ambient CO_2[1]. Methane presents a unique set of advantages for active matter – it is both a carbon and energy source simultaneously. It is ubiquitous in the environment in the form of biogas, and abundantly present from organic decomposition. Methanotrophy can enable active matter systems to achieve the most impressive functions of living materials. Our current DOE program learns from and applies the CH_4 chemistry of bacterial methanotrophs to create nanoparticle complexes that extend it to active matter systems. This is accomplished through three interconnected thrusts: (i) development of synthetic methanotrophic membranes that mimic the membrane-bound methane monooxygenase (MMO) of natural bacteria, (ii) demonstrate self-powered systems capable of methanotrophic biofilm growth and repair from methane, and (iii) demonstrate a pathway from methane to locomotive power of synthetic organisms as active matter systems, utilizing H_2O_2 as a methane derived oxidation fuel. Central to our contribution to this space is our development of the methanotrophic catalytic couple: two inter-connected catalytic cycles that we have engineered to mimic the key methanotrophic chemistry of living organisms. An Fe or Cu based partial oxidation catalyst for methane creates an alcohol for dehydrogenation at a coupled catalytic cycle. The pair generates a hydrogen peroxide H_2O_2 intermediate that can be used to power the partial oxidation – enabling carbon fixation and repair, materials that literally grow from ambient carbon – or as an energy source itself, powering coordinated locomotion. We show that this chemistry is easily transferrable to many different active matter systems – from

films and interfaces to particle swarms and swimmers. In this way, methanotrophy extends some of the most powerful active matter functions found in nature to synthetic, human derived systems for the first time, advancing the basic goals of the field.

Recent Progress

1. Biomimetic Synthetic Methanotrophic Catalytic Membrane Assembly

To give active matter systems access to a simultaneous carbon and energy source, our strategy has been to look to nature. Natural methanotrophs oxidize methane via membrane-bound particulate methane monooxygenase (pMMO), a copper-dependent enzyme that activates the methane C-H bond using electron transfer chain[2]. Inspired by this, we have developed a synthetic analog to this: a catalytic couple consisting of iron-modified ZSM-5 zeolite (Fe-ZSM-5) and immobilized alcohol oxidase (AOX) working in concert[3]. In this system, methane reacts at Fe-ZSM-5 to produce methanol (*Reaction 1*), which is then immediately oxidized by a nearby AOX to formaldehyde and H_2O_2 (*Reaction 2*). The H_2O_2, in turn, can subsequently react back at the original Fe-ZSM-5 to again convert methane, perpetuating the catalytic chain. The self-sustaining catalytic couple mirrors the redox cycling of pMMO. It imparts to an active matter system the ability to harness usable carbon, in the form of the C1 formaldehyde and an energy source, H_2O_2, commonly used in laboratory systems to power propulsion and actuation. Formaldehyde is easily polymerized to create a myriad of functional materials, which can grow and repair when coupled with the methanotrophic couple. Taken together, this catalytic couple, which we term the synthetic methanotroph, has been refined to achieve methane-to-formaldehyde conversion at room temperature where active matter systems are desired for study. We also demonstrate urea-formaldehyde polymer growth matching or exceeding those of living methanotrophic organisms, as the first realization of a synthetic methanotroph.

$$CH_4 + H_2O_2 \rightarrow CH_3OH + H_2O \quad (1)$$

$$CH_3OH + O_2 \rightarrow HCHO + H_2O_2 \quad (2)$$

Net: methane → carbon source + fuel source

Building on these results, we advance this work by assembling Fe-ZSM-5 and AOX into a membrane architecture, which we term the methanotrophic catalytic membrane assembly (Figure 1). We achieve this by immobilizing Fe-ZSM-5 and AOX on porous carbon paper, which, when assembled, forms a biomimetic membrane-like architecture with a triple-phase interface that enables efficient gas delivery and H_2O_2 and methanol turnover.

The catalytic membrane assembly has been integrated into a continuous flow reactor, forming an artificial methanotrophic cell that continuously metabolizes methane to C_1 products with high productivity and stability.

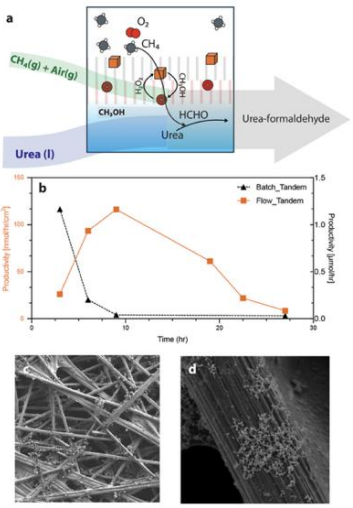


Figure 1. Biomimetic synthetic methanotrophic membrane assembly for ambient methane valorization into polymer. a, Schematic of the triple-phase catalytic system where methane and air are delivered as a gas mixture to the AOX/Fe-ZSM-5 catalytic membrane interface. **b**, Time-on-stream productivity comparison between batch tandem (black) and continuous-flow tandem (orange) operation, showing sustained productivity in the flow system versus rapid decay in batch. **c, d,** SEM image of the carbon paper support with the immobilized Fe-ZSM-5 and AOX.

2. Methanotrophic Biofilm Growth and Repair Powered by Methane

A key output of our synthetic methanotrophic system is formaldehyde, which serves as a reactive C_1 monomer for urea-formaldehyde (UF) polymerization. Natural methanotrophs use formaldehyde similarly, as the entry point for carbon assimilation into biomass (e.g., Ribulose monophosphate cycle), and we leverage this analogy to demonstrate methane-driven biofilm growth. UF condensation is strongly acid-catalyzed, proceeding rapidly below pH 4 and negligibly near neutral pH. The monomer of urea and formaldehyde, MMU dominates under neutral pH. This pH sensitivity provides a handle for spatially controlling biofilm growth by locally acidifying the reaction environment at a surface.

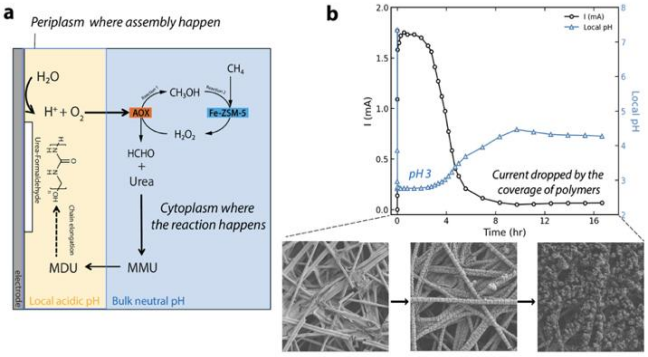


Figure 2. Polymer biofilm growth from methane-derived formaldehyde. a, Schematic of the biomimetic architecture of the local acidic pH zone (periplasm analog, yellow) where assembly occurs and the bulk neutral pH zone (cytoplasm analog, blue) where methane-to-formaldehyde reaction happens. Formaldehyde reacts with urea to form MMU, which converted to methylene diurea (MDU) and UF polymer via a subsequent chain elongation. **b,** Local pH (right axis) and current (left axis) during the polymerization. The local pH drops sharply to ~3, driving urea-formaldehyde condensation for the growing polymer. SEM images below show the evolution of the biofilm.

The polymerization can actively proceed selectively at the defined zone, producing a structured solid deposit directly from the methane-derived monomer.

3. H_2O_2-Powered Synthetic Organisms as Chemically Driven Active Matter

The promise of methanotropy for active matter is that methane itself can be both a carbon source and a fuel to power functions. Accordingly, we explored the use of H_2O_2 from the cycle to enable actuation of propulsion of synthetic organisms. H_2O_2 is a high-energy-density chemical fuel generated by our catalytic couple and is well-suited to powering microscale autonomous motion.

To mathematically characterize the dynamics of our synthetic methanotrophic system and identify the conditions under which stable H_2O_2 concentrations emerge, we formulate a dimensionless model (Equations (3)-(6)) for a continuous stirred-tank reactor (CSTR).

$$\frac{d\eta_{CH_4}}{d\chi} = 1 - \eta_{CH_4} - D_{a1}\eta_{CH_4}\eta_{H_2O_2} \tag{3}$$

$$\frac{d\eta_{H_2O_2}}{d\chi} = -\eta_{H_2O_2} - D_{a1}\eta_{CH_4}\eta_{H_2O_2} + D_{a2}\eta_{CH_3OH} \tag{4}$$

$$\frac{d\eta_{CH_3OH}}{d\chi} = \eta_{CH_3OH,0} - \eta_{CH_3OH} + D_{a1}\eta_{CH_4}\eta_{H_2O_2} - D_{a2}\eta_{CH_3OH} \tag{5}$$

$$\frac{d\eta_{HCHO}}{d\chi} = -\eta_{HCHO} + D_{a2}\eta_{CH_3OH} \tag{6}$$

where $\eta_i = \frac{C_i}{C_{CH_4,0}} (i = CH_4, CH_3OH, HCHO, H_2O_2)$, $\chi = \frac{t}{\frac{V}{q}}$, $D_{a1} = k_1 C_{CH_4,0} \frac{V}{q}$, $D_{a2} = k_2 \frac{V}{q}$ and C_i is the concentration of specie i, V is the volume of the reactor, q is the flow rate, k_1 and k_2 are the kinetic coefficients for *reaction 1* and *reaction 2*.

These four equations concisely encode the dynamics of the methanotropy, allowing the study of its non-linear dynamics to be tractable. By analyzing the steady-state solutions and transient trajectories of this system, we can delineate the parameter space – particularly in terms of the Damköhler numbers D_{a1} and D_{a2} – over which sustained H_2O_2 accumulation, and thus autonomous organism motility, is achievable. Our work develops design rules for harnessing chemical couples like this one for active matter systems.

We develop several classes of H_2O_2-powered synthetic organisms to this end. The first exploits geometric asymmetry to generate materials with spontaneous oscillatory mechanics: coupled particles with broken symmetry undergo sustained beating in the presence of the air-liquid interface powered by H_2O_2, with emergent collective oscillation arising from hydrodynamic coupling between neighboring units[4] (Figure 3). The second class in an attempt to implement chemotactic steering: particles trace isochemical contours in a chemical gradient field by coupling asymmetric H_2O_2 decomposition to directed propulsion, enabling autonomous navigation toward chemical sources without external control, mimicking natural chemotaxis[5]. H_2O_2, acting as a stimulus, alters the resistance of the sensor and the conformation of the actuator. These systems with synthetic organisms demonstrate that H_2O_2 generated by our synthetic methanotrophic

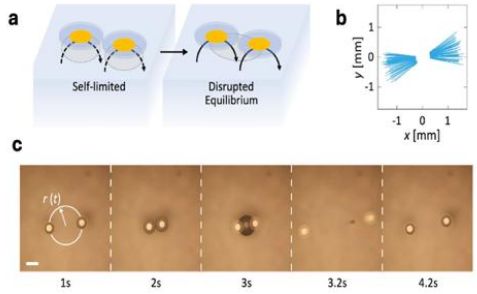


Figure 3. H_2O_2-Powered Synthetic Organisms as Chemically Driven Active Matter. a, Schematic of a two-particle system, exhibiting an emergent and self-sustained beating behaviour as the bubble merger restores the previously hindered reactivity, thus disrupting the equilibrium state. **b,** Tracked coordinates of a two-particle system with emergent beating. **c,** Micrograph of a two-particle system with emergent beating. Adapted from Ref. 4.

platform can, in principle, be directly harvested to power mechanical work at the microscale. Future work seeks to create materials that collective "beat" in regular mechanical contractions, similar to cardiac muscle, powered by methanotrophy.

Future Plans

The three thrusts described above – synthetic methanotrophic catalytic membrane, methane-derived biofilm growth, and chemically powered synthetic organisms – will be integrated into a unified chemically powered active matter platform. The system will demonstrate end-to-end methane-to-material conversion within concomitant active mater functions. The ability to control the direction and location of carbon fixation enables active matter systems to mimic the most powerful functions of living materials. In this way, our work is advancing the science of active matter: moving from systems powered by external fields or pre-stored fuels to systems that generate their own chemical energy and carbon fixation from the natural environment in direct analogy with living organisms.

References

1. Kwak, S. *et al.* Polymethacrylamide and Carbon Composites that Grow, Strengthen, and Self-Repair using Ambient Carbon Dioxide Fixation. *Advanced Materials* **30**, (2018).
2. J. Tucci, F. & C. Rosenzweig, A. Direct Methane Oxidation by Copper- and Iron-Dependent Methane Monooxygenases. *Chem. Rev.* **124**, 1288–1320 (2024).
3. Lundberg, D. J., Kim, J., Tu, Y. M., Ritt, C. L. & Strano, M. S. Concerted methane fixation at ambient temperature and pressure mediated by an alcohol oxidase and Fe-ZSM-5 catalytic couple. *Nat. Catal.* **7**, (2024).
4. Yang, J. F. *et al.* Emergent microrobotic oscillators via asymmetry-induced order. *Nat. Commun.* **13**, (2022).
5. Brooks, A. M., Yang, S., Kang, B. H. & Strano, M. S. A Microrobotic Design for the Spontaneous Tracing of Isochemical Contours in the Environment. *Advanced Intelligent Systems* **6**, (2024).

Publications (past 2 years, supported by BES)

1. Brooks, A. M., Yang, S., Kang, B. H. & Strano, M. S. A Microrobotic Design for the Spontaneous Tracing of Isochemical Contours in the Environment. *Advanced Intelligent Systems* 6, (2024).
2. Zhang, G. et al. High energy density picoliter-scale zinc-air microbatteries for colloidal robotics. *Science Robot*ics, 9, (2024).
3. Kim, J. & Strano, M. S. Methanotrophic catalysis for methane oxidation to formaldehyde. *Nature Catalysis* 7, 1270–1271 (2024).
4. Lundberg, D. J., Kim, J., Tu, Y. M., Ritt, C. L. & Strano, M. S. Concerted methane fixation at ambient temperature and pressure mediated by an alcohol oxidase and Fe-ZSM-5 catalytic couple. *Nature Catalysis* 7, (2024).

In review

Kang, B.H., Yang, S., Min, H., Strano, M. S. Steering 2D Microrobots via Microscale Force Balance Modulation. Under review in *Small*

Under preparation

Kim, J., Jiang, Y., Strano, M. S. Zero-waste Room-Temperature Upcycling of Waste Methane and Nitrogen Effluent into Polymeric Material.

Dynamics of Superstructure Formation from Supramolecular Assemblies

Samuel I. **Stupp**, Department of Materials Science and Engineering, Department of Chemistry, Department of Biomedical Engineering, Department of Medicine, Center for Regenerative Nanomedicine, Northwestern University

Keywords: Supramolecular polymers, dynamics, organic ferroelectrics, photocatalysis

Research Scope

Cells rely on compartmentalization to perform functions across length scales, from the outer membrane down to organelles with distinct metabolic and transport functions. It has been suggested that liquid–liquid phase separation (LLPS) occurs because of incompatibility between two fluid-forming materials such as hydrophilic and lipophilic domains or condensed and dilute phases, leading to systems that are highly dynamic, despite having a high degree of order. In our previous research funded by the DOE Biomolecular Materials program, we observed the growth of ordered arrays of filamentous nanostructures in water driven by repulsive electrostatic interactions as well as the formation of superstructures of these assemblies enabled by the dynamic exchange of molecules to allow optimal cohesion between the molecules.[1–3] We present here two projects involving catalysis in superstructures. In the first project, we investigate the use of confinement to enhance catalytic turnover of enzymes and peptide-based enzyme mimetics for reactions like the reduction of CO_2 and the production of H_2O_2 within the superstructures. In the second project, we use organic ferroelectric/piezoelectric materials, which generate electrical signals with mechanical deformation, to enhance photocatalysis. We previously reported on these supramolecular polymers composed of segments of the widely used ferroelectric polymer poly(vinylidene fluoride) in which peptide hydrogen bonding enhances the content of the ferroelectric phase.[4] Our recent research on the effects of macromolecular crowding on the ferroelectric behavior of these assemblies unexpectedly revealed that the ferroelectric supramolecular polymers can enhance photocatalytic production of fuels using supramolecular assemblies of chromophore amphiphiles (CAs) as photosensitizers. We are now exploring these systems with catalysts that can increase conversion to interesting fuels.

Recent Progress

Based on our understanding of charged and uncharged PA–polymer structures developed previously with BES support, we are studying how PA scaffolds and macromolecular crowders influence the recruitment and catalytic activity of enzymes that can mediate the interconversion of CO_2 and potential fuel molecules. As a proof of principle, we explored formate dehydrogenase (FDH) and its "forward" reaction converting formic acid to CO_2 using nicotinamide adenine dinucleotide (NAD^+) as a redox mediator (Figure 1). Since our goal is to use the PA bundles as confined reaction environments for enzyme cascades, we examined how enzyme-scaffold interactions vary across three PAs: anionic palmitoyl $V_3A_3E_3$ (E3), cationic palmitoyl-$V_3A_3K_3$ (K3), and an uncharged PA bearing histidine and PEG groups for solubility at low pH. Confocal

microscopy shows that enzyme recruitment is governed primarily by PA charge rather than crowding conditions. At its optimal operating pH of 8, FDH is negatively charged and shows minimal colocalization with the anionic E3 fibers, consistent with electrostatic repulsion even at high dextran concentrations. In contrast, FDH exhibits strong recruitment to the cationic K3 fibers, with high colocalization in both 0 wt.% and 5 wt.% dextran. Notably, in the absence of dextran, FDH appears to crosslink K3 fibers acting as a multivalent, negatively charged protein bridging positively charged fibers. For the uncharged histidine-PEG PA, FDH displays intermediate behavior: partial adsorption to fiber surfaces and partial partitioning into the dextran-rich phase. We also observed, by testing multiple enzymes in the uncharged PA–polymer system, that crowding plays a secondary role that depends on protein size, with larger enzymes experiencing stronger partitioning. Enzyme activity measurements further support the idea that the nature of scaffold–enzyme interactions determines catalytic efficiency. For example, the enzymatic activity is nearly eliminated with K3 PA, consistent with strong electrostatic adsorption leading to immobilization, misorientation of the active site, or partial enzyme unfolding. In samples using E3 PA, FDH does not partition into bundles, yet activity still decreases, suggesting indirect effects such as sequestering of the cofactor NAD^+ by the anionic PA network. Lastly, for the uncharged histidine-PEG PA, activity decreases with increasing PA concentration. This supports a model in which weak, reversible adsorption and confinement are sufficient to dampen catalytic turnover, even without strong electrostatic binding. Together, these results show that PA filaments can modulate enzyme function through a combination of physical confinement and non-specific interactions, and that scaffold peptide sequence provides a tunable parameter for controlling both recruitment and activity.

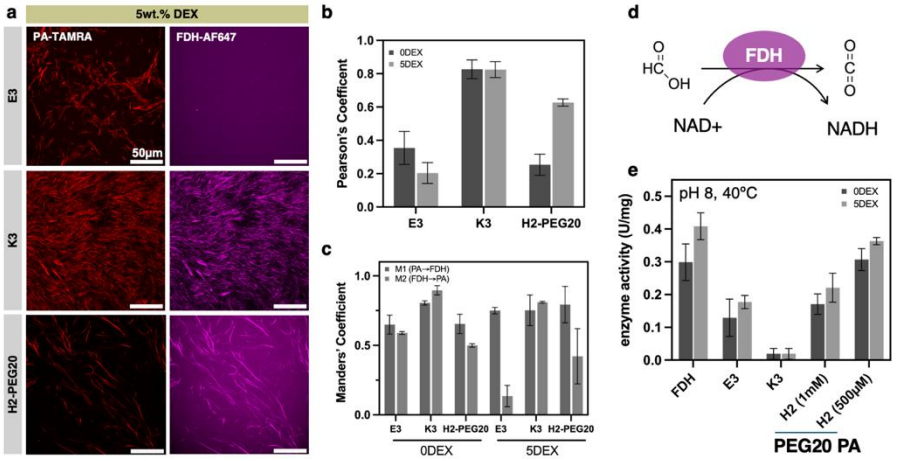


Figure 1. Enzyme recruitment and activity in PA–polymer systems. (a) Confocal micrographs of FDH colocalizing with E3, K3, and uncharged histidine-PEG PA bundles. (b) Pearson's coefficient and (c) Mander's coefficients comparing colocalization in 0 wt.% and 5 wt.% dextran PA–polymer solutions. (d) Schematic showing FDH forward reaction converting formic acid to CO_2 mediated by nicotinamide adenine dinucleotide (NAD^+). (e) FDH enzyme activity in PA–polymer systems with 0 wt.% and 5 wt.% dextran. N=3; error bars report standard deviation.

In a second project, we are studying the effects of our recently developed supramolecular ferroelectric/piezoelectric materials incorporating oligo(vinylidene fluoride) on photocatalysis (Figure 2). We began our investigation by bundling OVDF-PA assemblies with perylene monoimide ribbons, which we have previously reported to be useful for solar fuels production with visible light given their ability to efficiently harvest light.[5] Our approach here involved introducing pre-annealed OVDF-PA assemblies into an aqueous solution containing PMI nanostructures serving as photosensitizers, molybdenum sulfide clusters as catalysts, and ascorbic acid as a sacrificial electron donor. Liquid atomic force microscopy (AFM) revealed that at pH ~4 OVDF-PA fibers colocalize with PMI nanoribbons, with their ferroelectric polarization direction aligning along the π–π stacking axis. Based on these images, we speculate that the proximity and alignment between OVDF-PA and PMI nanoribbons provides a cooperative interaction between ferroelectric domains and chromophore assemblies, potentially enhancing charge separation and transport.

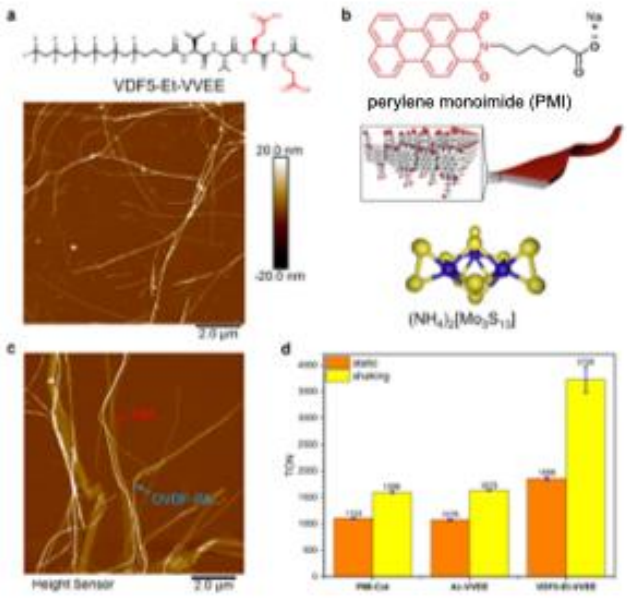


Figure 2. Improved photocatalytic H_2 production by introducing supramolecular ferroelectric nanostructures. (a) Chemical structure of an OVDF-PA molecule VDF_5-Et-VVEE and AFM image of the ferroelectric assemblies. (b) Chemical structure of PMI and illustration of the ribbon-like PMI assembly and the molybdenum sulfide catalyst crystal structure. (c) AFM image of bundles formed by VDF_5-Et-VVEE assemblies and PMI nanoribbons in the hydrogen-evolving solution. (d) H_2 evolution TON values after 18 h of white light illumination on solutions containing only PMI/catalyst (PMI-Cat), control with the addition of non-ferroelectric acetate-capped peptide (Ac-VVEE), and sample with ferroelectric VDF_5-Et-VVEE assemblies.

Photocatalytic hydrogen evolution assays were conducted under simulated solar irradiation (~3× sun intensity) of these samples in sealed vials. After 18 hours of illumination with gentle agitation (motion on the s^{-1} timescale), hydrogen accumulation in the headspace was quantified and used to calculate catalytic turnover numbers (TONs). Incorporation of ferroelectric OVDF-PA assemblies resulted in more than a twofold increase in TON relative to both the PMI/catalyst (PMI-Cat) system and the non-ferroelectric control with the acetamide-capped peptide (AcVVEE). While the source of this enhancement is not well understood based on current literature, we speculate that it is related to better mass transport of reagents, products, and ions in these materials when the ferroelectric OVDF-PA is used. It could also be related to changes in polarization in and around the catalytic site. We plan to quantify the mass transport enhancement through fluorescence recovery after photobleaching (FRAP) experiments similar to those previously performed on PMI nanoribbons.

Future Plans

In the first project, we will examine how intermolecular cohesion and nanostructure rigidity of the PA assemblies influence catalytic turnover, thereby establishing how supramolecular dynamics govern enzyme behavior under confinement. In parallel, we will also pursue the reverse FDH reaction to convert CO_2 to formic acid and implement a tandem FDH and glucose dehydrogenase (GDH) system for cofactor regeneration to sustain continuous formic acid production within PA–polymer bundles. As we transition from single-enzyme systems to tandem reactions, additional constraints will certainly arise from differences in optimal pH, cofactor dependence, and kinetic rates among natural enzymes confined within the same architecture. We also want to expand the range and architectural flexibility of the PA–polymer platform with enzyme-mimetic peptides as modular catalytic components that complement natural enzymes and enable the development of hybrid reaction systems. In the second project, we will leverage our previous work by introducing other chromophore amphiphiles. While PMIs have been extensively studied for their hydrogen evolution reactions, ullazines and aminonaphthalene monoimides have band gaps and lowest unoccupied molecular orbital (LUMO) levels that can drive more challenging reactions such as peroxide formation and carbon dioxide reduction. One of the key aspects that distinguishes our supramolecular approach to piezo-photocatalysis from the use of traditional inorganic piezoelectric materials is the programmability of dynamic supramolecular assemblies versus fixed crystal lattices, which can tune the vibration frequency responsiveness. We hypothesize that the frequency response of the supramolecular assemblies is a unique handle for controlling the photocatalytic activity linked by the mechanical properties of these supramolecular polymers, and aims to establish design rules for materials stiffness, dimensions and input energies versus chromophore bandgap and turnover frequencies. This materials stiffness will be further tuned by the combination of depletion force-induced bundling of the OVDF-PA / CA assemblies upon addition of polymers, providing orders-of-magnitude differences in vibration frequency from gentle shaking at Hz to ultrasonic vibrations at MHz.

References

1. R. Freeman, M. Han, Z. Álvarez, J. A. Lewis, J. R. Wester, N. Stephanopoulos, M. T. McClendon, C. Lynsky, J. M. Godbe, H. Sangji, E. Luijten, and S. I. Stupp, *Reversible Self-Assembly of Superstructured Networks*, Science **362,** *362*, 808 (2018).
2. Z. Álvarez, A. N. Kolberg-Edelbrock, I. R. Sasselli, J. A. Ortega, R. Qiu, Z. Syrgiannis, P. A. Mirau, F. Chen, S. M. Chin, S. Weigand, E. Kiskinis, and S. I. Stupp, *Bioactive Scaffolds with Enhanced Supramolecular Motion Promote Recovery from Spinal Cord Injury*, Science **374**, 848 (2021).
3. A. N. Edelbrock, T. D. Clemons, S. M. Chin, J. J. W. Roan, E. P. Bruckner, Z. Alvarez, J. Edelbrock, K. S. Wek, and S. I. Stupp, *Superstructured Biomaterials Formed by Exchange Dynamics and Host–Guest Interactions in Supramolecular Polymers*, Advanced Science **8**, 2004042 (2021).
4. Y. Yang, H. Sai, S. A. Egner, R. Qiu, L. C. Palmer, and S. I. Stupp, *Peptide Programming of a Supramolecular Vinylidene Fluoride Ferroelectric Phase,* Nature **634** 833 (2024).
5. A. S. Weingarten, R. V. Kazantsev, L. C. Palmer, M. McClendon, A. R. Koltonow, A. P. S. Samuel, D. J. Kiebala, M. R. Wasielewski, S. I. Stupp *Self-Assembling Hydrogel Scaffolds for Photocatalytic Hydrogen Production* Nature Chemistry **6** 964 (2014).

Publications

1. S. A. Egner, M. Agrawal, H. Sai, L. C. Palmer, and S. I. Stupp, *Functional Design of Peptide Materials Based on Supramolecular Cohesion,* Journal of the American Chemical Society **147** 6829 (2025).
2. Y. Yang, H. Sai, S. A. Egner, R. Qiu, L. C. Palmer, and S. I. Stupp, *Peptide Programming of a Supramolecular Vinylidene Fluoride Ferroelectric Phase,* Nature **634** 833 (2024).
3. J. S. W. Seale, S. Sharma, C. K. Lee, H. Han, T. Jaynes, E. W. Roth, S. Shafie, Y. Qiu, L. Malaisrie, M. I. Bardot, L. Zhang, Y.-K. Xing, D. J. Kim, S. I. Stupp, R. D. Astumian, E. A. Scott, W. R. Dichtel, J. F. Stoddart *Active Transport of Macrocycles into Micelles Using Molecular Pumps* Angewandte Chemie International Edition **64**, e202512899 (2025).
4. R. Qiu, W. Ji, Z. Álvarez, H. Sai, Z. Gao, F. Chen, A. A. Linton, N. J. Lanzetta, A. M. Goodwin, H. J. Brecort, J. Li, J. Inglis, S. Kurapaty, S. R. Stock, W. K. Hsu, E. L. Hsu, S. I. Stupp *Motion of Molecules in Supramolecular Scaffolds Enhances Bone Regeneration,* Journal of the American Chemical Society **147** 21586 (2025).
5. H. Du, R. Qiu, X. Lou, S. A. H. Jansen, H. Sai, Y. Wang, E. W. Meijer, S. I. Stupp *Mapping in situ the assembly and dynamics in aqueous supramolecular polymers* Nature Communications **16**, 4837 (2025).
6. R. Z. Pavlović, Y. Vorobyov, S. A. Egner, A. Metlushko, H. Sai, A. L. Hansen, C. Yuan, D. Conroy, S. Wang, S. Biswas, M. R. Karver, T. J. Jaynes, L. C. Palmer, S. I. Stupp *Probing Supramolecular Motion with Nuclear Magnetic Resonance in Bioactive Scaffolds that Promote Neural Regeneration in the Central Nervous System* Journal of the American Chemical Society **148** 18004 (2026).
7. J. V. Passarelli, Y. Yang, C. S. Smith, J. Hao, D. R. Dave, A. Narayanan, Z. Álvarez, B. K. Johnson, K. A. Marshall, I. Fithian, H. Sai, R. Qiu, C. L. Stern, L. C. Palmer, E. Kiskinis, S. I. Stupp *Peptide-Induced Ferroelectricity in Charge-Transfer Supramolecular Materials* Advanced Materials **38** e14940 (2026).
8. R. Emmanuele, J.-S. Chen, H. Sai, S. D. Namgung, D. J. Gosztola, Y. Wang, J. Lou, S. I. Stupp, M. C. Hersam, X. Ma *Efficient Second-Harmonic Generation from Molecular Monolayers* ACS Nano **20** 14627 (2026).
9. T. J. Jaynes, Luka Đorđević, H Sai, S. Weigand, J. F. Stoddart, S. I. Stupp *Dynamic Self-Assembly Mediated by Stored and Released Electrons in Pimer Supramolecular Polymers of Chromophore Amphiphiles* Chem **12** 103075 (2026).
10. Z. Syrgiannis, M. A. Alvarez-Saavedra, N. A. Sather, I. R. Sasselli, Z. Álvarez, S. Incontro, R. Z. Pavlović, C. S. Smith, O. A. Carballo-Molina, F. Jiménez-Ángeles, S. Kewalramani, D. Simkin, T. Fyrner, M. L. Musella, J. Extremet, M. Strong, S. Murphy, J. P. Sandler, F. Lancia, F. Chen, S. Rodriguez, M. R. Karver, S. J. Weigand, T. D. Clemons, C. A. Waudby, A. L. Hansen, J. E. Kupferberg, R. J. Nap, I. Szleifer, L. C. Palmer, M. J. Bedzyk, E. Kiskinis, M. Olvera de la Cruz, D. Debanne, S. I. Stupp *Dense Ion Clouds in Supramolecular Biomaterials Boost Neuronal Development and Neurotransmission,* In revision.

Simulation-driven design for experimental realization of 3D complex nanostructures

Petr **Šulc** (Arizona State University)

Keywords: inverse design, coarse-grained models, molecular simulation, self-assembly, DNA nanotechnology

Research Scope

We develop inverse design methods to realize self-assembled materials at nanoscale, with the goal of uncovering fundamental design principles that govern the assembly, as well as investigating the thermodynamics and kinetics of self-assembled materials which consist of multiple different components. From design space, it presents a challenge in terms of large number of parameters of possible solutions, as well as long timescales associated with system assembly, making computational design difficult. The goal is to establish modeling and simulation methods to understand the free energy landscape and kinetics of self-assembly of multicomponent periodic as well as finite-size structures. Towards this goal, we develop new efficient algorithms to search the design space as well as multiscale simulation approaches, representing individual building blocks at different resolutions in trade-off between speed and accuracy. We develop the theory for inverse design of self-assembling systems and then apply it to proof-of-principle to systems in DNA nanotechnology, which we also realize and characterize experimentally using DNA origami nanostructures used as a basic building block.

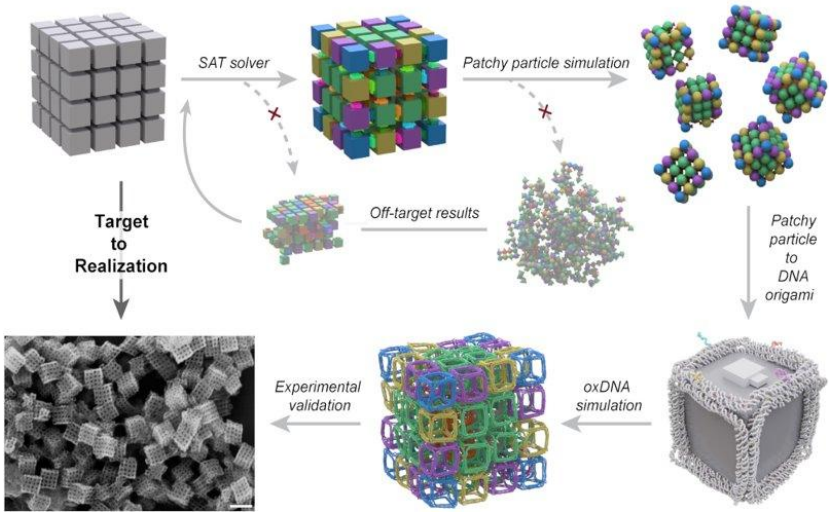


Figure 1: Design pipeline for nanoscale self-assembly of arbitrary target: For a specified target (a finite size structure or periodic crystal lattice) our models find a minimal number of distinct building blocks that are required for reliable self-assembly in high-yield. As a proof of principle, we verified the assembly experimentally using DNA nanostructures.

Recent Progress

We developed a complete theory-to-experiment pipeline for the inverse design of multicomponent self-assembling systems [1]. It is applied to aa universal polycube platform for programmable assembly of arbitrary three-dimensional nanostructures out of cubic-shaped boxes (Figure 1). We established the “minimal kit” concept, defining the smallest set of distinct components needed for

high-fidelity assembly. Using multiscale modeling, inverse thermodynamics, and DNA origami-based fabrication, we achieved predictive design and experimental realization of complex finite as well as crystalline, reconfigurable, and multifunctional nanostructures, including hierarchical DNA assemblies with up to 400 distinct components, which presents the largest non-crystalline 3D nucleic acid structure demonstrated to date. These results establish a predictive, model-driven framework linking microscopic interaction rules to macroscopic material behavior and provide new capabilities for engineering programmable nanoscale materials.

Future Plans

We will extend the inverse-design framework to the programmable self-assembly of tetrahedral open colloidal crystals using a single DNA-origami scaffold. The work will focus on demonstrating that crystal lattice topology can be controlled through encoded interaction rules rather than particle geometry. A computational pipeline combining SAT-based inverse design, positive and negative design principles, and patchy-particle simulations will be developed to identify interaction schemes that selectively stabilize target lattices while suppressing competing structures, which are some of the main reason for the difficulty of achieving complex open lattices. These designs will then be experimentally realized using tetrahedral DNA-origami building blocks with programmable binding sites and orthogonal DNA sticky-end interactions. Systematic studies of assembly conditions, thermodynamic phase behavior, kinetics, and defect formation will be performed across multiple lattice types to establish general design principles for selective self-assembly.

References

1. Thong Diep, Hao Liu, Joshua Evans, Michael Matthies, Matthew Sample, Subhajit Roy, Daniel Podbielski, Sneha Vaidyanathan, Dewight Williams, Kyoungdu Kim, Lukas Kroc, Haozhi Wang, Yonggang Ke, Joshua Hihath, Hao Yan, Petr Sulc: *Universal 3D Nanoscale Assembly with DNA Polycubes,* in revision in Science Robotics, preprint: doi:10.26434/chemrxiv-2025-qbk3f

Publications

1. Camilla Beneduce, Giuseppe Mastriani, Petr Sulc; Francesco Sciortino, John Russo: *"Inverse Thermodynamics: Designing Interactions for Targeted Phase Behavior*", Journal of Physical Chemistry. B, Volume **129**, p. 10153-10161 (2025)
2. Diogo Pinto, Petr Sulc, Francesco Sciortino, John Russo, "*Automating Blueprints for the Assembly of Colloidal Quasicrystal Clusters*", ACS Nano, **19(1)**, 512-519 (2024)
3. Camilla Beneduce, Diogo Pinto, Lorenzo Rovigatti, Flavio Romano, Petr Sulc, Francesco Sciortino, John Russo, "*Falsifiability Test for Classical Nucleation Theory*", Physical Review Letters, **134(14)**, 148201 (2025)

Rational Chemical Design of Dynamic Protein Materials

F. Akif **Tezcan**, University of California, San Diego

Keywords: Protein-Based Materials, Dynamic/Stimuli-Responsive/Adaptive Systems, Protein-Polymer Interface, Computational Protein Design

A. Research Scope. The overarching goal of our DOE-funded research program is to develop design strategies inspired by principles of supramolecular, inorganic and polymer chemistry for controlling the arrangement of proteins into dynamic high-order architectures. Through these efforts, our laboratory has established new approaches (e.g., metal- and disulfide-directed protein self-assembly), which, in turn, led to state-of-art protein materials (e.g., hyperstable protein assemblies, coherently dynamic protein crystals, protein-metal-organic frameworks, polymer-integrated protein crystals). These materials not only display unprecedented physical and mechanical properties, but also provide new platforms for studying and understanding biomolecular self-assembly, enabled by their externally-controllable mode of construction. While we are still pursuing methodology development for designing new protein *architectures* (see Objective 1), a considerable fraction of our ongoing efforts now centers on engineering adaptive protein-based materials, and programming their macroscale structural dynamics and functional/mechanical properties through atomic-scale interventions (Objective 2). Importantly, an important new focus of our research program is to design dissipative protein architectures, which, like natural cytoskeletal assemblies, require constant energy input/consumption for maintaining their self-assembled states (Objective 3).

B. Recent Progress

***Objective 1. Control of protein assembly through host-guest interactions*:** As an alternative to designing responsive protein structures exclusively through non-covalent networks, the use of discrete chemical bonding interactions provides an expedient route. Such chemical bonds occupy very small footprints on protein surfaces, rendering these bonds straightforward to engineer and easy to engage/disengage through external stimuli. Building on our previous work with metal- and disulfide-directed protein assembly, we have implemented here a different type of chemical

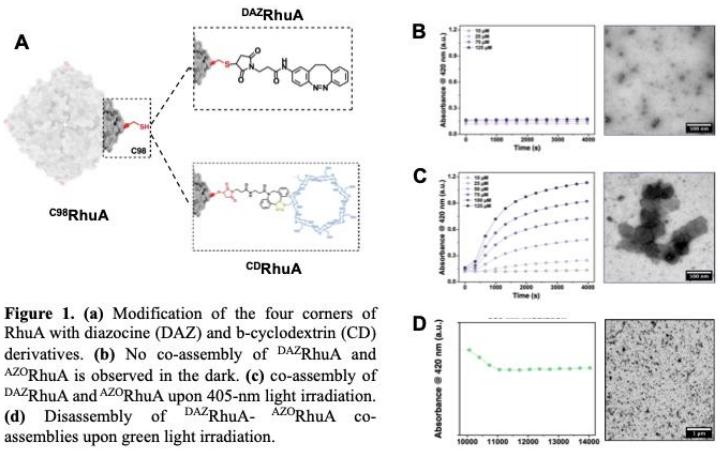


Figure 1. (a) Modification of the four corners of RhuA with diazocine (DAZ) and b-cyclodextrin (CD) derivatives. **(b)** No co-assembly of ^{DAZ}RhuA and ^{AZO}RhuA is observed in the dark. **(c)** co-assembly of ^{DAZ}RhuA and ^{AZO}RhuA upon 405-nm light irradiation. **(d)** Disassembly of ^{DAZ}RhuA- ^{AZO}RhuA co-assemblies upon green light irradiation.

interaction motif, namely non-covalent host-guest (HG) interactions. Earlier we demonstrated that RhuA (a C_4 symmetric tetrameric protein) could be functionalized in its four corners with β-cyclodextrin (CD) or azobenzene (AZO) groups, and the resulting variants (^{CD}RhuA and ^{AZO}RhuA) paired with one another to form well-ordered 1D nanotubes and crystalline 2D nanosheets (Chem, 2025, Publication 3). These assemblies, which form with the azo group in the thermodynamically favored trans (E) state, could be dissociated upon UV irradiation to cause the trans-to-cis (E-to-Z) isomerization of azo. In this period, our efforts focused primarily on synthesizing cyclic/constrained-derivatives of AZO, namely diazocines (DAZ), whose ground-state conformation is the Z state and can only pair with CD hosts (**Fig.1A**) upon visible light irradiation (followed by thermal relaxation to reverse-isomerize), thus opening the path the generate dissipative/non-equilibrium protein assemblies. Indeed, the co-assembly of ^{DAZ}RhuA and $^{\beta CD}$RhuA does not occur in the dark (**Fig.1B**) but could be initiated by irradiation with 405-nm light, leading to the formation of stacked 2D crystals (**Fig.1C**) as induced by the Z-to-E isomerization of DAZ. Yet these nanosheets did not dissociate upon removal of light and could only be disassembled upon prolonged exposure to 530-nm light (**Fig.1D**). Our TEM analyses and computational modeling suggest the E form of DAZ still be able to form kinetically stabilized HG interactions with CD groups within the 2D sheets (manuscript in preparation).

Objective 2a. Dual-energy control of dissipative enzyme assembly and catalysis: Living systems integrate multiple energy sources to regulate molecular function far from equilibrium. Chemical energy and environmental cues such as light cooperate to control protein assembly, enzymatic activity, and metabolism across multiple length and time scales. Although significant advances have been made in engineering stimuli-responsive proteins and dissipative biomolecular systems, synthetic protein assemblies generally rely on a single energy source and rarely couple transient structural states to programmable biological function. Consequently, general design principles for engineering protein systems that integrate multiple energy inputs remain largely unexplored.

Building on our recent development of an ATP-driven dissipative protein assembly based on the AAA+ ATPase FtsH (Nat. Chem. Biol. 2025, Publication 2), we asked whether distinct energy sources could be programmed to perform complementary functions within a single protein system. We coupled ATP-dependent FtsH assembly to a visible-light-responsive photoacid that converts photon flux into reversible changes in proton concentration (**Fig.2A**). In this design, ATP and light play fundamentally different yet cooperative roles. ATP activates FtsH into an assembly-competent state, whereas light creates the chemical environment required for nanotube

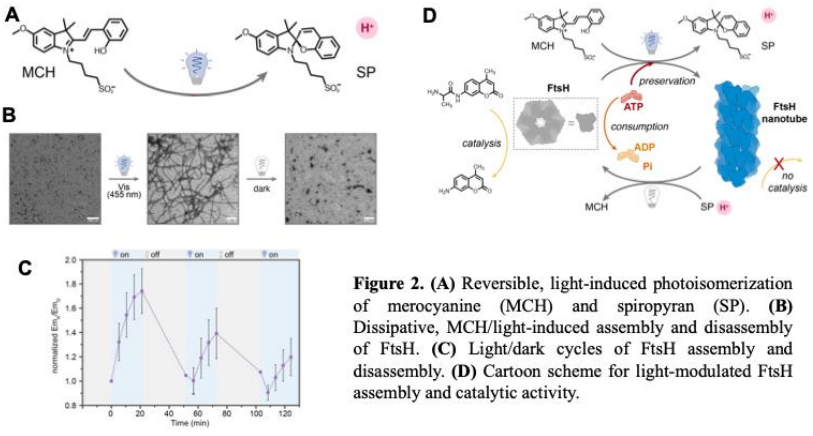


Figure 2. (A) Reversible, light-induced photoisomerization of merocyanine (MCH) and spiropyran (SP). **(B)** Dissipative, MCH/light-induced assembly and disassembly of FtsH. **(C)** Light/dark cycles of FtsH assembly and disassembly. **(D)** Cartoon scheme for light-modulated FtsH assembly and catalytic activity.

formation. Neither energy source alone is sufficient; only their simultaneous presence produces a transient assembled state that rapidly dissipates upon removal of light (**Fig.2B,C**). Thus, the structural state of the protein is governed by the integration of independent chemical and photonic energy inputs rather than either stimulus alone. Most importantly, the assembly state directly determines enzymatic function. Free FtsH protomers actively hydrolyze peptide substrates, whereas assembly into nanotubes allosterically suppresses proteolysis without altering the catalytic center itself (**Fig.2D**). Light therefore reversibly switches enzyme activity by controlling dissipative assembly rather than by directly modifying catalysis. Because ATP hydrolysis occurs primarily in the unassembled state, light-driven assembly also suppresses ATP consumption, allowing one energy source to regulate utilization of another. Together, these findings establish a new strategy for engineering protein systems in which multiple energy inputs cooperatively regulate structural organization, catalytic activity, and energy consumption.

Objective 2b. Designing an artificial, ATP-dissipative protein dimerization motif: Our efforts to construct protein dissipative materials have emphasized engineering NTPases to build extended protein assemblies. The ATP/GTP binding/hydrolysis requires large, evolutionarily conserved sequence/structural motifs. Clearly, the addition of modular motifs that bind and hydrolyze ATP/GTP into the protein design toolbox would greatly enhance our ability to design dissipative protein materials. To this end, we set out to leverage advances in deep-learning-based tools to design two complementary protein units that dimerize upon ATP binding/activation and become active for ATP hydrolysis (**Fig.3A**).

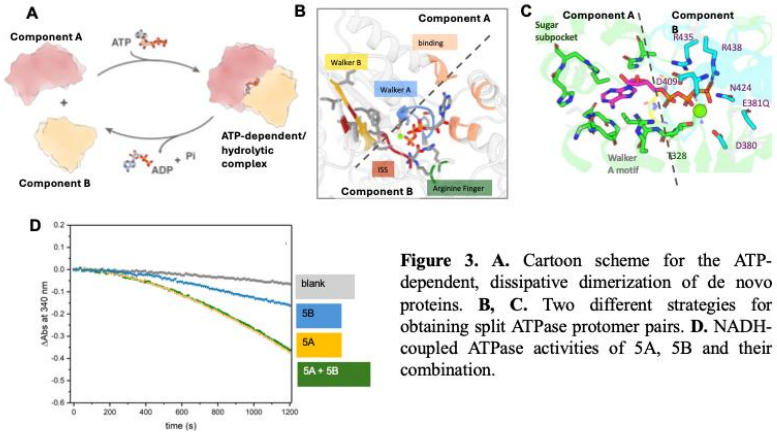


Figure 3. A. Cartoon scheme for the ATP-dependent, dissipative dimerization of de novo proteins. **B, C.** Two different strategies for obtaining split ATPase protomer pairs. **D.** NADH-coupled ATPase activities of 5A, 5B and their combination.

Using the active sites of the YME1 protein (an FtsH analog) as our template, we proceeded with the two distinct design/splitting strategies for the complementary protomers. In the first approach, we kept the original phosphate-binding interfaces (where catalytically important arginine residues are separated from the phosphate-binding P-loop) while we split the residues responsible for adenine and ribose binding into different protomers (**Fig. 3B**). The second strategy created two entirely new protomers: one housing all residues that primarily interact with ATP, and the other containing the residues that coordinate the γ-phosphate and Mg^{2+} ion (**Fig.3C**).

Following the first strategy, we experimentally tested seven complementary pairs after multiple rounds of *in silico* design. Gratifyingly, two pairs showed preliminary ATP hydrolysis via an NADH-coupled assay. Interestingly, one design (5A and 5B) showed increased ATP hydrolysis from the 5A and 5B mixture as well as from one protomer (5A) alone (**Fig. 3D**). We are currently investigating whether ATP hydrolysis occurs after the heterodimerization of 5A and

5B or after the homodimerization of 5A by implementing a tripartite GFP reporting system. At the same time, we proceeded with the second strategy and selected six candidates after screening and filtering more than 1000 designs *in silico*. Notably, AlphaFold3 predictions performed on one representative design suggested ATP-dependent complex stability. This was further supported by RMSD and potential energy calculations using steered MD simulations.

Objective 3. Programming Adaptive Protein Crystals: One of the central challenges in materials science is integrating the structural precision of crystalline materials with the adaptability and programmability characteristic of living systems. We sought to address this challenge by developing polymer-integrated protein crystals (PIX), a class of hybrid biomaterials that combines the long-range order of engineered protein crystals with the dynamic behavior of synthetic polymer networks. In earlier funding periods, we established that 1st-generation PIX (composed of ferritin crystals and polyacrylate-co-acrylamide polymers) underwent exceptionally large and reversible lattice expansion while preserving crystallinity, enabling self-healing, and reversible encapsulation of biomacromolecules. To understand the physical determinants of this unusual combination of crystallinity and adaptability, we combined small-angle neutron and X-ray scattering and multiscale MD simulations to elucidate the polymer-protein interface within PIX (JACS 2026, Publication 5). These studies revealed that lattice integrity is maintained through an extensive network of electrostatic, ion-mediated, H-bonding, and hydrophobic interactions that collectively stabilize the crystalline framework while accommodating large-scale structural motions.

This mechanistic understanding led us to ask whether we could convert adaptive behavior of 1st-generation PIX from an emergent property into a programmable one. To this end, rather than relying on diffuse electrostatic interactions, we site-specifically installed azobenzene guest molecules at the C_4-symmetric interfaces of ferritin crystals and incorporated β-CD host groups into the infiltrated polymer network (**Fig. 4A**). These host-guest (HG) interactions thus superimpose a molecularly encoded interaction layer onto the protein-polymer framework, allowing lattice mechanics to be programmed through precursor composition, molecular recognition, and external stimuli (Publication 6, in preparation). The resulting host-guest polymer-integrated protein crystals (HG-PIX) displayed several properties that distinguish them from 1st-generation PIX. Rather than expanding continuously until lattice integrity is lost, HG-PIX undergo finite and reproducible lattice expansion into discrete structural states whose final dimensions are programmed simply by varying the β-CD content of the polymer network (**Fig. 4B**). These structural states correspond to precisely defined inter-ferritin spacings spanning nearly an order of magnitude, thereby providing predictable control over lattice porosity and molecular transport. We further found that changing the azobenzene linker by only a few atoms markedly altered polymer mobility and expansion behavior, demonstrating that subtle molecular-scale changes are cooperatively amplified into material-scale mechanical responses.

Quantitative control over inter-protein spacing allowed us to achieve predictable size-selective encapsulation of proteins ranging from cytochrome *c* to chymotrypsin (**Fig. 4C**), while HG recognition enabled sequestration of negatively charged proteins that were completely excluded from 1st-generation PIX. By combining electrostatic retention with supramolecular recognition, we further demonstrated orthogonal, stimulus-specific cargo release, in which changes in pH selectively released electrostatically bound proteins while light independently released HG-bound cargo from the same crystal. Thus, this study begins to establish a general strategy for programming collective behavior in crystalline biomaterials by encoding molecular recognition into periodic protein architectures.

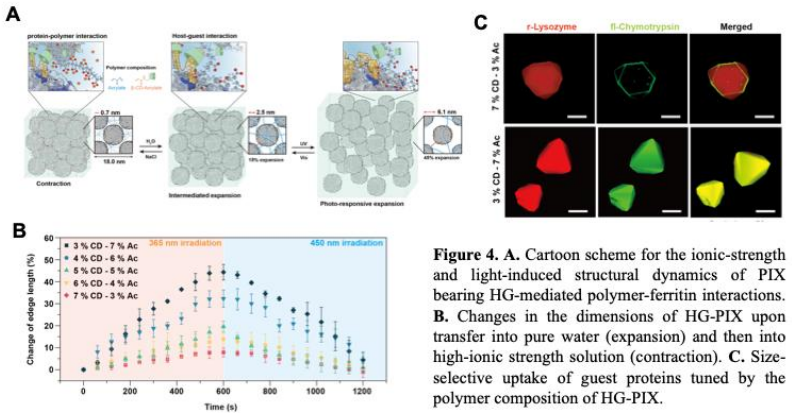


Figure 4. A. Cartoon scheme for the ionic-strength and light-induced structural dynamics of PIX bearing HG-mediated polymer-ferritin interactions. **B.** Changes in the dimensions of HG-PIX upon transfer into pure water (expansion) and then into high-ionic strength solution (contraction). **C.** Size-selective uptake of guest proteins tuned by the polymer composition of HG-PIX.

C. Future Plans. (Objective 1) We are currently synthesizing DAZ derivatives with functional groups that will (a) have longer linker lengths allow for in-plane bending of the 2D sheets to disfavor stacking and favor 1D nanotube formation, and (b) shorted excited state lifetimes compared DAZ. In parallel, we will also functionalize other proteins besides RhuA with our available AZO and DAZ groups to investigate their HG-mediated self-assembly. **(Objective 2)** We will express and purify all design candidates for ATP-mediated dimerization motifs, and determine their biochemical/biophysical properties (including ATP-dependent oligomerization and ATP hydrolysis). The successful pairs will be used to generate extended protein-based materials with dissipative properties. **(Objective 3)** We will use the HG-PIX platform to construct multi-enzyme platforms whose catalytic activities are coupled to the structural states of the crystalline framework. We will also investigate whether the scope of HG-PIX can be extended to the crystals of proteins besides ferritin.

D. Publications (2022-2024)

1) S. Vijayakumar, R. G. Alberstein, Z. Zhang, Y. Lu, A. Chan, C. E. Wahl, J. S. Ha, D. E. Hunka, G. R. Boss, M. J. Sailor*, F. A. Tezcan*, *Designed 2D Protein Crystals as Dynamic Molecular Gatekeepers for a Solid-State Device*, Nat. Commun., **15**, 6326 (2024).
2) Y. Li, J. Zhu, Z. Zhang, J. Wei, F. Wang, G. Meisl, T. P. J. Knowles, E. H. Egelman, F. A. Tezcan*, *Transforming an ATP-Dependent Enzyme into a Dissipative, Self-Assembling System*, Nat. Chem. Biol., **21**, 883-993 (2025).
3) Z. Zhang, H. T. Chiang, Y. Xia, N. Avakyan, R. R. Sonani, F. Wang, E. H. Egelman, J. J. De Yoreo, L. D. Pozzo, F. A. Tezcan*, *Design of Light- and Chemically-Responsive Protein Assemblies through Host-Guest Interactions*, Chem, **11**, 102407 (2025).
4) S. Srisantitham, A. L. Walker, U. Markel*, F. A. Tezcan*, *De Novo Design of Proteins for Autocatalytic Isopeptide Bond Formation*, J. Am. Chem. Soc., **147**, 12338-12346 (2025).
5) Y. Na, D. Le, P. Lin, Z. Zhang, J. Pombo, F. Jiménez-Ángeles , K. Han, L. Zhang, H. T. Chiang, C. Do, M. Olvera de la Cruz, A. Frañó, G. Arya, F. A. Tezcan*, *Role of Polymer-Protein Interactions in the Dynamics of Polymer-Integrated Protein Crystals*, J. Am. Chem. Soc., **148**, 18080-18094 (2026).
6) S. Kim, Y. Na, Y. Li, F. A. Tezcan*, *Supramolecular Programming of Adaptive Protein Crystals*, *to be submitted.*
7) Y. Li, V. H. Eng, F. A. Tezcan*, *Dual-energy control of dissipative enzyme assembly and catalysis*, *to be submitted.*

Patents:
1) K. Han, Y. Na, L. Zhang, F. A. Tezcan, "Controlled entrapment and release of molecular cargo", US Patent 12,195,620. Issued January 2025.

Merging non-equilibrium stat mech and AI for the design of intelligent adaptive bio-inspired materials

Suriyanarayanan **Vaikuntanathan**, University of Chicago

Keywords: non-equilibrium stat mech, physical learning

Research Scope

This research proposal aims to develop a novel framework combining non-equilibrium statistical mechanics with machine learning principles to create intelligent, adaptive bio-inspired materials. Understanding how force-generating biological materials can be tuned, built, and sustained can lead to the discovery of general design principles for the construction of non-equilibrium bioinspired materials with similar exotic adaptive properties. While machine learning methodologies have opened up new ways to design materials with such properties, the basic foundational principles for their bottom up design remains elusive. This is emerging as a grand challenge at the interface of statistical mechanics and artificial intelligence. Recent work from our group and others have shown how progress towards this grand challenge can be made by combining mathematical and computational frameworks developed in the context of machine learning with novel powerful non-equilibrium statistical mechanics frameworks, sone of which have been developed by our group. Our proposed work seeks to exploit this opportunity to develop a systematic framework for the design of bio-inspired materials that can adapt, learn and perform computations autonomously.

Recent Progress

In the first year of this project we have made progress along multiple fronts, both towards advancing the state of the art in non-equilibrium statistical mechanics and combining such advances with AI inspired techniques.

We showed that bioinspired chemical reaction networks (CRNs) can perform in-context learning (ICL), inferring a task rule at run time from a sequence of examples rather than from weights fixed during training. This in context learning property of transformers is thought to be responsible for their ability to generalize to unseen scenarios. ICL is normally tied to the pairwise dot-product attention of transformers, which has no natural physical/chemical realization Here we found how ICL can be achieved using a new geometric mechanism: rather than comparing the query to each context element pairwise, the CRN projects the full context vector onto a set of learned encoding vectors, and successful inference amounts to positioning those vectors so they cover the pairwise-comparison subspaces of the input space, the regions where a given context element matches the query. Similarity is thus read out from which subspace a steady state can classify, not from any explicit dot product. Our theory (and numeric calculations) predict onset of accurate ICL across first-order, autocatalytic, and winner-take-all kinetics; nonlinear winner-take-all dynamics can exploit thresholding to succeed below this count. The same subspace-coverage mechanism lets

CRNs solve regression and anomaly-detection ICL tasks with accuracy matching multilayer perceptrons, and because it depends only on the dimensionality of the controllable parameters rather than the details of the dynamics, it should extend to other physical substrates such as elastic and resistor networks. These results give a concrete design target for adaptive synthetic chemistry and candidate mechanisms for contextual computation in cells.

Future Plans

Moving forward, we plan to explore how some of the above described physical learning mechanisms generalize to more complex setups (as described in the proposal).

References

1. C. Floyd, H. Lopez, A. Dinner, S. Vaikuntanathan. *In context learning emerges in chemical reaction networks without attention, under revision, Nat Comm, 2026*

Publications

1. C. Floyd, H. Lopez, A. Dinner, S. Vaikuntanathan. *In context learning emerges in chemical reaction networks without attention, under revision, Nat Comm, 2026.*
2. C. Floyd, A. Dinner, S. Vaikuntanathan. *Learning to control non-equilibrium dynamics using local imperfect gradient (in Press) Newton 2026.*

Polymer Origami – A Blueprint for Hierarchical Folding Multiblock Copolymers

Thi **Vo**, Chemical and Biomolecular Engineering, Johns Hopkins University

Keywords: Single-Chain Nanoparticles, Foldamers, Self-Assembly, Polymers, Theory/Modeling

Research Scope

Directing macromolecular organization into spatially and orientationally defined nanostructures presents a grand challenge for bottom-up materials engineering. Common approaches borrow from protein design to create foldamers (folding oligomers), wherein information about desired morphology is programmed directly into its molecular sequence. However, due to their sequence-specific synthesis requirements, state-of-the-art approaches are mostly constrained to be oligomeric in nature. Along the same vein, directed folding of polymeric macromolecules via hydrophobic collapse – single chain nanoparticles (SNPs) – serves as a promising alternative, but are mostly limited to globular structures with close-packed, amorphous internal ordering. Our project combines self-consistent field theory, scaling theory, and molecular dynamic simulations to characterize how the interplay between stiff and flexible polymeric domains can be leveraged to sculpt hierarchical chain folding. Our findings showcase newer avenues for programming multiscale complexity into synthetic macromolecules, encoding chains to not only spontaneously fold into monodispersed morphologies but also hierarchically organized into structures previously unattainable using traditional polymers[1]. The former serves as a critical step for establishing a truly synthetic analog of protein folding while the latter expands the library of morphological diversity accessible to block copolymers for technological applications across filtration, templating, and nanostructured materials.

Recent Progress

Here, we report our recent progress in predicting polymer conformations and designing polymer architectures to target chain folding into ordered nanostructures. Our major findings for this report span two polymer designs (**Fig. 1**):

1) Folding of achiral homopolymers into chiral, helical nanostructures (**Fig. 1a**)
2) Assembly of foldameric copolymers into ordered nanostructures (**Fig. 1b**)

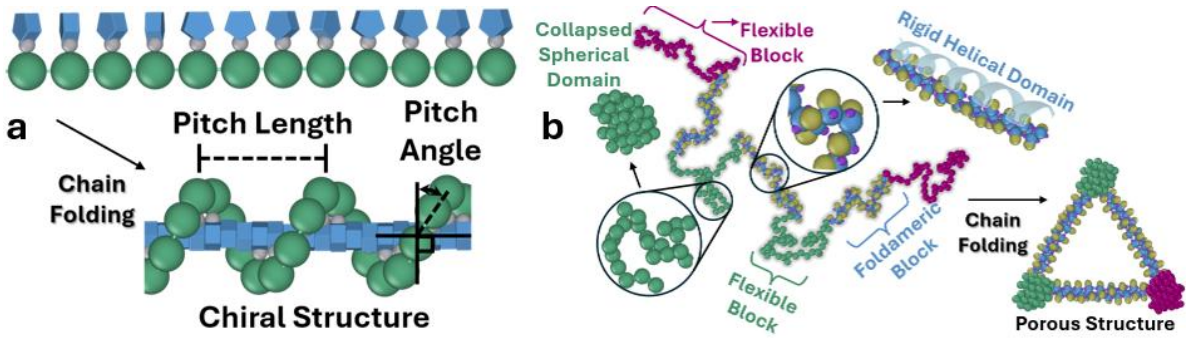


Figure 1. Overview of Major Findings. We showcase two designed polymer architectures that fold into a) chiral nanostructures and b) porous, patchy polygonal nanostructures.

Folding of Achiral Homopolymers into Chiral, Helical Nanostructures. Our previous works have shown that monomer anisotropy and connectivity impose strong entropic constraints that can impact chain conformation[2]. Building upon this idea, we develop an achiral homopolymer that self-folds into chiral nanostructures with tunable pitches (**Fig. 2**). We first employ theory to highlight the complex conformational space accessible in chain folding for our designed polymers. Specifically, we compute the free energy per monomer (E_N) between two neighboring pendant groups at varying backbone separation distance (r_{eq}). Plotting the predicted energy yielded a non-monotonic trend (**Fig. 2c**), where tilted pendant alignments (**Fig. 2b,** II) and not perfect π-π

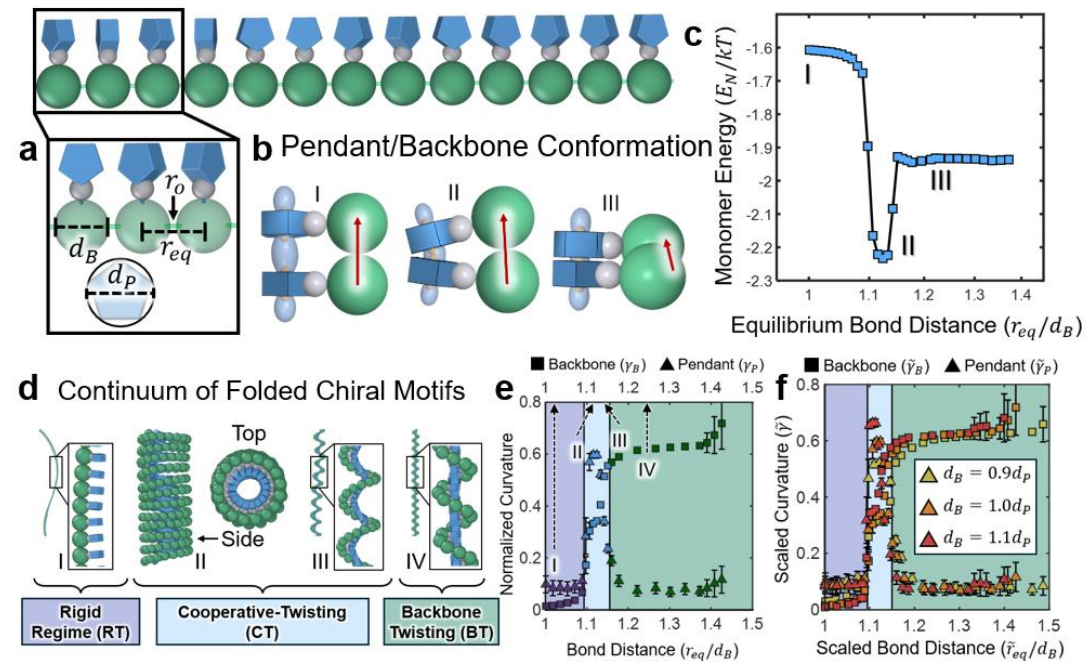


Figure 2. Folding of Achiral Homopolymers into Chiral, Helical Nanostructures. a) Design of homopolymer with chiral folding properties. b) Visualization of equilibrium conformation between neighboring monomers for equilibrium bond distances (r_{eq}) of $1.0d_B$, $1.12d_B$, and $1.22d_B$ (left to right). c) Energy as a function of equilibrium bond length, showing a non-monotonic trend and optimal chain energy at intermediate regimes (Region II). d) Simulation snapshots of folded chain showing rigid chain (I), hollow helical tube (II), e) expanded twisted spring (III), and twisted backbone with homochirality (IV). e) Computed curvature for $d_B = 1.0d_P$ for backbone and pendant particles. f) Scaling collapse of curvature across all simulated results. Scatter points indicate simulation results and backgrounds are phase characterization for RT, CT, and BT.

pendant stacking (**Fig. 2b**, III) are the lowest in energy. Such findings indicate that chain twisting can be obtained at intermediate r_{eq}.

To corroborate theory, we study the equilibrium conformation of the designed polymers in coarse-grained molecular dynamics simulations. Characterization of the folding results reveal three dominant chain conformations (**Fig. 2d**): rigid (RT), cooperative-twisting (CT), backbone-twisting (BT). These regimes exactly correspond to the distinct regions of pendant energies computed in **Fig. 2c**. Here, the rigid regime (RT) reflects the short r_{eq} limit where the backbone is so stiff that bending constraints completely suppress favorable pendant-pendant interactions, thereby locking the chain into a linear conformation (**Fig. 2d,** I). Conversely, large r_{eq} give rise to a backbone-twisting (BT) regime, where significant backbone flexibility produces: 1) a linearly rigid cylindrical core that arises from pendant stacking, and 2) a helical coil wrapped around the cylindrical core due to backbone twisting (**Fig. 2d,** III and IV). More importantly, at intermediate r_{eq}, we observe chain folding into helical coils with varying pitch length and angle (**Fig. 2d,** II) due to cooperative twisting (CT) between both pendant and backbone. Additionally, we perform quantitative analysis of the folded conformations to corroborate the various twisting regimes observed (**Fig. 2e**). Lastly, we further show that the observed behavior is universal across different monomer sizes (**Fig. 2f**), all of which can be theoretically predicted using a corresponding state-like universal twisting curve for the designed class of folding polymers. Combined, these findings indicate that chiral nanostructures can be obtained as a product of relieving geometric frustration between backbone rigidity and pendant-pendant associations. The former deepens our fundamental understanding of chain folding while the latter expands the library of chemical space available for use in chiral materials engineering.

Foldameric Copolymer Assembly into Porous Nanostructures and Open Lattices. We next develop a polymer design that synergistically merges self-folding helices (foldamer) with flexible SNP-like domains into a unified architecture. Specifically, we construct block polymers exhibiting alternating regions of flexible (SNP-like) and foldameric sequences (**Fig. 3a**). These hybrid polymers utilize the foldameric blocks to define rigid structural domains within the polymer and the flexible blocks to organize the rigid domains into ordered nanostructures. Here, our design is a diblock copolymer with a repeating A_x-$[B$-$A_x]_n$- motif, where A_x define a flexible segment of degree of polymerization x, B define a helix-forming foldameric sequence, and n is the number of repeat units of the B-A_x motif (**Fig. 3a**). Characterization of the folding behavior using coarse-grained molecular dynamics simulations reveal that chains readily fold into porous triangular ($n = 3$), square ($n = 4$), pentagonal ($n = 5$), and hexagonal ($n = 6$) nanostructures, respectively (**Fig. 3b**). Importantly, quantitative characterization of the folded structures indicates that the measured edge lengths are identical for the same foldamer block length across all systems (**Fig. 3c**). These findings indicate that increasing the number of foldameric segments purely serves as a handle to

control the emergent shape of the folded copolymer. In other words, geometrical features such as edge lengths and pore areas can be *a priori* designed for each folded nanostructure via tuning the synthesized foldamer block lengths. To further confirm the universality in folding behaviors, we additionally show that all folded chains results ($n = 3 – 6$) readily collapse onto a composite phase diagram that can be defined using the foldamer length (N_h), flexible length (N_f), and insphere radius (a_p) of each folded nanostructure (**Fig. 3d**).

We additionally posit that inter-chain associations between the collapsed flexible domains are possible if the nanostructures are aligned vertex-to-vertex relative to each other (**Fig. 3e**), meaning that the folded nanostructures can be hierarchically organized. Indeed, simulating a system of interacting folded nanostructures results in the formation of open network morphologies as shown in **Fig. 3g**. Characterization of the interior angles (**Fig. 3f**) across all nanostructures reveal values that directly match those computed from polygonal geometry (black lines). These findings indicate that the folded nanostructures maintain their shape and do not refold in the presence of neighboring

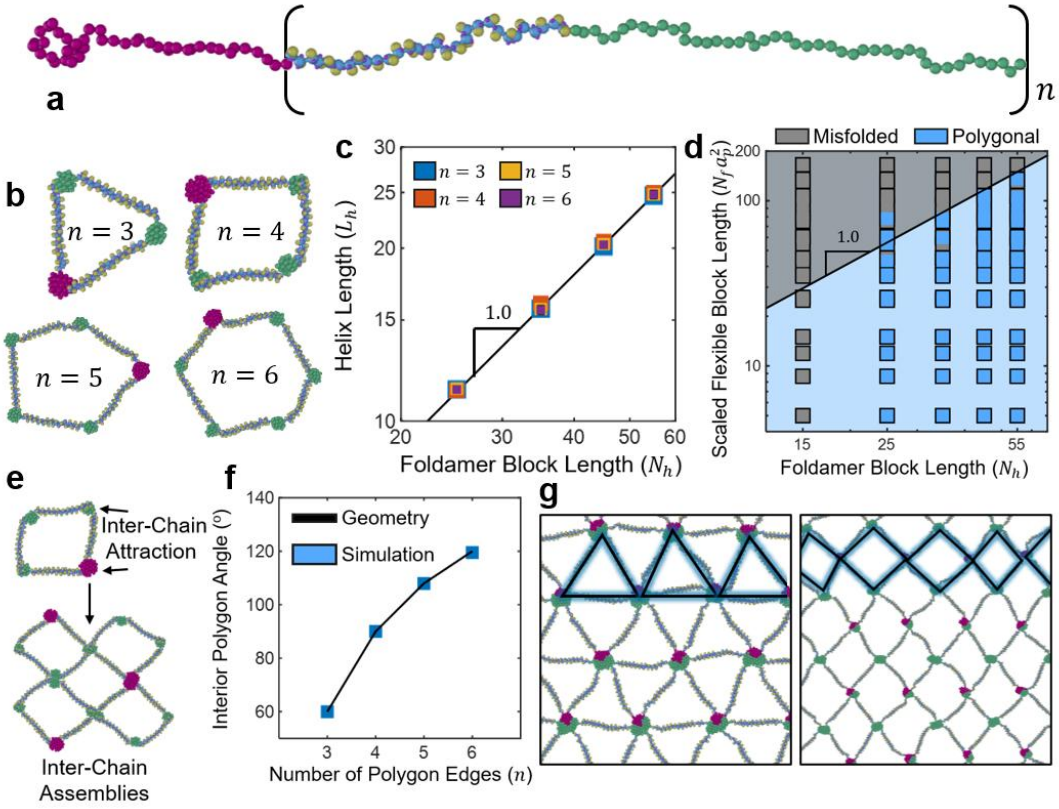


Figure 3. Copolymer Folding and Hierarchical Assembly. a) Polymer architecture for nanostructure folding. b) Snapshots of folded chains across all polygonal nanostructures. c) Helix lengths across nanostructures show identical scaling (1.0) and length for all systems. d) Scaling collapsed of morphology phase diagrams across all simulated polymers, solid line indicates theoretical folded-misfolded transition in the collapsed landscape of $N_f a_p^2 \sim N_h$, where a_p is the circumcircle radius for each respective folded nanostructure geometry. e) Inter-chain interactions mediated by collapsed flexible blocks serving as "patchy" interaction sites. f) Measurements of interior angle of each folded nanostructures within the ordered network compared to idealized geometrical values. g) Assemblies of folded triangular (left) and square (right) nanostructures into porous, open networks.

chains. Through this lens, our polygonal nanostructures can be viewed as polymeric analogs of patchy nanoparticles that are commonly used in colloidal self-assembly[3,4]. Combined, our study presents new avenues for engineering programmable soft materials with applications in molecular separations, adaptive membranes, sensing platforms, and reconfigurable devices.

Future Plans

For our on-going works, we anticipate that we can combine the different components highlighted above to obtain folded polymers whose structural complexity can rival their protein-inspired counterparts. More specifically, we plan to expand the design rules obtained for porous 2D nanostructures (**Fig. 3**) to access 3D porous nanocages and leverage those designs to create network/membrane structures transport/separations applications. Similarly, we plan to study how the designed chiral folding polymers (**Fig. 2**) can be deployed as novel polymeric brushes for advanced sensing and electrochemical applications. We additionally plan to expand folding polymer designs across the suite of experimentally accessible molecular polyhedral monomers (polyoctahedral silsesquioxanes, carboranes, triptycene etc…) to access folded polymers with crystalline internal ordering. This will augment the range of crystal motifs accessible from polymer folding, providing a more expansive suite of scaffolding morphology for use in catalyst design.

References

1) Bates, C. M., Bates, F. S. *50th Anniversary Perspective: Block Polymers-Pure Potential*. Macromolecules **50**, 3–22 (2017).
2) Akkunuri, K., Zhang, X., Vo, T. *Elucidating the Interplay between Entropy-Driven and Patch-Mediated Bonding in Directing Nanoscale Assemblies*. Mol. Syst. Des. Eng **10**, 19-31 (2025).
3) Kim, A., Kim, C., Waltmann, T., Vo, T., Kim, E. M., Kim, J., Shao, Y.-T., Michelson, A., Crockett, J. R., Kalutantirige, F. C., Yang, E., Yao, L., Hwang, C.-Y., Zhang, Y., Liu, Y.-S., An, H., Gao, Z., Kim, J., Mandal, S., Muller, D. A., Fichthorn, K. A., Glotzer, S. C., Chen, Q. *Patchy Nanoparticles by Atomic Stencilling*. Nature **646**, 592–600 (2025).
4) Zhu, B., Chen, J., Li, R., Ren, J., Wang, Y., Zhong, Y., Liu, Y., Yasuhara, A., Kakefuda, M., Aoyama, Y., Vo, T., Ye, X. *Superstructural Phase Transitions in Polymer-Grafted Nanooctahedra*. Science Advances **11**, eadw2740 (2025).

Publications

1) Zhu, B., Chen, J., Li, R., Ren, J., Wang, Y., Zhong, Y., Liu, Y., Yasuhara, A., Kakefuda, M., Aoyama, Y., Vo, T., Ye, X. *Superstructural Phase Transitions in Polymer-Grafted Nanooctahedra*. Science Advances **11**, eadw2740 (2025).
2) Jeong, H., Vo, T. *Assembly of Foldameric Copolymers into Ordered Nanostructures and Crystalline Networks*, **Under Review**.
3) Zhang, X., Vo, T. *Chiral Emergence in Self-Folding of Achiral Homopolymers*, **Under Review**.
4) Akkunuri, K, Vo, T. *Self-Folding of Conjugated Bottlebrush Polymers into Biomimetic Shape Amphiphiles*, **Under Review**.
5) Mullangi, D, Wang, D., Jeong, H., Miao, Y., Vo, T., Tsapatsis, M., Kokkoli, E.. *DNA Sequence and Amphiphile Architecture Direct Self-Assembly and Enantioselective Catalysis in DNA-Based Artificial Metalloenzymes*, **Under Review**.

Steering the Pathways of Hierarchical Self-assembly at Solid Surfaces

Tao **Ye** (lead PI),[1] Yonggang **Ke**,[2] and Gaurav **Arya**[3]

[1]Chemistry & Biochemistry, University of California, Merced; [2]Biomedical Engineering, Emory University and Georgia Institute of Technology; [3]Mechanical Engineering and Materials Science, Duke University

Keywords: DNA origami, self-assembly, simulation, surface patterning

Research Scope

This project aims to 1) gain a quantitative, mechanistic understanding of the interactions between DNA origami and nanopatterned solid materials, and 2) rationally engineer these interfacial interactions so that DNA origami can be accurately and selectively placed on surface patterns and programmably interconnected, enabling 2D and 3D hierarchical networks.

Recent Progress

Mechanistic understanding of DNA origami placement on nanografted self-assembled monolayer patterns:

Precise placement of nanomaterials on patterned surfaces is a prerequisite for many nanoelectronic and nanophotonic circuits. A promising strategy is DNA origami placement (DOP),[1,2] which uses lithographically generated binding sites within a passivating background to selectively bind and align DNA origami, which in turn can display nanomaterials in arbitrary arrangements with few-nanometer lateral resolution.

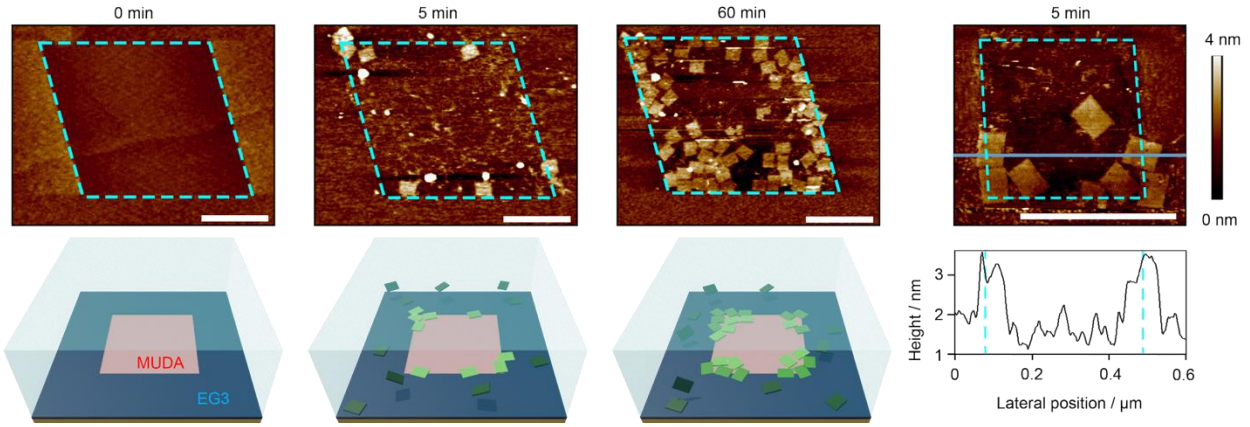


Figure 1. In situ AFM images of diluted DNA origami deposition on a large (1000 nm × 1000 nm) MUDA binding site within EG3 background, before incubation, 5 min after incubation, and 60 min after incubation. Origami tiles colored in bright green represent tiles that are visible under AFM, and tiles colored in dark green are invisible under AFM due to high mobility. Right image: Higher resolution AFM image of diluted DNA origami deposition on a large (400 nm × 400 nm) MUDA binding site within EG3 background 5 min after incubation. A cross-sectional height profile is shown below the image. Scale bars: 400 nm.

In the previous project period, we discovered that charge-neutral, hydrophilic background functional groups dramatically improve the yield, alignment precision, and speed of DOP relative to hydrophobic groups. However, the mechanism of this acceleration remained unclear. To discriminate between 2D and 3D diffusion pathways, the Ye group studied DNA origami deposition on an oversized binding site, which permitted in situ AFM imaging as DOP proceeded (Figure 1). Deposition preferentially occurs at the edge of the binding site. This edge preference is readily explained by the 2D diffusion pathway: origami transiently trapped by the background must cross the binding-site boundary to be captured. Consistent with this, the higher-resolution snapshot in Figure 1 (right) captures numerous tiles straddling the boundary, supporting diffusion along the hydrophilic background into the binding site.

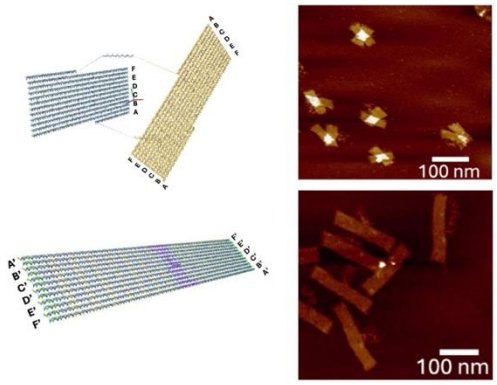


Figure 2. Top: Double layer DNA origami Bottom: Connector DNA origami.

Surface mediated DNA origami interconnection:

We aim to achieve programmable interconnection between surface-bound DNA origami using multiple layers linked by flexible tethers. The bottom layer binds the surface, allowing the second layer to interconnect via DNA origami connectors. In the previous reporting period, the Ye and Ke groups designed and assembled both the multilayer origami and the connector origami (Figure 2), demonstrated that double-layer origami connect with origami in homogeneous solution, and showed that the bottom layer selectively binds to mercaptoundecanoic acid (MUDA) binding sites within an oligoethylene glycol SAM background that resists nonspecific adsorption. The bottom layer was imaged successfully, but the tethered top layer moved in and out of the tip-surface junction too rapidly to be visualized by AFM. We overcame this challenge using Ni^{2+}, which immobilizes DNA origami more strongly, allowing both layers to be visualized. We further found that an OEG6 background aligns double-layer origami better than OEG3: whereas OEG3 binding sites often induce side-by-side

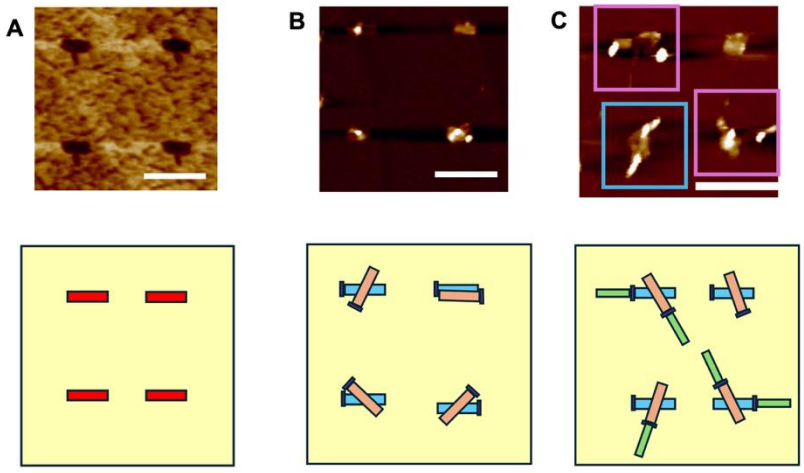


Figure 3. Surface-mediated DNA origami interconnection. A, MUDA binding sites are patterned into OEG6 background. B, Deposition of double-layer DNA origami onto the binding sites. C, After binding of connector DNA origami to the double layer DNA origami. The top row includes AFM images and the bottom row includes schematics.

adsorption of both layers, OEG6 favors selective adsorption of the bottom layer, owing to the larger energetic for misalignment. We also found that the connector tile binds the surface-bound double-layer origami (Figure 3C).

In parallel, the Arya group developed an analytic model for the configuration-dependent free energy of the tethered two-layer origami assembly, treating the two DNA tethers as ideal polymer chains and the origami layers as rigid bodies. Minimizing this free energy predicts the preferred interlayer angle as a function of the distance between tether connection points. The predicted angular variation agrees well with molecular dynamics simulations, showing that the interlayer angle can be tuned between ~20° and ~180° by manipulating the tethering points (Figure 4A). Extending the model with an analytical treatment of the rotational entropy of the upper layers, we determined the minimum bond strength required to directly interconnect pairs of tethered origami layers: bonds stronger than ~10 k_BT (6 kcal/mol) are needed, and this threshold rises with increasing tether-point separation (Figure 4B). We are now extending the model to interconnection via externally supplied origami connectors in solution, mirroring the experiments above.

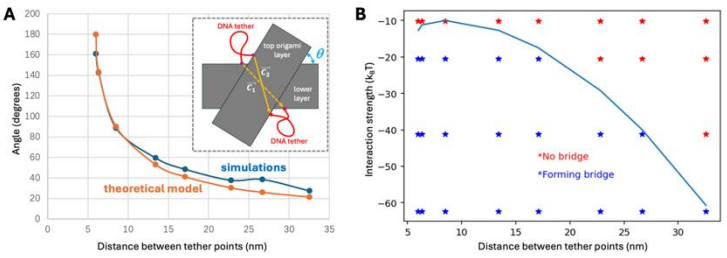


Figure 4. Theoretical modeling of DNA origami interconnection. A, Model predictions for the relative angle between the surface-bound origami layer and tethered origami layer above as a function of the distance between single-stranded DNA tether points, assuming similar tether points on both layers, i.e., d = $|\mathbf{C}_1| = |\mathbf{C}_2|$. B, Diagram showing the possibility (probability>50%) of two surface-tethered origami (width=6 nm) interconnecting as a function of the distance between the tether points and the bond interaction strength.

Patterning of DNA Origami on Surfaces using Polymer Brushes:

Controlling the local arrangement and long-range order of DNA origami on surfaces remains a central challenge. Surface-assisted self-assembly of symmetric, non-interacting origami offers a facile route to 2D superlattices, but typically yields close-packed arrays with little control over inter-origami spacing. Combining experiments (Ke group) and simulations (Arya group), we demonstrated a new strategy for regulating lateral spacing during assembly. Growing uniform single-stranded polynucleotide brushes from the origami surface modulates their effective geometry by introducing longer-ranged entropic repulsion, enabling precise, adjustable control of inter-origami distances across macroscopic areas. Systematic variation of brush length, surface adsorption strength, and brush density yields tunable patterns across different origami shapes (Figure 5). This approach advances DNA-templated nanofabrication by providing highly programmable templates with precise spatial control, and offers a foundation for integrating functional nanomaterials. It is also synergistic with the present project: brushes can regulate origami-surface interactions to further improve DOP accuracy and yield, and brush-functionalized

origami can be used for multilayer assembly of origami on surfaces, as brushes have been shown to reduce unwanted nonspecific origami-origami interactions.

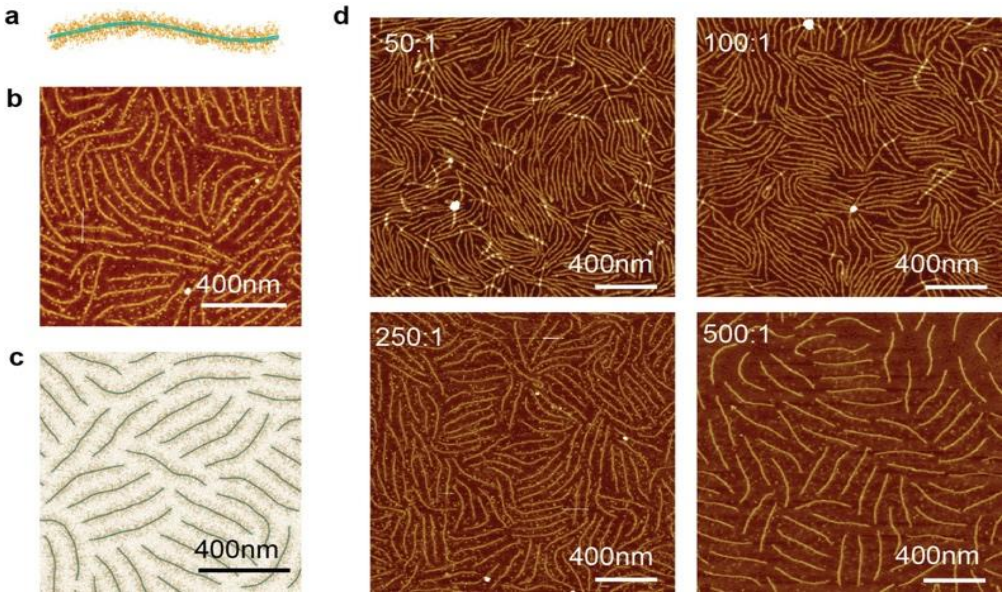


Figure 5. Control DNA origami placement with DNA polymer brushes. (a) Single-stranded DNA brushes can be grown on DNA origami in a programmable manner. (b) and (c) experimental data and simulation showed the brushed DNA origami can form nematic pattern on surface with regular inter-origami spacing. (d) the inter-origami spacing can be readily

Future Plans:

We will quantify the surface forces and dynamics of mesoscale DNA origami self-assembly on nanopatterned solid supports and rationally engineer interfacial interactions so that top-down techniques can program 2D and 3D origami superstructures.

Elucidate how interfacial interactions drive the binding of DNA origami on nanopatterned solid supports. We will use a novel single-molecule force spectroscopy method to quantify the adhesion and lateral forces between DNA origami and the patterned surface, and to understand how they impact DOP. These measurements, coupled with mesoscopic modeling and simulations, will reveal how interfacial forces determine DOP dynamics.

Design interfacial interactions for constructing 3D hierarchical networks. We hypothesize that the bottleneck for interconnecting pattern-bound origami lies in competing demands: the conformational freedom needed for facile interconnection *versus* the confinement imposed by binding to lithographic patterns. We will explore how a strategy based on DNA origami multilayers can meet both needs.

References:

1. Gopinath, A., Miyazono, E., Faraon, A., & Rothemund, P. W. (2016). Engineering and mapping nanocavity emission via precision placement of DNA origami. *Nature*, *535*(7612), 401-405.
2. Gopinath, A., Thachuk, C., Mitskovets, A., Atwater, H. A., Kirkpatrick, D., & Rothemund, P. W. (2021). Absolute and arbitrary orientation of single-molecule shapes. *Science*, *371*(6531), eabd6179.

Publications

(1) Petrek, Z., DeMello, A., Giagou, T., Zhang, Y., Dudkin, R., Lwin, B., ... & Ye, T. (2025). Surface crowding effects in molecular recognition by thrombin binding aptamers conjugated to gold nanoparticles. *Langmuir*, *41*(39), 26730-26737.
(2) Li, Y., Shao, Y., Sterling, S., Goodlad, M., Ke, Y., Arya, G., & Ye, T. (2025). Engineering Surface Interactions for High-Precision Placement of DNA Origami onto Nanoscale Lithographic Patterns. Under Revision
(3) Wang, S., Lin, P.-A., Zauscher, S., Arya, G., & Ke, Y. (2026). Tunable Patterning of DNA Origami on Surfaces using Steric Brushes. *Angew. Chem. Int. Ed.* e8367703.
(4) Lin, P.-A., Ren, S., Piland, J., Collins, L.M., Zauscher, S., Ke, Y., & Arya, G. (2026). Deep Inverse Design of Patchy Particles for Mesoscale Assembly of Superlattices, Submitted (preprint available on *ChemRxiv*)

Laboratory Abstracts

Bio-inspired Durable Storage of CO_2

Principal Investigator: Chun-Long **Chen**, Pacific Northwest National Laboratory (PNNL) and University of Washington (UW)

Co-Principal Investigators: Jim De Yoreo (PNNL/UW), Chris Mundy (PNNL/UW), Kevin Rosso (PNNL), Wendy Shaw (PNNL), Marvin Bayro (University of Puerto Rico)

Keywords: Peptoids, CO_2 mineralization, crystal nucleation and growth, phase transformation

Research Scope: The overarching vision of this project is to establish fundamental principles for the design of high-information content polymers that would promote selective nucleation and growth of nanostructured materials. We have been progressing toward this vision by advancing our understanding of molecular interactions with CO_2, water, carbonate minerals, and the constituent ions focusing on the design of peptoid materials that promote CO_2 hydration and carbonate formation. Progress achieved during the current project has shown that our long-term vision for enabling cost-effective CO_2 usage is viable. Promotion of CO_2 hydration, accelerated conversion of bicarbonate to carbonate, and accelerated metal carbonate formation can significantly reduce the time required for carbonate formation and enable new energy technologies.

Recent Progress

Promotion of $CaCO_3$ nucleation by carboxyl- and amine-terminated peptoid nanotubes (***Langmuir,*** *2026*)**.** The use of surfaces to promote heterogeneous nucleation of $CaCO_3$ has been extensively studied to develop bioinspired approaches for synthesizing composite materials, and as a route towards accelerating CO_2 mineralization. Recently, we investigated the ability of films of self-assembled -NH_2 and -COOH terminated peptoid nanotubes to promote the nucleation of $CaCO_3$ (Figure 1).[1] Using a combination of atomic force, scanning electron and optical microscopy, we found that interwoven films of nanotubes formed from peptoids with -NH_2 side chains promoted the preferential formation of vaterite with the (001) plane parallel to the film and exhibit a lower interfacial energy than that reported for inorganic surfaces. In contrast, the film of -COOH-functionalized peptoid nanotubes is a much stronger promoter, giving a particle density five orders of magnitude larger than for the -NH_2 terminated peptoid nanotubes and enabling complete coverage of individual peptoid tubes with $CaCO_3$ nanoparticles that results in a composite material with a 50-fiold increase in Young's modulus. Thus, interwoven films of peptoid nanotubes provide a useful platform for investigating the impact of specific chemical groups on nucleation and offer potential application to accelerated

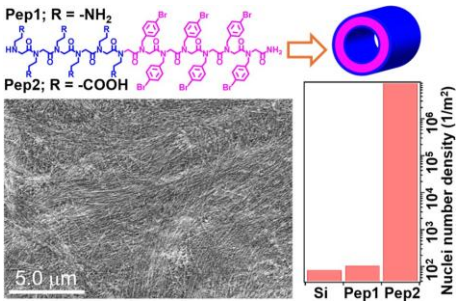


Fig. 1. Peptoid assemblies with aligned -COOH groups accelerate the nucleation of calcium carbonate crystals. The films of nanotubes assembled from Pep2 promote the nucleation of vaterite crystals much more significantly than those from Pep1.

mineralization of CO_2 for removal from the environment or modulation of mineralogy and properties of carbonate-based building materials.

Accelerated phase transformation of magnesium carbonates by self-assembled carboxyl-containing peptoid nanosheets and nanotubes. Magnesium carbonates, such as magnesite, are a class of very important mineral materials for long-term storage of carbon dioxide. However, the formation of magnesites in natural environments is very slow due to the strongly hydrated character of Mg^{2+}. By assembling Mg^{2+}-binding carboxyl groups of amphiphilic peptoids into crystalline nanosheets and nanotubes, we demonstrated that these well-organized carboxyl groups were able to accelerate the transformation of amorphous magnesium carbonates (AMC), which is stable at room temperature for many days, into much more thermodynamically stable crystalline phases: nesquehonite, hydromagnesite, and magnesite. We found that peptoid nanosheets and nanotubes exhibited distinct acceleration in the phase transformation of AMC. Specifically, while peptoid nanosheets accelerated the transformation of AMC into nesquehonite crystals, peptoid nanotubes led to the formation of much more thermodynamically stable hydromagnesite, as revealed by liquid-cell TEM results (Figure 2). We further demonstrated that the number of carboxyl groups and the assembled peptoid architecture and crystallinity are significant for such accelerated transformation. Solution NMR results suggest that peptoid assemblies regulate AMC crystallization by creating a confined interfacial reaction environment that retains Mg^{2+} and carbonate species while facilitating proton-transfer processes. The nanotube architecture maintains this reactive interface longer than nanosheets, providing a mechanistic basis for its direct transformation of AMC into hydromagnesite. Molecular dynamics (MD) simulations were performed to understand this acceleration process and showed that increased carboxyl content raises the surface density of solvent-exposed groups at the membrane–water interface before reaching a saturation regime. Carboxyl density contributes to a more nuanced mechanistic role than a simple enhancement of interfacial binding. Carboxyl groups appear to control the probability and persistence of the initial peptoid-AMC association; once that association becomes sufficiently extensive, the interface can sustain the local ionic flux needed for rapid

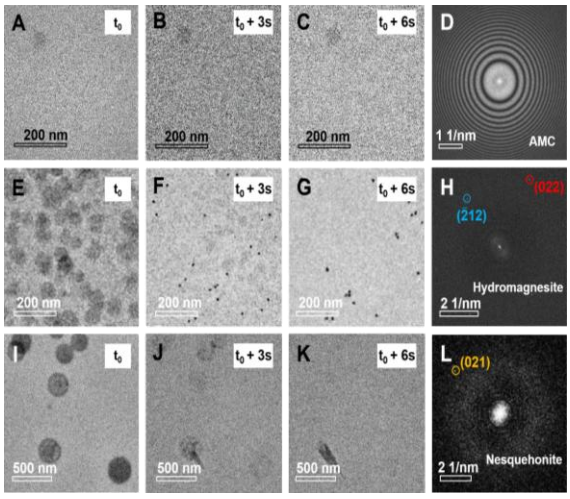


Fig. 2. -COOH containing peptoid sheets and tubes accelerate the transformation of amorphous magnesium carbonates (AMC) into crystalline phases, revealed by in situ liquid-cell TEM observation of the time-resolved transformation of AMC in the absence and presence of self-assembling peptoids. (A-D) Control AMC showing no observable dissolution or recrystallization within 6 s. (E-H) AMC incubated with $Nbrpm_6Nce_{12}$ nanotubes showing synchronous dissolution of AMC and nucleation of hydromagnesite; FFT pattern (H) confirms the indexed reflections. (I-L) AMC incubated with $Nbrpe_6Nce_{12}$ nanosheets showing rapid nucleation and growth of nesquehonite; FFT pattern (L) confirms the indexed reflection.

transformation. Furthermore, we demonstrated that these peptoid nanosheets and nanotubes were able to accelerate the transformation of AMC into magnesite under 50 °C and 90 bar CO_2. Both peptoid nanosheets and nanotubes remained intact after such acceleration under high temperature and high pressure. These results establish a new platform of using crystalline self-assembled peptoid nanomaterials to accelerate the formation of magnesite and offer great potential for permanent CO_2 storage.

Role of histidine-containing peptoids in accelerating the kinetics of calcite growth (*Adv. Funct. Mater., 2026*). Previously we discovered that amphiphilic peptoids were able to accelerate the calcite step speeds by more than an order of magnitude at only nanomolar concentrations.[2] Recently, we found that peptoid accelerators have multiple roles, including facilitating HCO_3^- deprotonation and Ca^{2+} desolvation, and disrupting the interfacial hydration structure at the calcite surface. Collectively these effects combine to determine the magnitude of peptoid-driven acceleration of calcite growth.[3] Drawing inspiration from carbonic anhydrase (CA), we designed a class of histidine-containing peptoids capable of coordinating with Zn^{2+} ions to act as CA mimetics for accelerating calcite step growth (Figure 3). Our results revealed that these peptoids significantly enhance step advancement, with a more pronounced effect observed when combined with Zn^{2+} ions and under higher calcium-to-carbonate activity ratios, indicating that peptoids facilitate the incorporation of CO_3^{2-} ions into step edges. Solution NMR and three-dimensional atomic force microscopy (3D AFM) analyses showed that the coordination of peptoids with Zn^{2+} promote both the deprotonation of HCO_3^- to CO_3^{2-} and restructure the interfacial hydration layers on calcite, collectively lowering the activation barrier for step growth. These findings establish a design framework for sequence-defined synthetic polymers to regulate carbonate mineralization, offering promising applications in CO_2 capture and long-term storage.

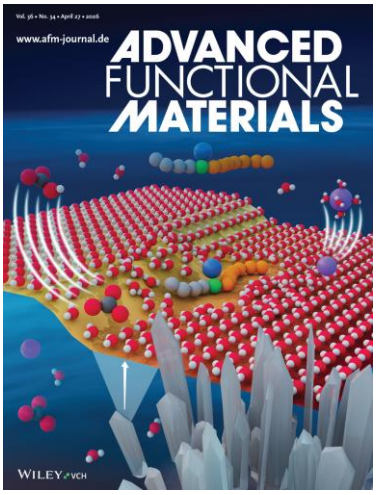


Fig. 3. We designed a class of histidine-containing peptoids that, coordinating with Zn^{2+}, form carbonic anhydrase (CA) mimetics. These mimetics act as calcite growth accelerators by facilitating the deprotonation of bicarbonate ions. Peptoids were found to enhance step growth rates, and the acceleration effect becomes more pronounced when combined with Zn^{2+} addition.

Computational understanding of peptoid-promoted $CaCO_3$ nucleation. The central modeling development of this period is GB*, a correction to the Generalized Born (GB) implicit-solvent model that makes it accurate for the short-range ion interactions that govern $CaCO_3$ nucleation. Standard GB describes these interactions poorly, overstabilizing Ca^{2+} pairing by up to ~2 kcal/mol and missing the solvent-separated minima and desolvation barriers. Building on the project's STEPs-SOL peptoid force field, GB* adds a PMF-derived potential that matches full explicit-solvent simulations while reducing an ion-binding calculation from hours to minutes and reaching the dilute conditions explicit solvent cannot. This is already moving the modeling from rationalization toward prediction: for the calcite-growth-accelerator $Pep_{8,4}$: Nce_8Npe_4,[3] GB* reproduced the Ca^{2+}-induced change in carboxyl dynamics measured by NMR and predicted that

the ion-binding region alone could not explain it, directing new experiments that identified the hydrophobic block as the controlling element. The next step turns this toward nucleation itself: pairing GB* with aggregation-volume-bias Monte Carlo (AVBMC) sampling to directly simulate ion clustering and the formation of critical $CaCO_3$ nuclei on peptoids, a rare-event process long out of reach for atomistic simulation, while folding local-pH and protonation chemistry into GB* makes the growth environment realistic. Together these keep the multiscale problem accurate yet cheap enough to be used for design: computationally proposing peptoid sequences that control $CaCO_3$ nucleation, toward the goal of durable CO_2 capture and storage.

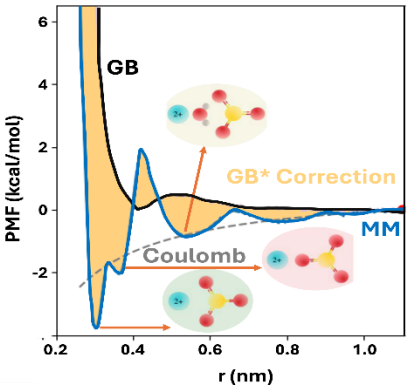


Fig. 4. Potential of mean force (PMF) between Ca^{2+} and CO_3^{2-} from full all-atom simulation (blue) and the uncorrected GB model (black). GB fails to capture the short-range interactions that govern ion pairing; the GB* correction reproduces the all-atom PMF with quantitative accuracy at orders-of-magnitude lower cost.

Understanding peptoid-$CaCO_3$ interfacial dynamics using solid-state NMR. To address a current gap in our molecular understanding of the peptoid-mineral interfaces, we have utilized solid state nuclear magnetic resonance (ssNMR) to characterize the site-specific dynamics of peptoids associated with carbonate mineral surfaces. To distinguish the interfacial behavior of these two regions, the calcite-growth-accelerator: $Pep_{8,4}$: Nce_8Npe_4 was selectively ^{13}C-enriched at the Cα positions of either the hydrophobic block or the hydrophilic block, enabling site-resolved measurements of ^{13}C transverse relaxation times T_2 and rotating-frame spin–lattice relaxation times $T_{1\rho}$. In the absence of mineral surfaces, the labeled sites in the hydrophobic and hydrophilic blocks exhibit comparable ^{13}C T_2 and $T_{1\rho}$ values. Upon interaction with calcite, the hydrophilic block displays a longer ^{13}C T_2 but a shorter ^{3}C $T_{1\rho}$ than the hydrophobic block, suggesting that the carboxyl-rich block remains dynamically active at the calcite interface. By contrast, the slower dynamics in the hydrophobic block may arise from hydrophobic clustering, aromatic packing, or hydration shells around the phenyl-containing residues. Replacing $CaCO_3$ with $CdCO_3$ produced only minor changes in the ^{13}C T_2 and $T_{1\rho}$, suggesting that the observed peptoid dynamics are not governed solely by a rigid inner-sphere metal–carboxyl binding.

Future Plans

Our future plans center on continuing to develop a molecular understanding of peptoid-promoted CO_2 hydration and mineralization by advancing three scientific objectives: 1) Determine the molecular-scale interactions and reactions by which peptoids act as soluble additives to accelerate carbonate crystal growth; 2) Understand how peptoid orientation and packing within crystalline peptoid scaffolds promote carbonate crystal nucleation with control over mineral phase and orientation; 3) Determine how active site organization and peptoid sequence translate into efficient hydration of CO_2 and accelerated deprotonation of HCO_3^- into CO_3^-, coupled to mineralization of metal carbonates, to form hierarchical peptoid-carbonate composite materials. Synthesis, in situ

characterizations, simulations, and measurements of function will be integrated to establish the scientific basis for making peptoid materials that accelerate CO_2 hydration and mineralization.

References

(1) Mondarte, E. A. Q.; Hao, B.; Bard, A. B.; Zhang, M.; Chakma, P.; Bae, Y.; Zhang, S.; Ginovska, B.; De Yoreo, J. J.; Tao, J.; et al. Promotion of CaCO3 Nucleation by Carboxyl- and Amine-Terminated Peptoid Nanotubes. *Langmuir* **2026**, *42* (17), 11728-11736. DOI: 10.1021/acs.langmuir.5c06875.
(2) Chen, C. L.; Qi, J. H.; Zuckermann, R. N.; DeYoreo, J. J. Engineered biomimetic polymers as tunable agents for controlling CaCO3 mineralization. *J. Am. Chem. Soc.* **2011**, *133* (14), 5214-5217. DOI: 10.1021/ja200595f.
(3) Zhang, M.; Chen, Y.; Wu, C.; Zheng, R.; Xia, Y.; Saccuzzo, E. G.; Trinh, T. K. H.; Mondarte, E. A. Q.; Nakouzi, E.; Rad, B.; et al. A molecular view of peptoid-induced acceleration of calcite growth. *Proceedings of the National Academy of Sciences* **2024**, *121* (45), e2412358121. DOI: 10.1073/pnas.2412358121.

Publications since 2024 PI meeting.

1. P. Chakma, Y. Chen, B. S. Harris, Y. W. Elhady, R. Zheng, M. E. Bowden, T. K. H. Trihn, C. J. Mundy, M. D. Baer, C.-L. Chen, *Assembly of Sequence-defined Peptoids into Crystalline Nanomaterials as Carbonic Anhydrase Mimics for Promoted Hydration and Sequestration of CO_2.* ***Nature Comm.*** 16 (1), 7348 (2025), https://doi.org/10.1038/s41467-025-62366-w.

2. E. G. Saccuzzo-Close, Y. Chen, A. S. Lipton, J. Tao, M. E. Bowden, K. Fontanez, M. J. Bayro, C.-L. Chen, W. J. Shaw, *Molecular interactions between a designed peptoid and the $CaCO_3$ surface characterized by solid-state NMR.* ***J Phys Chem C.*** 129 (28), 13010 (2025), https://doi.org/10.1021/acs.jpcc.5c02180.

3. E. A. Q. Mondarte, B. Hao, A. B. Bard, M. Zhang, P. Chakma, Y. Bae, S. Zhang, B. Ginovska, J. J. De Yoreo, J. Tao and C.-L. Chen, Promotion of CaCO3 Nucleation by Carboxyl- and Amine-Terminated Peptoid Nanotubes. ***Langmuir***, *42*, 11728 (2026). https://doi.org/10.1021/acs.langmuir.5c06875.

4. Y. W. Elhady, B. S. Harris, C. J. Mundy, M. D. Baer, *STEPs-SOL a Peptoid Force Field Parameterization to Include Solvent Effects.* ***J Phys Chem B.*** 129, 23, 5901 (2025), https://doi.org/10.1021/acs.jpcb.5c02834.

5. M. Zhang, Y. Chen, C. Shi, P. Chakma, J.J. De Yoreo, C.-L. Chen, *Role of histidine-containing peptoids in accelerating the kinetics of calcite growth*, ***Advanced Functional Materials****.* 36, 34, e22918 (2026). https://doi.org/10.1002/adfm.202522918.

6. H. Du, T. K. H. Trihn, O. C. Brandon, R. Zheng, H. Wang, K. Corry, T. R. Wood, C.-L. Chen, E. Nance, Nicotinamide-loaded Peptoid Nanotubes for Energy Regeneration in Acute Brain Injury. ***ACS Nano***. 20, 16, 12250 (2026). https://doi.org/10.1021/acsnano.5c19897.

7. L. Ge, T. K. H. Trihn, C. Li, L. Mayer, J. M. Chin, C.-L. Chen and M. R. Reithofer, *Directed Synthesis of Gold Nanoparticle Superstructures Using Self-Assembling Peptoids Containing Metal-Bonding N-Heterocyclic Carbenes*, ***Nano Lett.*** 25, 31, 12049 (2025). https://doi.org/10.1021/acs.nanolett.5c02998.

8. T. K. H. Trihn, B. Jin, R. N. Zuckermann and C.-L. Chen, *Assembly of Metalloporphyrin Peptoids into Crystalline Nanomaterials as a Multifunctional System for Biomimetic Catalysis and Sensing*, ***ACS Appl. Mater. Interfaces.*** 17 (31), 44347 (2025). https://doi.org/10.1021/acsami.5c05546.

9. H. Feng, F. Suwayyid, M. Zia, J. Wee, Y. Hozumi, C.-L. Chen and G.-W. Wei, *Commutative Algebra Machine Learning─A Case Study on Protein–Ligand Binding Affinity Prediction.* ***J. Chem. Inf. Model.***, 65, 6732-6743 (2025). https://doi.org/10.1021/acs.jcim.5c00940.

10. P. Chakma, B. S. Harris, C. Shi, B. Hao, K. Whitaker, M. D. Baer and C.-L. Chen, *Multi-stimuli Responsive Nanomaterials Assembled from Spiropyran-containing Peptoids.* ***Nanoscale.*** (2025) DOI: 10.1039/D5NR03491D.

Precision synthesis and assembly of ionic and liquid crystalline polymers

Paul **Nealey**[1], Matthew Tirrell[1], Jie Xu[2], Joan Montes de Oca[1], Juan J de Pablo[1], Wei Chen[1]

[1]Materials Science Division, [2]Nanoscience and Technology Division, Argonne National Laboratory, USA

Keywords: mixed conductors, dual-network, phase separation, AI-guided robotic experiments

Research Scope

This project advances the discovery of new principles toward a fundamental understanding of the chemistry, physics, and materials science of charged, nanostructured, and functional polymer and soft-matter systems, both at equilibrium and far from equilibrium. Our approach relies on the synthesis of polymers with precise composition, and on processing these materials through controlled molecular self- and directed self-assembly, which encode specific intra- and intermolecular interactions that drive assembly with hierarchical structure. A unifying strength of the project is the combination of experiment, autonomous laboratories, theory, computation, and data-driven approaches to accelerate materials discovery and design. Our effort is organized along three interrelated thrusts: Thrust 1: Fundamental Investigation of Water Absorption and Ion Transport Mechanisms in Homopolymer and Block Copolymer Electrolytes; Thrust 2: High-Throughput Robotic Experimentation and Computation for Designing Mixed Conducting Polymers; and Thrust 3: Hybrid Coacervation, Surface Interactions and Their Modification with Polyampholytes. Fundamental materials and principles discovered here will impact a wide array of energy technologies, ranging from fuel cells, electrolyzers, and desalination to energy storage, energy-efficient and neuromorphic microelectronics, and electrochemical sensors, as well as antifouling coatings for separation membranes.

Recent Progress

During the last project cycle, substantial progress was achieved across all three thrusts. In Thrust 1, we established how water content, local solvation, and nanoscale connectivity govern ion transport, providing design principles for ionic conductors that retain high conductivity at reduced hydration while minimizing swelling and mechanical degradation[1']. In Thrust 3, we combined rheology, coherent X-ray scattering, simulations, and AI-assisted analysis to reveal how interparticle interactions and cooperative rearrangements govern yielding and recovery

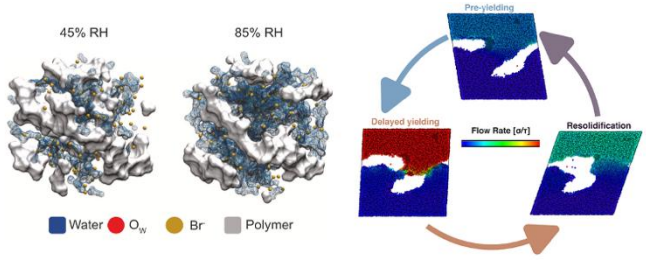


Fig. 1. Recent progress across the program. Thrust 1 explored water-mediated ion transport in hydrated polyelectrolytes (left) while Thrust 3 revealed how microscopic interactions control yielding pathways in charged soft materials (right).

in charged soft materials, enabling microscopic control over when these materials flow, arrest, or restructure under stress[2].

For this DOE/BES Biomolecular Materials Principal Investigators' Meeting, we will highlight progress in research Thrust 2, which integrates AI, data-driven analysis, and robotic experimentation to navigate the chemical, morphological, and processing design space of mixed ionic and electronic conducting polymers (MIECPs)[1-3]. Our goal is to determine how polymer structure and assembled morphology govern coupled ion transport and electronic charge mobility, ultimately establishing design principles for durable dry-state mixed conductors.

Our work spans three interconnected efforts. First, we investigate post-polymerization functionalization as an automation-compatible synthetic strategy and understand how the resulted linkage chemistry regulates the physical properties of polymerized ionic liquids. Second, we designed AI-guided autonomous experimentation to study how polymer chain packing influences mixed ionic/electronic conduction under conventional aqueous electrolyte conditions. Third, we develop dual-network, interpenetrating morphologies for efficient dry-state mixed conduction through a newly developed AI-guided autonomous experimentation platform. Results from each of these research directions are described below.

Influence of linkage chemistry and side-chain polarity on ion transport in click-functionalized polymerized ionic liquids. Post-polymerization functionalization offers precise molecular weight control and enables the high-throughput investigation of structure–property relationships in polymer research. However, post-polymerization functionalization strategies often introduce additional linkage chemistry,and its role in the physical properties of polymerized ionic liquids (PILs) has yet to be explored. In this work, a series of PILs were synthesized using Cu(I)-catalyzed azide–alkyne cycloaddition (CuAAC), with comparison made to N-alkylation substitution chemistry. The triazole ring introduced by CuAAC chemistry was found to induce extensive ion aggregation and deteriorate ion transport. The impact of linkage chemistry on ion transport can be alleviated by incorporating polar ethylene glycol spacers in the side chain, achieving an ionic conductivity of 2.1×10^{-4} S/cm at 30 °C. Furthermore, the effect of polar spacer placement was explored, revealing that overalls ide-chain polarity, rather than polarity in the vicinity of the ionic group, governs ion aggregation and ion transport in PILs.[3]

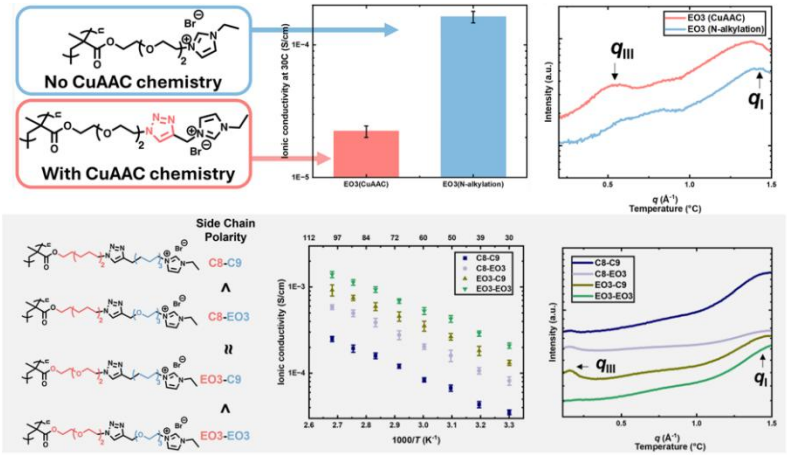


Fig.2: Chemical structures, ionic conductivity, and WAXS profiles comparing CuAAC and N-alkylation linkages (top) and polymers with varied side-chain polarity (bottom)

Understand the impact of assembled microstructure diversity on mixed conducting properties using adaptive autonomous robotic platform. To achieve effective ionic and electronic conduction in MIECPs, we hypothesized that the preferred morphology of MIECPs for achieving the high mixed conduction property relies on three key features: (1) planar chain conformation that extend π-electron delocalization, (2) sufficient π–π stacking for efficient interchain electronic charge-carrier hopping and (3) large interfacial areas to enhance ion-electron coupling. However, achieving control over the assembly of MIECPs into the hypothesized film morphology through solution processing remains challenging owing to the highly non-equilibrium conditions that can lead to unpredictable morphological variability. To explore a broad processing conditions to facilitate the formation of diverse packing, we developed an adaptive AI-driven robotic platform for solution-shearing MIECP films on nanogrooved substrates, with the conditions informed by autonomous device characterizations on the films (Fig. 2). Using organic electrochemical transistors (OECT) to evaluate the mixed-conducting figure of merit, defined as the product of charge-carrier mobility and volumetric capacitance (μC*), our platform achieved a broad μC* range from 166 to 1,275 F cm^{-1} V^{-1} s^{-1} in just 64 autonomous trials. The analysis identified two key structural factors for higher volumetric capacitance: larger crystalline lamellar spacing and higher specific surface area, and uncovered a previously unknown polymer polymorph[7'].

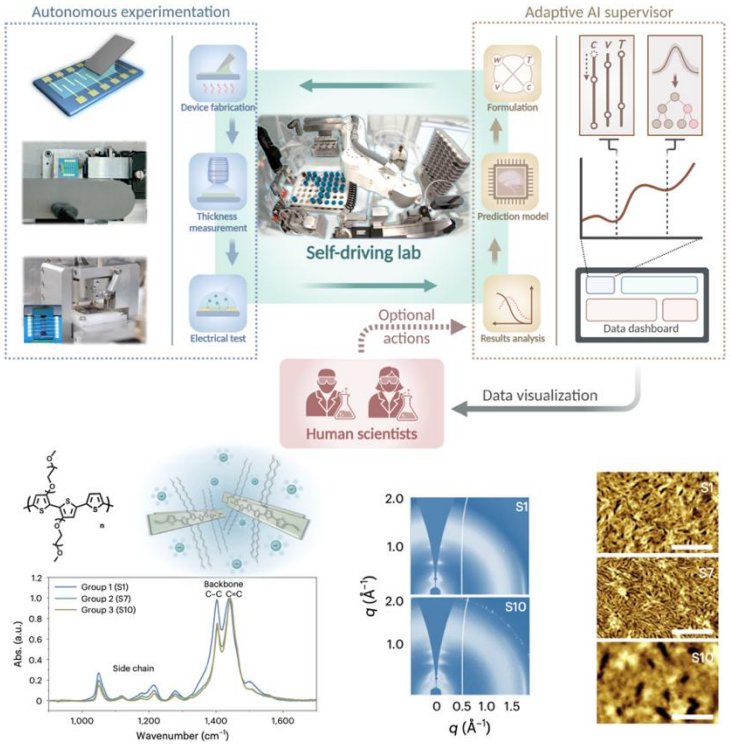


Fig. 3: (Top) AI-robotic platform for automated OECT fabrication, μC* measurement, and AI-guided experimentation. (Bottom) Multiscale characterization of representative MIECPs (S1 is the best one) by Raman spectroscopy, X-ray scattering, and AFM[7'].

Dual-network, interpenetrating morphologies to enable efficient mixed conduction in the dry state through a newly established dry-state AI-guided autonomous experimentation platform. We hypothesize that dual-continuous pathways for ion and electron transport, formed by MIECPs and an ionically conductive polymer matrix within a single assembled microstructure, can enable effective dry-state mixed conduction. To realize such architectures, we explored two strategies: (1) promoting the assembly of percolated MIECP networks within a polymerized ionic monomer matrix through solvent exchange, and (2) leveraging Li salts to suppress macrophase separation in

MIECP/ionic polymer blends and drive the formation of interconnected nanostructures. Both approaches exhibited effective dry-state mixed conduction behavior (Fig. 3).

To systematically investigate these dual-network systems, we developed an integrated autonomous screening pipeline encompassing metric definition, device standardization, automated fabrication, and data infrastructure. We established a quantitative figure of merit (FOM) that can be extracted directly from solid-state measurements, enabling rapid, physically meaningful ranking of candidate materials without multiple independent measurements or thickness calibration. We also developed a standardized multilayer OECT platform for reproducible fabrication and direct FOM extraction, together with an autonomous glovebox workflow integrating solution preparation, film deposition, thermal annealing, device assembly, and electrical characterization. A dedicated data-management system automatically captures and standardizes experimental metadata and results. The platform generates two continuously expanding datasets: one for high-throughput performance screening and one for long-term operational stability, supporting machine-learning-guided analysis and closed-loop discovery of high-performance, durable solid-state OMIECs.

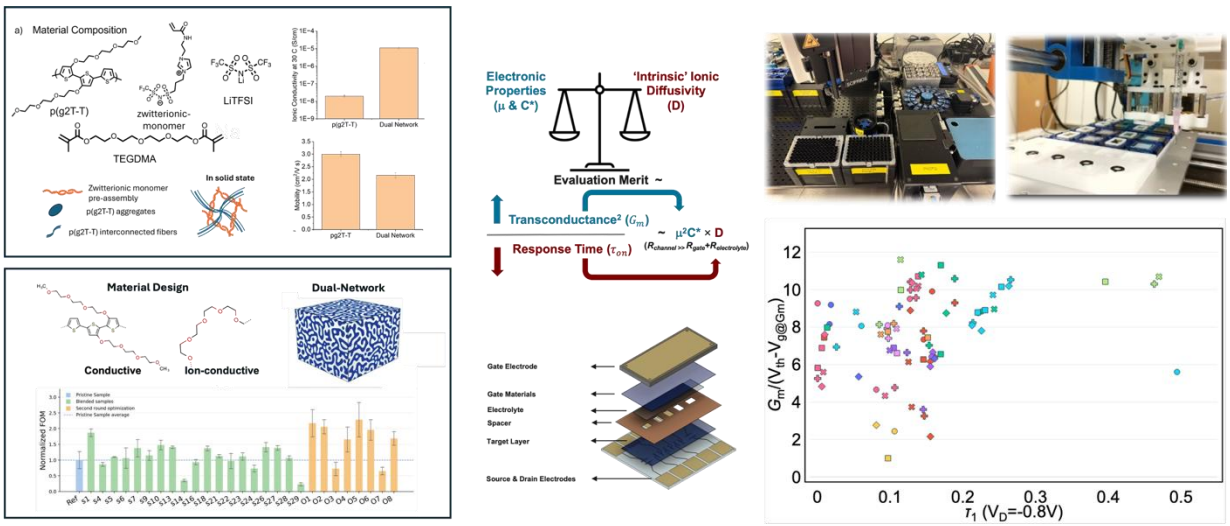


Fig.4: (Left) Two strategies for forming dual-continuous ion- and electron-transport networks. (Middle) Thickness-independent FOM screening using a standardized OECT test structure[4,5]. (Right) Glovebox-integrated autonomous fabrication, data processing, and AI-ready infrastructure for high-throughput performance and long-term stability evaluation of dry-state MIECPs. The lower-right panel shows the ongoing high-throughput screening of MIECP.

In ongoing work, we are leveraging this platform to explore large chemical, formulation, and processing design spaces to uncover the fundamental design principles governing dry-state mixed-conducting polymers. In parallel, we are integrating experiments with simulations to investigate how electronic polymeric materials undergo damage under internal electric fields during operation and cycling. These efforts aim to enable the synergistic design of functional electronic polymers that simultaneously achieve functional properties and long-term durability.

References

1. Jones, S. D., Nguyen, H., Richardson, P. M., Chen, Y.-Q., Wyckoff, K. E., Hawker, C. J., Clément, R. J., Fredrickson, G. H., & Segalman, R. A. Design of Polymeric Zwitterionic Solid Electrolytes with Superionic Lithium Transport. ACS Central Science, 8(2), 169–175. (2022).
2. Paulsen, B. D., Tybrandt, K., Stavrinidou, E., & Rivnay, J. Organic mixed ionic–electronic conductors. Nature Materials, 19(1), 13–26. (2020).
3. Tom, G., Schmid, P. S., Baird, G. S., Cao, Y., Darvish, K., Hao, H., Lo, S., Pablo-García, S., Rajaonson, M. E., Skreta, M., Yoshikawa, N., Corapi, S., Akkoc, D. G., Strieth-Kalthoff, F., Seifrid, M., & Aspuru-Guzik, A. Self-Driving Laboratories for Chemistry and Materials Science. Chemical Reviews, 124(16), 9633–9732. (2024).
4. Bernards, D. A., & Malliaras, G. G. Steady-State and Transient Behavior of Organic Electrochemical Transistors. Advanced Functional Materials, 17(17), 3538–3544. (2007).
5. Bisquert, J., & Tessler, N. Transient Current Responses of Organic Electrochemical Transistors: Evaluating Ion Diffusion, Chemical Capacitance, and Series Elements. Advanced Functional Materials, 35(16), 2419000. (2024).

Publications

1'. Wang, Z.; Sun, G.; Lewis, N. H. C.; Mandal, M.; Sharma, A.; Kim, M.; Montes De Oca, J. M.; Wang, K.; Taggart, A.; Martinson, A. B.; Kohl, P. A.; Tokmakoff, A.; Patel, S. N.; Nealey, P. F.; De Pablo, J. J. Water-Mediated Ion Transport in an Anion Exchange Membrane. Nat. Commun., 16 (1), 1099. (2025)

2'. He, H.; Liang, H.; Chu, M.; Jiang, Z.; De Pablo, J. J.; Tirrell, M. V.; Narayanan, S.; Chen, W. Bridging Microscopic Dynamics and Rheology in the Yielding of Charged Colloidal Suspensions. Proc. Natl. Acad. Sci., 122 (42), e2514216. (2025)

3'. N. Shan, J. Xu, S. Wang, P. F. Nealey, Influence of Linkage Chemistry and Side-Chain Polarity on Ion Transport in Click-Functionalized Polymerized Ionic Liquids, Macromolecules 59, 7123–7130 (2026).

4'. Montes De Oca, J. M.; Dong, R.; Zaldivar, G.; Sun, G.; Wang, Z.; Patel, S. N.; Nealey, P. F.; De Pablo, J. J. IEC-Independent Coupling between Water Uptake and Ionic Conductivity in Anion-Conducting Polymer Films. Macromolecules, 58 (12), 6134–6148. (2025)

5'. Wang, Z.; Wang, K.; Eom, C.; Chen, Y.; Sun, G.; Kim, M.; Montes De Oca, J. M.; Liang, D.; Bagchi, K.; Patel, S. N.; De Pablo, J. J.; Nealey, P. F. Role of Crosslinking and Backbone Segmental Dynamics on Ion Transport in Hydrated Anion-Conducting Polyelectrolytes. Adv. Funct. Mater., 35 (52), e14589. (2025)

6'. Han, M.; Sun, G.; Nealey, P. F.; De Pablo, J. J. Attention-Based Functional-Group Coarse-Graining: A Deep Learning Framework for Molecular Prediction and Design. Npj Comput. Mater., 11 (1), 355. (2025)

7'. Dai, Y.; Chan, H.; Vriza, A.; Fan, J.; Kim, F.; Wang, Y.; Liu, W.; Shan, N.; Xu, J.; Weires, M.; Wu, Y.; Cao, Z.; Miller, C. S.; Divan, R.; Gu, X.; Zhu, C.; Wang, S.; Xu, J. Adaptive AI Decision Interface for Autonomous Electronic Material Discovery. Nat. Chem. Eng., 2 (12), 760–770. (2025)

8'. Emeršič, T.; Bagchi, K.; Fitz, S.; Jensen, A.; Nealey, P. F.; De Pablo, J. J. Stable Non-Equilibrium Structures in Chiral Nematics under Microfluidic Flow. J. Phys. Chem. B, 128 (46), 11441–11449. (2025)

9'. Sokolov, A.; Katuri, J.; De Pablo, J. J.; Snezhko, A. Synthetic Active Liquid Crystals Powered by Acoustic Waves. Adv. Mater., 37 (19), 2418846. (2025)

10'. Zaldivar, G.; Dong, Y.; Montes de Oca, J. M.; Sun, H.; Alessandri, R.; Arges, C. G.; Patel, A. J.; Nealey, P. F.; de Pablo, J. J. The Role of Water Volume Fraction on Water Adsorption in Anion Exchange Membranes. Macromolecules, 58 (18), 9972–9982. (2025)

Adaptive Interfacial Assemblies Towards Structuring Liquids

Thomas P. **Russell**[1,2], Paul D. Ashby[3], Brett Helms[3], Ahmad K. Omar[1,4], Peter Ercius[3]

[1]Materials Sciences Division, Lawrence Berkeley National Laboratory, Berkeley, CA
[2]Polymer Science and Engineering Department, University of Massachusetts Amherst, Amherst, MA
[3]Molecular Foundry, Lawrence Berkeley National Laboratory, Berkeley, CA
[4]Materials Science and Engineering Department, University of California Berkeley, Berkeley, CA

Keywords: Interfacial nanoparticle surfactant assemblies, droplet interface bilayers, responsive assemblies, shape evolution, ion transport

Research Scope

Structuring liquids by the formation, binding, and assembly of nanoparticle surfactants (NPSs) at fluid interfaces remains central to this FWP. Our advances and recent discoveries open new opportunities for energy generation, storage and transduction that capitalize on the dynamics, responsiveness, and adaptability of the NPS assemblies. Intuitively, NPSs form monolayers at liquid interfaces, recent studies indicate the assemblies may be more complex. We will high resolution microscopies and microfluidic liquid cells for TEM to visualize NPS assemblies in situ with single NP-size resolution to resolve the structure and dynamics of the interfacial assemblies. The high interfacial coverage of NPSs imparts an elasticity to the assemblies. These elastic assemblies allow droplets encapsulating active particles to assume nonequilibrium shapes with a shape-evolution needing a statistical mechanical description of the soft membrane and their response to the active media. Pore formation in NPS bilayers between liquid droplets uncovered behavior relevant to neuromorphic computing. We will use dynamic covalent chemistries to form responsive NPS bilayers. By modulating external stimuli dynamic covalent bonding will control the NPS assemblies and tune pore formation, acting as adaptive, reconfigurable channels for ions and molecules, akin to synaptic plasticity, where the strength of connections (pores) can be adjusted dynamically. By programming response to specific external stimuli, we will emulate memory processes, e.g., signal propagation, threshold gating, and transduction pathway reinforcement, leading to liquid-based neuromorphic systems that integrate computation with environmental adaptability.

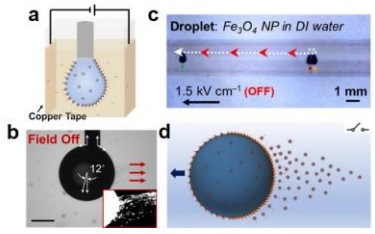


Fig. 1 (**a**) Schematic of a pendant drop with negatively charged NPs in oil with cationic surfactants in a DC E-field; (**b**) optical image with field removed; (**c**) droplet self-propulsion, (**d**) asymmetric explosive emulsification scheme.

Recent Progress

Self-Propulsion by Directed Explosive Emulsification (**Helms, Ashby, Omar, Russell**, ***Adv. Mater.*** **2024**, 36 (19). e2310435.https://doi.org/10.1002/adma.202310435) An active droplet system, programmed to repeatedly move autonomously at a specific velocity in a well-defined direction, was shown. Coulombic energy is stored in oversaturated interfacial assemblies of charged nanoparticle-surfactants by an applied DC electric field and can be released on demand. Spontaneous emulsification is suppressed by an increase in the stiffness of the oversaturated assemblies (Figure 1). Rapidly removing the field releases the stored energy in an explosive event that propels the droplet, where thousands of charged microdroplets are ballistically ejected from the surface of the parent droplet. The ejection is made directional by a symmetry breaking of the interfacial assembly, and the combined interaction force of the microdroplet plume on one side of the droplet propels the parent droplet distances tens of times its size, making the droplet active. The propulsion is autonomous, repeatable, and agnostic to the chemical composition of the nanoparticles. The symmetry-breaking in the nanoparticle assembly controls the microdroplet velocity and direction of propulsion. d as higher current and power generation systems.

Ion Transport Through Reconfigurable Nanoparticle-surfactant Stabilized Droplet Interface Bilayers (Ercius, Helms, Ashby, Omar, Russell, Proc. Nat. Acad. Sci., 123 (8), e2522349123 (**2026**)). https://doi.org/10.1073/pnas.2522349123) Nanoparticle-surfactant (NPS) stabilized droplet interface bilayers (NPS-DIBs) enable mechanically robust, chemically reconfigurable ion transport platforms that operate without ionophores or nanochannel-forming proteins (Figure 2). We show that jammed interfacial assemblies spontaneously or electrically generate nanoscopic, ion-selective channels, supporting size- and charge-specific transport along with neuromorphic functions, such as short- and long-term plasticity. These nanoscopic channels emerge from packing defects in the jammed interfacial assemblies of the charged NPSs and support size and charge selective, hysteretic ion transport governed by interfacial electrostatics and dimensional constraints. The NPS-DIBs exhibit memristive ionic conduction and maintain structural integrity under strong stimuli, overcoming the stability and tunability limitations of lipid systems. This versatile approach couples soft-matter mechanics with interfacial ionic functionality, offering a generalizable route to adaptive iontronic devices and synthetic synapses with applications in neuromorphic computing, and nanofluidic separation.

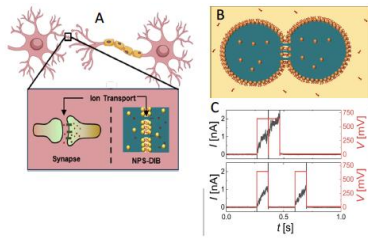


Fig. 2 ((A,B) Schematics of nanochannels within the droplet interface bilayer mimicking that of biological synapses; (C) paired-pulse facilitation behavior.

Self-Assembly of Anisotropic Particles on Curved Surfaces (Russell, Omar, ACS Nano, 2025, 19**,** 38803**.** https://doi.org/10.1021/acsnano.5c15378) The surface curvature of membranes, interfaces, and substrates plays a crucial role in shaping the self-assembly of particles adsorbed on these surfaces. However, little is known about the interplay between particle anisotropy and surface curvature and how they couple to alter the free energy landscape of particle assemblies. Using molecular dynamics simulations, we investigate the effect of prescribed curvatures on a quasi-2D assembly of anisotropic patchy particles (Figure 3). By varying curvature and surface coverage, we uncover a rich geometric phase diagram, with curvature inducing ordered structures entirely absent on planar surfaces. Large spatial domains of ordered structures can contain hidden microdomains of orientational textures imprinted by the surface on the assembly. The dynamical landscape is also reshaped by surface curvature, with a glass- like state emerging at modest densities and high curvature. Changes to the symmetry of the surface curvature are found to result in distinct structures, including phases with mesoscale ordering. Our findings show that the coupling between surface curvature and particle geometry opens an unexplored space of morphologies and structures that can be exploited for material design.

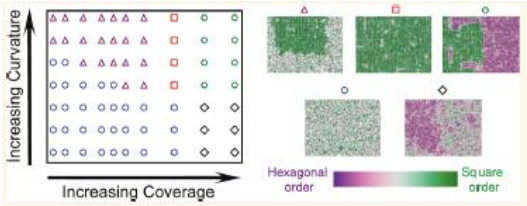


Fig. 3 Mapping of hexagonal and square ordering of NPs on curved surfaces as a function of curvature and areal density.

Transient Structuring of Liquids using Dissipative Interfacial Assemblies (**Ashby, Russell, Helms, *Matter* 2024**, 7 (3): 1092-1105. https://doi.org/10.1016/j.matt.2023.12.025) To prescribe a lifetime for structured liquids requires that the interfacially trapped material eventually reverts to molecularly dissolved species. Here, it was shown that poly(acrylic acid) fueled with carbodiimide segregates to an oil-water interface and forms assemblies of aggregates, solidifying the interface. With fuel consumed, the assembly changes into soluble polymer chains, destroying any out-of- equilibrium structure imparted to the liquid, dissipating energy. Crossover points in the interfacial storage and loss moduli at times commensurate with the fuel concentration were determined, evidencing transitions from solid-like to liquid-like assemblies.

Oscillatory and Collective Dynamics of Gold-Nanoparticle-Laden Droplets Driven by Photothermal-Induced Thermocapillarity (Russell, Adv. Mater. 2026, 38, e14793. DOI: 10.1002/adma.202514793) Droplets have long intrigued researchers due to their ability to exhibit complex and fascinating behavior when subjected to external stimuli. Here, we investigate a coupled oscillatory behavior of gold-nanoparticle-surfactant-laden aqueous droplets at an oil–oil interface stimulated by light. We show that the interaction between light and the droplets gives rise to a range of oscillatory modes, including bouncing and clustering, where droplets exhibit collective movement (Figure 4). From experiment and numerical simulations, we elucidate the underlying mechanism: upon laser irradiation, gold nanoparticles convert light into heat, generating asymmetric temperature gradients that drive an upward thermocapillary flows and a hydrodynamic force from photothermal convection. These forces compete with gravity and buoyancy to induce droplet bouncing, while the resulting asymmetric flow fields bias neighboring droplets toward the illuminated droplet, leading to clustering. Our findings not only expand the library of dynamic droplet behavior but also offer insights into the potential applications of light-driven systems in materials science, soft robotics, and microfluidics.

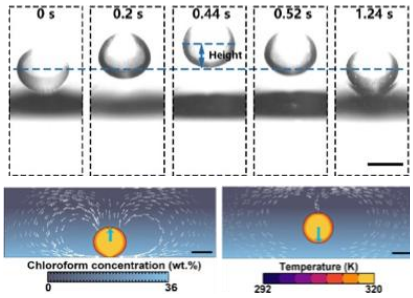


Fig. 4 (top) Successive side-view snapshots of a 2-μL aqueous droplet during one bouncing cycle under laser illumination. The scale bar is 1 mm. (bottom) Simulations (0.02 s after the beginning of heating) of convection. Blue arrows denote net forces acting on the droplets.

Future Plans

Recent findings in our laboratories have uncovered new energy transduction pathways that demand investigation. Only by the development of novel chemistries, theories to quantify the interfacial assembly and dynamics of NPSs, and the development of methodologies to characterize the assemblies with NP-resolution *in-situ* and in real time will we be able to capitalize on these discoveries. We will pursue three independent, though interrelated research foci to meet these challenges. Thrust 1. *In-situ* Imaging and Manipulating Interfacial NPS Assemblies, Thrust 2. Evolutionary Structured Liquids from Confined Active Matter and Thrust 3. Using Dissipative Reactions to Impart Responsiveness and Adaptability. We will develop chemistries that impart responsiveness to the packing and dynamics of the NPS assemblies to build-in, dissipative processes and external triggers (*Thrusts 1,3*). We will use *in-situ* liquid transmission electron microscopy (LTEM) and super-resolution optical microscopy to visualize the nanoparticle surfactant assemblies and their dynamics at liquid-liquid interfaces with single NP resolution (*Thrust 1*) to obtain unprecedented insights into jamming and vitrification, long-standing challenges in materials science. Our recent findings of NPS-ladened droplet interface bilayers show charge transduction behavior comparable to that seen in synapse junctions (*Thrust 1*). Non-equilibrium thermodynamic arguments are being used to predict the shape evolution of structured

liquids confining active matter that will be experimentally validated by varying interfacial tension, (*Thrust 2*), drawing on the imaging capabilities of *Thrust 1* and the dissipative assembly studies in *Thrust 3*. Recent high resolution fluorescence confocal microscopy studies suggest more complex interfacial assemblies at high ligand concentrations (*Thrust 1*). These challenges can only be met by integrating the different expertise of the PIs in this FWP.

Publications

(1) Kim, P. Y.; Zhu, S.; Forth, J.; Xie, G.; King, D. A.; Helms, B. A.; Ashby, P. D.; Omar, A. K.; Russell, T. P. Shape-Evolving Structured Liquids. *Adv Mater* **2025**, *37* (28), e2500804. DOI:10.10002/adma.202500804.
(2) Bordia, G.; Russell, T. P.; Omar, A. K. Self-Assembly of Anisotropic Particles on Curved Surfaces. *ACS Nano* **2025**, *19* (44), 38803–38813. DOI: 10.1021/acsnano.5c15378.
(3) Jiang, S.; Zhu, S.; Kim, P. Y.; Fink, Z.; Yang, Z.; Li, P.; Chu, Z.; Russell, T. P.; Xie, G. Oscillatory and Collective Dynamics of Gold-Nanoparticle-Laden Droplets Driven by Photothermal-Induced Thermocapillarity. *Adv Mater* **2026**, *38* (4), e14793. DOI: 10.1002/adma.202514793.
(4) Wu, X.; Xue, H.; Fink, Z.; Xia, Z.; Sarma, N. A.; Gan, X.; Katsaras, J.; Ercius, P.; Rad, B.; Helms, B. A.; et al. Ion Transport through Reconfigurable Nanoparticle-Surfactant Stabilized Droplet Interface Bilayers. *Proc Natl Acad Sci U S A* **2026**, *123* (8), e2522349123. DOI: 10.1073/pnas.2522349123.
(5) Sarma, N. A.; King, D. A.; Wu, X.; Helms, B. A.; Ashby, P. D.; Russell, T. P.; Omar, A. K. Dynamic Permeability in Metastable Droplet Interfacial Bilayers. *Soft Matter* **2026**, *22* (21), 3759–3773. DOI: 10.1039/d6sm00150e.
(6) Xia, Z.; Rastogi, P.; Wu, X.; Fink, Z.; Ashby, P. D.; Helms, B. A.; Russell, T. P. Chemically Fueled Interfacial Supramolecular Polymerization. *ACS Nano* **2026**. DOI: 10.1021/acsnano.6c06152.
(7) Lu, X. Y.; Zou, J.; Pham, M.; Rana, A.; Liao, C. T.; Subramanian, E. C.; Wu, X. F.; Lo, Y. H.; Bevis, C. S.; Karl, R. M.; et al. Self-Assembled Magnetic Nanoparticle Layers: Structural Control for Reconfigurable Magnetism and Functional Applications. *ACS Applied Nano Materials* **2025**, *8* (13), 6643–6650. DOI: 10.1021/acsanm.5c00461.
(8) Raykh, A.; Paulsen, J. D.; McGlasson, A.; Joshi, C.; Atherton, T. J.; Kandula, H. N.; Hoagland, D. A.; Russell, T. P. Shape-Recovering Liquids. *Nature Physics* **2025**, *21* (6). DOI: 10.1038/s41567-025-02865-1.
(9) Hashemi, S. A.; Panahi-Sarmad, M.; Ghaffarkhah, A.; Rad, V.; Soroush, M.; Russell, T. P.; Rojas, O. J.; Arjmand, M. Stabilization of Miscible Aqueous Phases via Diffusion-Controlled Multifunctional Nanoparticle-Ligand Complexation. *Advanced Functional Materials* **2026**. DOI: 10.1002/adfm.202524954.
(10) Zhao, S.; Wang, Y.; Tang, X.; Zhang, J.; Wu, W.; Fu, Y.; Chu, S. T.; Ren, Y.; Liu, X.; Guan, X.; et al. Structured liquid-based reconfigurable all-liquid optical fibers. *Nat Commun* **2025**, *17* (1), 1186. DOI: 10.1038/s41467-025-67954-4.

Dynamics of Active Self-Assembled Materials

PI: Alexey **Snezhko**. Co-Investigators: Andrey Sokolov, Andreas Glatz

Argonne National Laboratory

Keywords: active matter, out-of-equilibrium self-assembly

Research Scope

Self-assembly, a natural tendency of simple building blocks to organize into complex architectures, is a unique opportunity for materials science. Materials that can spontaneously organize into hierarchical structures with unique and complex properties are currently exhibited only by living systems. Achieving in-depth understanding of out-of-equilibrium collective dynamics, active microscopic transport and dynamic self-assembly mechanisms is essential for the rational design of advanced materials and the discovery of tailored self-assembled architectures that can adapt to environmental conditions, self-heal, and regulate physical properties. Developing fundamental understanding and control of self-assembled out-of-equilibrium (*active*) materials, however, poses a significant challenge as they are intrinsically complex, with often hierarchical organization occurring on many nested length and time scales.

The program is focused on the fundamental aspects of out-of-equilibrium dynamics and self-organization of bio-inspired materials. Current research directions focus on the design and exploration of novel active materials based on out-of-equilibrium colloids powered by external electromagnetic fields and synthetic active liquid crystals. The difference between the two thrusts is in the way the injected energy is utilized: active colloids transform it into a mechanical particle motion, while in active liquid crystals it is used for reorientation of a local nematic order. We investigate the role of chiral behavior, spontaneous synchronization, confinement and memory effects on the onset of special and temporal coherence in active ensembles; we develop fundamental understanding and control of emergent patterns and topological defect dynamics in active nematic materials energized by acoustic waves. The program is aimed at advancing understanding and providing access to novel dynamic self-assembled materials that exhibit tunable structural and transport characteristics at the microscale unattainable under equilibrium conditions.

Recent Progress

In the past two years, we discovered and explored novel active colloidal molecules with reconfigurable chiral behavior dynamically self-assembling in binary mixtures of spherical rollers powered by Quincke phenomenon. We investigated spontaneous phase separation by chiral state and synchronization in chiral active colloidal fluids. We explored the role of shape anisotropy and chiral behavior in the collective memory of emergent self-organized structures in active colloidal ensembles. The program yielded the inversion of the global collective behavior in active chiral fluids in response to complex interplay between temporal activity modulations, shape-anisotropy and ensemble's collective memory [1, 2]. We utilized the emergent collective behavior of active

magnetic colloids to demonstrate the self-organization of a colloidal swarm into a dynamic architecture capable of controlled transport of passive cargo particles [3]. We demonstrated turbulent-like behavior of quasi two-dimensional dense suspensions of motile colloids with memory [4]. We explored complex behavior of active nematic droplets energized by acoustic waves and discovered the onset of spontaneous spinning and locomotion [5]. The research also yielded evidence of topological charge polarization at active-passive interfaces in active liquid crystals energized by an acoustic field [6].

Reconfigurable chiral colloidal molecules encode emergent dynamics of active fluids. Nature uses chirality and shape reconfiguration as pathways to achieve structural variety and adaptive functionalities. Unlike biological active matter, their synthetic counterpart – active colloidal particles– are typically rigid, operate at constant force and often lack the flexibility of their shape significantly limiting their dynamic behavior. Here, we report active colloidal molecules with reconfigurable chiral behavior dynamically self-assembling in binary mixtures of spherical rollers powered by Quincke phenomenon. The intricate balance between electrostatic and hydrodynamic interactions results in the formation of robust heterogenious bound pairs of rollers moving on curved trajectories, see Figure 1. The structural flexibility of the pair enables its motion to adapt to environmental changes through variations in trajectory curvature and even inversion of chiral handedness. We demonstrate that the chiral pairs form collective dynamic states ranging from a global polar state to a multi-vortical state comprised of free-standing self-organized vortices with quasi-antiferromagnetic arrangements of their vorticities (Figure 1c). In a global polar state the pairs imprint the dynamic state of the whole ensemble forming a state memory that facilitates robust polar state reversals of the whole ensemble upon activity cycling. By combining experiments and computational modeling we demonstrate that the heterogeneous pair formation is promoted by electrostatic interaction between spheres of different diameters once certain threshold is met. We find that in a global polar state the pairs imprint the dynamic state of the whole ensemble forming a collective state memory that facilitates robust polar state reversal of a whole ensemble upon the

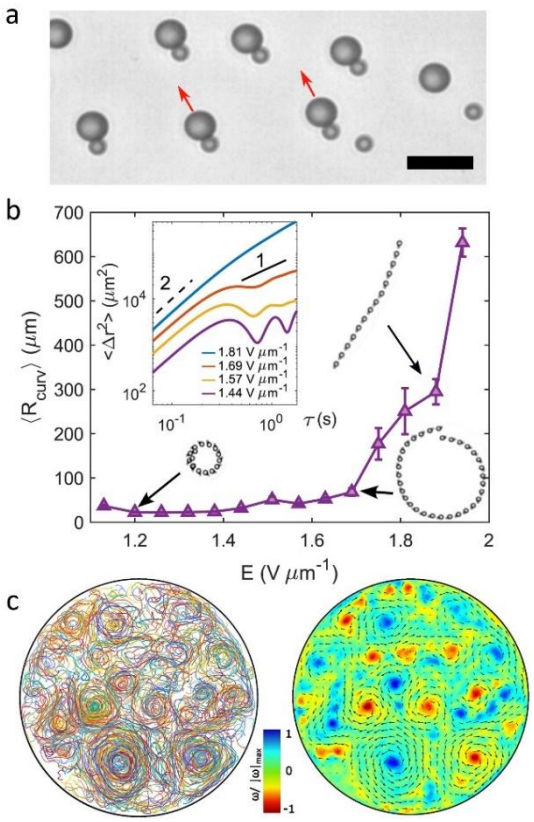


Figure 1. (a) Spontaneous formation of particle pairs in binary mixtures of Quincke roller. The red arrows indicate the propagation directions. Scale bar 20μm. (b). Radius of curvature of the trajectories is controlled by the applied electric field. Insert: Time evolution of the mean square displacement of paired Quincke rollers shown for a set of driving electric field strengths. (c) self-localized free-standing vortices comprised of roller pairs: trajectories (left) and corresponding vorticity field (right).

cessation of activity beyond all relevant timescales and subsequent activity restoration. The reversal driven by the self-assembled reconfigurable pairs results in up to one order of magnitude decrease in the characteristic reversal time demonstrated by spherical rollers. We show that the swift reversal is driven by symmetry breaking at the level of heterogeneous pairs, in striking contrast to the polar-state reversal observed in systems of purely spherical rollers, where the reversal is facilitated by the accumulation of local positional asymmetries within the ensemble [2]. Our findings provide insights into the dynamics of active heterogeneous ensembles with collective motion orchestrated by dynamically assembled, structurally flexible colloidal molecules, suggesting a design pathway for responsive active materials at the microscale.

Topological charge polarization at active-passive interfaces in acoustically powered active liquid crystals. The behavior of topological defects in nonhomogeneous active materials with modulated activity or coexisting phases (nematic/isotropic) is nontrivial. It was predicted that in the mixtures of active and passive nematics, the nematic-isotropic interfaces become topologically charged. In acoustically powered liquid crystals, the interference of the driving field naturally creates spatially nonuniform activity, separating the material into neighboring active and passive regions [7]. The characteristic size of these regions, and therefore the spacing of the active-passive interfaces, is tuned by the acoustic wave excitation frequency. We used this nonuniform activity to investigate how topological defects respond to activity gradients within the same material [6]. The conversion of acoustic energy into local extensile stresses of the liquid-crystalline medium results in the emergence of an undulation instability (with the characteristic wavelengths governed by the amplitude of the acoustic field) and proliferation of topological defects [7]. We find that in the presence of an active-inactive interface positively charged +1/2 topological defects, which are motile and sensitive to the activity gradient, preferentially reorient and migrate towards the passive zone, while negative defects remain immobile (see Figure 2a). This asymmetric defect transport produces a layer with net topological charge at the interface, forming a polarized state [6] with the strength of the polarization tuned by activity. Following the cessation of acoustic excitations, defect generation stops and the polarized layer gradually relaxes through annihilation of opposite topological charges. This process resembles charging and discharging of a capacitor, but with topological defects playing the role of mobile charges. The

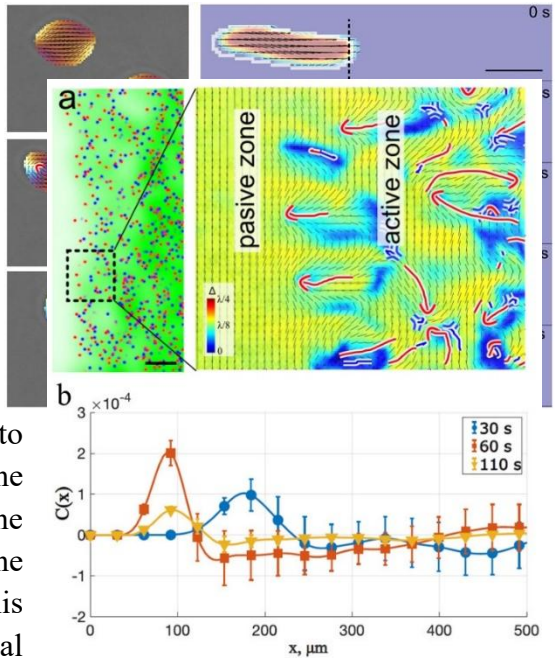


Figure 2. (a) Topological charge polarization at active-passive interfaces in acoustically energized liquid crystals. Positive topological defects migrate into passive zone. (b) Topological charge density across interface taken at different times. The interface is topologically charged with negative topological defects.

findings highlight the potential of activity patterning for manipulation of topological defect dynamics, storage and release of topological charges in active liquid crystals.

Dynamics of Acoustically Energized Active Nematic Droplets. Active nematics confined in droplets support diverse spatiotemporal patterns and dynamics [8]. We investigate the behavior of nematic tactoids in a thin quasi-2D film of DSCG liquid crystal subject to acoustic waves. The acoustically energized active liquid crystal provides a controlled environment where the activity is manipulated by the amplitude of the excitation signal. We demonstrate that at low acoustic field amplitude nematic tactoids primarily undergo stretching and bending. As the activity increases, tactoids exhibit a directional rotation with an oscillating rate. At high activity levels nematic droplets demonstrate shape changes, fission and spontaneous self-locomotion [5] (see Fig. 3 left panel). The behavior is driven by an interplay of active extensile stresses introduced at the microscopic level, nematic order, hydrodynamics and elasticity of the droplets. Our work provides fundamental insights into the behavior of synthetic active nematic droplets powered by acoustic fields. The results suggest strategies for the design and control of active nematic states, and tunable transport at the microscale.

Figure 3. Dynamics of acoustically energized active nematic droplets. Left panel: Topological transformation of nematic droplets. Actively spinning droplets transition into circular shape with two +1/2 point defects, and as activity increases, the defects merge into a single +1 defect, forming a toroid with an isotropic phase in the center. Right panel: Emergence of droplet self-propulsion. Nematic droplet stretches and bends while moving forward reminiscent of biological cells. The dashed line indicate the initial position of the droplet. The local nematic orientational order is shown by color and line

Future Plans

We plan to continue focusing our research on new approaches to discovery, synthesis and characterization of active (out-of-equilibrium) colloidal materials stemming from advances of our program. We will explore a nontrivial interplay between chiral motion, spontaneous synchronization, confinement, and emergent memory in a broad class of active colloidal materials. We plan to systematically investigate the emergence of correlated states in heterogeneous active ensembles supporting the formation of reconfigurable active colloidal units and architectures with out-of-equilibrium collective states controlled by a spontaneous symmetry breaking at multiple scales - from particle, and molecules to collectives. We will continue to advance the fundamental understanding of active liquid crystals powered by acoustic waves focusing on controlling the transport of individual topological defects with activity patterning, and exploring their use as functional elements in active materials. We plan to design and utilize activity landscapes to orchestrate large scale behavior of topological currents in active liquid crystalline materials.

References

1. B. Zhang, A. Snezhko, *Shape-anisotropy inverses the behavior of emergent vortices in active chiral fluids*, Communications Physics **8**, 243 (2025).
2. B. Zhang, H. Yuan, A. Sokolov, M. Olvera de la Cruz, A. Snezhko, *Polar state reversal in active fluids*, Nature Physics **18**, 154 (2022).

3. K. Han, A. Glatz, A. Snezhko, *Self-assembled reconfigurable pump architectures via magnetic colloidal swarms*, Physical Review Applied **22**, 064073 (2024).
4. R. Luo, A. Snezhko, P.M. Vlahovska, *Turbulent-like flows in quasi two-dimensional dense suspensions of motile colloids*, Soft Matter **21**, 6852–6858 (2025).
5. T. Emersic, J. J. de Pablo, A. Snezhko, A. Sokolov, *Dynamics of Acoustically Energized Active Nematic Droplets*, Phys. Rev. Lett. **135**, 048301 (2025).
6. A. Sokolov, T. Emersic, P. Nealey, J. de Pablo, A. Snezhko, *Evidence of topological charge polarization at active-passive interfaces in acoustically powered active liquid crystals*, Phys. Rev. Research **8**, 023060 (2026).
7. A. Sokolov, J. Katuri, J. J. de Pablo, A. Snezhko, *Synthetic Active Liquid Crystals Powered by Acoustic Waves*, Advanced Materials **37**, 2418846 (2025).
8. L. J. Ruske and J. M. Yeomans, *Morphology of Active Deformable 3D Droplets*, Physical Review X **11**, 021001 (2021).

Publications

1. K. Han, A. Snezhko, *Field-Driven Out-of-Equilibrium Collective Patterns for Swarm Micro-Robotics*, ACS Nano **19**, 16248 (2025).
2. Sokolov, J. Katuri, J. J. de Pablo, A. Snezhko, *Synthetic Active Liquid Crystals Powered by Acoustic Waves*, Advanced Materials **37**, 2418846 (2025).
3. T. Emersic, J. J. de Pablo, A. Snezhko, A. Sokolov, *Dynamics of Acoustically Energized Active Nematic Droplets*, Phys. Rev. Lett. **135**, 048301 (2025).
4. B. Zhang, A. Snezhko, *Shape-anisotropy inverses the behavior of emergent vortices in active chiral fluids*, Communications Physics **8**, 243 (2025).
5. K. Han, A. Glatz, A. Snezhko, *Self-assembled reconfigurable pump architectures via magnetic colloidal swarms*, Physical Review Applied **22**, 064073 (2024).
6. R. Luo, A. Snezhko, P.M. Vlahovska, *Turbulent-like flows in quasi two-dimensional dense suspensions of motile colloids*, Soft Matter **21**, 6852–6858 (2025).
7. C Cha, J Seo, B Park, A Snezhko, J Choi, K Han, *Hierarchical fractal assemblies from dual-anisotropic building blocks fabricated via magnetic field-assisted thermo-mechanical deformation*, Chaos, Solitons & Fractals **209**, 118461 (2026).
8. A. Sokolov, T. Emersic, P. Nealey, J. de Pablo, A. Snezhko, *Evidence of topological charge polarization at active-passive interfaces in acoustically powered active liquid crystals*, Phys. Rev. Research **8**, 023060 (2026).